The petrography and geochemistry of the Kadinhani area, Central Turkey.

by

Huseyin KURT, B.Sc., M.Sc. (Selcuk University, Turkey)

A thesis submitted for the degree of Doctor of Philosophy

Dept. Geology & Applied Geology

Glasgow University.

March, 1994

ProQuest LLC.
789 East Eisenhower Parkway
P.O. Box 1346
Ann Arbor, MI 48106 – 1346

I dedicate this thesis to my mother Mevlude, My father Emin, my sisters, and my brothers.

DECLARATION

The material presented in this thesis summaries the results of of three years research work carried out in the Department of Geology, University of Glasgow between March 1991- March 1994 under the supervision of Prof.Dr B.E.Leake.

I declare that the contents of this thesis are the results of my own work, have not been accepted in substance or in part for any other degree, and are not currently being submitted for any other degree. All other works referred to in this thesis have been acknowledged.

Huseyin Kurt.

I certify that Huseyin Kurt has undertaken the bulk of the work involved in this thesis. Specifically; background geology, sample preparation, examinations and analyses, and their interpretation. I have assisted with advice and help of a general, technical, conceptual nature, as would be expected in the course of normal PhD. supervision and advice. Huseyin Kurt has written the thesis himself, and is responsible for its content.

Professor B.E.Leake.

ACKNOWLEDGEMENTS

This research was caried out at the Department of Geology & Applied Geology.

I am indebted to Dr. C.D. Gribble, the head of the department, for allowing me the use of the facilities and a friendly atmosphere in the department.

I especially thank Professor B.E. Leake for his informed supervision, his guidance, hospitality, continued advice, involving several days in the field and criticism of my work during the last three years. This research would have never completed on time without his help.

I would like to present my sincere appreciation and gratitude to Professor Russel, Professor Ramsay, Dr.Dempster, Dr.Bell, Dr.Bowes and Dr. Fallick for their help and support.

I wish to thank Dr. C. Farrow for his consistent help with the computing facilities.

The technical staff of the departments made many a task much easier during the course of this research. Their help and advice has been invaluable; R.Morrison, D.Turner, R.Mc Donald, J.Gallagher, M.Macleod, J. Gilleece, J.Kavanagh, A.Jones and W. Higgison.

I wish to acknowledge my gratitude to the Rector of Selcuk universty (Konya-Turkey), member of the Engineering & Architecture Faculty and staff members of the Geology Department for having awarded me a scholarship to pursue this degree.

I am very grateful to Professor Dr. H. Bas for his supervision in Turkey and for his continued interest in my work.

I am also very grateful to the people of Turkey for providing a grant towards the financing of my research.

The post-grad fraternity of the department, both past and present, made my period of research a pleasure. Thanks for friendship and humour; Sherif, Ali, Nasir, Mohammed, Hameed, Nejmi, Jan, Esam, Daud, Fethi, Rona, Carolyn, Susan, Campbell, Ali, Vojtech, John, Garry, Calum, Richard, Amar, Mansur, Colin, Chris, Tim, Robert, Ahmed, Zafer, Helen, David, Paul, Shuang, Mark, Abdullah, Salem,

I would particularly like to thank Mehmet, Veysel, Kerim, Gemma, Bulent , Abdurrahman, Edi, John, Patrica, Joe, Devit, Fiona, Clarea, Juanna, Liz, Izobel, Kerin, Lee, Marie, Mary and students of the Turkish society, for being friendly, understanding and giving continued support during my stay in Britain.

Finally, I would like to offer sincere appreciation to my parents, especially to my mother and my father, brothers and sisters, for their love, their unfailing encouragement and support.

CONTENTS PAGE

DECLARATION ii
ACKNOWLEDGMENTS iii
CONTENTS iv
LIST OF TABLES vi
LIST OF FIGURES viii
LIST OF PHOTOGRAPHS xi
ABSTRACT xii
CHAPTER -I. INTRODUCTION 1-4
1.1. Description of the area 1
1.2. Previous work 3
1.3. The aim of the research 4

CHAPTER -II. SAMPLING AND ANALYTICAL METHODS 5

CHAPTER - III. STRATIGRAPHY 7
3.1. Introduction 7
3.2.Esiragil Formation 8
3.3.Bagrikurt Formation 8
3.4.Kursunlu Formation 10
3.5.Metatrachyandesite 10
3.6.Metabasaltic andesite 10
3.7.Metahornblende gabbro 11
3.8.Metadolerite 11
3.9.Lorasdagi Formation 11
3.10.Osmankayasi Tepe Formation 11
3.11.Dacite 12
3.12.Toprakli Formation 12
3.13.Alluvium 12

CHAPTER -IV. STRUCTURAL GEOLOGY 13

CHAPTER -V. PETROGRAPHY AND MINERAL CHEMISTRY 23
5.1. Esiragili Formation 23
5.2. Bagrikurt Formation 26
5.3. Kursunlu Formation 36
5.4. Metatrachyandesite 36
5.5. Metabasaltic andesite 46
5.6.Metahornblende gabbro 54
5.7.Metadolerite 60

5.8.Lorasdagi Formation 64
5.9.Osmankayasi Tepe Formation 64
5.10.Dacite 64

CHAPTER - VI. GEOCHEMISTRY 72
6.1. Psammite and Quartzite 72
6.2.Metachert 87
6.3.Pelite, Basic schist, and Calc silicate rocks 92
6.4. Carbonate rock 105
6.5. Meta-igneous and igneous rocks 109
6.5.1.Meta-igneous rocks 109
6.5.1.1.Metatrachyandesite and metabasaltic andesite 109
6.5.1.2.Metahornblende gabbro and metadolerite 126
6.5.2. Igneous rocks 146
6.5.2.1.Dacite 146

CHAPTER - VII.METAMORPHISM 156

CHAPTER- VIII. THE TECTONIC EVOLUTION OF TURKEY AND EVOLUTION OF THE PRESENT AREA 164

IX - CONCLUSIONS 168

REFERENCES 173

Appendix 1. A geological map of Kadinhani area, Turkey.
Appendix 2. Cross-sections for the geological map of Kadinhani area, Turkey

LIST OF TABLES

Table Title	Page
1. Table showing formation name and age in studied area.	7
2. Composition of dolomite and ankerite minerals in carbonate rocks.	25
3. Composition of muscovite in metapelitic rocks.	29
4. Composition of chloritoid in metapelitic rocks.	29
5. Composition of tourmaline in metapelitic rocks.	30
6. Composition of rutile in metasedimentary rocks.	30
7. Composition of plagioclase in metapelitic rocks.	31
8. Composition of epidotes in calc-silicate rocks.	32
9. Composition of chlorite in in pelitic rocks.	34
10. Composition of amphiboles in metabasic schist.	35
11. Composition of magnetite in metapelite and metabasic schist.	35
12. Compositionof plagioclases in metatrachyandesite.	41
13. Composition of clinopyroxene in metatrachyandesite.	42
14. Composition of amphiboles in metatrachyandesite.	42
15. Composition of pumpellyite in metatrachyandesite.	43
16. Composition of chlorites in metatrachyandesite.	43
17. Composition of epidotes in metatrachyandesite.	44
18. Composition of micas in metatrachyandesite.	44
19. Composition of magnetites in metatrachyandesite.	45
20. Composition of plagioclase in metabasaltic andesite.	50
21. Composition of clinopyroxene in metabasaltic andesite.	50
22. Composition of amphiboles in metabasaltic andesite.	51
23. Composition of stilpnomelane in metatrachy andesite.	51
24. Composition of biotites in metabasaltic andesite.	52
25. Composition of white micas in metabasaltic andesite.	52
26. Composition of epidote and chlorites in metabasaltic andesite.	53
27. Composition of feldspars in metahornblende gabbros.	57
28.Composition of amphiboles in metahornblende gabbros.	57
29. Composition of chlorites in metahornblende gabbro.	58
30. Composition of epidote in metahornblende gabbro.	58
31. Composition of muscovite, pyroxene and magnetite minerals in metahornblende gabbro.	59
32. Composition of feldspar in metadolerite.	62
33. Composition of clinopyroxene in metadolerite.	62
34. Composition of white micas in metadolerite.	63
35.Composition of feldspars in dacite.	66
36. Composition of amphiboles in dacite.	66

37. Composition of biotite and magnetite in dacite. 67
38. Major and trace elements of psammites. 83
84
39. Major and trace elements of quartzite. 85
86
40. Rare earth element data for the psammite and quartzite. 86
41. Major and trace elements of cherts. 91
42. Rare earth element data for the cherts. 91
43. Major oxides and trace elements of metapelitic rocks. 99
100
44. Major oxides and trace elements of the metabasic schist. 101
102
45. Major oxides and trace elements of calc silicate rocks. 103
104
46. Some important major oxides and trace elements contents in different carbonate rocks. 107
47.Major oxides and trace elements contents in carbonate rocks. 107
108
48. Major oxides, trace elements and CIPW norms of the metatrachyandesite. 121
122
49. Major oxides, trace elements and CIPW norms of the metabasaltic andesite. 123
124
50. Rare earth element data for the metatrachyandesite and metabasaltic andesite. 125
51. Major oxides, trace elements and CIPW norms of the metahornblende gabbros. 141
142
143
52. Major oxides, trace elements and CIPW norms of the metadolerite. 154
53. Rare earth element data for the metahornblende gabbro and metadolerite. 145
54. Major oxides, trace elements and CIPW norms of the dacite. 153
154
55. Rare earth element data for the dacite. 155
56. Metamorphic minerals in greenschist and blueschist metamorphism for different rocks in the studied area. 163

LIST OF FIGURES

Fig. Title	Page
1.Location map of the area studied.	2
1a. Tectonic map of Turkey.	2
2. Chemical composition of chlorites in metapelitic and metasedimentary rocks.	33
3. Classification of amphiboles in metabasic schist.	33
4. Albite in the metatrachyandesite.	37
5. Composition of cpx, in metatrachyandesite.	37
6.Compositional variations of clinopyroxene phenocrysts from the metatrachyandesite in terms of Ti, Ca, Na, Cr and Al using discriminant diagrams.	38
7. Classification of amphiboles in metatrachyandesite.	39
8. Composition of chlorite, in metatrachyandesite.	40
9. Muscovite and phengite Al-Si composition of metatrachyandesite.	41
10. Plagioclase in metabasaltic andesite.	46
11. Composition of cpx, in metabasaltic andesite.	47
12. Compositional variations of clinopyroxene phenocrysts from the metabasaltic andesite in terms of Ti, Ca, Na, Cr and Al using discriminant diagrams.	47
13. Classification of amphiboles in metabasaltic andesite.	48
14. Composition of chlorite, in metabasaltic andesite.	49
15. Chemical composition of plagioclase plotted on the Or-Ab-An diagram in metahornblende gabbro.	54
16. Classification of amphiboles in metahornblende gabbro.	55
17. Composition of chlorite, in metahornblende gabbro.	56
18. Plagioclase in the metadolerite.	60
19. Composition of cpx, in metadolerite.	60
20. Compositional variations of clinopyroxene phenocrysts from the metadolerite in terms of Ti, Ca, Na, Cr and Al using discriminant diagrams.	61
21. Composition of feldspar in dacite.	65
22. Classification of psammite.	72
23. Harker variation diagram for psammite and quartzite.	73
24. Plot of Niggli mg vs Niggli Si for psammite and quartzite.	74
25.Major oxides and trace element values vs Niggli al-alk for psammite and quartzite.	75
26. Major oxides and trace elements plots for psammite and quartzite.	76
27. Plot of Log (K_2O/Na_2O) vs SiO_2 for psammite and quatrzite.	78
29. Plot of discrimination function F_1 and F_2 showing the position of psammite and quartzite.	78
30. Plot of discrimination function F_1 and F_2 showing the provenance of psammite and quartzite.	79
31. AFM diagram for psammite and quartzite.	80
32. K_2O: Na_2O: MgO triangular diagram for psammite and quartzite.	81
33. La/Th against TiO_2 diagram for psammite and quartzite.	82
34. Chondrite - normalised REE patterns for psammite and quartzite.	83
35. Plot of Al_2O_3 vs. K_2O+Na_2O and Al_2O vs. FeO*(total) in metacherts.	87

36. Plot of Ce/Ce* vs. some major oxides diagram for metacherts. 88
37. The total REE vs some major oxides for metacherts. 88
38. Some REE vs. al-alk diagram for metacherts. 89
39. Chondrite normalised REE patterns for metacherts. 90
40. Niggli c vs. mg plot for metapelites, metabasic schist and calc silicate rocks. 93
41. Niggli al-alk vs. c plot for metapelites, metabasic schist and calc silicate rocks. 93
42. Plots of Niggli al-alk against some oxides and trace elements for metapelites, metabasic schist and calc silicate rocks. 95
43. Plots of K_2O against Pb, Ba, Th and Al_2O_3 for metapelites, metabasic schist and calc silicate rocks. 96
44. CaO vs. Sr for metapelites, metabasic schist and calc silicate rocks. 96
45. Zr/TiO_2 vs. Ni for metapelites, metabasic schist and calc silicate rocks. 97
46. AFM diagram for metapelites, metabasic schist and calc silicate rocks. 98
47. Plots against Al_2O_3 for carbonate rocks. 105
48. Zr/TiO_2 vs. Nb/Y for metatrachyandesite and metabasaltic andesite. 110
49. Zr/TiO_2 vs. Ga for metavolcanics. 110
50. TiO_2 vs. Zr/P_2O_5 discrimination diagram for metavolcanics. 111
51. SiO2 vs FeO*/MgO plot for metavolcanics. 111
52. Harker diagram for metavolcanics. 112
113
53. Plots of major oxides and trace elements and Niggli ti versus Niggli mg for metavolcanics. 114
54. Ti vs. Zr plot for metavolcanics. 115
55. Cr versus Y plot for metavolcanics. 116
56. Zr/Y versus Zr diagram for metabasaltic andesite. 117
57. MORB-normalized incompatible element patterns for representative samples of the metavolcanics. 118
58. Primordial mantle - normalized multi-element pattern for representative samples of metavolcanics. 118
59. Chondrite- normalized rare earth element patterns for metavolcanics. 119
60. CIPW nomenclature and classification of the metahornblende gabbro and metadolerite, ANOR vs, Q' plot. 126
61. Zr/P_2O_5 versus TiO_2 discrimination diagram for metahornblende gabbro and metadolerite. 127
62. SiO_2 vs. FeO*/MgO for metahornblende gabbro and metadolerite. 127
63. Harker diagrams for metahornblende gabbro and metadolerite. 129
130
64. Trace elements concentrations vs. Zr for metahornblende gabbro and metadolerite. 131
65. Plots of major oxides versus Niggli mg, for metahornblende gabbro and metadolerite. 132
65a. Plots of trace elements versus Niggli mg, for metahornblende gabbro and metadolerite. 133
134
66. Ti versus Zr for the metahornblende gabbro and metadolerite. 135
67. Zr/P_2O_5-TiO_2 plot for the metahornblende gabbro and metadolerite. 135
68. MORB-normalized patterns for averages of metahornblende gabbro and metadolerite. 136
69. Primordial mantle - normalized multi - element patterns for averages of metahornblende

gabbro and metadolerite. 137
70. Chondrite-normalized rare earth element distribution patterns for the metahornblende gabbro and metadolerite. 138
71. Chemical classification diagram of dacite. 146
72.Chemical classification diagramof dacite. 146
73. Plot of normative plagioclase composition versus normative colour index for dacite. 147
74. Chemical discrimination diagram of dacite. 147
75. Chemical discrimination diagram of dacite. 147
76. AFM diagram of dacite. 148
77. Harker diagram of dacite. 149
150
78. Y versus Nb, La, and CaO plots for dacite. 151
79. Chondrite - normalized rare earth element patterns for dacite. 152
80. NaM^{IV} vs. Al^{IV} diagram for metahornblende gabbro and metatrachyandesite. 157
81. Amphibole analyses plotted on a Al^{VI} against Si diagram for metabasic schist and metatrachyandesite. 158
82.Compositional variations of pumpellyite. 160
83. Plot of mg against Na for muscovite and white mica analyses from high and low pressure areas. 161
84. Chlorite Al-Fe-Mg composition diagram. 162

LIST OF PHOTOGRAPHS Page

1. Photograph showing the mesoscopic F_1 folds recognized are isoclinal and recumbent. 18
2. Photograph showing S_1 schistosity folded by S_2. 18
3. Photograph showing conjugate kink folds in laminated pelitic rocks. 19
4. Photograph showing Systematic and non-systematic joints. 19
5. Photograph showing joints and lineation on marble. 20
6. Photograph showing D3 upright plunging folds in Esiragili Formation carbonate. 20
7. Photomicrograph from pelitic rocks, showing early S_1 foliation in micaschist is folded or crenulated by S_2. 21
8. Photomicrograph from pelitic rocks, showing S_1 distorted around a chloritoid porphyroblast. 21
9. Photomicrograph from quartz-albite-epidote actinolite schist, showing needle-like actinolite grains with a preferred orientation, marks the foliation S_1. 22
10. Photomicrograph from pelitic rocks, showing post tectonic chloritoid rosette preserving relict foliation. 68
11. Photomicrograph of metatrachyandesite, showing salite surrounded by riebeckite minerals. 68
12. Photomicrograph of metatrachyandesite, showing pumpellyite aggregates surrounded by epidote, chlorite, salite and quartz minerals. 69
13. Photomicrograph of metabasaltic andesite, showing augite porphyroblast with glaucophane and fibrous actinolite rim. 69
14. Photomicrograph of metabasaltic andesite, showing aggregates of stilpnomelane. 70
15. Photomicrograph of metahornblende gabbro, showing epidote, plagioclase, quartz, chlorite and hornblende which was replaced by crossite and riebeckite. 70
16. Photomicrograph of dacite, showing sieve texture. 71

ABSTRACT

The petrographic and geochemical investigations of the Kadinhani metamorphic, igneous and sedimentary rocks indicate a great range in petrography and geochemistry.

The stratigraphy in the area starts with the metasedimentary Esiragili Formation which is followed upwards in the Devonian by the Bagrikurt Formation which is characterized by metavolcanic rocks, cherts, metasedimentary rocks, pelite, carbonate, calc-silicate and block limestone.The formation is overlain by the upper Devonian-lower Carboniferous Kursunlu formation limestone, which reflects a shelf environment and is cut by intrusive dykes. The Lorasdagi Formation carbonate was deposited in the an open shelf environment in the Jurassic to Cretaceous, overlies the older rocks unconformably and continues up to the unconformably overlying upper Miocene-Pliocene Osmankayasi Tepe Formation limestone which is overlain by dacite which itself is overlain by the Plio-Quaternary Toprakli Formation.

Three phases of deformation (D_1-D_3) have been recognized in the present area.The microstructural and petrographic investigations show distinct phases of deformation and different metamorphic events. The apparent absence of any mineral growth during D_2 and the post tectonic mineral overgrowth, indicates a metamorphic relaxation followed the M_1 metamorphism. The second metamorphic event involves retrogression with pseudomorphic replacement of chloritoid, biotite, amphibole and feldspar.

The area was metamorphosed first under the conditions of the greenschist facies (the most important minerals, muscovite, chlorite, chloritoid, actinolite and stilpnomelane) and then later under the blueschist facies metamorphism which gave rise to magnesio riebeckite, crossite, glaucophane, phengite and albite minerals.

The psammite and quartzites have a passive or active continental margin setting. The cherts have been deposited in a relatively shallow-water environment similar to recent continental shelf slope environment. The pelitic rocks were originally shales in which the main control in composition was the sheet silicates. The metabasic schists were possibly tuffs in the pelites. The calc silicate rocks were originally impure siliceous limestones with variable amounts of clay material. The carbonate rocks

contains variable amounts of terrigenous material and dolomite is possibly of late diagenetic origin.

The meta-igneous and igneous rocks are of a subalkaline character. The metahornblende gabbros were derived from a subalkaline basaltic melt with oceanic affinity. The metadolerites reveal a parental magma source similar to subduction- related lavas in a continental margin environment. The parental magma of the metadolerite involved a mix of subcontinental lithosphere and subduction components. The possiblity of derivation of the metatrachyandesite from basaltic magma via crystal fractionation of mafic minerals conflicts with the degree of REE fractionation of the metabasaltic andesite.

The dacites were evolved mainly by amphibole fractionation under hydrous conditions at shallow levels in the continental crust and probably formed by fractional crystallization from an andesitic parental magma.

The thesis contain 18 REE analyses, 153 XRF analyses of metamorphic, igneous and sedimentary rocks, microprobe analyses of feldspars, sheet silicates, amphiboles, pyroxenes, carbonate minerals, stilpnomelane, chloritoids, tourmalines, rutiles, epidotes, pumpellyites and magnetites. There is a new geological map of the area.

I - INTRODUCTION

1.1. DESCRIPTION OF THE AREA

This account describes the results of a systematic geological investigation of the Kadinhani area, Konya, Central Anatolia. The mapped area covers about 300km^2 and is situated about 60 kilometers NW of Konya (Figure,1).

The general relief is low hills and shallow valleys. Rocks in the mapped area are well exposed with most arable land limited to the Neogene rocks.

The lower most visible unit in the area is the Silurian - Devonian age Esiragili Formation, comprised metacarbonate, phyllite and psammites. This formation is overlain by the Devonian Bagrikurt Formation, of schist, phyllites, marbles, cherts, quartzites, basic schist, calc silicate, pelites and psammites and also metavolcanic rocks such as metatrachyandesite and metabasaltic andesite. The formation is overlain by Devonian and Carboniferous age Kursunlu Formation limestone.

The meta-igneous rocks such as metahornblende gabbro and metadolerite cut the Permian limestone, which is outside the studied area, and older rocks in the present area.

The Lorasdagi Formation, of Jurassic Cretaceous age, overlies the Kursunlu and Bagrikurt Formations unconformably and continues up to the unconformably overlying upper Miocene- Pliocene Osmankayasi Tepe Formation.

The upper Miocene-Pliocene is overlain by dacite which itself is overlain by the Plio -Quaternary Toprakli formation.

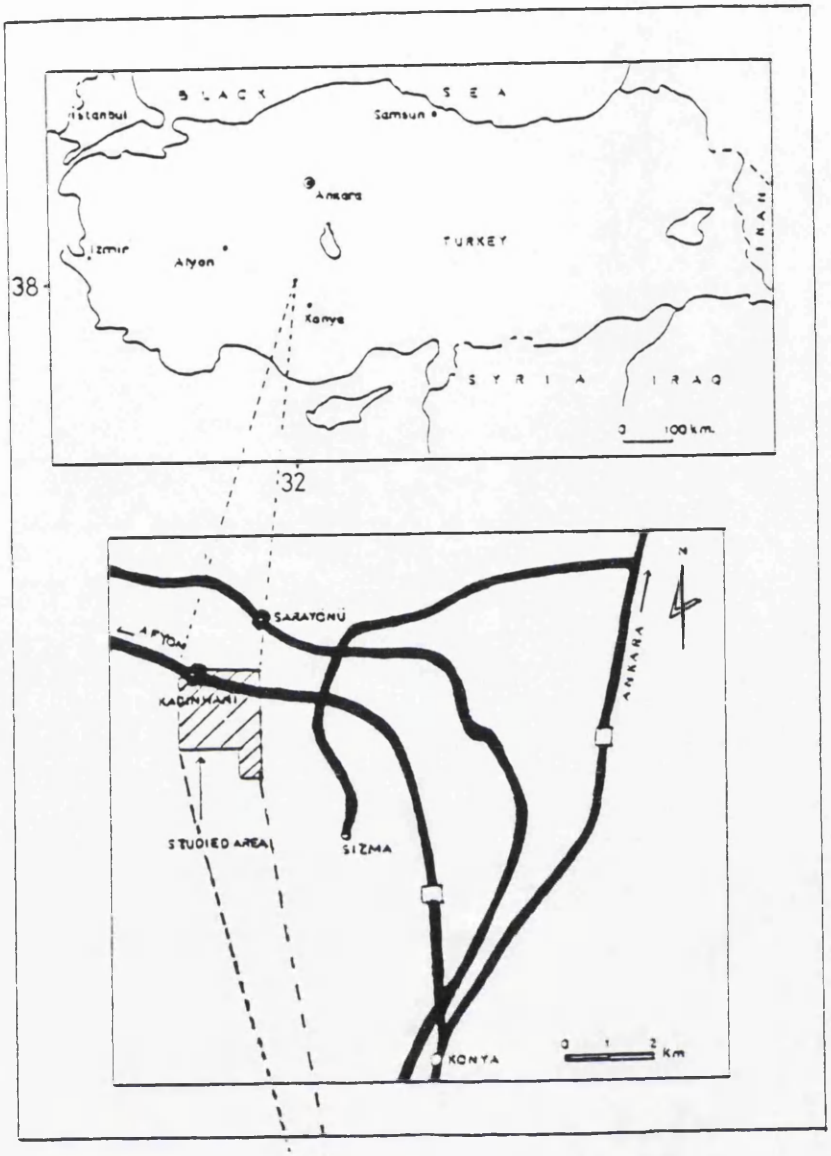

Figure. 1. Location map of the area studied.

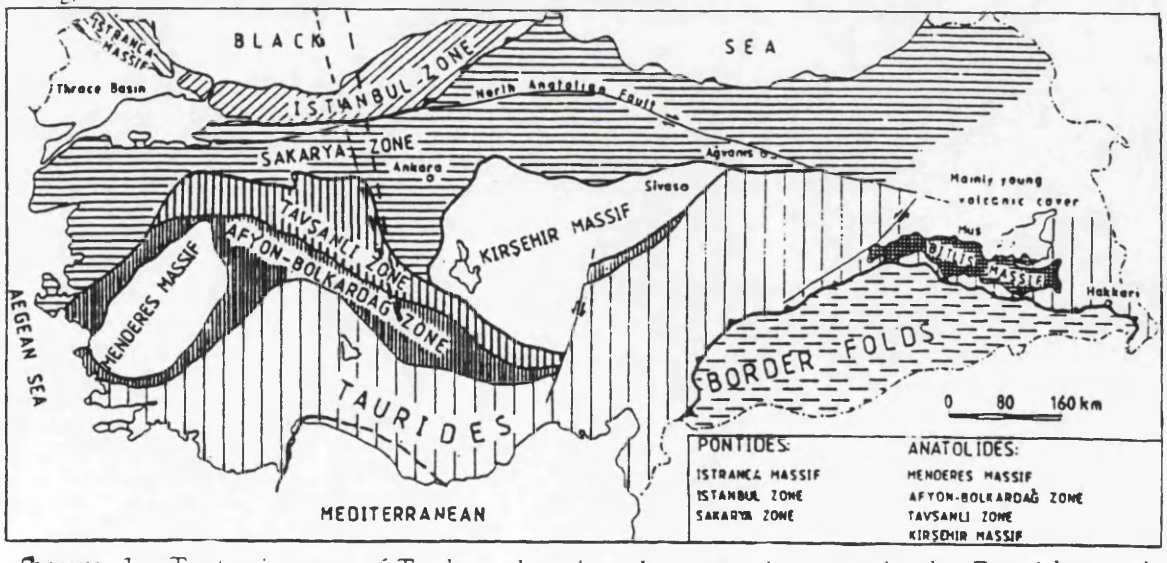

Figure. 1a. Tectonic map of Turkey showing the tectonic zones in the Pontides and Anatolides. Heavy lines indicate major sutures.

1.2. PREVIOUS WORK

Considerable work has been carried out on the geology of the region as result of mercury deposits in the neighbouring area. Pilz (1937), Schumacher (1937), and Kovenko (1939) made regional surveys of the geology with Niehoff(1964) compiling a regional geological map at 1:100,000. Petrascheck (1964), Maucher (1964), Kaaden (1964), Weisner (1964) and Holl (1966) carried out investigations into ore deposits and the economic geology.

The first detailed study of the area was made by Weisner, (1968) who proposed that the mercury deposits are related to andesitic volcanism. The oldest formation in the region is metamorphosed Silurian limestone which is overlain with an angular unconformity by Lower Devonian phyllite with Upper Devonian - Carboniferous phyllite and quartzite following conformably and then Lower-Middle Carboniferous limestone. Weisner(1968) described the magmatic activity which produced "andesite porphyrite" and "andesite".

Bayic (1968) and Banger (1987) studied the petrography of the adjacent area to the east. They found stilpnomelane and glaucophane minerals and suggested that these were the result of burial metamorphism.

Dogan (1975) , Ustundag (1987) and Eren(1993), described the stratigraphy of the adjacent area to the east.

Pehlivan (1976) and Motorcu (1987), considered the origin of the mercury deposits.

Guzel(1983) carried out hydrogeological studies on the schist underlying the limestone. This author considered the volcanic rocks as andesites of Paleogene age.

1.3. THE AIM OF THE RESEARCH

Almost all previous workers were satisfied with a brief description of the lithology, without intensive study of the petrography and geochemistry. Geochemistry is a very important aspect of the present work.

The aim of this research is to decipher the geological history and the petrology of the area investigated which so far has never been studied in detail. In order to do this a 1:25,000-scale geological map of the area was completed, the stratigraphy and tectonics examined and mineralogical and chemical studies undertaken in order to understand the petrology of the rocks concerned.

The bulk rock composition was examined by the use of X-Ray fluorescence, and ICP analysis. Electron microprobe analysis was used to study the mineral compositions

II - SAMPLING AND ANALYTICAL METHODS

The ultimate goal of the present study is to reconstruct the original rock compositions in order to deduce the source terranes and interpret these compositions in terms of tectonic models.

Sampling involved collection of fresh unweathered specimens from various localities in the Kadinhani area. Sample locations are given in Tables in chapter VI.

Bearing in mind any possible contamination, large samples were initially trimmed to remove weathered surfaces using a hydraulic press. The samples were then crushed into small pieces depending on the number of the required test specimens which were subsequently used to make thin and polished sections and, chemical analyses.

Mineral analyses were obtained using a Cambridge instrument Microscan 5 Machine. This uses X-ray radiation generated by an electron beam striking finely made and carbon coated thin probe sections. Each element produces a characteristic x-ray energy spectrum which is measured by a solid state detector for a counting time of 100 seconds.

Chemical analyses in conjuction with petrography are important means of examining compositional variation in rock samples. Therefore 153 samples were subjected to X-ray fluorescence analysis for both major and trace elements.

The first step consists of reducing the size of the samples to 100 mesh and then to 250 mesh. The former size is suitable for major element analyses and the latter for the trace elements. The methods of analyses are those described by Harvey et al. 1981 and Harvey et al. 1973 for trace and major elements repectively, using fused discs for major elements and pressed fine powders for trace elements.

The FeO contents of samples were determined by the method of titration with potassium - dichromate as the X-ray spectrometer gives only total iron. Fe_2O_3 is calculated by subtracting FeO multiplied by 1.1114, from the total iron as Fe_2O_3.

The amounts of H_2O and CO_2 were determined by a method of combustion, adsorbtion and gravimetry (Riley, 1958). In some samples, volatile contents were determined by measuring loss on ignition.

REE were analyzed by ICP-mass spectrometry (ICP-MS) at the Scottish Universities Research and Reactor Centre. Sample dissolution prior to introduction into the ICP-MS was achieved by HNO_3-HF-$HClO_4$ microwave digestion in sealed Teflon beakers, as detailed elsewhere (Murray et al. 1991a). Samples were prepared and run in random order, and on different analytical runs, days, and ICP-Ms instruments. Data was reduced using a modified version of the elemental data reduction software.

III - STRATIGRAPHY

3. 1. INTRODUCTION

The area is composed of Paleozoic Mesozoic and Cenozoic rocks in the following stratigraphical order;

Table,1.Lithostratigraphy

NAME	AGE	THICKNESS (m)
Alluvium		
(Unconformity)		
Toprakli Formation)	Plio-Quaternary	120
(Unconformity)		
Dacite		30
(Unconfomity)		
OsmankayasiTepeFormation	upperMiocene-Pliocene	300
(Unconformity)		
Lorasdagi Formation	Jurassic-lower Cretaceous	650
(Unconformity)		
Metadolerite		
Meta hornblende gabbro		
Meta trachyandesite		150
Meta basaltic andesite		
Kursunlu Formation	middle Devonian-lower Carboniferous	200
Bagrikurt Formation	Devonian	700
Esiragil Formation	Silurian ?- lower Devonian	300

3.2. ESIRAGIL FORMATION

The oldest formation exposed in the area is the Esiragil Formation. The lower part of this formation is mostly of metacarbonate with phyllite and psammite. Towards the top of the formation, the carbonate beds within the formation increase in proportion and the phyllite and psammite decrease.

The psammites are fine-grained yellow-brown siliceous rocks. Cream-yellowish metacarbonate units are interbedded with phyllite.

Weisner(1968) first observed and named this formation as "yellow-grey limestone". Dogan (1975) named them the "Ertugrul limestone stage" and Ustundag (1987) observed them within Esiragil Village and named them the Esiragil Formation.

Exposures occur on Yapraklibasi Tepe (35200-19100), Gulbek Tepe (38700-14700) and Tulbent Tepe (37500-13500) (appendix-1).

This formation passes upwards into the Bagrikurt Formation (table,1) with a gradational contact, defined at the top of the metacarbonate which underlies a consistently purple coloured phyllite which itself forms the base of the Bagrikurt Formation. The boundary of the two formations can be seen very clearly in the Ketele Dere. The bottom of the formation is nowhere seen in the present area but the formation is overthrust onto ophiolitic rock outside the studied area to the southest.

No fossils were found. Weisner (1968) tentatively suggested a Silurian ?-Devonian age for the formation due to the stratigraphy.

3.3. BAGRIKURT FORMATION

This formation is the commonest in the area (appendix-1) and includes phyllite, schist, marble, quartzite, metachert, psammite, pebbly quartzite, milky quartz veins, metaconglomerate and block limestone. It is overlain conformably by Middle Devonian limestone.

Ustundag (1987) named the formation after Bagrikurt Village but good exposure also occurs in Kadinhani town (33000-31000), Bulgurpinari village (25700-21500) and on Tavsankayasi (32500-19000), Kartal Yaylasi (39000-18400) and Kara Tepe (35000-33400).

Generally the schist and pelite have brownish-purple-grey weathered surface but fresh rocks are greenish in colour, with a well developed schistosity. Intercalations of micaschist, phyllite, psammite, quartzite and limestone occur. It is dominated by a penetrative schistosity and shows the later development of crenulation cleavages. The bedding planes of the phyllite were not observed in the field due to strong development of the foliation. Milky quartz veins are parallel to the foliation of the phyllite and are synmetamorphic.

Occasionally, conglomerates occur with rounded clasts varying from 3 cm to 10 cm in diameter of phyllite, metachert, quartzite and limestone fragments. The pebbles show elongation in one direction and flattening in the other direction which is in the cleavage. Pebbly quartzite is exposed in the area, with 0.2 - 2 cm grain size in best preserved pebbly horizons. The pebbly horizons consist of abundant pebbles of quartz, with some feldspar and mica minerals. The pebbles are elongated in length up to 0.5-1cm. and sedimentary grading is well preserved. Dark grey limestone and marble occur as lenses surrounded by schists and phyllite and are up to 20 -40 cm thick.

Basic schists occur in the formation and are generally concordant with the schistosity of the host rocks. They are green to dark green in colour and have a fine to medium grain size.

Metacherts, from 15cm to 15m in thickness are interbedded with metapelites. The bed thicknesses of the metacherts range between 3cm and 15cm.

Grey and white quartzites up to 10 m thick are interlayered with pelites and occur on the highest ridges in the area.

Psammites vary in colour from pale-grey to pink. Occasionally the rocks are found interbedded with pelite bands (3cm to 15 cm thick). Generally they occur close to the quartzite. The grains are flattened in the foliation and elongated to lengths up to 0.5cm. Bedding planes are well developed in this rocks. Graded sandstones occur in cyclic sequence probably as result of turbidity currents.

Block limestone have a very sharp contact with pelites.

The formation underlies the Kursunlu Formation conformably (table 1). The boundary is at the top of the schist which underlies a persistent limestone which itself forms the base of the Kursunlu Formation. The boundary can be seen very clearly around the Sivri Tepe (27000-29000) Imamcal Tepe (31500-29500).

Weisner(1968) suggested a Devonian age for the formation due to the stratigraphy, as this formation underlies the Kursunlu Formation which has Middle Devonian-lower Carboniferous fossils However, this assumes the sucession is right way up which seems likely.

3.4. KURSUNLU FORMATION

The formation is dark black bituminous limestone, first named by Dogan (1975) from Kursunlu Village

It occurs in the vicinity of Karacam Tepe (39000-20600), Dellal Tepe (34300-27500), on Imamcal Tepe (31500-29500), Elmaliagili Tepe (38.800-30900) and Sivri Tepe (27000-29000) (appendix-1).

The lower parts of the Formation are recrystallized, massive, beige-light grey and medium bedded. The top of the unit is medium to thick bedded, dark grey dolomitic limestone.The formation contains an abundant microfauna which is difficult to identify , due to metamorphism and recrystallization. The following fossil was identified in this study Amphipora ramosa (PHILLIPS) which indicates a Middle Devonian age .

The formation is overlain by the Lorasdagi Formation with unconformity (table,1).

3.5. METATRACHYANDESITE

The rocks are green coloured with large (0,5x1.5 cm) plagioclase phenocrysts and with good foliation which is conformable with the country rock foliation. These rocks occur on Tasli Tepe (33000-32500), Bostanligin Tepe (32.700-31800), north of the Imamcal Tepe (28.800-31.300) and south of Mecidiye Village(32000-33000) (appendix-1) in the Bagrikurt Formation. The age of these rocks is unknown.

3.6. METABASALTIC ANDESITE

The rocks are green coloured and generally concordant with the main schistosity of the host rocks. These rocks occur as a sill in Karanlik Dere (40500-17500) (appendix-1). The age of the rocks is unknown and possibly of the same age as the metatrachyandesite .

3.7. METAHORNBLENDE GABBRO

Gabbro dykes containing Na-amphibole, hornblende and plagioclase have a NW strike, vary in width from 1-5m, outcrop in exposures up to 300m long. The dykes are often nearly vertical (80-90 dip) and were intruded into the metasediments at right angles to the middle Carboniferous limestone bedding planes or older rock foliations. Exposures occur at Elmaliagili tepe (38.800-30900), Igdeli Burnu (37200-28700), Unluk Tepe (38.000-25000) (appendix-1).

3.8. METADOLERITE

A few metadolerite dykes containing augite and plagioclase have a NW strike, vary in width from 1-3m, outcrop in exposures up to 500m and cross the Middle Carboniferous and older rocks. The dykes may be the same age as the metahornblende gabbro. The exposures occur on Ces Tepe (39700-22700) and west of Kurucay Dere (39000-22400) (appendix-1).

3.9. LORASDAGI FORMATION

This formation consists of grey recrystallized fossiliferous limestones named by Goger et al (1969). According to Eren (1993), the following fossils were identified Trocholina cf. alpina (LEUPOLD) which indicates a Jurassic-lower Cretaceous age. Exsposures occur on Aydalcatagi Tepe (30000-19000), Somakli Tepe (27200-21900) and Uyuz tepe (27600-19700) (appendix-1).

The formation is overlain by the Osmankayasi Tepe Formation with unconformity (table,1).

3.10. OSMANKAYASI TEPE FORMATION

This pale marly limestone is richly fossiliferous and named from Osmankayasi Tepe in this study. Exposures also occur on Osmankayasi Tepe (40800-11900) and Ogudunkafa Tepe(37300-12300) (appendix-1).

It unconformably overlies the Esiragili Formation and is unconformably overlain by the Toprakli Formation (table,1). In this study the following fossils were determined ; Cymnocodium, Lithophyllum, Litttomnium and Cymopolla which indicate a Upper Miocene-Pliocene age. The formation is probabably lacustrine in origin.

3.11. DACITE

Dacite lavas and agglomerates sometimes with cooling joints, were erupted to form volcanic domes. Dacite occurs in the vicinity of Asarkale Tepe (37700-14700) (appendix-1). The rock contains phenocrysts of feldspar, hornblende, biotite and quartz. The Osmankayasi Tepe Formation underlies the dacite unconformably on Yaziyeri. It is younger than Upper Miocene.

3.12.TOPRAKLI FORMATION

The lithology comprises mainly marls and marly limestones with clays, tuff, sandstone, pebbles and conglomerate. Eren (1993) named the formation.

The formation overlies the other formations unconformably and is generally horizontal. The facies have terrestrial and lacustrine characteristics.

It overlies the Osmankayasi Tepe Formation (table,1) and it is probably Plio-Quaternary in age.

3.13 ALLUVIUM

The lithology comprises mainly gravel, sand and clay along streams.

IV - STRUCTURAL GEOLOGY

Except for the Quaternary rocks all the older units have been complexly deformed in the Hercynian and Alpine orogenic movements. The Cenozoic rocks are only affected by low N-S compression.

The term schistosity describes a planar, penetrative fabric of metamorphic origin, also referred to as slaty cleavage. Original bedding or compositional layering is referred to as S_0.

In the study area three phases of deformation have been recognized (D_1-D_3). The first deformation event was synchronous or just before the regional metamorphism that affected the whole area. The strike of S_1 is dominantly NNW-SSE but due to later movements it can be NE-SW (appendix-1). In general, the mesoscopic F_1 folds recognized are sharp and the flattened limbs are often sheared-out parallel and into the regional S_1. The F1 folds often display "S" and "Z" shapes, and they are both symmetrical and asymmetrical (Plate, 2). The second and third phases of deformation (D_2, D_3) represent post-metamorphic episodes and developed type 3 and type 2 refolded folds, crenulation cleavages (S_2, S_3), kink bands and lineation (Plate 1, 2, 3).

D1 Deformation

The structures formed during the first phase of deformation are widespread in the area. This deformation is responsible for the development of major F_1 folds (appendix-1) and they are the earliest folding about NNW-SSE striking axial planes (appendix-1) .

The early cleavage (S_1) development depends on the lithology of the rock in which it develops and also on the intensity of the deformation. This S_1 cleavage is strongly developed in the schist and pelite and clearly seen in the field (plate, 1, 2)

The mineral lineation is generally very poorly or weakly developed. However, L_1 lineations are strongly developed on calc schist and limestone surfaces (plate, 5)

The main faults are NNW-SSE and both strike slip, and dip slip faults have been recognized (appendix, 1).

D_2 Deformation

The D_2 structures are most evident in the schist and pelite. This deformation produces a strong crenulation cleavage (S_2). However there are a few localities where the S_2 fabric can be seen in the field (plate 1, 2).

Evidence from field studies indicates that there are major F_2 folds in the studied area with ENE-WSW striking axial planes (appendix- 1).

The L_2 lineations in the area are mainly developed in the marble and calc schist (plate, 5).

SSW-NNE faults and strike slip faults have been recognized (appendix-1).

D3 Deformation

This deformation produces warps to open upright folds (plate 6) and kink bands structures are found in pelite and schist (plate, 3). As (S_3) Fabric has been observed in the area (plate, 1).

Joints

Joints are very prominently developed in the present area. More than one set of joints have been recognized. The most common joints are oblique extension joints (plate 4, 5), some are filled with limonitic material.

Veins

Numerous quartz and calcite veins can be seen in the present area. Some of them are 0-3 m. and they follow the deformation directions. Metadolerite and metahornblende gabbro veins are developed in a N50-70W direction (appendix-1).

MICROSTRUCTURE

Microstructures observed in thin sections reveal two regional metamorphic events, outlasting three phases of deformation. The microstructures observed during the first metamorphic event (M_1) are regarded as being syntectonic to D_1. The second metamorphic event (M_2) was post-tectonic (post-D_2). The third phase of deformation has no major imprint on a micro-scale,being post-metamorphic.

1-Microstructural Characteristics of the First Metamorphic Event (M_1).

a) Microstructure of sheet slicates;

Well preserved S_1 schistosity is well developed in the more micaceous layers where the foliation is defined by a compositional layering, clearly distinguishable in hand specimen. These compositional layers consist mainly of sheet silicates.

The first phase of deformation produced tight isoclinal folds with an axial-planar foliation. Microscopic F_1 folds have been observed (see Plate 7). A second phase of deformation (D_2) is recognized in the folded S1 foliation forming the F_2 folds.

b) Chloritoid microstructure

Skeletal chloritoid has been observed in a few rock specimens, chloritoids found in some rocks show evidence of syntectonic rotation and deformation, with wrapping of the foliation around the porphyroblasts (Plate, 8), indicating a possible early syn-D_1 origin. In more micaceous rocks the sheet-silicate foliation (S_1) bends or wraps around deformed chloritoids, with a sheath of chlorite flakes in the pressure shadows along the foliation.

The foliation of the rock is marked by parallel needle-like chlorite and some muscovite flakes (Plate 8). Also post-tectonic chloritoid rosettes enclosing a relict foliation exist (Plate 10).

c) Amphiboles in the pelitic schists;

Large, actinolites occur in the pelitic schists. Due to syntectonic ductile shearing the amphiboles sometimes develop into needle-like grains with a preferred orientation, marking the foliation (Plate 9).

Comment:

The regional M_1 metamorphic event produced the distinct S_1 foliation that can be recognized throughout the mapped area. The most important minerals, i.e. muscovite, chloritoid, actinolite crystallized and grew during this event.

Before the onset of the second metamorphic event; the second phase of deformation locally crenulated the S_1 foliation to form a S_2 crenulation foliation (Plate 7).

2. Microstructural characteristics of the second metamorphic event (M_2)

The sheet-silicate fabric

In the study area, the early S_1 foliation in some micaceous quartzites and schists is folded or crenulated on a microscale to form a crenulation foliation (S_2).

Recrystallization of muscovite in the hinge zones of the S_2 crenulation foliation and around large mica "fish" (see plate 7), coincides with the M_2 metamorphic event. The mica initially recrystallized as small, flakes but the size of the M_2 recrystallized muscovite is variable, usually a few microns and the muscovite grains are weakly orientated (Plate 7).

3. Microstructures of the third metamorphic event

The third metamorphic event can be distinguished as a retrograde event, with pseudomorphic replacement of chloritoid, plagioclase, pyroxene, amphibole and biotite porphyroblasts. Chloritoid rims and cracks alter to chlorite. Biotite breaks down to Fe-rich chlorite. Ca-plagioclase has been transformed to Na-plagioclase. Hornblende is replaced by riebeckite, crossite, winchite and actinolite and actinolite often shows partial replacement by winchite and riebeckite. Augite and salite were replaced by sodic amphibole and actinolite. Epidote grains often overgrow sheet silicates and feldspar. Epidotes occur in many rocks and it is often impossible to determine whether they are early minerals or secondary alteration products.

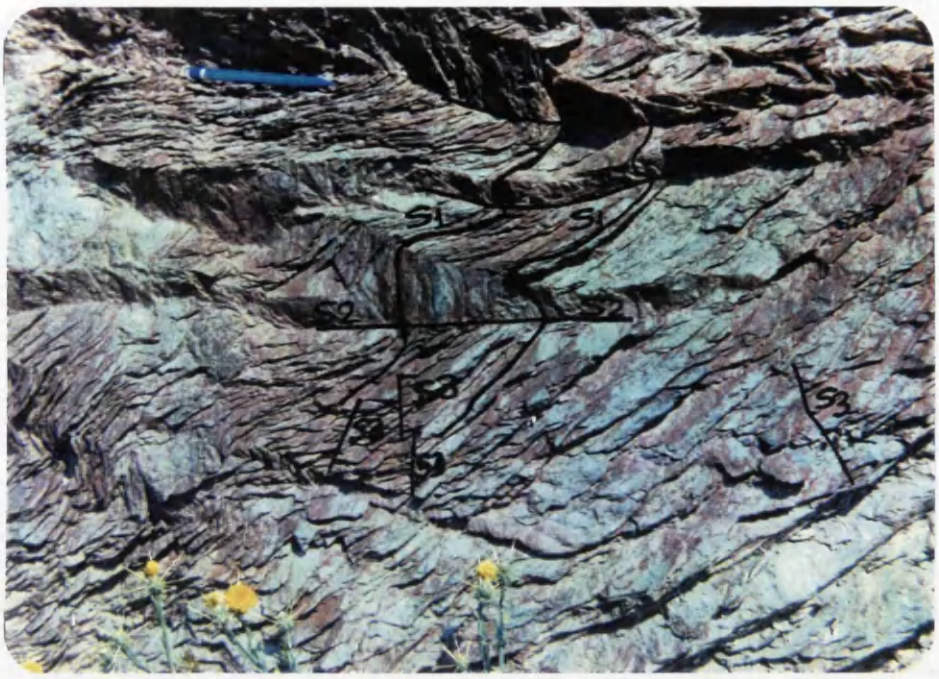

Plate.1. The mesoscopic F_1 folds recognized are isoclinal and recumbent. The hinge zones are sharp and the flattened. Limbs are often sheared-out parallel to the regional S_1. The second and third phases of deformation (D_2,D_3) represent post-metamorphic episodes and developed type 3 and type 1 refolded folds, crenulation cleavage (S_2, S_3). South of the Sogutozu (27550-25950), Bagrikurt formation.

Plate.2. S_1 schistosity folded by D_2. Successive stages in a symmetrical folding. South of Kartal Tepe (24250-22650), Bagrikurt Formation.

Plate .3. Conjugate kink folds in laminated pelitic rocks.
Ketele Dere (35750-20100), Bagrikurt Formation.

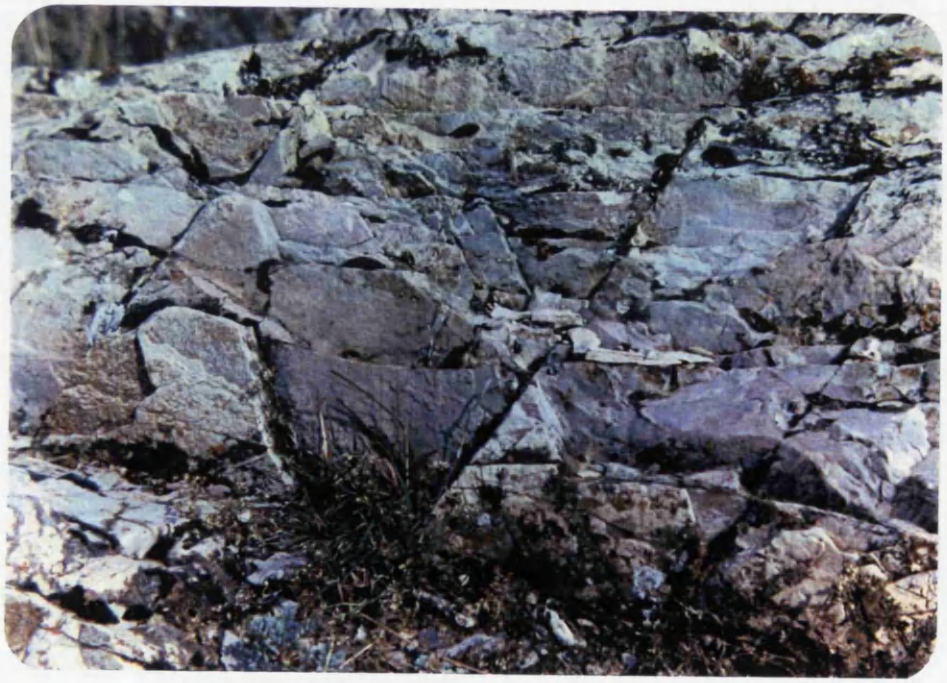

Plate. 4. Systematic and non-systematic joints .
South of Sivri Tepe (27400-28350), Kursunlu Formation.

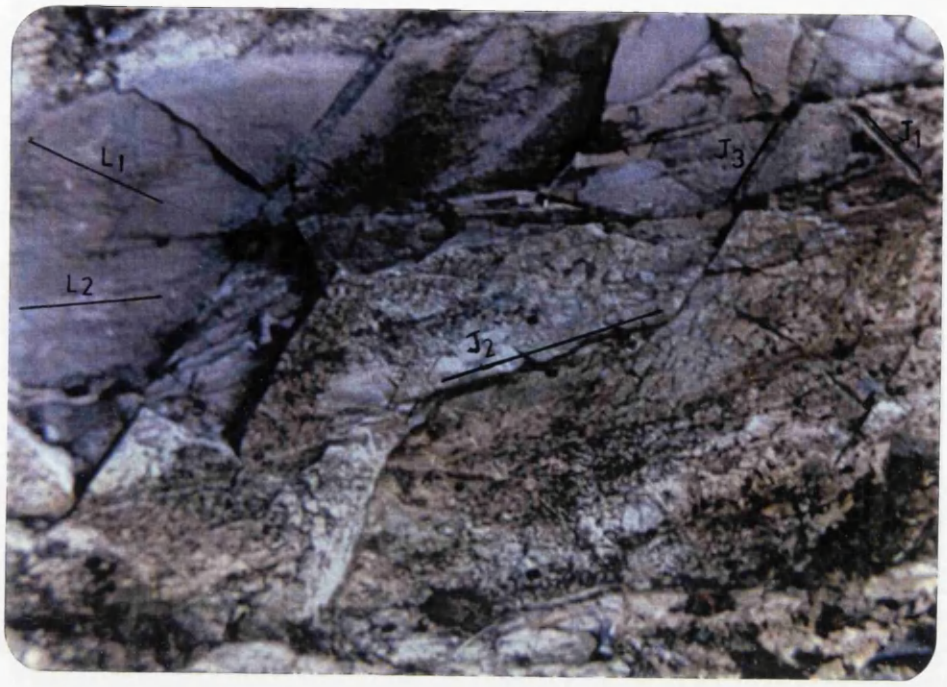

Plate 5. Joints and lineation on marble.
South of Sivri Tepe (27450-28500), Bagrikurt Formation

Plate. 6. D3 upright plunging folds in Esiragil Formation carbonate.
Ketele Dere (35800-19500), Esiragil Formation.

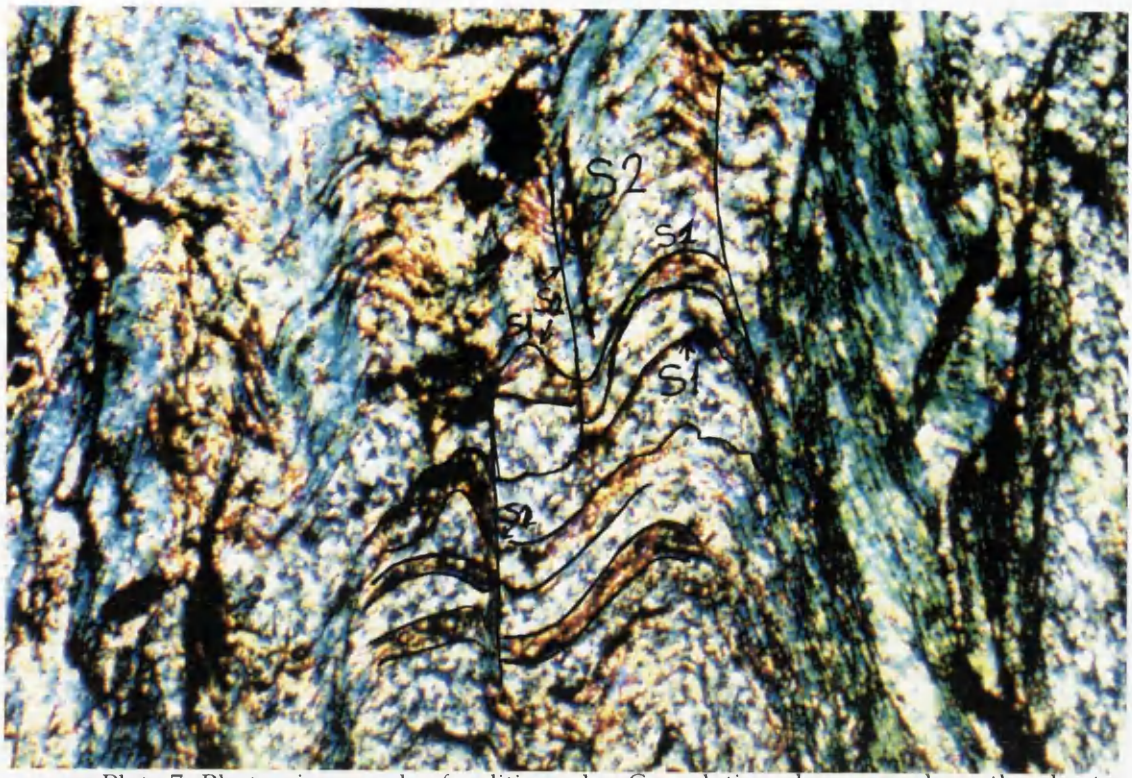

Plate.7. Photomicrograph of pelitic rocks. Crenulation cleavages along the short limbs of symmetric microfolds in a schist fabric. The early S_1 foliation in micaschist is folded or crenulated by S_2. [Crossed Nicol] x 2.5. Sample 289, Locality (37675-18250), Bagrikurt Formation.

Plate.8. Photomicrograph of pelitic rocks. S_1 distorted around a chloritoid porphyroblast. [Crossed Nicol] X 2.5. Sample 429, Locality (35050-33375), Bagrikurt Formation.

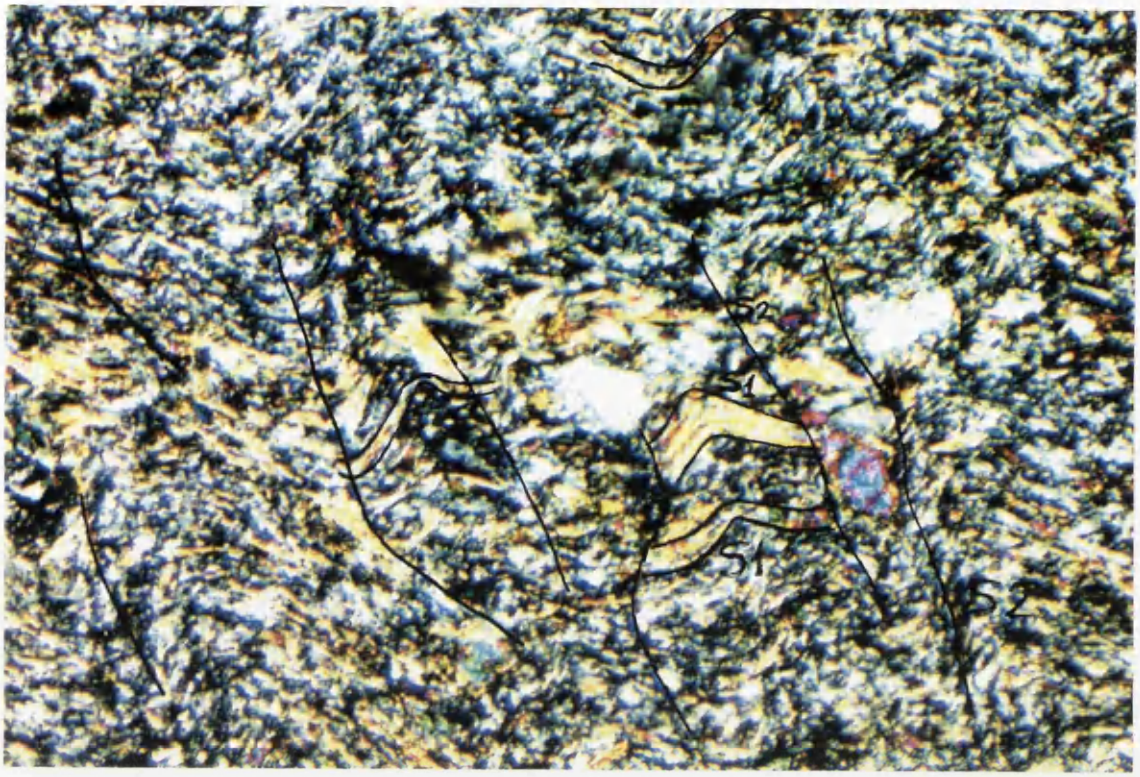

Plate.9. Photomicrograph from quartz-albite- epidote-actinolite schist. Needle-like actinolite grains with a preferred orientation, marks the foliation S_1. [Crossed Nicol] X 2.5. Sample 62, Locality (33250-22600), Bagrikurt Formation.

V - PETROGRAPHY AND MINERAL CHEMISTRY

From about 600 samples collected during mapping about 200 thin sections were examined and representative rocks were studied with the electron microprobe

5.1. ESIRAGIL FORMATION

CHLORITE-CALC SCHIST

The schist is composed of 50-60% calcite, 15-25% quartz, 5-10% chlorite, 3-5% muscovite, and accessory magnetite, all in a schistose texture with a preferred grain shape orientation. Relict quartz grains commonly have well developed deformation features, including deformation bands, undulose extinction,and deformation lamellae, subgrains and sutured grain boundaries. Quartz also forms fibrous fringes, commonly in association with fibrous chlorite, indicating that solution transfer processes operated during deformation (Ramsay&Huber 1983). Twinned calcite and deformation banding in calcite is common.

PHYLLITES

These rocks are composed of 45-56% quartz, 30-35 % sericite, 5-8% chlorite, 3-6% opaque minerals and accessory tourmaline, in a fine-grained schistose texture.

A very high degree of orientation is characteristic, with an elongation of fine-grained (0.2-0.3 mm) quartz and sericite as thin lenses, and with sericite and chlorite in parallel foliation. The growth of the quartz grains has been retarded by the presence of numerous small mica flakes. Grain boundaries are slightly curved or straight. Undulose extinction is very common. Mica flakes are less than one mm in length, exhibiting a preferred orientation. The chlorite grains are generally less than 0.3 mm in diameter, and are intergrown with the white mica. Some grains reach 10mm in diameter. Irregular crenulations occur.

CALC- SCHISTS

These schists have bands of fine-grained calcite, dolomite and fine-grained (1-2mm) quartz, micas and hematite which are probably relict bedding. Deformation twinning is conspicuous in much of the coarse calcite. The grain size distribution is unimodal. The calcite grain boundaries are sutured and the quartz porphyroblasts have undulose extinction, are fragmented and set in a secondary calcite cement. There are also calcite inclusions within the quartz grains. The rocks show sheety and laminated zones.

QUARTZ -BEARING MARBLES

These consist of 50-70% calcite-dolomite, 20-40% quartz, accessory ankerite and an Fe-oxide in a cataclastic texture. In strongly altered rocks close to mineralization, ferroan dolomite and ankerite occur (table 2). The texture is dominated largely by the individual dolomite grains, which show a strong elongation in the plane of foliation and characteristically have irregular and interlocking boundaries. The larger porphyroblasts (4mm) show strain, and extremely fine-grained dolomite is found interstitial to the larger grains. Ankerites are fine to medium grained. Fractures have developed within coarse calcite and quartz crystals and all fractures have been filled by microcrystalline calcite. Some coarse calcite crystals show deformation twinning and inclusion trails.

Table 2. Composition of dolomite and ankerite minerals.

Sam. No	460 Dolomite	460 Dolomite	460 Dolomite	460 Dolomite	460 Ankerite	460 Ankerite
SiO_2	0.09	0.09	0.07	0.05	0.69	0.60
TiO_2	0.06	0.01	0.02	0.00	0.05	0.04
FeO*	0.30	0.40	0.39	0.26	12.87	12.86
MgO	21.44	20.91	21.25	21.04	17.36	17.36
CaO	30.39	29.69	30.20	31.18	24.95	24.93
Na_2O	0.21	0.19	0.08	0.00	0.19	0.19
K_2O	0.03	0.01	0.02	0.02	0.03	0.03
Total	52.52	51.3	52.03	52.55	56.14	56.01
	Formula on the basis of 6 Oxygens					
Si	0.00	0.00	0.00	0.00	0.02	0.02
Ti	0.00	0.00	0.00	0.00	0.00	0.00
Fe	0.01	0.01	0.01	0.01	0.34	0.34
Mg	0.95	0.96	0.95	0.96	0.81	0.86
Ca	1.03	1.02	1.03	1.03	0.82	0.77
Na	0.01	0.01	0.01	0.00	0.01	0.01
K	0.00	0.00	0.00	0.00	0.00	0.00
Total	2.00	2.00	2.00	2.00	2.00	2.00

LITHIC ARENITES

These consist of 60-80 % quartz, 3-4% muscovite, and 5-15% of groundmass which comprises calcite, sericite, chlorite, ilmenite, hematite and accessory tourmaline and zircon in a lepidoblastic texture.

Angular to sub-rounded quartz is set in a fine-grained matrix, which consists of fine quartz grains, chlorite, calcite and sericite. Quartz grains are dimensionally elongated and crystallographically strongly orientated. The mica flakes (up to 0.4mm) are, in general, oriented parallel to the bedding but small laths may occur as inclusions in quartz grains. The carbonate cement includes iron-bearing types showing faint brownish oxidation streaks. Calcite is replaced by euhedral secondary quartz, and secondary calcite forms fine anhedral grains.

5.2.BAGRIKURT FORMATION

PHYLLITES

These contain 30% sericite, 25-30 % quartz, 5-10 % calcite, 3-5% chlorite, 3-5% chloritoid, 3-5% muscovite, 3-5% hematite and ilmenite in a fine-grained texture.

The matrix has equidimensional grains, and a fine layering which is predominantly parallel to the cleavage.

The cleavage wraps around the chloritoid and chlorite porphyroblasts sigmoidaly and the ends of the porphyroblasts are rounded in contact with the cleavage (Plate 7). Inclusions of quartz and sericite are common in all the porphyroblasts. There are post-tectonic muscovites later than the schistosity, which are undeformed and perpendicular to the schistosity. The syntectonic and coarse anhedral calcite crystals are wrapped around by the foliation. The magnetite occurs as dendritic grains.

QUARTZITES

These consist of 80-90% quartz, 3-5% sericite, chlorite, 3-5% albite, K-felspar, tourmaline, zircon, magnetite, hematite with Fe-oxides in a granoblastic texture.

The polygonal-granoblastic quartz grains are generally small, (0.4-0.6 mm in diameter) with slightly curved grain boundaries and have weak undulose extinction.

Fine sericite and greenish chlorite flakes, (0.4mm) have a preferred orientation. Small, recrystallized muscovite flakes in the quartzites are common. Smaller flakes are sometimes enclosed in quartz grains, often displaying rounded ends in the quartz.

METACHERT

This dominantly consists of fine-grained quartz with cryptocrystalline and microcrystalline quartz, radiolaria, calcite, hematite, graphite and limonite.

The size of the grains is very uniform and so fine-qrained that the texture is effectively cryptocrystalline with crystallized areas of secondary quartz. The quartz is dominantly in veins . The groundmass is essentially made up of quartz and carbonate. In some assemblages quartz veinlets are noted inside fractured granules.

A radial texture occurs in some specimens due to pigmentation of limonite in the core of granoblastic quartz. In the outer zone, a concentric texture occurs due to alternating zones or rings of iron-oxide pigments.

SUBLITHARENITE

These consist of 60-75% quartz 15 % calcite 5 % muscovite and 15% groundmass, in which are calcite, sericite, chlorite, quartz and accessory zircon, ilmenite, hematite and Fe-oxides in a lepidoblastic texture.

Original quartz grains have been recrystallized to produce a granoblastic -polygonal texture, with an average grain size of 0.4 mm. Mica is small (0.2mm) and grows on quartz grain boundaries disseminated through the rock, exhibiting a preferred grain growth orientation. The coarse calcite shows twinning and elongated grain shapes.

BLOCK LIMESTONE

These are rich in white, grey and cream calcite, and show bedding with a granoblastic to schistose texture with late fractures and deformation twinning in the calcite. Magnetite also occurs in the rocks.

CHLORITE- MUSCOVITE SCHISTS

These comprise 40-50% muscovite, 25-30% quartz, 5-10% chlorite, 5-10% magnetite, hematite and accessory tourmaline.

The muscovite, quartz and chlorite may have all crystallized syntectonically. Crenulation cleavage has developed in the fine grained rocks.

There are micaceous-rich zones, corresponding to crenulation cleavages along alternate limbs of symmetric microfolds in a differentiated S_1 layering fabric. The S_1 fabric trends are overprinted by an S_2 crenulation cleavage. Irregular shaped masses of quartz in the hinges of micaceous layers (Plate. 7) have been recrystallised in the fold hinges.

CHLORITE-MUSCOVITE-CHLORITOID SCHISTS

These contain 35-47% chloritoid, 20-30% quartz, 5-20% muscovite, 3-5% chlorite, 3-5% tourmaline, albite and hematite, ilmenite and rutile.

Muscovite, chlorite and quartz porphyroblasts have different orientations and overprint an earlier stage of fabric development. Some chlorites are aligned parallel to the schistosity.

Muscovite is present in five of the analysed specimens (Table 3). A paragonite component of between 3.9 and 12.55 mol % has been determined by microprobe.

Chloritoid grains, 2-3mm long, show pale green (β) to blue green (γ) pleochroism. Some chloritoid crystals occur as rosette-like clusters (Plate, 10). They show post-crystalline deformation. No aluminium silicates such as kaolinite or pyrophyllite occur with chloritoid.

Present techniques do not allow routine distinction of Fe^{+2} and Fe^{+3}, hence for most cases, total Fe is used as Fe^{+2} in chloritoid, because usually Fe^{+3} is low in chloritoid (Deer et al. 1982).

The analyzed chloritoids (Table,4) from Kadinhani are characterized by low Mg. Chloritoid from carbonate free samples (237) is much more magnesian (Fe/Mg = 8.96-9.55) than that from carbonate bearing sample (44). Chloritoid is characteristically high in Al_2O_3 and has (Fe/Mg) ratios above 0.6. Ti and Mn are present in very low, but extremely variable amounts within individual crystals.

Tourmaline is present as irregular shaped crystals in the plane of foliation. The colour is pale yellow-brown to brownish. Tourmaline was analyzed by electron microprobe in two samples. Significant compositional variation occurs for FeO, MgO, and CaO. Changes in SiO_2 and Al_2O_3 and small TiO_2 variations are, with one exception, also small. Representative microprobe analyses of tourmaline are given in Table 5.

Magnetite and rutile are the dominant Fe-Ti oxide minerals. Rutile contains >98 % TiO_2, approximately 0.5% FeO, and minor amounts of Si and Al (Table 6).

Quartz occurs as fine-grained and porphyroblastic crystals. Polycrystalline quartz porphyroblasts are surrounded by a fine-grained matrix of quartz, chlorite and muscovite. Plagioclase porphyroblasts have albite twinning and are $An_{0.5\text{-}1.1}$ (Table 7).

Table 3. Composition of muscovite

Sample No	239	306	134	134	191
SiO_2	48.00	46.00	46.41	46.25	45.84
TiO_2	0.17	0.19	0.64	0.80	0.20
Al_2O_3	35.55	30.90	30.36	30.50	34.41
Fe_2O_3	1.53	3.28	2.09	2.32	1.51
FeO	0.24	0.52	0.33	0.36	0.24
MnO	0.05	0.07	0.00	0.01	0.00
MgO	0.00	1.85	2.20	2.24	0.84
CaO	0.00	0.05	0.02	0.03	0.00
Na_2O	1.00	0.70	0.60	0.29	0.80
K_2O	9.47	9.77	10.57	10.43	9.55
TOTAL	96.01	93.03	93.22	93.23	93.39
Recalculated to 22 Oxygens					
Si	6.21	6.25	6.34	6.32	6.40
Ti	0.01	0.02	0.06	0.08	0.00
Al^{+6}	1.78	1.74	1.65	1.67	1.59
Al^{+4}	3.64	3.12	3.24	3.23	3.21
Fe^{+3}	0.15	0.34	0.21	0.23	0.40
Fe^{+2}	0.02	0.06	0.03	0.04	0.07
Mn	0.00	0.00	0.00	0.00	0.00
Mg	0.19	0.38	0.44	0.45	0.30
Ca	0.00	0.00	0.00	0.00	0.00
Na	0.25	0.18	0.15	0.07	0.16
K	1.56	1.55	1.84	1.81	1.74
Total Cat.	13.81	13.64	13.96	13.90	13.87
End member of the muscovite minerals					
Muscovite	78.25	77.80	91.87	90.95	87.05
Paragonite	12.55	9.45	7.92	3.90	8.15

Fe^{+3} is calculated by ratio according to Schumacher (1991)

Table 4. Composition of chloritoids

Samp.N	44	44	237	237	237	237	237
SiO_2	24.95	23.28	24.43	25.94	24.01	24.98	24.44
TiO_2	0.96	0.29	0.47	0.18	0.54	0.86	0.12
Al_2O_5	37.17	38.74	39.77	39.60	39.43	39.59	39.94
FeO*	26.03	26.41	23.52	22.11	25.44	24.41	24.22
MnO	0.20	0.13	0.17	0.24	0.22	0.17	0.17
MgO	1.53	1.65	2.47	2.80	1.99	2.43	2.35
CaO	0.06	0.37	0.03	0.00	0.00	0.01	0.00
Na_2O	0.04	0.00	0.00	0.00	0.00	0.00	0.00
K_2O	0.03	0.00	0.01	0.07	0.01	0.00	0.00
TOTAL	91.97	90.87	90.87	90.94	91.64	92.45	91.24
Recalculated to 12 Oxygens							
Si	2.11	1.98	2.04	2.14	2.02	2.07	2.04
Ti	0.06	0.01	0.03	0.00	0.00	0.00	0.00
Al	3.71	3.89	3.91	3.86	3.91	3.87	3.93
Fe	1.84	1.88	1.64	1.53	1.79	1.69	1.69
Mn	0.01	0.13	0.01	0.01	0.01	0.01	0.01
Mg	0.19	0.21	0.30	0.34	0.35	0.30	0.29
Ca	0.00	0.00	0.00	0.00	0.00	0.00	0.00
Na	0.00	0.00	0.00	0.00	0.00	0.00	0.00
K	0.00	0.00	0.00	0.00	0.00	0.00	0.00
Total Cat.	7.92	8.01	7.93	7.88	8.08	7.94	7.96

Total Fe as FeO*

Table 5. Composition of tourmalines

Sample No	244	244	244	244	244
SiO_2	34.69	34.77	34.54	35.18	35.62
TiO_2	1.64	1.38	1.71	0.77	1.40
Al_2O_3	32.62	32.54	32.48	32.28	32.38
FeO*	11.23	10.61	11.12	7.86	6.98
MnO	0.03	0.05	0.05	0.01	0.07
MgO	4.74	4.95	5.13	8.54	8.45
CaO	0.84	0.66	0.77	0.68	0.40
Na_2O	1.05	1.17	1.06	1.59	1.39
K_2O	0.09	0.04	0.03	0.06	0.03
TOTAL	86.93	86.17	86.89	86.97	86.72
Recalculated to 31 Oxygens					
Si	5.87	5.9	5.85	5.95	5.99
Ti	0.23	0.19	0.24	0.10	0.18
Al	7.05	7.02	6.99	6.79	6.89
Fe	1.75	1.66	1.73	1.15	1.00
Mn	0.00	0.00	0.00	0.00	0.00
Mg	1.32	1.38	1.42	2.23	2.13
Ca	0.16	0.13	0.15	0.13	0.25
Na	0.39	0.40	0.39	0.50	0.45
K	0.02	0.01	0.00	0.00	0.00
Total Cat.	16.79	16.69	16.77	16.85	16.89
Total Fe as FeO*					

Table 6. Composition of rutiles

Sample No	244	244	244
SiO_2	0.30	0.24	1.23
TiO_2	98.47	99.08	97.94
Al_2O_3	0.04	0.02	0.21
FeO*	0.40	0.46	0.68
MnO	0.00	0.01	0.00
MgO	0.00	0.00	0.09
CaO	0.12	0.00	0.00
Na_2O	0.08	0.01	0.02
TOTAL	99.11	99.82	100.17

Table 7. Composition of plagioclases

Sample No	320	320	320	320	320
SiO_2	68.00	67.85	67.15	68.09	67.33
TiO_2	0.00	0.00	0.15	0.1	0.03
Al_2O_3	20.22	20.41	20.79	20.90	20.49
FeO*	0.44	0.61	0.60	0.04	0.03
MnO	0.05	0.07	0.05	0.02	0.07
MgO	0.42	0.44	0.70	0..69	0.60
CaO	0.11	0.18	0.17	0.23	0.13
Na_2O	10.86	10.49	9.72	10.68	10.72
K_2O	0.68	0.67	0.79	0.94	0.86
TOTAL	100.78	100.72	100.12	101.69	100.26
Recalculated to 32 oxygens					
Si	11.8	11.78	11.72	11.75	11.73
Ti	0.00	0.00	0.00	0.00	0.00
Al	4.12	4.18	4.28	4.24	4.21
Fe	0.06	0.01	0.08	0.00	0.00
Mn	0.00	0.00	0.00	0.00	0.00
Mg	0.10	0.01	0.01	0.01	0.15
Ca	0.02	0.03	0.02	0.04	0.00
Na	3.64	3.53	3.29	3.57	3.62
K	0.15	0.14	0.17	0.20	0.19
Total Cat.	19.89	19.68	19.56	19.81	19.90
End member of the plagioclase minerals as below					
An	0.50	0.80	0.80	1.10	0.60
Ab	95.60	95.5	94.80	93.70	94.60
Or	3.80	3.70	4.40	5..20	4.80

FeO* is total iron as FeO.

CALCITE- EPIDOTE BEARING SCHISTS

These schists consist of 40-50% epidote, 25-30% calcite, 15-20% quartz, 5-10% chlorite, 5-10% sericite, 3-5% albite, 3-5% amphibole, and accessory apatite, hematite and magnetite, in a schistose texture. They are fine grained, strongly foliated and lineated schists, dominated by epidote and calcite. The epidote occurs as aggregates of spongy crystals. The amphibole is mostly deep green winchite often showing patchy replacement by magnesian riebeckite. Most of the rock is composed of a fine-grained groundmass of mafic minerals containing thin bands, rich in quartz and albite. The foliation is crenulated.

Representative microprobe analyses of epidote are given in Table 8.

Table 8. Composition of Epidotes

Sam.N	289	289	41	41	281	281	456cor	456ri
SiO_2	36.40	36.00	36.59	36.00	36.20	36.20	36.30	36.89
TiO_2	0.07	0.02	0.19	0.08	0.04	0.08	0.18	0.17
Al_2O_3	22.50	22.65	23.44	23.00	23.78	23.85	23.95	23.17
Fe_2O_3	15.27	15.80	14.49	14.54	14.92	14.94	15.27	14.57
FeO	0.67	0.61	0.54	0.64	0.70	0.66	0.77	0.69
MnO	0.06	0.21	0.25	0.22	0.27	0.18	0.27	0.39
MgO	0.36	0.21	0.20	0.12	0.06	0.00	0.07	0.17
CaO	23.27	23.70	22.53	23.67	22.60	22.49	22.21	22.70
Na_2O	0.05	0.08	0.00	0.05	0.16	0.05	0.00	0.12
TOTAL	98.65	99.05	98.23	98.32	98.73	98.45	99.02	98.87
	Recalculated to 25 Oxygen							
Si	6.19	6.17	6.14	6.23	6.29	6.25	5.85	5.93
Ti	0.00	0.00	0.02	0.01	0.00	0.01	0.02	0.02
Al	4.31	4.48	4.64	4.36	4.14	4.32	4.17	4.20
Fe^{+3}	1.76	1.59	1.41	1.66	1.83	1.70	1.97	1.76
Fe^{+2}	0.09	0.08	0.07	0.08	0.09	0.09	0.10	0.09
Mn	0.09	0.03	0.03	0.02	0.03	0.02	0.03	0.05
Mg	0.09	0.05	0.05	0.02	0.01	0.00	0.01	0.04
Ca	4.06	4.08	4.05	4.09	4.09	4.04	3.83	3.91
Na	0.01	0.02	0.00	0.01	0.05	0.01	0.00	0.03
Total Cat	16.51	16.50	16.41	16.46	16.53	16.44	15.98	16.03
Pistasite	28.99	26.19	23.3	27.57	30.65	28.23	32.08	29.53

$Fe^{+3}$is calculated by ratio according to Schumacher (1991).

ALBITE- CHLORITE- AMPHIBOLE- EPIDOTE SCHISTS

These consist of 25-30%epidote, 20-25% amphibole, 15-18% quartz, 15-17% chlorite, 5-10% albite and accessory magnetite, sphene and apatite. This is a medium grained, strongly foliated schist dominated by epidote and green amphibole, with minor winchite and magnesian riebeckite.

Epidote occurs most commonly as porphyroblasts (0.05mm). It is pleochroic from pale yellow to colourless.

Fine-grained green chlorite is ubiquitous and representative microprobe analyses of epidote are given in table 9. Using the nomenclature of Hey (1954) the chlorite is pycnochlorite (Figure 2).

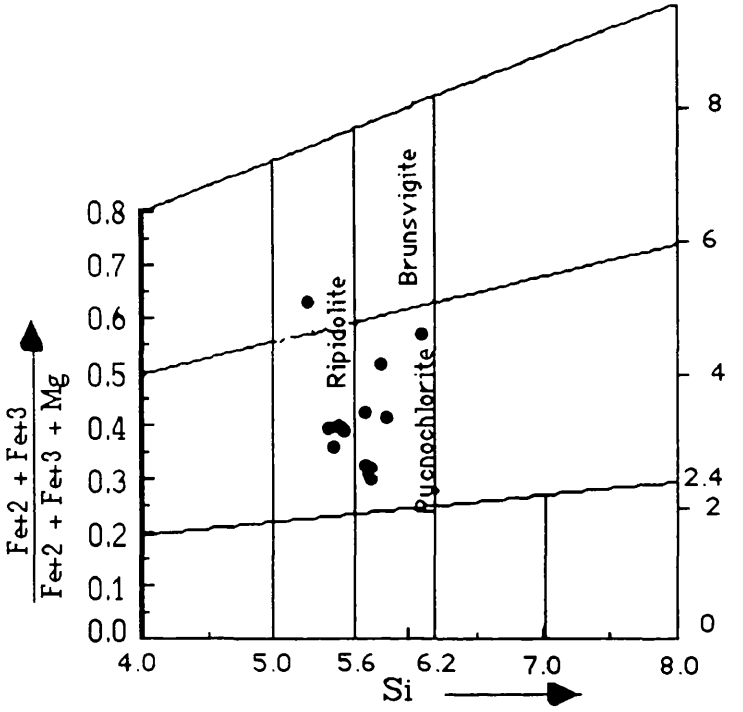

Figure 2. Chemical composition of chlorites plotted on Hey's (1954) diagram.

Amphiboles (Table 10) occur as tiny green needles, rarely 0,5-2mm long. According to the classification of Leake (1978), the amphiboles are actinolites, magnesio-riebeckite, magnesio-hornblende and winchite (Figure 3). The green magnesian hornblende and actinolite often show partial replacement by winchite and magnesian riebeckite.

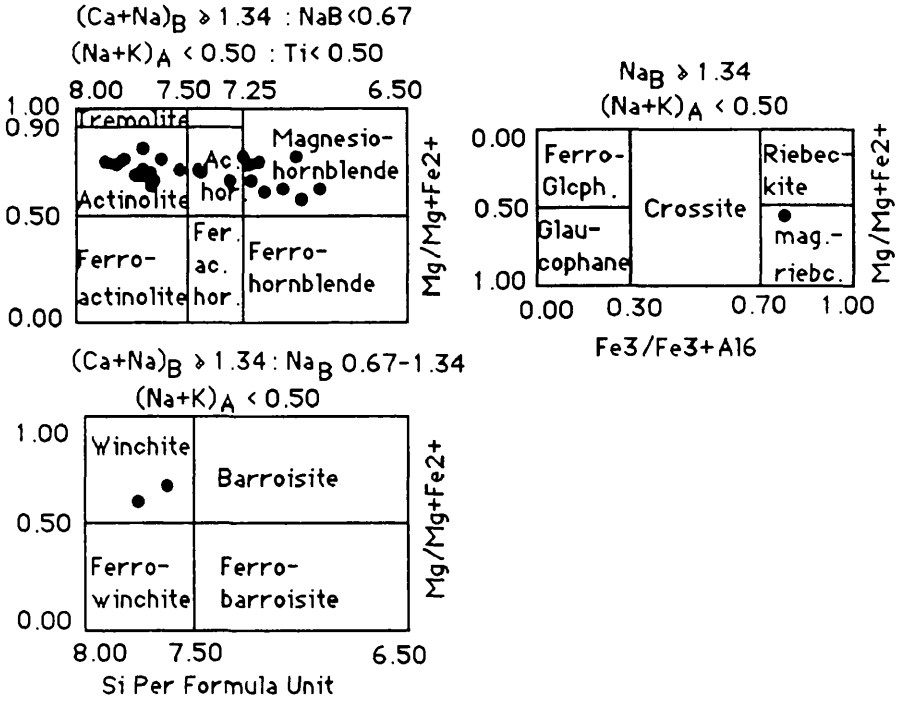

Figure 3. Classification of amphiboles (after Leake, 1978; Hawthorne, 1981).

The albite has lamellar twinning . The most common type is a simple twin composed of two individuals. It is generally fairly clear and of very fine grain size.

Magnetite ranges from fine to coarse grained. It also occurs in strongly recrystallized assemblages which show the relict outline of magnetite granules. Many of the magnetites are oxidized to euhedral hematite. Representative analyses are given in Table 11.

Table 9. Composition of chlorites

Smp. No	320	281	281	281	281	307
SiO_2	28.79	27.90	28.30	28.00	27.60	25.90
TiO_2	0.05	0.07	0.00	0.01	0.00	0.00
Al_2O_3	19.10	18.30	19.00	18.84	18.20	19.90
Fe_2O_3	5.73	3.91	3.67	4.00	3.80	4.26
FeO	20.64	14.08	13.23	14.40	13.68	15.35
MnO	0.38	0.40	0.40	0.40	0.39	0.24
MgO	10.86	21.10	21.80	21.03	21.50	18.99
CaO	0.30	0.08	0.08	0.11	0.00	0.10
Na2O	0.08	0.09	0.07	0.02	0.16	0.06
K2O	0.19	0.00	0.00	0.00	0.00	0.00
TOTAL	86.12	85.93	86.55	86.81	85.33	84.80
Recalculated to 28 Oxygens						
Si	6.08	5.71	5.72	5.68	5.69	5.43
Ti	0.00	0.01	0.00	0.00	0.00	0.00
Al	4.76	4.42	4.52	4.50	4.42	4.92
Fe^{+3}	0.91	0.60	0.55	0.61	0.59	0.67
Fe^{+2}	3.64	2.41	2.23	2.44	2.36	2.69
Mn	0.06	0.06	0.06	0.06	0.06	0.04
Mg	3.42	6.44	6.56	6.41	6.61	5.93
Ca	0.06	0.02	0.02	0.00	0.00	0.02
Na	0.03	0.03	0.03	0.04	0.06	0.02
Total Cat.	18.96	19.70	19.69	19.74	19.79	19.70
End member of the chlorite minerals as below						
Mg-Cl	34.21	64.44	65.68	64.11	66.14	59.39
Fe-	36.49	24.13	22.37	24.44	23.62	26.94
Fe*/(Fe*+mg)	0.57	0.31	0.30	0.32	0.29	0.36

$Fe^{+3}$is Calculated by ratio according to Schumacher (1991).

Table 10. Composition of amphiboles

Sam. No	41.ac	41.ac	62.ac	62.mh	6.mrb	6.ac	456.w	456.w
SiO_2	52.49	52.38	54.55	51.70	53.98	53.60	52.76	52.72
TiO_2	0.13	0.08	0.02	0.76	0.03	0.02	0.05	0.07
Al_2O_3	3.00	3.82	3.00	6.70	2.49	1.90	4.05	4.07
FeO*	12.20	12.66	12.65	12.10	22.96	8.92	16.19	15.87
MnO	0.21	0.28	0.33	0.39	0.45	0.45	0.25	0.22
MgO	15.28	14.95	16.00	15.40	8.94	18.11	12.54	10.60
CaO	12.16	11.88	8.63	9.22	0.85	12.70	7.06	7.89
Na_2O	0.65	0.60	1.51	0.93	7.24	0.55	3.43	4.24
K_2O	0.39	0.11	0.05	0.06	0.00	0.04	0.13	0.23
TOTAL	96.51	96.76	96.74	97.77	96.94	96.29	96.25	95.91
Recalculated to 23 Oxygens								
Si	7.65	7.53	7.71	7.22	7.96	7.69	7.61	7.77
Al^{+4}	0.34	0.46	0.18	0.77	0.03	0.30	0.28	0.29
AlT	0.51	0.66	0.51	1.14	0.41	0.32	0.80	0.79
Al^{+6}	0.17	0.19	0.33	0.36	0.37	0.01	0.55	0.53
Ti	0.01	0.00	0.00	0.08	0.00	0.00	0.00	0.00
Fe^{+3}	0.09	0.22	0.16	0.30	1.27	0.17	0.30	0.00
Mg	3.32	3.26	3.48	3.33	1.89	3.87	2.69	2.24
Fe^{+2}	1.39	1.33	1.25	1.16	1.45	0.89	1.29	1.52
Mn	0.02	0.03	0.04	0.04	0.05	0.05	0.03	0.02
FMT	13.02	13.06	13.27	13.30	13.06	13.02	13.08	13.30
Ca	1.91	1.86	1.34	1.53	0.12	1.95	1.09	1.20
NaM4	0.07	0.07	0.37	0.16	1.80	0.02	0.82	0.00
NaT	0.18	0.17	0.42	0.26	1.99	0.15	0.95	1.16
NaA	0.11	0.09	0.05	0.10	0.18	0.12	0.13	0.00
K	0.072	0.021	0.01	0.011	0.00	0.008	0.02	0.04

Fe^{+3} is calculated by estimation according to Spear and Kimball (1984).

ac: actinolite mh: magnesian hornblende mrb: magnesian riebeckite

w: winchite

Table 11. Composition of magnetites

Samp. N	314	314	457	457	457
SiO_2	0.48	0.49	0.54	0.47	0.40
TiO_2	0.44	0.00	0.00	0.10	0.00
Al_2O_3	0.25	0.00	0.39	0.16	0.27
Fe_2O_3	68.38	68.46	66.58	68.65	67.15
FeO	32.26	31.38	28.72	30.73	28.9
MnO	0.18	0.00	0.10	0.06	0.04
MgO	0.11	0.0	0.38	0.07	0.25
CaO	0.07	0.06	0.08	0.05	0.09
Na2O	0.00	0.23	0.23	0.22	0.31
TOTAL	102.1 0	100.62	97.02	100.51	97.41
Recalculated to 32 Oxygens					
Si	0.08	0.06	0.02	0.02	0.02
Ti	0.01	0.00	0.00	0.00	0.00
Al	0.01	0.00	0.02	0.00	0.01
Fe3	1.85	1.92	1.96	1.98	1.99
Fe2	1.04	0.98	0.96	0.98	0.95
Mn	0.01	0.00	0.00	0.00	0.00
Mg	0.01	0.00	0.02	0.00	0.01
Ca	0.00	0.00	0.00	0.00	0.00
Na	0.00	0.04	0.02	0.02	0.02
Total Cat.	3.00	3.00	3.00	3.00	3.00

Fe+3 is calculated by cation balance according to Schumacher (1991).

End member of the minerals as below

Mg-ferrite	0.06	0.00	1.324	0.039	0.869
Magnetit	99.64	99.99	97.77	99.596	98.483

5.3. KURSUNLU FORMATION

This formation is a grey, black limestone composed of micrite cement, dolomite, biomicrite and Fe-oxide. Recrystallization has produced large sparry calcites derived from primary fossil fragments. Very small calcite grains are found mainly in the groundmass, but sometimes fill fossil cavities. The calcites often show deformation twin lamellae. Poorly developed stylolites rarely occur. Dolomite has almost obliterated the original structure of the fossils.

5.4. METATRACHYANDESITE

This rock is composed of 35-50% plagioclase, 13-17% clinopyroxene, 5-15% mica, 5-13% amphibole, 3-10% chlorite, 2-8% quartz, 0-8% calcite, 1-1.5% epidote, 0-1% pumpellyite, 5-7% sanidine, with accessory magnetite, sphene and apatite.

The original porphyritic and amygdaloidal texture of the rocks is preserved in some samples, but commonly is deformed and wrapped around by granules and prisms of epidote, pumpellyite and flakes of chlorite.

The groundmass is made of plagioclase, iron oxide, clinopyroxene, quartz, amphibole, sericite, chlorite, epidote and pumpellyite.

Generally euhedral plagioclase phenocrysts (<6mm) are normally zoned. Plagioclase phenocrysts have been totally transformed into sodic plagioclase with a composition of An_{0-2} up to Or_{0-4}. Also, plagioclases are partially replaced by epidote and sericite. Albitization is marked by a dusty appearance. Twins are generally preserved but zoning is partially destroyed. Sanidine is common in the groundmass. Analyses of plagioclase are presented in Table 12, and Figure 4.

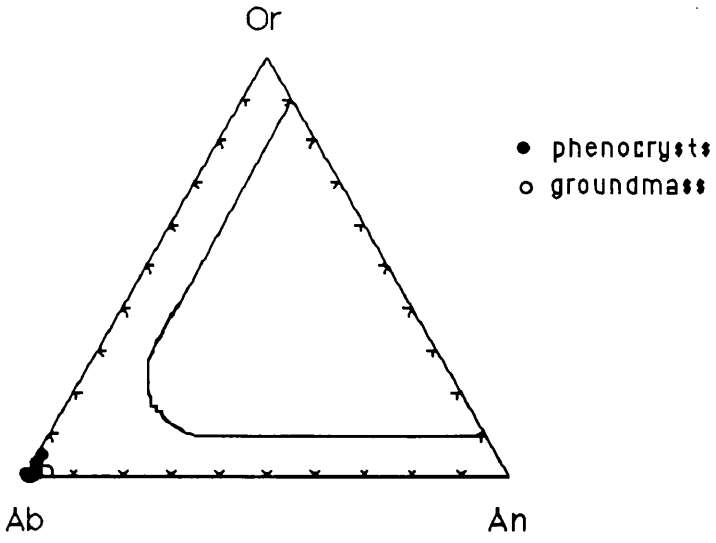

Figure 4. Albite in the metatrachyandesite.

Clinopyroxene occurs as phenocrysts (0.5-2mm) and in the groundmass. The mineral occurs as minute colourless to pale green crystals. The composition is the salite according to Poldervaart et al.(1951, figure, 5). The composition is $Wo_{45.5-47.2}$, $En_{36.7-42,4}$, $Fs_{12.2-17.6}$. High Wo contents are suggested to result from a substantial Ca-Tschermak's component (e.g, Brown, 1967: Barberi et al . 1971; Huebner, 1980). Groundmass clinopyroxenes (<0.2 mm) locally form parallel intergrowths. The analyses are characterized by relatively low TiO_2 (0.10-0.27) and low Al_2O_3 (0.99-1.48) contents. Analyses of phenocrysts are presented in Table 13.

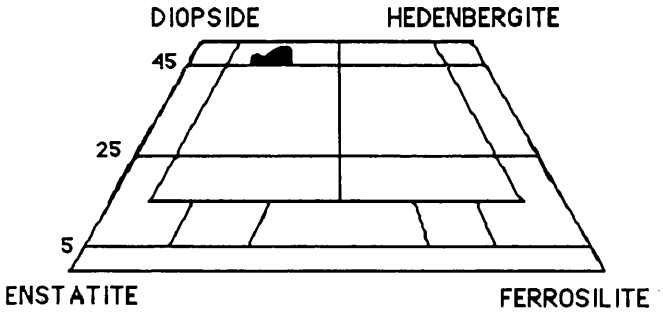

Figure 5. Composition of clinopyroxene, plotted on the diagram after Poldervaart et al. (1951).

The pyroxene compositions plotted in Figure 6. a, c indicate tholeiitic and calc-alkali character. Figure 6. b, shows that they plot in the orogenic field.

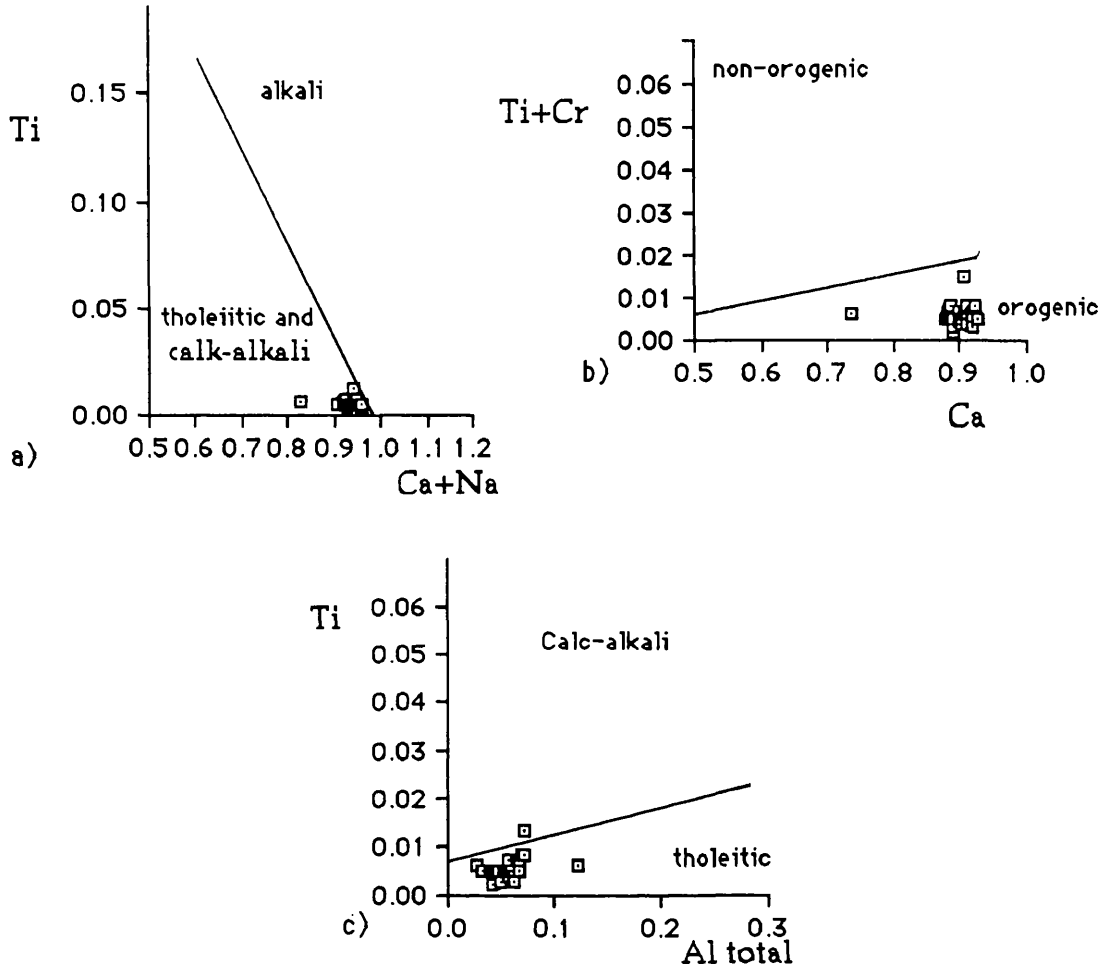

Fig. 6 a, b and c. Composional variations of pyroxene phenocrysts from the metatrachyandesite in terms of Ti, Ca, Na, Cr and Al using the discriminant diagrams of Leterrier et al. (1982).

Amphibole phenocrysts are olive-green to pale lavender blue . Actinolite is fairly abundant as tiny needles and prisms, and as bundles of pale bluish green needles. Needles are up to 0.15 mm long and prisms up to 0.5 mm long are common. Al_2O_3 values averaged are less than 1.5 percent. Most sodic amphibole commonly forms rims around the salite (Plate, 11) and is lavender blue to violet. Most riebeckites in these rocks show pleochroism which is α= blue to indigo β= yellow to brown, γ=grey blue. Crossite is partly replaced by actinolite, and has α= yellow, β = blue, γ= violet. According to the classification of Leake (1978.; Figure 7), the

amphiboles are actinolites, ferro- winchite (which is green-blue), winchite, magnesio-riebeckite, crossite and, less frequently, calcian ferro glaucophane, which is blue . Analyses of amphibole are presented in Table 14.

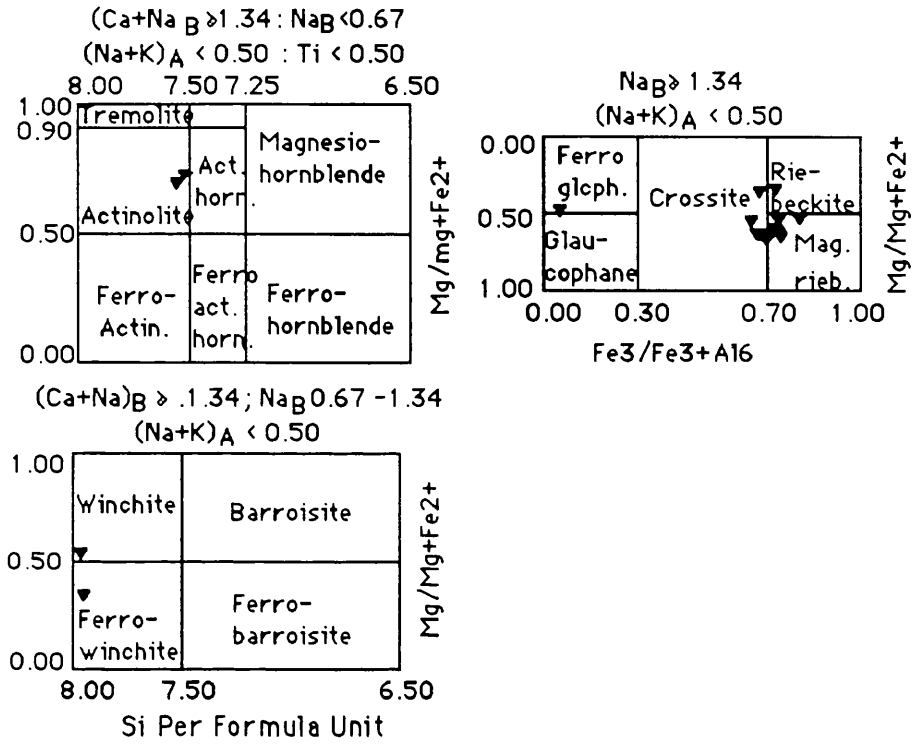

Figure 7. Classification of amphiboles (after Leake, 1978; Hawthorne, 1981).

Amygdales range in size from 0.5-2mm to 3-4mm in diameter. Poly and monomineralic amygdales are distinguishable and a mineral zonation from rim to core is common. A narrow rim of pumpellyite, epidote, chlorite and quartz is generally present, followed towards the centre by calcite , chlorite, epidote, quartz and pumpellyite (Plate, 12). Common mineral assemblages in amygdales are pumpellyite, chlorite, epidote and quartz. Brownish green pumpellyite predominates in the amygdales. Pumpellyite forms tiny acicular prisms and spherulitic sheaves displaying strong pleochroism and dispersion, with fan-like, radial extinction. Some fibres occur intergrown with epidote which is readily distinguished from other minerals by its higher relief and birefringence. The iron content (FeO*) ranges from 8.26 to 11 %. The compositions of pumpellyites are given in Table 15.

Chlorite occurs as flaky or feathery aggregates, pale-green and yellowish, green-brown groundmass material, where it forms either from alteration of volcanic glass or from fine-grained primary minerals, and as infill of amygdales. The compositions of the chlorites are given in Table 16; they are pycnochlorites (Hey 1954) Figure 8.

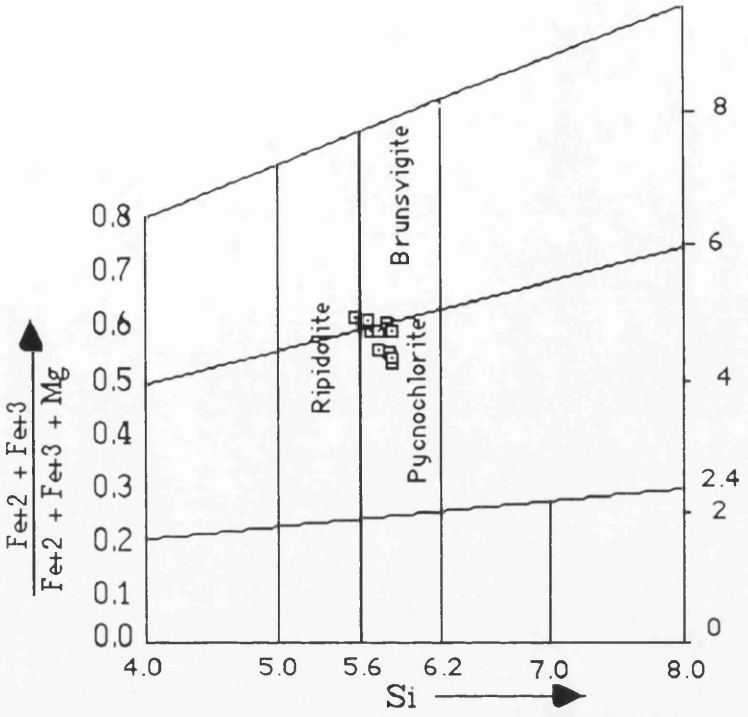

Figure 8. Composition of chlorites plotted on Hey's (1954) diagram.

Yellow epidote results from the alteration of groundmass clinopyroxene, and as filling in amygdales (Table 17). The pistacite component is 23 to 26.55.

Occasional larger flakes of white mica and phengite (Figure, 9) which are yellowish green, and muscovite occur scattered throughout the rocks. Also white micas occur particularly within albitized plagioclase, and are frequently a pale yellowish in thin section. Selected analyses of these larger flakes are included in Table 18. End member compositions of the micas vary between paragonite (0.1-43) and margarite (0.75-5.93).

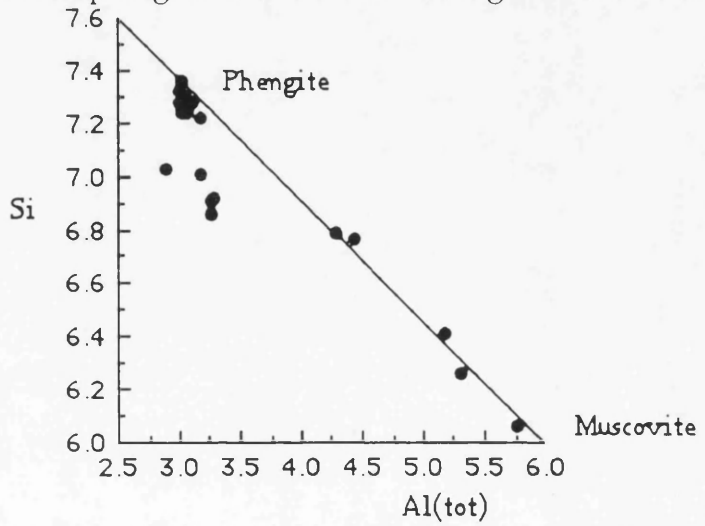

Figure 9. Muscovite and phengite Al-Si composition of metatrachy andesite.

Magnetite (Table, 19) forms subhedral to anhedral microphenocrysts which grade into minute particles in the groundmass.

Quartz phenocrysts (<2mm) are partly resorbed and contain inclusions of colourless to pale brown glass. Quartz is also present in most amygdales. Accessory minerals are euhedral sphene and apatite, commonly as inclusions in plagioclase, magnetite and amphibole.

Table 12. Composition of plagioclases

Sm.N	227 micr	227 phe	183 core	183 mid.	183 rim	183 core	183 mid.	183 rim	323 mic	323 phe
SiO_2	68.68	70.59	66.89	67.46	67.93	67.63	68.02	67.35	70.62	68.17
TiO_2	0.07	0.22	0.00	0.00	0.01	0.00	0.07	0.00	0.00	0.02
Al_2O	19.29	18.79	19.72	19.08	19.64	19.79	19.65	19.89	18.41	19.56
Feo*	0.06	0.05	0.02	0.00	0.00	0.84	0.00	0.43	0.32	0.03
MnO	0.00	0.03	0.00	0.00	0.00	0.00	0.00	0.13	0.02	0.02
MgO	0.00	0.00	0.00	0.00	0.00	0.00	0.07	0.108	0.02	0.00
CaO	0.05	0.01	0.45	0.27	0.14	0.23	0.31	0.149	0.00	0.26
Na_2O	11.57	10.01	11.01	11.09	11.69	11.49	10.90	11.33	9.62	11.18
K_2O	0.04	0.55	0.06	0.10	0.14	0.79	0.10	0.13	0.75	0.03
TOT.	99.76	100.25	98.15	98.00	99.55	100.77	99.30	99.12	99.74	99.27
	Recalculated to 32 Oxygens									
Si	12.04	12.42	11.89	11.95	11.85	11.85	11.90	11.88	12.52	11.96
Ti	0.01	0.03	0.00	0.00	0.00	0.00	0.01	0.00	0.00	0.00
Al	3.97	3.48	4.13	4.04	4.15	4.15	4.14	4.13	3.43	4.04
Fe	0.01	0.07	0.00	0.00	0.01	0.01	0.00	0.00	0.58	0.00
Mn	0.00	0.06	0.00	0.00	0.00	0.00	0.00	0.00	0.00	0.00
Mg	0.00	0.00	0.00	0.00	0.00	0.00	0.02	0.02	0.00	0.00
Ca	0.09	0.02	0.09	0.05	0.04	0.04	0.05	0.03	0.00	0.05
Na	3.92	3.41	0.09	3.87	3.98	3.96	3.75	3.88	3.30	3.80
K	0.09	0.12	3.79	0.02	0.02	0.01	0.02	0.03	0.17	0.01
T.Cat	20.13	19.56	19.94	19.93	20.04	20.02	19.91	19.94	19.49	19.86
	End member of the plagioclase minerals									
An	0.20	0.48	2.20	1.30	0.70	1.08	0.50	0.70	0.00	1.20
Ab	99.60	95.95	97.60	97.90	98.90	97.90	99.30	98.50	95.05	98.60
Or	0.20	3.48	0.40	0.60	0.60	0.40	0.00	0.80	4.40	0.20

FeO* is total iron as FeO.

Table 13 . Composition of clinopyroxenes

Sa.No	227	227	227	323	227	373	373 Core	373 rime
SiO_2	52.87	51.80	51.55	52.40	52.35	51.52	52.58	51.89
TiO_2	0.10	0.14	0.27	0.19	0.19	0.22	0.18	0.20
Al_2O_3	1.00	1.18	1.48	1.35	0.99	1.39	1.27	1.29
FeO*	9.48	9.60	9.88	9.37	9.35	9.49	9.52	8.99
MnO	0.40	0.37	0.46	0.30	0.38	0.37	0.28	0.28
MgO	13.69	12.97	13.00	12.84	13.11	12.61	13.18	13.37
CaO	22.40	22.79	22.40	22.19	22.92	22.72	22.17	22.60
Na_2O	0.60	0.43	0.54	0.70	0.42	0.57	0.57	0.54
K_2O	0.00	0.00	0.00	0.00	0.00	0.00	0.00	0.03
T0tal	100.54	99.28	99.58	99.04	99.71	98.89	99.75	99.19
	Recalculated to 6 oxygens							
Si	1.99	1.99	1.93	1.99	1.98	1.99	1.99	1.98
Ti	0.00	0.00	0.00	0.00	0.00	0.00	0.00	0.00
Al+6	0.04	0.05	0.06	0.05	0.04	0.06	0.05	0.05
Al+4	0.00	0.00	0.00	0.01	0.00	0.00	0.00	0.01
Fe+3	0.07	0.07	0.09	0.01	0.05	0.06	0.04	0.07
Fe^{+2}	0.21	0.23	0.21	0.21	0.23	0.23	0.25	0.21
Mn	0.01	0.01	0.01	0.01	0.01	0.01	0.00	0.00
Mg	0.75	0.70	0.72	0.72	0.73	0.70	0.73	0.74
Ca	0.88	0.91	0.90	0.90	0.91	0.91	0.88	0.90
Na	0.04	0.03	0.03	0.00	0.03	0.04	0.04	0.04
K	0.00	0.00	0.00	0.00	0.00	0.00	0.00	0.00
Total	4.00	4.00	4.00	4.00	4.00	4.00	4.00	4.00
	End member of the clinopyroxene minerals as below							
wo	45.56	46.87	46.15	47.00	47.00	47.37	46.04	46.66
En	38.73	37.10	37.22	36.56	37.39	36.57	38.06	38.39
Fs	15.69	16.00	16.62	16.36	15.59	16.05	15.89	14.94

Fe^{+3} is calculated by normalization according to Schumacher (1991).

Table 14. Composition of amphiboles

Sa.N	227 mgr	373 mgr	227 Cr	373 Cr	227 w	373 w	183 Fw	183 ac	183 ac	373 cfg
SiO_2	55.80	54.60	52.00	55.37	54.35	54.27	53.25	55.99	53.92	56.00
TiO_2	0.00	0.02	0.73	0.00	0.12	1.15	0.00	0.10	0.17	0.96
Al_2O	2.20	2.76	2.85	3.00	2.94	3.12	2.13	1.37	1.41	3.13
FeO*	18.57	18.96	27.93	18.64	20.55	17.96	20.99	14.62	14.97	17.90
MnO	0.30	0.40	0.21	0.25	0.22	0.34	0.33	0.33	0.48	0.18
MgO	10.69	10.94	4.37	10.60	9.40	9.79	9.32	12.74	11.79	9.60
CaO	3.39	2.59	1.46	2.50	3.20	4.07	7.11	11.51	11.12	3.63
Na_2O	5.00	5.76	6.37	5.50	4.60	5.04	3.10	1.00	1.39	5.61
K2O	0.10	0.20	0.16	0.16	0.23	0.12	0.11	0.10	0.09	0.12
Total	96.05	96.23	96.08	96.03	95.59	95.86	96.23	97.66	95.25	97.13
	Recalculated to 23 Oxygens									
Si	7.98	7.92	7.93	7.96	7.97	7.94	7.95	8.08	7.98	8.16
Al^{+4}	0.01	0.07	0.06	0.03	0.02	0.05	0.04	0.00	0.00	0.00
AlT	0.36	0.47	0.51	0.51	0.51	0.54	0.37	0.23	0.25	0.53
Al^{+6}	0.34	0.39	0.44	0.48	0.49	0.49	0.33	0.00	0.00	0.00
Ti	0.00	0.00	0.08	0.00	0.01	0.12	0.00	0.01	0.01	0.10
Fe^{+3}	1.04	1.00	0.87	0.98	0.74	0.36	0.39	0.00	0.00	0.00
Mg	2.36	2.36	0.99	2.31	2.09	2.17	2.07	2.74	2.65	2.08
Fe^{+2}	1.26	1.29	2.68	1.29	1.82	1.87	2.22	1.76	1.89	2.18
Mn	0.04	0.04	0.03	0.03	0.02	0.04	0.04	0.04	0.06	0.02
FmT	13.05	13.11	13.11	13.11	13.19	13.08	13.07	12.87	12.90	13.10
Ca	0.53	0.40	0.24	0.39	0.51	0.65	1.13	1.78	1.80	0.56
NaM	1.40	1.47	1.65	1.49	1.28	1.26	0.79	0.00	0.00	0.00
NaT	1.43	1.62	1.88	1.56	1.33	1.45	0.90	0.27	0.40	1.58
NaA	0.03	0.14	0.23	0.06	0.05	0.19	0.10	0.00	0.00	0.00
K	0.015	0.027	0.003	0.048	0.061	0.0	0.158	0.0	0.0	0.0

Fe^{+3} is calculated by estimation according to Spear and Kimball (1984)

Mgr: magnesio-riebeckite Cr: Crossite w: Winchite Fw: Ferro-winchite ac: actinolite Cfg: Calcian ferro glaucophane

Table 15. Composition of pumpellyites

Sample No	183 Core	183 rim	183	183	183
SiO_2	36.06	35.13	36.49	37.34	37.35
TiO_2	0.18	0.05	0.181	0.189	0.13
Al_2O_3	23.58	21.98	21.88	22.29	23.21
FeO*	10.02	11.00	8.78	8.26	8.50
MnO	0.34	0.28	0.173	0.22	0.15
MgO	2.29	4.11	2.58	2.57	1.64
CaO	21.39	19.31	22.19	22.27	22.92
TOTAL	93.86	91.86	92.27	93.14	93.90
Recalculated to 51 Oxygens					
Si	12.31	12.29	12.60	12.73	12.62
Ti	0.05	0.01	0.05	0.05	0.03
Al	9.49	9.07	8.90	8.96	9.25
Fe	2.86	3.29	2.53	2.35	2.40
Mn	0.09	0.09	0.05	0.06	0.04
Mg	1.16	2.14	1.32	1.31	0.82
Ca	7.82	7.13	8.21	8.14	8.30
Total Cat.	33.73	34.02	33.61	33.60	33.46

Total Fe as Feo*

Table 16. Composition of chlorites

Samp. No.	183	183	183	183
SiO_2	28.20	27.56	28.20	28.49
TiO_2	0.01	0.00	0.08	0.00
Al_2O_3	18.90	20.30	19.08	20.70
Fe_2O_3	5.85	5.86	5.87	5.71
FeO	21.06	21.12	21.13	20.56
MnO	0.53	0.56	0.49	0.45
MgO	13.63	12.19	12.95	12.20
CaO	0.20	0.30	0.20	0.20
Na_2O	0.20	0.23	0.15	0.07
K_2O	0.00	0.00	0.00	0.00
TOTAL	88.38	88.12	88.15	88.38
Recalculated to 28 Oxygens				
Si	5.82	5.71	5.82	5.79
Ti	0.00	0.01	0.00	0.00
Al^{+6}	4.59	4.97	4.46	4.96
Al^{+4}	0.90	0.91	0.91	0.87
Fe^{+3}	3.63	3.66	3.65	3.49
Fe^{+2}	0.09	0.09	0.08	0.08
Mn	4.19	3.77	3.98	3.70
Ca	0.05	0.07	0.04	0.00
Na	0.09	0.09	0.06	0.03
K	0.00	0.00	0.00	0.00
Total Cations	19.36	19.28	19.00	18.92
End member of the chlorite minerals as below				
Mg-Cl	41.93	37.70	39.87	37.00
Fe-Cl	36.36	36.36	36.52	34.99
Fe*/(Fe*+mg)	0.52	0.54	0.53	0.54

Fe^{+3} is calculated by ratio according to Schumacher (1991).

Table 17. Composition of epidotes

Sample No	183	183	183	183	183	183
SiO_2	38.10	37.33	37.72	38.37	38.13	38.60
TiO_2	0.14	0.11	0.08	0.67	0.00	0.09
Al_2O_3	24.17	23.43	23.74	22.45	22.80	23.75
Fe_2O_3	11.51	11.54	12.17	12.69	11.75	11.15
FeO	0.54	0.54	0.57	0.60	0.55	0.52
MnO	0.07	0.03	0.27	0.10	0.00	0.09
MgO	0.08	0.20	0.00	0.26	0.19	0.51
CaO	23.48	22.46	22.93	20.59	21.05	22.18
Na_2O	0.00	0.00	0.00	0.00	0.00	0.00
K_2O	0.03	0.05	0.04	0.03	0.02	0.01
TOTAL	98.12	95.69	97.52	95.76	94.49	96.90
Recalculated to 25 oxygens						
Si	6.03	6.04	6.02	6.18	6.12	6.13
Ti	0.02	0.01	0.01	0.08	0.00	0.01
Al	4.51	4.47	4.46	4.26	4.35	4.45
Fe^{+3}	1.37	1.40	1.46	1.54	1.50	1.33
Fe^{+2}	0.07	0.07	0.07	0.08	0.08	0.07
Mn	0.01	0.00	0.04	0.01	0.00	0.01
Mg	0.02	0.05	0.00	0.06	0.05	0.12
Ca	3.98	3.90	3.92	3.55	3.82	3.78
Na	0.00	0.00	0.00	0.00	0.00	0.00
K	0.01	0.02	0.01	0.01	0.01	0.02
Total Cat.	16.02	15.96	15.99	15.77	15.93	15.92
pistasite	23.29	23.85	24.66	26.55	25.64	24.00

Fe^{+3} is calculated by ratio according to Schumacher (1991).

Table 18. Composition of micas

Sm.N	227 Phg.	227 Phg.	227 Phg.	373 Phg	373 Phg.	183 mus	183 mus	183 mus	183 mus	183 mus
SiO_2	52.00	49.87	49.40	50.64	49.23	47.93	51.00	48.67	51.48	45.84
TiO_2	0.32	1.22	1.41	1.72	1.50	0.14	0.07	0.06	0.13	0.09
Al_2O	18.74	19.97	19.89	19.46	19.80	37.65	29.00	33.31	27.68	32.89
Fe_2O	5.18	6.26	5.91	4.90	5.66	0.24	0.94	0.71	1.67	1.71
FeO	0.82	0.99	0.93	0.77	0.90	0.03	0.15	0.11	0.26	0.03
MnO	0.00	0.01	0.08	0.04	0.07	0.01	0.06	0.17	0.08	0.07
MgO	4.67	4.25	4.00	4.07	4.11	0.87	3.78	1.39	3.60	1.08
CaO	0.10	0.69	0.80	1.01	0.86	0.58	0.60	0.04	0.68	0.14
Na_2O	0.01	0.12	0.10	0.00	0.08	0.35	0.20	0.18	0.35	0.17
K_2O	10.70	10.49	10.27	10.17	10.54	10.85	10.59	11.12	10.68	10.79
Total	92.54	93.87	92.79	92.78	92.75	98.65	96.38	95.76	96.61	92.81
Recalculated to 22 Oxygens										
Si	7.23	6.9	6.91	7.00	6.86	6.06	6.76	6.41	6.78	6.25
Ti	0.03	0.12	0.14	0.17	0.15	0.01	0.00	0.00	0.01	0.01
Al^{+6}	0.76	1.09	1.08	0.99	1.14	1.93	1.23	1.58	1.21	1.74
Al^{+4}	2.31	2.16	2.19	2.17	2.11	3.82	3.19	3.58	3.08	3.55
Fe^{+3}	0.54	0.65	0.62	0.51	0.59	0.02	0.09	0.07	0.16	0.17
Fe^{+2}	0.01	0.11	0.11	0.09	0.10	0.04	0.02	0.01	0.03	0.03
Mn	0..00	0.00	0.01	0.00	0.01	0.00	0.01	0.02	0.01	0.01
Mg	0.10	0.87	0.83	0.84	0.85	0.16	0.70	0.27	0.68	0.22
Ca	0.01	0.10	0.12	0.15	0.13	0.08	0.08	0.00	0.09	0.02
Na	0.02	0.03	0.03	0.00	0.22	0.09	0.05	0.05	0.09	0.04
K	0.90	1.85	1.83	1.79	1.88	1.75	1.70	1.87	1.72	1.88
T.Cat.	13.87	13.94	13.90	13.83	13.95	13.94	13.84	13.90	13.88	13.95
End member of the mica minerals as below										
Mus	95.0	91.74	90.68	87.49	88.63	87.55	84.60	93.45	86.45	94.00
Par	0.10	1.58	1.33	0.10	1.04	4.30	2.40	2.40	4.30	2.25
Mar	0.75	5.05	5.93	7.35	6.10	3.95	4.05	0.30	4.60	1.10

Fe^{+3} is calculated by ratio according to Schumacher (1991).

Mus:muscovite Phg:phengite Par:paragonite Mar:marcasite

Table 19. Composition of magnetites

Analyses No	227	227	227	227
SiO_2	0.00	0.50	0.80	0.49
TiO_2	0.18	0.11	0.60	0.20
Al_2O_3	0.08	0.56	0.63	0.53
Fe_2O_3	53.38	58.21	66.79	54.9
FeO	47.98	42.39	32.68	41.88
MgO	0.07	0.00	0.00	0.04
CaO	0.18	0.20	0.07	1.38
Na_2O	0.89	0.67	0.16	0.58
Total	0.17	0.00	0.69	0.06
TOTAL	102.9	102.6	102.42	100.06
Recalculated to 32 oxygen				
Si	0.05	0.03	0.02	0.03
Ti	0.00	0.00	0.05	0.00
Al	0.00	0.00	0.01	0.07
Fe3	1.27	1.46	1.79	1.30
Fe2	1.27	1.19	0.99	1.11
Mn	0.00	0.00	0.00	0.00
Mg	0.01	0.01	0.00	0.08
Ca	0.04	0.03	0.01	0.00
Na	0.01	0.00	0.00	0.00
Total	3.00	3.00	3.00	3.00

Fe+3 is calculated by cation balance according to Schumacher (1991)

5.5. METABASALTIC ANDESITE

These rocks consist of 30-50% plagioclase, 30-45% clinopyroxene, 10-20% epidote, chlorite, white mica, stilpnomelane and biotite, 0-5% amphibole and accessory sphene, apatite and magnetite.

The original porphyritic textures are preserved in the rocks. All the primary plagioclase has recrystallized completely to albite (Ab 95-99 An 0-8 Or 0-3; Table, 20. Figure 10). associated with epidote. The phenocrysts are euhedral to subhedral and are enriched with epidote and sericite inclusions. They show strong undulatory exinction and are tabular with simple twins.

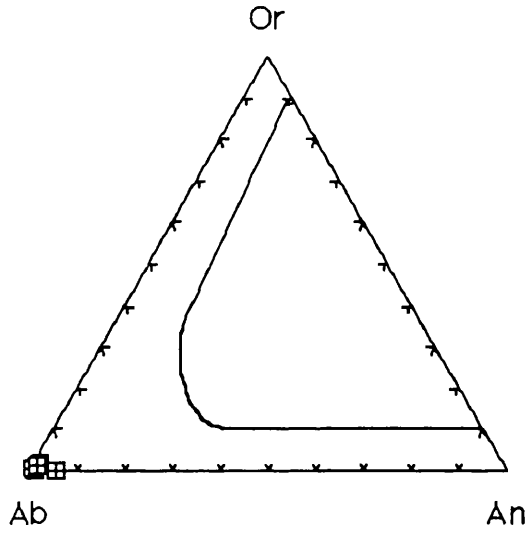

Figure 10. Plagioclase observed in metabasaltic andesite.

Minor quartz crystals occur which are elongated parallel to the schistosity. Also some quartz occurs as fine-grained aggregates scattered throughout the groundmass.

The clinopyroxene grains occur as euhedral to subhedral microphenocrysts and phenocrysts. The composition of the pyroxene is augite (Figure 11; Table, 21). Relict colourless or pale brown augites are common, which are subhedral with an average diameter of about 0.5 mm . Common alteration products of the pyroxene are calcite, chlorite, epidote and amphibole. They are generally replaced marginally by green metamorphic actinolite or sodic amphibole (Plate, 13). The igneous augite is charecterized by low Ca and high Ti, being $Wo_{(37.16-43.87)}$, $En_{(40.7-45.1)}$, $Fs_{(11.38-19.82)}$ as tabulated in Table 21.

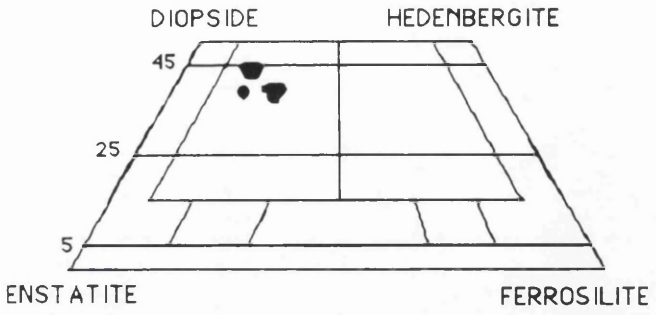

Figure 11. Composition of cpx, plotted on the diagram of Poldervaart et al. (1951).

The Ti, Cr, Ca, Na and Al contents of the pyroxene phenocrysts indicate that the chemistry of the metabasaltic andesite is of orogenic and tholeiitic affinities (Figure 12. a-c).

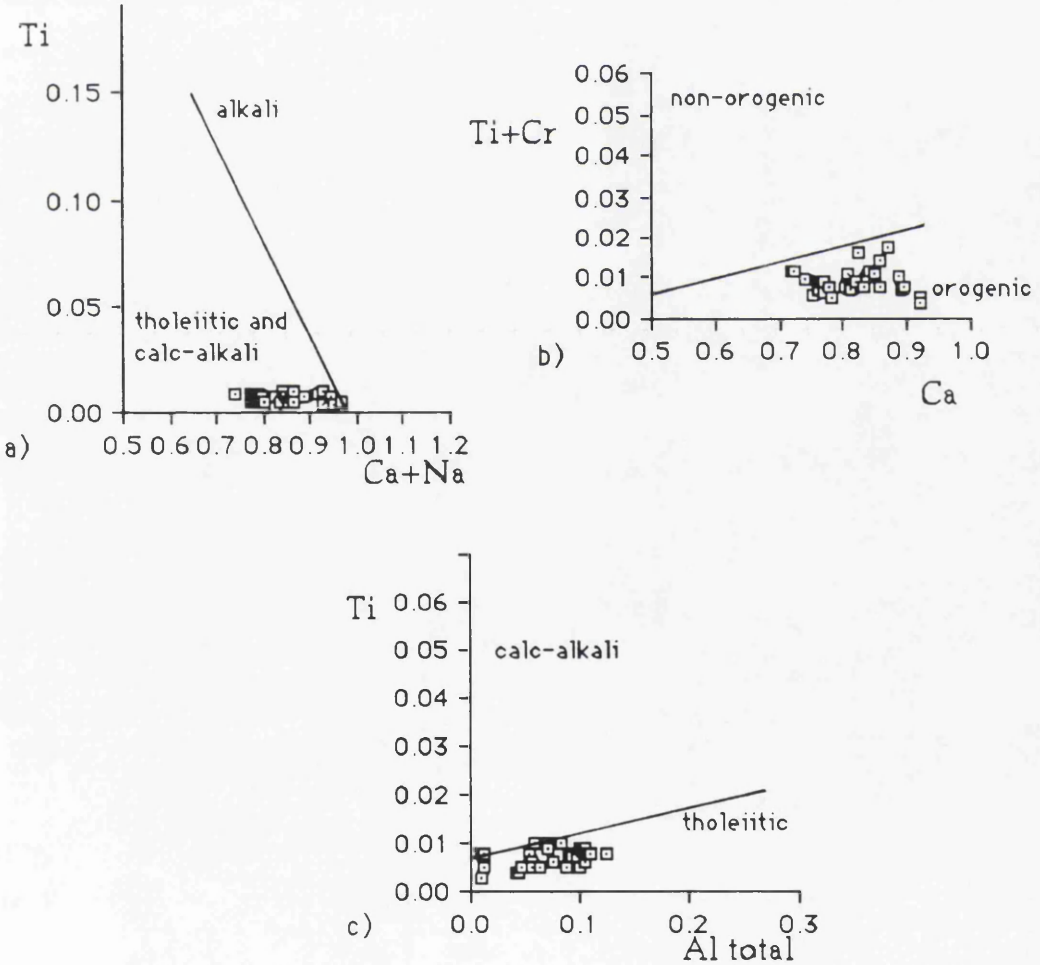

Fig. 12. a, b and c. Compositional variations of clinopyroxene phenocrysts from the metabasaltic andesite in terms of Ti, Ca, Na, Cr and Al using the discriminant diagrams of Leterrier et al. (1982).

Amphibole is ubiquitous with both sodic and calcic amphiboles (Table 22). Actinolite occurs in rocks as prismatic crystals (0.1mm long) and needles (0.15mm long). It shows ∝= pale green, β= pale yellow green, γ=colourles. It has Mg/(Mg+Fe) ratios of 0.56 to 0.63. Glaucophane shows ∝=yellow, β=blue and γ=violet colours. They occur around relict augite (Plate,13). All amphiboles formed as secondary phases from clinopyroxene. According to the classification of Leake (1978), these are actinolite, richterite and ferro-glaucophane (Figure 13).

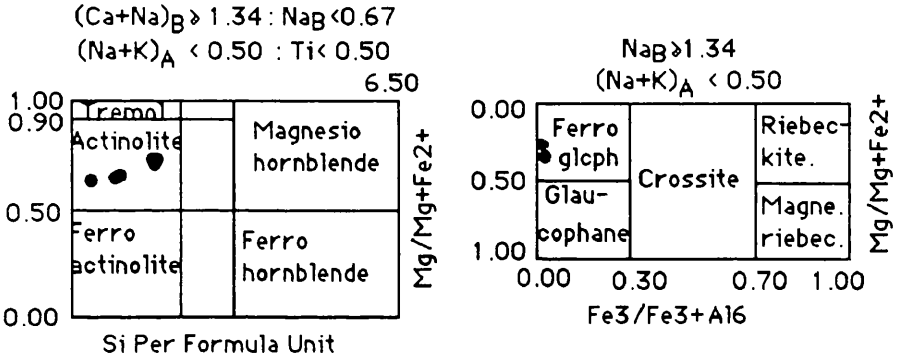

Figure 13. Classification of amphibole (after Leake, 1978; Hawthorne, 1981).

Stilpnomelane appears as ∝=light golden yellow to β=brown needles in the matrix, and single and acicular crystals in the phenocryst phases (Plate, 14), suggesting a considerable ferric iron content. The composition of stilpnomelane is given in Table 23. The Fe/(Fe*+mg) ratios are 0.68, and in Al (0.39-0.44), in Si 2.66-2.85).

Biotite forms partly resorbed phenocrysts (2-4mm) exhibiting green to dark coffee brown pleochroism, or reddish orange where oxidized, and altered to chlorite. Individual plates may be up to 0.1 mm across. Analyses of biotite phenocrysts show relatively high TiO_2 (1.29-4.80) content and an Fe/(Fe+Mg) ratio of (0.42-0.50) (Table 24).

Two types of white micas (Table 25) are recognised in these rocks. One is a fine-grained white mica or sericite, generally included within feldspar and pyroxene. The other type of mica is scarce and appears as small flakes aligned parallel to the schistosity.

The epidote formed from primary augite as small irregular patches, or scattered in the groundmass. Also it occurs as radiating clusters . The composition is shown in Table 26.

Pale green chlorite (Table, 26) occurs as platy and fibrous aggregates replacing the pyroxene and amphiboles, and tends to align along the schistosity with some chlorite pseudomorphs after biotite. The composition of chlorite are pycnochlorite and brunsvigite (Figure 14) with 0.43-0.54 Si/(Si+Al) ratio.

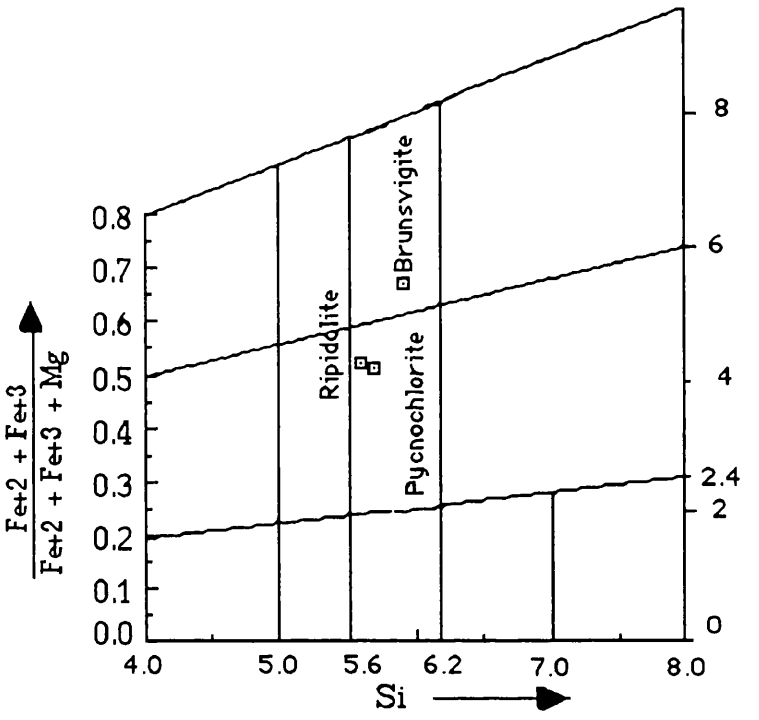

Figure 14. Composition of chlorites plotted on Hey's (1954) diagram.

Oxides are completely recrystallized to fine-grained (0.5-0.8 mm) sphene .Magnetite occurs as small granules concentrated in the groundmass.

Table 20. Composition of plagioclases

Sample N	272 microlit	277 pheno	405 pheno	405 rim	405 core	405 pheno
SiO_2	68.19	67.26	69.03	68.36	67.60	66.85
TiO_2	0.02	0.00	0.03	0.01	0.00	0.00
Al_2O_3	20.22	19.32	19.15	19.84	19.18	19.88
FeO*	0.32	0.16	0.04	0.02	0.94	0.22
MnO	0.02	0.00	0.01	0.00	0.10	0.08
MgO	0.28	0.00	0.10	0.28	1.17	0.25
CaO	0.14	0.20	0.03	0.23	0.20	0.30
Na_2O	11.05	11.50	10.97	11.02	10.66	10.71
K_2O	0.35	0.09	0.03	0.20	0.13	0.62
TOTAL	100.59	98.53	99.39	99.96	99.98	98.91
Recalculated to 32 oxygens						
Si	10.85	10.80	11.92	11.90	11.71	11.81
Ti	0.00	0.00	0.00	0.00	0.00	0.00
Al	4,10	4.05	4.03	4.07	4.03	4.14
Fe	0.05	0.03	0.02	0.03	0.02	0.04
Mn	0.00	0.00	0.00	0.00	0.01	0.11
Mg	0.07	0.00	0.00	0.07	0.31	0.07
Ca	0.02	0.02	0.00	0.04	0.03	0.06
Na	3.83	3.87	3.69	3.72	3.68	3.67
K	0.01	0.01	0.00	0.04	0.03	0.14
Total Cat.	20.04	20.03	19.96	19.92	20.10	19.99
End member of the plagioclase minerals as below						
An	0.70	0.99	0.20	1.10	0.90	1.40
Ab	98.90	98.30	99.20	97.10	98.30	95.00
Or	0.30	0.49	0.60	1.10	0.80	3.50

FeO* is total iron as FeO.

Table 21. Composition of clinopyroxenes

Sam.N	272	272	272	272	272	272	272	272
SiO_2	51.44	50.79	51.50	51.51	51.15	51.63	52.43	51.65
TiO_2	0.32	0.30	0.32	0.31	0.24	0.18	0.17	0.19
Al_2O_3	2.37	2.14	2.32	2.41	2.24	2.88	1.69	2.60
FeO*	12.04	13.57	11.79	11.25	7.62	6.95	7.64	8.26
MnO	0.35	0.32	0.32	0.31	0.14	0.14	0.22	0.20
MgO	14.30	14.21	15.23	14.85	15.98	15.78	15.93	15.76
CaO	19.25	18.19	18.13	19.13	22.12	21.25	20.75	21.04
Na_2O	0.32	0.81	0.24	0.27	0.21	0.26	0.28	0.24
TOTAL	100.39	100.33	99.85	100.04	99.70	99.07	99.11	99.94
Recalculated to 6 Oxygens								
Si	1.91	1.91	1.91	1.91	1.88	1.91	1.94	1.91
Ti	0.01	0.01	0.01	0.01	0.006	0.005	0.004	0.005
Al^{+6}	0.08	0.09	0.08	0.08	0.10	0.88	0.06	0.09
Al^{+4}	0.02	0.00	0.02	0.02	0.00	0.03	0.02	0.02
Fe^{+3}	0.07	0.11	0.06	0.05	0.13	0.06	0.04	0.09
Fe^{+2}	0.30	0.23	0.30	0.29	0.10	0.16	0.19	0.17
Mn	0.01	0.01	0.01	0.01	0.00	0.00	0.07	0.00
Mg	0.79	0.83	0.84	0.82	0.87	0.87	0.88	0.86
Ca	0.76	0.71	0.72	0.76	0.87	0.84	0.82	0.83
Na	0.02	0.05	0.02	0.02	0.01	0.02	0.02	0.02
TotalCat.	4.00	4.00	4.00	4.00	4.00	4.00	4.00	4.00
End member of the clinopyroxenes as below								
Wo	39.43	37.40	37.16	39.18	43.87	43.58	42.29	42.44
En	40.74	43.49	43.43	42.31	44.09	45.03	45.17	44.21
Fs	19.82	19.09	19.39	18.49	12.03	11.38	12.53	13.34

Fe^{+3} is calculated by normalization according to Schumacher (1991).

Table 22. Composition of amphiboles

Sam. No	272 ac	272 rich.	405 ac	405 ac	405 Fgl	405 Fgl
SiO_2	53.08	55.81	52.10	53.81	57.56	53.45
TiO_2	0.05	0.02	0.00	0.00	0.02	0.27
Al_2O_3	1.29	6.81	1.43	0.50	2.59	1.78
FeO*	16.95	12.57	14.57	15.12	21.28	23.19
MnO	0.17	0.10	0.40	0.49	0.18	0.20
MgO	12.10	8.73	14.33	14.18	5.58	7.23
CaO	11.95	8.79	11.44	12.26	1.03	1.62
Na_2O	0.35	4.44	0.67	0.38	5.86	5.96
K_2O	0.17	0.09	0.13	0.04	0.20	0.22
TOTAL	96.11	97.46	95.08	96.97	94.43	93.92
Recalculated to 23 O xygens						
Si	7.92	8.04	7.77	7.91	8.66	8.28
Al^{+4}	0.00	0.00	0.22	0.08	0.00	0.00
AlT	0.22	1.11	0.25	0.08	0.45	0.32
Al^{+6}	0.00	0.00	0.29	0.04	0.00	0.00
Ti	0.00	0.00	0.00	0.00	0.00	0.03
Fe^{+3}	0.00	0.00	0.16	0.03	0.00	0.00
Mg	2.69	1.81	3.18	3.10	1.25	1.67
Fe^{+2}	2.11	1.46	1.65	1.83	2.67	3.00
Mn	0.02	0.01	0.05	0.06	0.02	0.03
FMT	12.99	12.46	13.09	13.03	13.08	13.35
Ca	1.91	1.31	1.82	1.93	0.16	0.27
NaM4	0.00	0.00	0.08	0.03	0.00	0.00
NaT	0.10	1.20	0.19	0.10	1.71	1.79
NaA	0.00	0.00	0.11	0.08	0.00	0.00
K	0.03	0.02	0.02	0.09	0.04	0.04

Fe^{+3} is calculated by estimation according to Spear and Kimball (1984).
ac:actinolite rich:richterite Fgl:Ferro-glaucophane

Table 23. Composition of stilpnomelanes

Sam. No	408	408	278	272	277	408	408
SiO_2	46.69	47.08	48.78	48.21	48.52	48.76	47.47
TiO_2	0.15	0.14	0.13	0.20	0.11	0.10	0.15
Al_2O_3	5.79	5.90	6.71	6.54	6.27	5.62	5.75
FeO*	26.97	27.21	27.22	25.97	25.91	25.68	26.92
MnO	1.62	1.81	0.78	0.55	0.73	1.74	1.71
MgO	6.93	6.81	7.09	6.26	5.48	6.83	6.72
CaO	0.11	0.17	0.22	0.24	0.73	0.17	0.14
NaO	0.61	0.24	0.31	0.31	0.43	0.27	0.29
K_2O	1.27	1.20	1.40	1.64	1.09	1.28	1.44
TOTAL	90.14	90.56	92.64	90.02	89.27	90.45	90.54
Recalculated to 8oxygens							
Si	2.66	2.67	2.69	2.62	2.85	2.71	2.66
Ti	0.01	0.01	0.01	0.09	0.01	0.01	0.01
Al	0.39	0.39	0.43	0.44	0.41	0.40	0.39
Fe	1.29	1.29	1.25	1.20	1.26	1.26	1.25
Mn	0.79	0.87	0.04	0.03	0.03	0.09	0.09
Mg	0.59	0.57	0.58	0.53	0.45	0.59	0.59
Ca	0.01	0.01	0.01	0.01	0.04	0.01	0.01
Na	0.07	0.03	0.03	0.03	0.04	0.03	0.03
K	0.09	0.09	0.01	0.12	0.09	0.01	0.10
TOTAL	5.20	5.17	5.15	5.13	5.07	5.17	5.18

Total Fe as FeO*

Table 24. Composition of biotites

Sample No	277	277	277	277	277	277
SiO_2	35.70	35.82	38.10	36.98	35.10	38.19
TiO_2	4.07	4.62	1.29	2.98	4.80	1.77
Al_2O_3	13.24	13.12	11.80	12.56	13.00	12.23
Fe_2O_3	3.68	3.65	3.56	3.68	3.49	3.58
FeO	18.77	18.64	18.16	18.79	17.81	18.27
MnO	0.36	0.30	0.31	0.30	0.32	0.40
MgO	9.26	9.81	12.04	10.36	9.95	11.39
CaO	0.09	0.07	0.02	0.10	0.34	0.06
Na_2O	0.13	0.16	0.28	0.27	0.37	0.29
K_2O	9.21	9.03	9.46	9.26	8.71	9.41
TOTAL	94.51	95.22	95.02	94.92	93.89	95.59
Recalculated to 22 Oxygens						
Si	5.57	5.52	5.87	5.70	5.48	5.84
Ti	0.48	0.53	0.15	0.35	0.56	0.20
Al	2.43.	2.38	2.14	2.28	2.39	2.20
Fe^{+3}	0.43	0.42	0.41	0.43	0.41	0.41
Fe^{+2}	2.45	2.40	2.34	2.42	2.33	2.34
Mn	0.04	0.04	0.04	0.04	0.04	0.05
Mg	2.15	2.25	2.76	2.38	2.31	2.59
Ca	0.01	0.01	0.00	0.02	0.06	0.01
Na	0.04	0.05	0.08	0.08	0.11	0.09
K	1.83	1.77	1.86	1.82	1.73	1.83
To.Cations	15.45	15.43	15.67	15.54	15.46	15.59
End member of the biotite as below						
Phlogopi	35.88	37.60	46.08	39.73	38.63	43.31
Annite	40.83	40.08	39.02	40.45	38.83	39.00

Fe^{+3} is calculated by ratio according to Schumacher (1991).

Table 25. Composition of white micas

Sample No	408	408	272	272	272
SiO_2	50.90	50.70	49.45	49.76	48.71
TiO_2	0.24	0.19	0.21	0.13	0.31
Al_2O_3	19.30	19.44	23.40	21.46	21.82
Fe_2O_3	6.61	7.00	5.78	6.35	8.74
FeO	1.05	1.11	0.91	1.01	1.38
MnO	0.05	0.03	0.01	0.11	0.10
MgO	4.69	4.81	4.31	5.00	3.80
CaO	0.00	0.12	0.01	1.48	0.48
Na_2O	0.00	0.08	0.00	0.00	1.43
K_2O	11.13	11.09	10.89	9.61	7.72
TOTAL	93.97	94.57	94.97	94.91	94.49
Recalculated to 22 Oxygens					
Si	7.05	6.97	6.74	6.80	6.67
TI	0.02	0.02	0.02	0.01	0.03
Al^{+6}	0.95	1.02	1.25	1.19	1.32
Al^{+4}	2.19	2.13	2.50	2.26	2.22
Fe^{+3}	0.69	0.72	0.59	0.65	0.90
Fe^{+2}	0.12	0.13	0.10	0.11	0.16
Mn	0.01	0.00	0.00	0.01	0.01
Mg	0.96	0.98	0.87	1.02	0.78
Ca	0.00	0.02	0.00	0.22	0.07
Na	0.00	0.02	0.00	0.00	0.38
K	1.96	1.95	1.89	1.67	1.36
Total Cat.	13.98	14.02	14.00	13.96	13.93
End member of the mica minerals as below					
muscovite	98.30	97.40	94.75	83.80	68.05
paragonite	0.00	1.10	0.10	0.00	19.15
marcasite	0.00	0.95	0.10	10.90	3.55

Fe^{+3} is calculated by ratio according to Schumacher (1991).

Table 26. Composition of epidote and chlorites

Sample No	272	272	404	404
SiO_2	37.99	38.43	25.79	27.17
TiO_2	0.15	0.17	0.10	0.00
Al_2O_3	22.91	22.21	17.92	17.85
Fe_2O_3	12.96	12.35	5.89	5.77
FeO	0.64	0.55	21.23	20.78
MnO	0.15	0.10	0.60	0.47
MgO	0.52	0.14	13.74	13.75
CaO	22.66	23.36	0.11	0.02
Na2O	0.02	0.01	0.05	0.07
K2O	0.04	0.03	0.00	0.00
TOTAL	98.04	97.35	85.43	85.88
Recalculated to 25 oxygens for epidote, 28 oxygens for chlorite				
Si	6.20	6.21	5.58	5.90
Ti	0.02	0.02	0.02	0.00
Al	4.35	4.46	4.57	7.65
Fe^{+3}	1.74	1.62	0.96	1.58
Fe^{+2}	0.09	0.06	3.84	6.32
Mn	0.02	0.01	0.11	0.14
Mg	0.11	0.04	4.43	3.86
Ca	3.91	4.09	0.02	0.09
Na	0.01	0.03	0.03	0.01
K	0.01	0.0	0.0	0.0
To.Cation	16.03	16.06	19.67	19.44
Pistasite	28.73	26.64		
End members of the chlorite as below				
			Mg-Cl	44.36	38.63
			Fe-Cl	38.46	40.45
			Fe*/(Fe*+mg)	0.52	0.67

Fe^{+3} is calculated by ratio According to Schumacher (1991).

5.6. METAHORNBLENDE GABBROS

The composition of the rocks is 25-40% plagioclase, 15-25% amphibole, 8-17% mica, 4-14% epidote, 9-13% quartz, 4-14% chlorite, 4-7% calcite, 1-3% augite and orthoclase, and accessory magnetite, sphene and apatite. The most common rock type is coarse grained and granular.

The feldspar occurs mostly as euhedral equant grains of albite (Ab 100-95 Or0-25) and rare oligoclase (An_{10} Ab_{85} Or_5). Large crystals display wavy extinction and twisted polysynthetic twinning. Some plagioclases are found as small hypidioblastic to idioblastic zoned crystals, with chlorite and epidote filling the intergranular space. Many plagioclase crystals are clouded with abundant oriented needles of opaque inclusions. Albite and quartz develop granophyric textures in the rock. Plagioclase is saussuritized, epidotized and sericitized. Microprobe analyses of plagioclase are given in Table 27 and Figure 15.

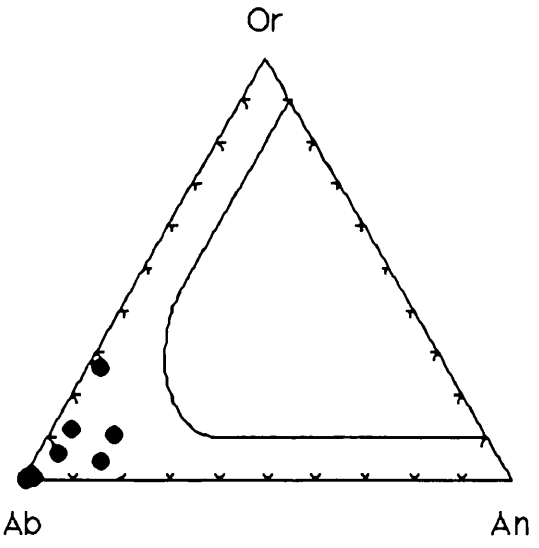

Figure 15. Chemical composition of plagioclase plotted on the Or-Ab-An diagram.

Hornblende occurs as large (up to 2-3mm diameter), green and brownish green crystals which are partially or completely replaced by actinolite, sodic amphibole, chlorite and epidote (Plate, 15). Secondary amphiboles formed at the expense of earlier amphiboles contain less Al and higher Si and Mg than the hornblende. Actinolite is usually green and prisms of up to 0.6 mm long are common Mg/(Mg+Fe) ratios of 0.49 to 0.57

, with the Mg/(Mg+Fe) ratio decreasing slightly with increasing Al. Following Leake's (1978) chemical classification, amphibole (Table 28) ranges from crossite, ferro winchite, winchite, magnesio-hornblende, ferri-hornblende, ferri-actinolitic hornblende to actinolite (Figure, 16). The winchite to crossite amphibole with lavender blue-purple colour occurs with actinolite.

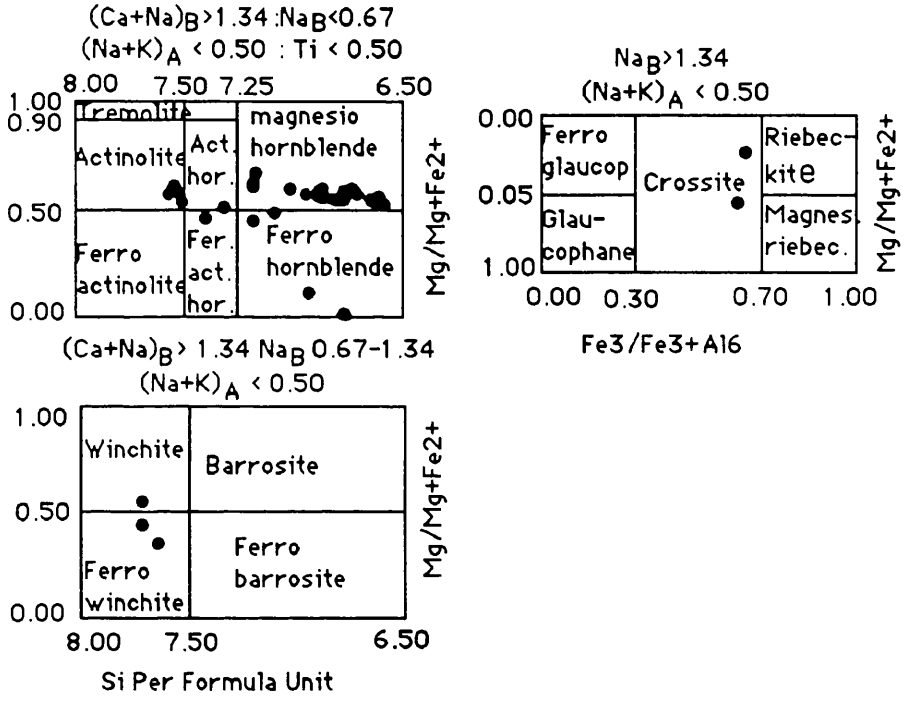

Figure 16. Classification of amphiboles from metahornblende gabbro (after Leake, 1978; Hawthorne, 1981).

The main types of chlorite are yellowish to golden brown diabanite, a pale-green phenochlorite and ripidolite (Hey,1954); (Table 29 and Figure 17). They occur as aggregates of plates which entirely replace hornblende and actinolite.

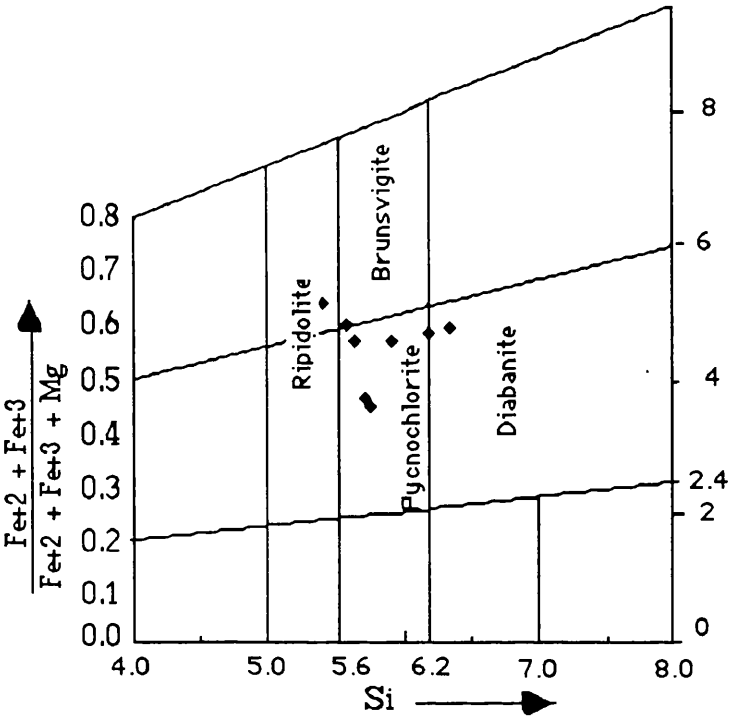

Figure 17. Composition of chlorites, plotted on Hey's (1954) diagram.

Pale yellow epidote (Table 30) is formed by saussuritization. Anhedral crystals are common, with some radiating crystals. Epidote is evenly distributed throughout the rock. It may have partially replaced plagioclase and actinolite.

Quartz, chlorite and albite are in part recrystallized.

Muscovite and sericite include paragonite (from 0.45 to 1.3 %) and margarite (from 1.2 to 1.65 %) as given inTable 31.

Rare clinopyroxene relics are augitic according to Poldervaart et al. (1951), as given in Table 31.

Magnetite and ilmenite are accessory minerals sometimes occurring as inclusions within amphibole porphyroblasts. The magnetite composition is given in Table 31.

Sphene is present in rocks as small, irregularly shaped grains of high relief. Apatite is also present. Calcite commonly occurs as inclusions within albitized plagioclase.

Table 27. Composition of feldspars

Samp.N	337	313	313	313	337	379	379
SiO_2	68.03	66.15	68.97	68.38	68.81	67.20	66.33
TiO_2	0.03	0.03	0.05	0.00	0.01	0.05	0.02
Al_2O_3	19.74	21.62	19.90	19.64	19.49	20.02	21.23
FeO*	0.20	0.34	0.22	0.28	0.44	0.08	0.01
MnO	0.00	0.02	0.03	0.00	0.02	0.04	0.00
MgO	0.44	0.95	0.15	0.11	0.03	0.10	0.30
CaO	0.57	o.438	0.12	0.107	0.12	0.16	2.64
Na_2O	10.96	7.20	12.11	11.59	11.70	11.11	8.50
K_2O	0.23	4.11	0.09	0.06	0.17	0.09	1.79
TOTAL	100.19	100.85	101.63	100.10	100.79	98.85	100.82
	Recalculated to 32 Oxygens						
Si	11.81	11.24	11.89	11.93	11.96	11.94	11.28
Ti	0.00	0.00	0.00	0.00	0.00	0.01	0.00
Al	4.16	4.68	4.04	4.04	3.99	4.03	4.53
Fe	0.31	0.36	0.32	0.42	0.65	0.01	0.30
Mn	0.00	0.00	0.00	0.00	0.00	0.01	0.00
Mg	0.12	0.26	0.41	0.30	0.00	0.03	0.09
Ca	0.11	0.86	0.22	0.20	0.22	0.03	0.51
Na	3.80	2.56	4.05	3.92	3.94	3.87	2.99
K	0.05	0.96	0.00	0.00	0.00	0.02	0.41
Total Cat.	20.36	20.17	20.10	20.00	20.01	19.97	20.14
	End member of the plagioclase m inerals as below						
An	2.9	2.2	0.59	0.50	0.60	0.80	12.76
Ab	95.6	66.00	98.79	99.00	98.99	98.50	72.76
Or	1.3	24.00	0.00	0.00	0.01	0.50	10.50

FeO* is total iron as FeO.

Table 28. Composition of amphiboles

Sa.No	344 W	344 Fw	379 Fw	344 c	337 ac	379 Fh-C	379 Fah-r	339 mh-C	379 mh-r
SiO_2	51.10	50.87	51.90	51.65	50.89	46.10	48.97	45.30	45.18
TiO_2	0.70	1.88	0.50	0.15	0.35	0.87	0.37	1.04	1.59
Al_2O_3	4.47	4.11	11.14	5.98	3.25	5.39	3.72	6.54	7.28
FeO*	19.63	19.13	15.57	22.39	20.90	22.29	22.46	18.98	19.80
MnO	0.21	0.23	0.39	0.20	0.40	0.44	0.38	0.32	0.31
MgO	9.58	9.00	4.83	10.10	11.72	9.56	9.18	10.49	10.28
CaO	3.66	5.00	7.35	1.19	9.62	9.81	11.54	10.59	10.04
Na_2O	4.69	5.30	4.67	5.87	0.86	1.08	0.77	1.30	1.70
K2O	0.11	0.17	0.18	0.04	0.11	0.23	0.11	0.13	0.12
Total	94.15	95.69	96.53	97.57	98.10	95.77	97.50	94.69	96.30
	Recalculated to 23 Oxygens								
Si	7.70	7.77	7.64	7.56	7.51	7.08	7.40	6.94	6.76
Al^{+4}	0.29	0.29	0.00	0.43	0.48	0.91	0.59	1.05	1.23
AlT	0.79	0.70	1.89	1.01	0.56	0.97	0.66	1.18	1.31
Al^{+6}	0.50	0.40	0.00	0.57	0.08	0.06	0.06	0.12	0.08
Ti	0.07	0.21	0.05	0.01	0.03	0.10	0.04	0.12	0.18
Fe^{+3}	0.60	0.12	0.00	0.89	0.34	0.55	0.40	0.57	0.59
Mg	2.15	1.95	1.03	2.16	2.57	2.18	2.06	2.39	2.34
Fe^{+2}	1.86	2.20	1.88	1.79	2.23	2.30	2.47	1.85	1.94
Mn	0.02	0.02	0.04	0.02	0.06	0.05	0.04	0.04	0.04
FmT	13.23	13.36	12.56	13.46	13.34	13.27	13.06	13.12	13.19
Ca	0.59	0.78	1.13	0.18	1.52	1.61	1.86	1.73	1.64
NaM_4	1.17	1.18	0.00	1.34	0.13	0.11	0.07	0.13	0.15
NaT	1.37	1.49	1.30	1.64	0.24	0.32	0.22	0.38	0.50
NaA	0.19	0.31	0.00	0.29	0.11	0.20	0.15	0.27	0.34
K	0.02	0.04	0.04	0.01	0.01	0.05	0.02	0.018	0.02

Fe^{+3} is calculated by estimation according to Spear and Kimball (1984).

w: winchite Fw: Ferro-winchite c: Ferro crossite ac: actinolite Fh: Ferro-hornblende Fah: ferro-actinolitic hornblende mh: magnesio-hornblende, C: core r: rim.

Table 29. Composition of chlorites

Sample No	337	313	337	313	313
SiO2	28.31	28.20	29.67	26.59	25.40
TiO2	0.03	0.02	0.01	0.03	0.09
Al2O3	19.28	19.00	19.40	17.96	19.40
Fe2O3	5.49	5.26	5.89	6.99	7.29
FeO	19.77	18.96	21.43	25.16	26.24
MnO	0.40	0.30	0.37	0.49	0.47
MgO	16.17	16.46	12.30	12.00	10.62
CaO	0.30	0.40	0.21	0.03	0.03
Na2O	0.26	0.25	0.17	0.08	0.10
K2O	0.04	0.08	0.03	0.04	0.02
TOTAL	90.05	88.93	89.48	89.37	89.66
Recalculated to 28 Oxygens					
SI	5.72	5.77	5.89	5.58	5.39
Ti	0.00	0.00	0.00	0.00	0.00
Al	4.59	4.56	4.58	4.44	4.85
Fe^{+3}	0.83	0.80	0.89	1.10	1.16
Fe^{+2}	3.34	3.23	3.55	4.41	4.66
Mn	0.06	0.05	0.06	0.08	0.08
Mg	4.87	4.96	3.70	3.75	3.36
Ca	0.06	0.08	0.04	0.00	0.00
Na	0.10	0.09	0.06	0.03	0.04
K	0.01	0.02	0.00	0.01	0.00
Total Cat.	19.58	19.61	18.77	19.63	19.59
End member of the chlorite minerals as below					
Mg-Cl	48.70	49.96	30.77	37.54	33.62
Fe-Cl	33.42	32.30	35.59	44.18	46.61
Fe*/(Fe*+mg)	0.46	0.45	0.54	0.59	0.63

Fe^{+3} is calculated by ratio according to Schumacher (1991)

Table 30. Composition of epidotes

Samp. No	344	344	337	313	313	337
SiO_2	37.00	37.10	37.06	38.17	37.47	37.79
TiO_2	0.01	0.01	0.00	0.00	0.00	0.04
Al_2O_3	23.20	23.81	22.45	23.19	23.00	22.91
Fe_2O_3	13.30	13.55	13.95	12.65	13.00	12.67
FeO	0.61	0.62	0.64	0.60	0.60	0.58
MnO	0.21	0.13	0.14	0.15	0.06	0.03
MgO	0.23	0.19	0.09	0.13	0.17	0.13
CaO	22.70	22.96	23.77	23.42	23.50	24.13
Na2O3	0.00	0.00	0.00	0.11	0.05	0.00
K2O	0.48	0.06	0.05	0.10	0.06	0.03
TOTAl	97.74	98.43	98.15	98.52	97.85	98.31
Recalculated to 25 Oxygens						
Si	6.26	6.49	6.17	6.21	6.20	6.22
Ti	0.01	0.02	0.00	0.00	0.00	0.03
Al	4.42	4.24	4.48	4.45	4.56	4.52
Fe^{+3}	1.74	1.66	1.75	1.72	1.61	1.56
Fe^{+2}	0.08	0.08	0.08	0.08	0.07	0.07
Mn	0.03	0.00	0.01	0.02	0.01	0.05
Mg	0.05	0.05	0.02	0.03	0.04	0.03
Ca	3.93	3.85	4.13	4.08	4.05	4.14
Na	0.0	0.05	0.0	0.04	0.01	0.00
K	0.1	0.03	0.01	0.02	0.01	0.00
Total Cat.	16.62	16.47	16.65	16.65	16.56	16.62
Pistacite	28.25	28.13	28.08	27.87	26.09	25.65

Fe^{+3} calculated by ratio according to Schumacher (1991).

Table 31. Composition of muscovite, Pyroxene and magnetite minerals

Sam.No	337mus	337mus	313mus	337cpx	313cpx	313mgn	313mgn
SiO_2	50.80	49.70	50.10	50.79	49.58	0.97	0.87
TiO_2	0.02	0.02	0.10	0.67	0.47	0.44	0.17
Al_2O_3	21.59	19.20	22.19	3.83	5.43	0.25	0.47
Fe_2O_3	8.00	9.32	6.38	0.00	0.00	0.00	0.00
FeO	1.27	1.48	1.01	8.43	12.35	88.60	88.67
MnO	0.08	0.02	0.06	0.17	0.22	0.18	0.00
MgO	4.30	4.44	3.85	17.20	13.83	0.11	0.06
CaO	0.23	0.16	0.09	18.79	15.61	0.07	0.61
Na_2O	0.01	0.09	0.03	0.15	0.15	0.00	0.06
K_2O	10.54	9.98	10.60	0.00	0.00	0.00	0.09
TOTAL	96.84	94.41	94.41	100.03	97.64	90.62	91.00
Recalculated to oxygens 22 for muscovite, 6 for pyroxene,32 for magnetite minerals							
Si	6.83	6.90	6.86	1.88	1.88	0.03	0.03
Ti	0.02	0.00	0.01	0.01	0.01	0.01	0.00
Al^{+6}	1.16	1.09	1.13	0.16	0.24	0.01	0.00
Al^{+4}	2.26	2.04	2.45	0.05	0.01	0.00	0.00
Fe^{+3}	0.81	0.97	0.65	0.05	0.01	1.88	1.65
Fe^{+2}	0.14	0.17	0.11	0.21	0.33	1.11	1.30
Mn	0.01	0.00	0.00	0.00	0.00	0.00	0.00
Mg	0.86	0.91	0.78	0.93	0.79	0.00	0.00
Ca	0.03	0.02	0.01	0.73	0.69	0.00	0.02
Na	0.02	0.02	0.00	0.01	0.04	0.00	0.00
K	1.81	1.76	1.85	0.00	0.00	0.00	0.00
Total Cat.	13.96	13.88	13.92	4.00	4.00	3.00	3.00
End member of the minerals as below							
mus	90.5	88.4	92.7	wo:38	wo:34.9	Mt:99	Mt:99.9
par	1.3	1.2	0.45	En:48.4	En:43	Usp:0.6	Usp:0.2
mar	1.6	1.2	0.75	Fs:13.58	Fs:13.5		

Fe^{+3} is calculated by ratio for muscovite, by normalization for pyroxene, by cation balance for magnetite according to Schumacher (1991).

Mus:muscovite Cpx:clinopyroxene Par:paragonite Mar:marcasite wo:wollastonite En:enstatite Fs:ferrosilite Mt:magnetite Usp:ulvospinel

5.7. METADOLERITES

These consist of 35-55% plagioclase, 30-45% clinopyroxene, 10-15% sericite, chlorite, calcite, epidote, ilmenite, sphene, quartz and apatite. The primary doleritic texture can still be recognized in the rocks.

Feldspars, occur as small laths and all feldspars are altered to albite (Table.32 and Figure 18) sericite,calcite and chlorite.

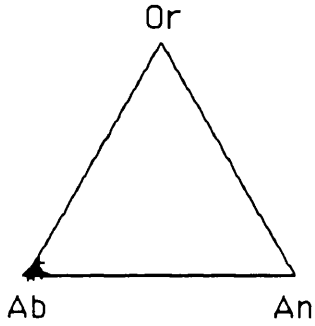

Figure 18.Plagioclase in the metadolerite

The clinopyroxene is strongly moulded on plagioclase laths to give a subophitic texture. The compositions are plotted on the Poldervaart (1951) diagram, which shows the augitic character (Figure 19). The clinopyroxene's composition is given in Table 33. While Fe, Ti and Mn increase from the core to the rim, Cr and Mg decrease.

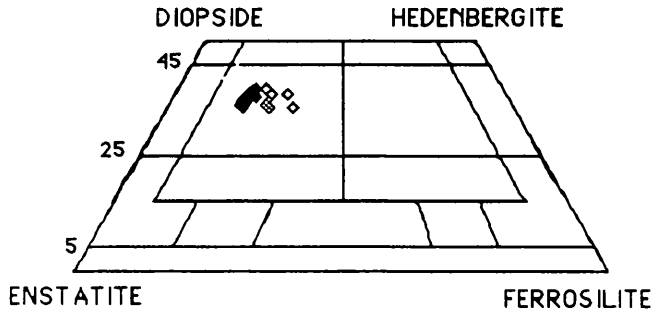

Figure 19. Composition of cpx, plotted on the diagram after Poldervaart et al. (1951).

The Ti, Cr, Ca, Na and Al contents of the pyroxene phenocrysts indicate that the chemistry of the metadolerite is non-orogenic according to Figure 20 ,with calcalkaline affinities (Figure 20).

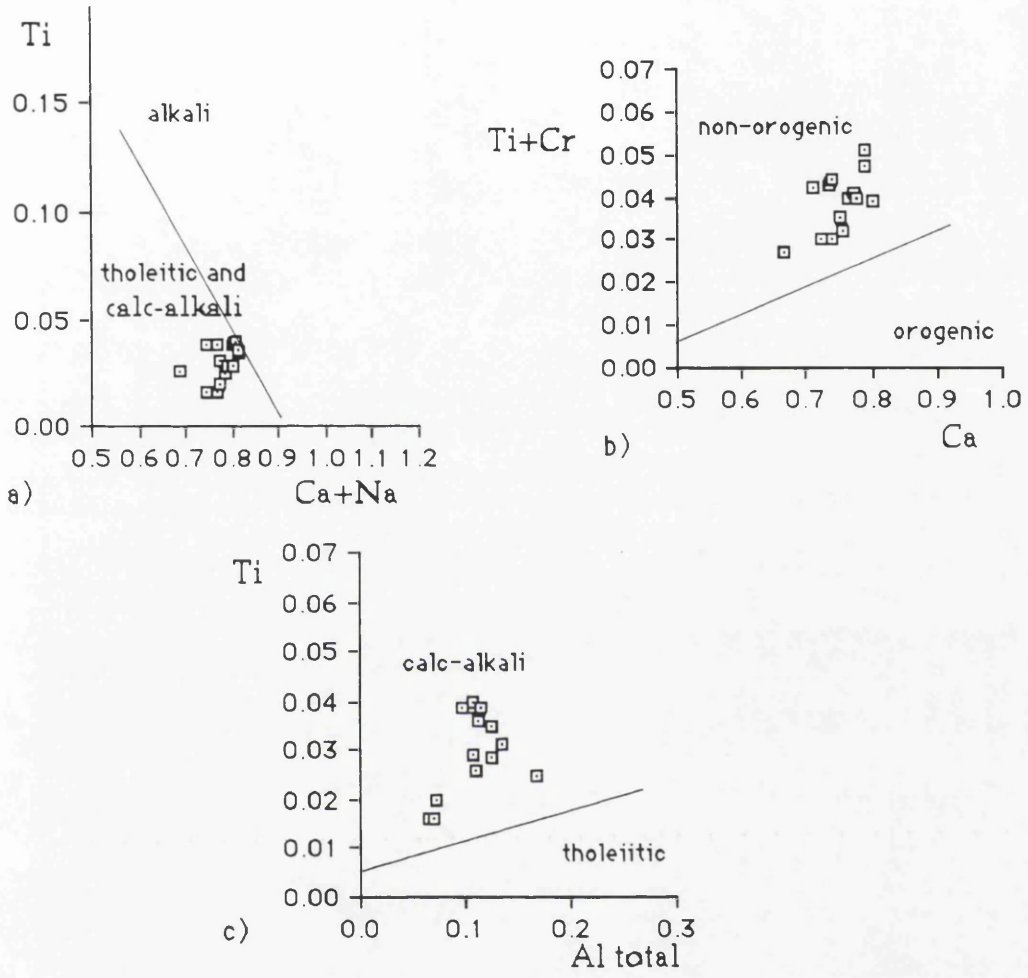

Fig. 20. a, b and c. Compositional variations of clinopyroxene phenocrysts from the metadolerite in terms of Ti, Ca, Na, Cr and Al using the discriminant diagrams of Leterrier et al. (1982).

Fine-grained white mica or sericite (Table. 34), replaces feldspar. Chlorite occurs as aggregates scattered in irregular patches. Epidote occurs as small irregular patches, or is scattered in the rock.

Ilmenite-magnetite intergrowths form scattered irregular aggregates as much as 0.4 mm in diameter. Ilmenite occurs in slender laths up to 0.3-0.5 mm in length.

Table 32. Composition of feldspars

Samp.No	414	414	414	414	417	417	417	417
SiO_2	67.24	66.55	66.67	66.58	66.99	66.88	68.36	66.73
TiO_2	0.00	0.12	0.05	0.06	0.12	0.12	0.07	0.16
Al_2O_3	20.01	20.10	20.06	20.01	20.29	20.18	19.85	19.70
FeO*	0.25	0.57	0.69	0.74	0.40	0.56	0.21	0.80
MnO	0.00	0.01	0.03	0.00	0.02	0.00	0.00	0.01
MgO	0.00	0.25	0.33	0.19	0.07	0.23	0.00	0.39
CaO	0.13	0.13	0.39	0.19	0.27	0.15	0.07	0.08
Na_2O	11.81	11.49	11.30	11.37	11.63	11.72	11.53	11.32
K_2O	0.06	0.14	0.41	0.50	0.07	0.06	0.08	0.29
Total	99.54	99.35	99.93	99.56	99.86	99.92	100.17	99.48
	Recalculated to 32 Oxygen							
Si	11.84	11.76	11.76	11.76	11.76	11.76	11.92	11.8
Ti	0.00	0.00	0.00	0.00	0.00	0.00	0.00	0.00
Al	4.16	4.20	4.16	4.16	4.20	4.16	4.08	4.12
Fe	0.04	0.08	0.12	0.12	0.04	0.08	0.04	0.12
Mn	0.00	0.00	0.00	0.00	0.00	0.00	0.00	0.00
Mg	0.00	0.08	0.08	0.04	0.00	0.04	0.00	0.12
Ca	0.04	0.04	0.08	0.04	0.04	0.04	0.00	0.00
Na	4.04	3.92	3.84	3.92	3.96	4.00	3.98	3.88
K	0.00	0.04	0.08	0.12	0.00	0.00	0.00	0.08
Total Cat.	20.12	20.12	20.04	20.16	20.00	20.08	20.38	20.18
	End member of the plagioclase minerals as below							
An	1.00	1.00	2.00	0.98	1.00	0.99	0.00	0.00
Ab	99.00	98.00	96.00	96.00	99.00	99.00	100.00	97.97
Or	0.00	1.00	2.00	0.98	0.00	0.00	0.00	2.02

FeO* is total iron as FeO.

Table 33. Composition of clinopyroxenes

Sm.N	414 core	414 rim	414 core	414 rim	414 core	414 rim	414 core	414 rim	414	414
SiO_2	50.50	50.80	50.36	53.57	52.84	51.19	52.40	50.49	52.86	50.28
TiO_2	1.20	1.40	1.39	0.93	0.60	1.06	0.61	1.37	0.73	1.47
Al_2O	2.87	2.59	2.46	2.48	1.52	2.50	1.65	2.21	1.68	2.43
FeO*	9.06	11.89	11.66	13.28	8.86	9.21	8.53	11.08	8.44	13.03
MnO	0.22	0.21	0.19	0.21	0.23	0.28	0.21	0.23	0.28	0.30
MgO	15.18	14.60	14.96	11.73	16.87	15.75	16.80	14.12	16.40	13.08
CaO	19.80	17.74	18.42	16.21	18.36	19.29	18.70	19.14	19.15	19.30
Na_2O	0.32	0.50	0.49	0.32	0.30	0.43	0.43	0.37	0.29	0.43
K_2O	0.00	0.06	0.00	0.33	0.04	0.05	0.00	0.00	0.01	0.10
Total	99.15	99.79	99.93	99.06	99.62	99.76	99.33	99.01	99.84	100.42
	Recalculated to 6 oxygens									
Si	1.90	1.90	1.88	2.05	1.94	1.89	1.93	1.90	1.95	1.88
Ti	0.04	0.04	0.04	0.03	0.02	0.03	0.02	0.04	0.02	0.04
Al	0.13	0.12	0.10	0.11	0.07	0.11	0.07	0.10	0.07	0.11
Fe^{+3}	0.05	0.04	0.09	0.00	0.02	0.06	0.04	0.04	0.00	0.07
Fe^{+2}	0.23	0.33	0.27	0.43	0.26	0.22	0.22	0.31	0.26	0.33
Mn	0.01	0.01	0.01	0.01	0.02	0.01	0.01	0.01	0.01	0.01
Mg	0.84	0.81	0.83	0.67	0.93	0.87	0.92	0.79	0.89	0.73
Ca	0.79	0.71	0.73	0.67	0.72	0.76	0.74	0.77	0.76	0.79
Na	0.02	0.04	0.04	0.02	0.02	0.03	0.03	0.03	0.02	0.03
K	0.00	0.00	0.00	0.02	0.00	0.00	0.00	0.00	0.00	0.01
Total	4.00	4.00	4.00	4.00	4.00	4.00	4.00	4.00	4.00	4.00
	End member of the clinopyroxene minerals as below									
Wo	41.117	37.35	37.99	37.64	37.52	39.68	38.24	40.20	39.26	40.29
En	43.842	42.75	42.92	37.88	47.96	45.06	47.78	41.24	46.76	37.97
Fs	15.042	19.89	19.08	24.46	14.51	15.25	13.96	18.55	13.97	21.73

Fe+3 is calculated by normalization according to Schumacher (1991).

Table 34. Composition of white micas

Sm. No	414	414	414	417	417	417	417
SiO_2	47.63	43.75	48.70	48.37	48.76	49.02	48.45
TiO_2	0.14	0.10	0.19	0.05	0.19	0.14	0.18
Al_2O_3	25.92	24.18	24.71	27.91	25.50	28.23	25.46
Fe_2O_3	5.31	8.05	5.98	3.82	5.12	4.09	5.70
FeO	0.84	1.28	0.95	0.61	0.81	0.65	0.91
MnO	0.00	0.00	0.07	0.00	0.04	0.01	0.04
MgO	3.94	7.34	4.23	2.40	2.86	2.81	3.50
CaO	0.25	0.63	0.04	0.02	0.05	0.05	0.08
Na_2O	0.20	0.45	0.15	0.11	0.02	0.21	0.33
K_2O	9.14	9.38	10.73	11.10	11.01	10.73	10.19
Total	93.37	95.06	95.75	94.39	94.36	95.94	94.84
	Recalculated to 22 oxygens						
Si	6.53	6.11	6.60	6.57	6.66	6.54	6.59
Ti	0.02	0.01	0.02	0.05	0.02	0.01	0.02
Al^6	1.47	1.88	1.40	1.42	1.33	1.46	1.40
Al^4	2.72	2.10	2.54	3.04	2.78	2.98	2.67
Fe^3	0.54	0.84	0.61	0.39	0.52	0.41	0.58
Fe^2	0.10	0.15	0.18	0.07	0.09	0.07	0.10
Mn	0.00	0.00	0.00	0.09	0.01	0.00	0.01
Mg	0.80	1.53	0.85	0.48	0.58	0.55	0.71
Ca	0.04	0.09	0.01	0.00	0.01	0.01	0.01
Na	0.05	0.12	0.04	0.03	0.01	0.05	0.09
K	1.60	1.32	1.86	1.92	1.92	1.83	1.77
Total	13.87	14.17	14.04	13.95	13.94	13.94	13.95
	End member of the white mica minerals as below						
Mus	79.90	65.85	92.75	96.20	96.05	91.35	88.45
Par	2.65	6.10	1.95	1.45	0.25	2.70	4.35
Mar	1.85	4.70	0.30	0.15	0.35	0.35	0.60

Fe^{+3} is calculated by ratio according to Schumacher (1991).

5.8. LORASDAGI FORMATION

These grey limestones consist of medium to coarse grained , calcite, and detrital grains such as quartz and Fe-oxide. The matrix grain size varies from a fine to coarse grain size. Micrite grains have increased in size due to recrystallization. Anhedral, interlocking crystals exhibit a polygonal texture Equant calcite crystals occur in fossil cavities as a cement.

5.9. OSMANKAYASI TEPE FORMATION

These cream, grey limestones have a micrite matrix. Microcrystalline calcite is found mainly in the groundmass. Calcite and clay are the dominant cement inside the fossil cavities. Needle-like and micrite grains act as cement. The needle-like grains of calcite line fossil cavities, whereas the micrites randomly fill fossil cavities. The masses of dark cryptocrystalline calcite are not completely homogeneous. Secondary sparry calcite has precipitated around the fossils. Some Fe-oxide pigments occur in the rims of the fossils.

5.10. DACITE

This rock contains phenocrysts of plagioclase 25-40%, quartz 20-25%, amphibole 15-20%, biotite 5-8%, sanidine up to 5-7% , oxides 2-3% and accessory sphene and apatite with a groundmass which is microcrystalline and equiqranular, cryptocrystalline and glassy .

Feldspar phenocrysts display oscillatory and reverse zoning with An_{50-30} Ab_{50-70} Or_{2-5} and Or_{75-40} Ab_{25-60} An 2-8, the latter being sanidine composition (Table 35, Figure, 21). Phenocrysts are mainly andesine in composition and the groundmass microcrystals are sanidine. Some phenocrysts have sieve texture (Plate, 16). previous studies have suggested that sieve texture in plagioclase results from the reaction of sodic feldspar becoming more calcic (Kuno, 1950; Anderson, 1976, Nixon and Pearce, 1987).

Zoning in plagioclase phenocrysts can be divided into fine-scale oscillatory zoning and larger -scale compositional shifts superimposed on fine-scale patterns. Fine scale zoning is thought to be controlled by the interplay of growth and diffusion rates in compositional and thermal boundary layers (unrelated to magma mixing) surrounding individual

crystals (Sibley et al., 1976; Kuo and Kirkpatrick, 1982; Loomis, 1982; Pearce and Kolisnik, 1990).

Sanidine in dacite is invariably rounded, embayed and mantled by plagioclase. Quartz is similarly rounded and embayed.

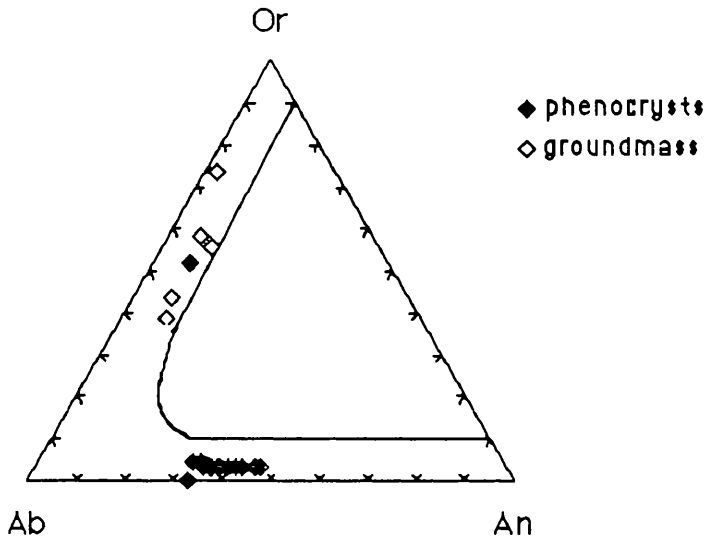

Figure 21. Composition of feldspar.

Hornblende is the second most abundant phenocryst phase (Table 36). It occurs as subhedral to anhedral crystals (4mm) and exhibits olive-green to pale brown pleochroism. Thin opaque rims, presumably formed by oxidation on extrusion, are found on many crystals and locally Fe-Ti oxides appear to have replaced entire phenocrysts. Inclusions within amphibole are plagioclase, magnetite, biotite, apatite, and rare zircon. Amphiboles are magnesio-hornblende, titanian pargasite, edenitic hornblende and magnesio-hastingsite (Leake,1978). The compositions are typical of amphiboles occuring in orogenic dacites (Jakes &White,1972; Ewart, 1979, 1982).

Biotite forms subhedral phenocrysts (2mm), with green to dark coffee brown pleochroism where oxidized. Breakdown of biotite forms opaque oxides rimmed or replaced by fine-grained intergrowths rich in titanomagnetite and amphibole. Analyses of biotite phenocrysts show relatively high TiO_2 and a uniformly magnesian composition as shown in Table 37.

Phenocrysts of magnetite (Table 37) (up to 0.5mm) are subhedral to anhedral whereas microphenocrysts are euhedral; some of the anhedral crystals are xenocrysts. Apatite and Fe-Ti oxides occur as inclusions.

Table 35. Composition of feldspars

An.Sp	271 rim	271 middle	271 core	271 pheno	271 pheno	271 pheno	271 microl	271 microl
SiO_2	57.33	59.84	60.29	59.21	71.43	59.81	57.55	67.84
TiO_2	0.30	0.03	0.04	0.04	0.07	0.05	0.04	0.08
Al_2O_3	27.14	24.85	24.74	25.61	17.68	25.98	27.00	18.63
FeO*	0.23	0.19	0.20	0.16	0.45	0.27	0.34	0.29
MnO	0.00	0.00	0.00	0.02	0.03	0.00	0.00	0.00
MgO	0.01	0.01	0.00	0.11	0.20	0.06	0.00	0.03
CaO	9.52	7.42	7.10	7.47	2.68	7.73	9.44	0.11
Na_2O	6.09	7.29	7.20	7.06	4.56	6.84	5.74	2.80
K_2O	0.53	0.67	0.67	0.63	3.06	0.58	0.53	12.66
TOTAL	101.15	100.30	100.24	100.31	100.16	101.32	100.64	102.44
Recalculated to 32 Oxygens								
Si	10.19	10.62	10.69	10.57	10.41	10.56	10.27	10.41
Ti	0.00	0.00	0.00	0.00	0.00	0.00	0.00	0.01
Al	5.79	5.32	5.29	5.42	3.56	5.40	5.68	3.56
Fe	0.03	0.03	0.03	0.02	0.07	0.04	0.05	0.04
Mn	0.00	0.00	0.00	0.00	0.00	0.00	0.00	0.00
Mg	0.00	0.00	0.00	0.02	0.05	0.01	0.00	0.00
Ca	1.78	1.38	1.32	1.38	0.52	1.46	1.80	0.14
Na	2.06	2.47	2.43	2.36	1.60	2.34	1.98	0.99
K	0.11	0.15	0.15	0.01	0.70	0.13	0.12	2.87
Total Cat	20.00	20.01	19.94	19.96	19.95	19.96	19.93	19.95
End member of the plagioclase minerals								
An	44.40	34.23	33.2	35.33	12.50	36.60	44.78	0.50
Ab	51.50	60.97	60.09	60.37	38.40	58.50	49.35	24.10
Or	3.00	3.60	3.70	3.53	17.00	3.30	3.07	71.80

FeO* is total iron as FeO.

Table 36. Composition of amphiboles

Sample No	271 Edh	271 Tipg	271 Mghast	271 Parg.horn
SiO_2	42.40	41.57	41.75	43.76
TiO_2	1.40	2.30	2.33	2.10
Al_2O_3	9.52	13.30	13.27	12.60
FeO*	17.78	11.10	9.57	13.39
MnO	0.50	0.00	0.24	0.20
MgO	10.30	14.00	14.70	10.76
CaO	11.80	11.60	11.00	10.26
Na_2O	1.40	2.32	2.10	1.86
K_2O	1.10	1.00	1.00	1.49
TOTAL	96.20	97.19	95.96	96.42
Recalculated to 23 Oxygens				
Si	6.55	6.18	6.09	6.46
Al^{+4}	1.44	1.81	1.90	1.53
AlT	1.69	2.27	2.22	2.24
Al^{+6}	0.25	0.46	0.32	0.70
Ti	0.16	0.25	0.25	0.23
Fe^{+3}	0.55	0.40	0.67	0.31
Mg	2.31	3.03	3.33	2.42
Fe^{+2}	1.68	0.94	0.46	1.61
Mn	0.06	0.00	0.03	0.02
FMT	13.04	13.09	13.07	13.01
Ca	1.91	1.80	1.84	1.66
NaM4	0.05	0.10	0.08	0.32
NaT	0.41	0.65	0.58	0.54
NaA	0.36	0.55	0.49	0.29
K	0.21	0.18	0.18	0.47

Fe^{+3} is calculated by estimation according to Spear and Kimball (1984)

Edh: Edenitic hornblende Tipg: Titanian-pargasite Mghast:magnesio hastingsite Parg horn: Pargasitic hornblende.

Table 37. Composition of biotite and magnetite minerals

Sample No	271	271	271	271
SiO_2	37.00	37.16	0.30	0.40
TiO_2	4.21	4.23	2.94	3.60
Al_2O_3	14.50	14.70	1.77	1.30
Fe_2O_3	3.50	3.43	64.00	62.39
FeO	15.85	15.51	23.40	32.40
MnO	0.35	0.33	0.97	0.80
MgO	11.36	11.36	0.65	0.97
CaO	0.01	0.05	0.15	0.00
Na_2O	0.36	0.48	2.17	0.15
K_2O	9.50	9.49	0.08	0.00
TOTAL	96.64	96.74	96.43	101.65
Recalculated to 22 oxygens for biotite, 32 oxygens for magnetite				
Si	5.49	5.50	0.01	0.01
Ti	0.45	0.50	0.08	0.09
Al	2.47	2.49	0.07	0.05
Fe^{+3}	0.38	0.37	1.9	1.72
Fe^{+2}	2.16	2.11	0.70	1.01
Mn	0.04	0.04	0.03	0.02
Mg	2.66	2.65	0.03	0.05
Ca	0.00	0.01	0.00	0.00
Na	0.10	0.13	0.15	0.01
K	1.76	1.74	0.00	0.00
Total Cation	15.55	15.54	3.00	3.00
End member of the biotite and magnetite minerals as below				
Phlogopite	15.55	15.54	Sp	4.66	2.95
Annite	44.76	44.60	Mt	94.97	89.21
			Mg-Fer.	0.00	2.61

Fe^{+3} is calculated by ratio according to Schumacher (1991).

Compositions of the hornblende can be used to estimate the pressure of formation of granitic rocks (Johnson and Rutherford, 1989). If the same calibration apply to dacites, the results indicate a pressure of 6-7 Kbar. The crystallization temperatures obtained from hornblende-plagioclase geothermometers suggest that the temperature was 743 (+75)°C to 789 (+75)°C (Blundy and Holland, 1990).

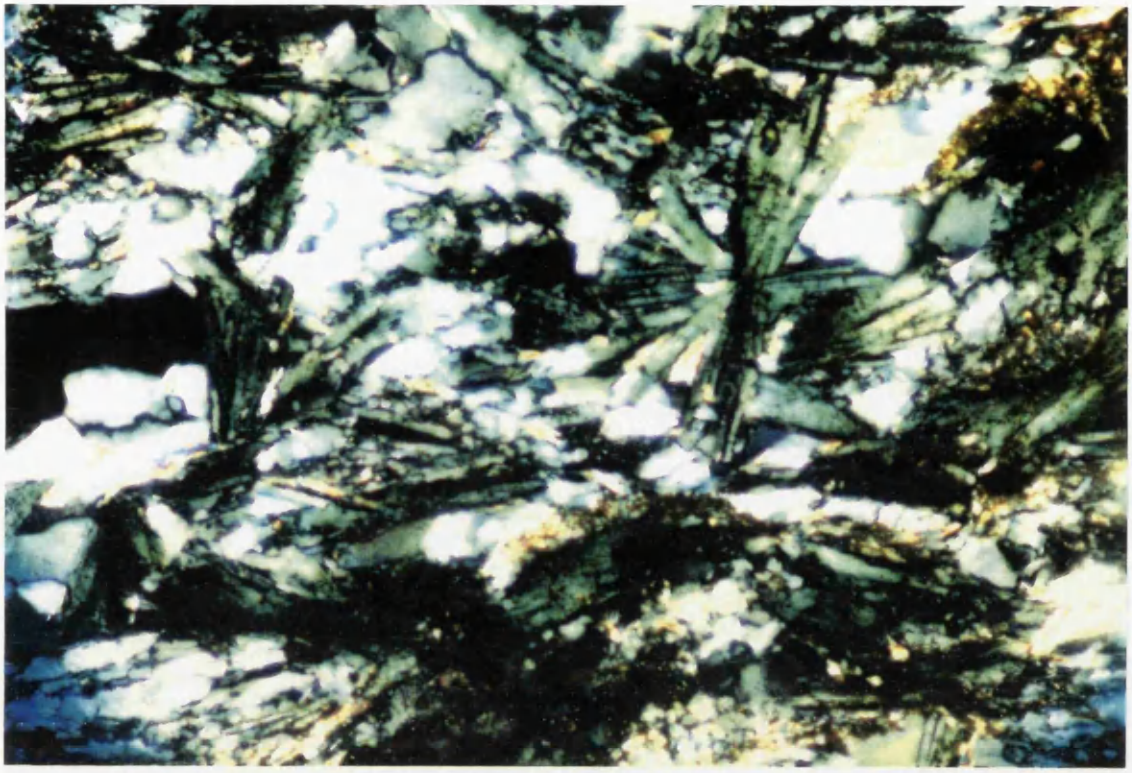

Plate.10. Photomicrograph of pelitic rock. Post-tectonic chloritoid rosette preserving relict foliation. No disequilibrium textures between chloritoid and quartz can be observed. Matrix minerals are quartz and chlorite. [Crossed Nicols] X 10.
Sample 237, Locality (34750-33500), Bagrikurt Formation.

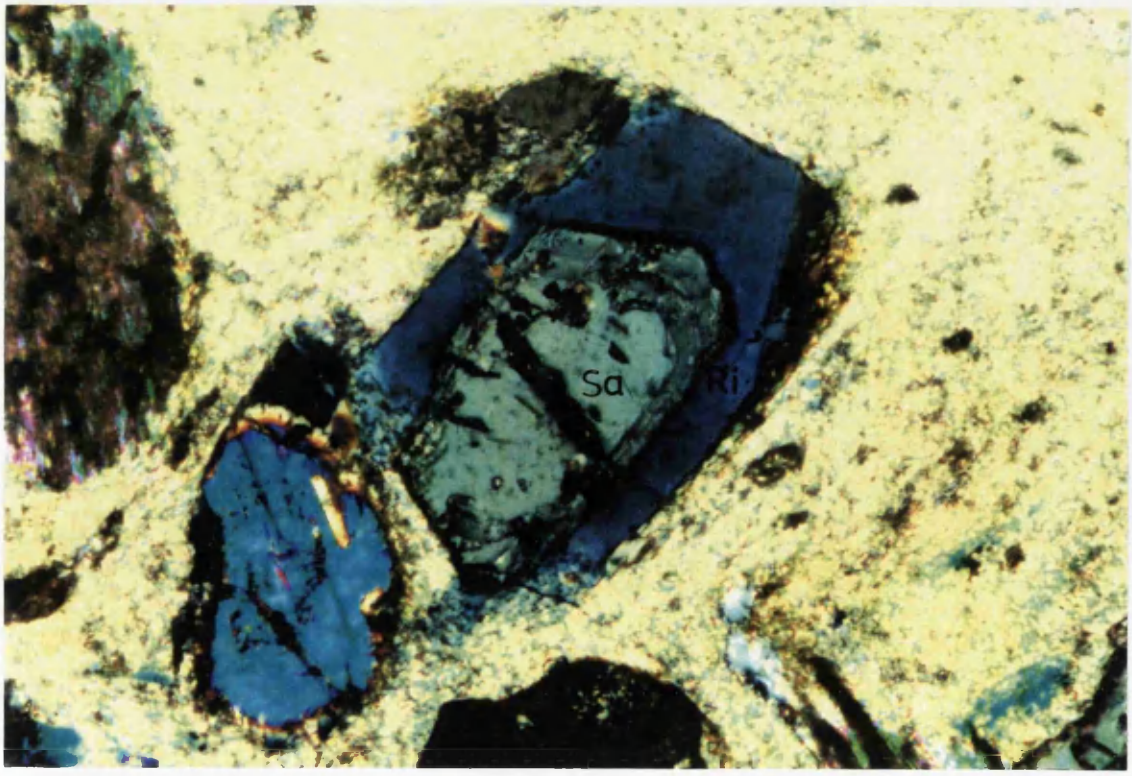

Plate.11. Photomicrograph of metatrachyandesite showing salite surrounded by riebeckite mineral [Crossed Nicol] X.10. Sample 373, Locality (33050-32275)
Sa: salite, Ri: riebeckite.

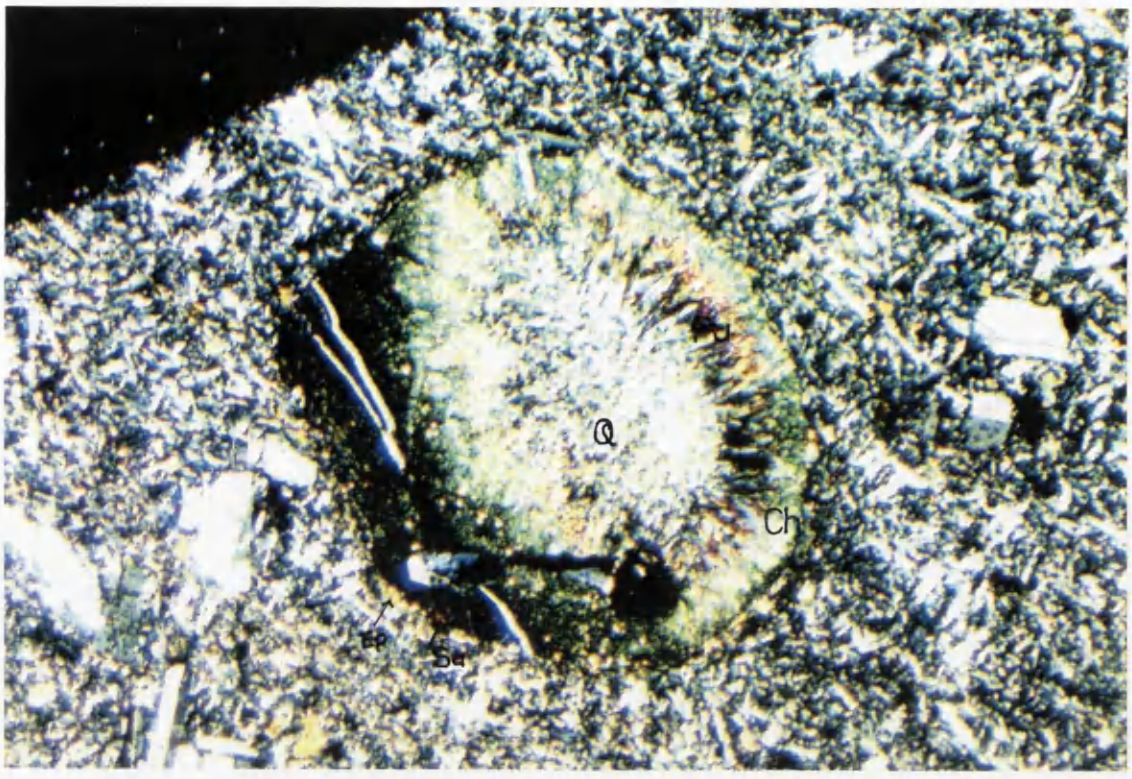

Plate.12. Photomicrograph of metatrachyandesite. Pumpellyite aggregates surrounded by epidote, chlorite, salite and quartz minerals. The central of the amigdaloid is quartz. [Crossed Nicol] X2.5. Sample 183, Locality(33050-32300).
Q: quartz, Pu: pumpellyite, ch: chlorite, Ep: epidote, Sa: salite.

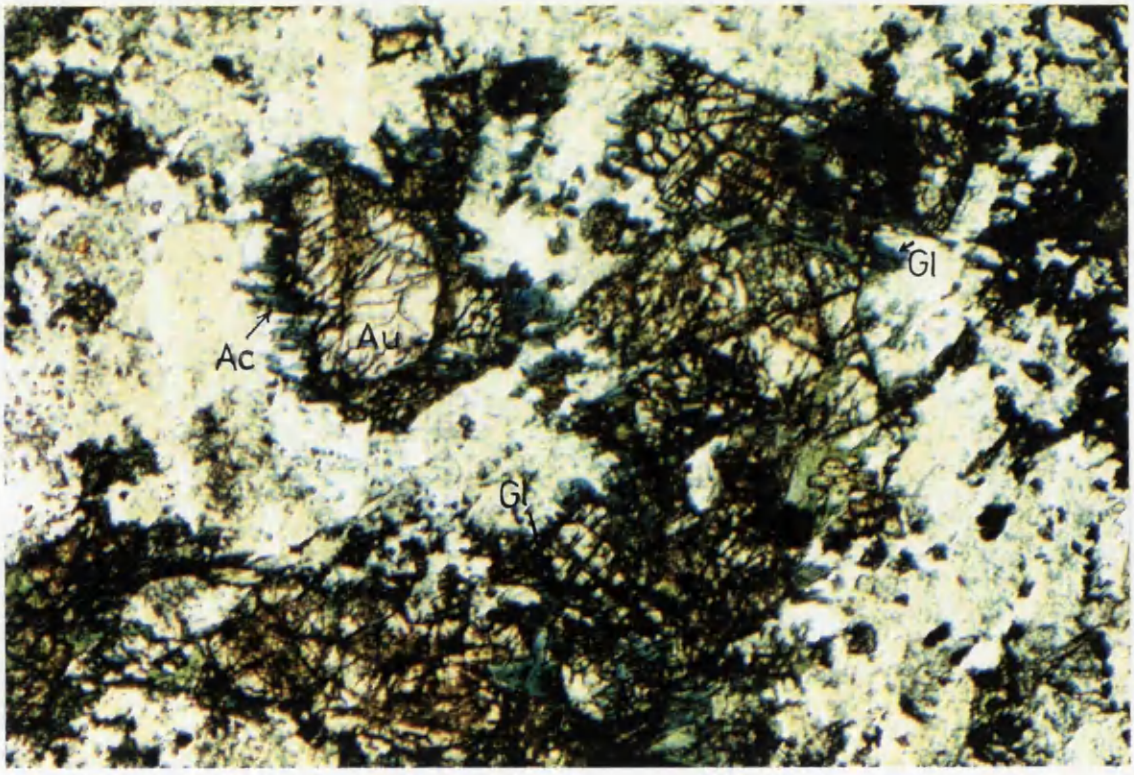

Plate.13. Photomicrograph of metabasaltic andesite. Augite porphyroblast with glaucophane and fibrous actinolite rim. [Plane-polarized] X 2.5.Sample 408, Locality (40550-17450). Gl: glaucophane, Ac: actinolite, Au: augite.

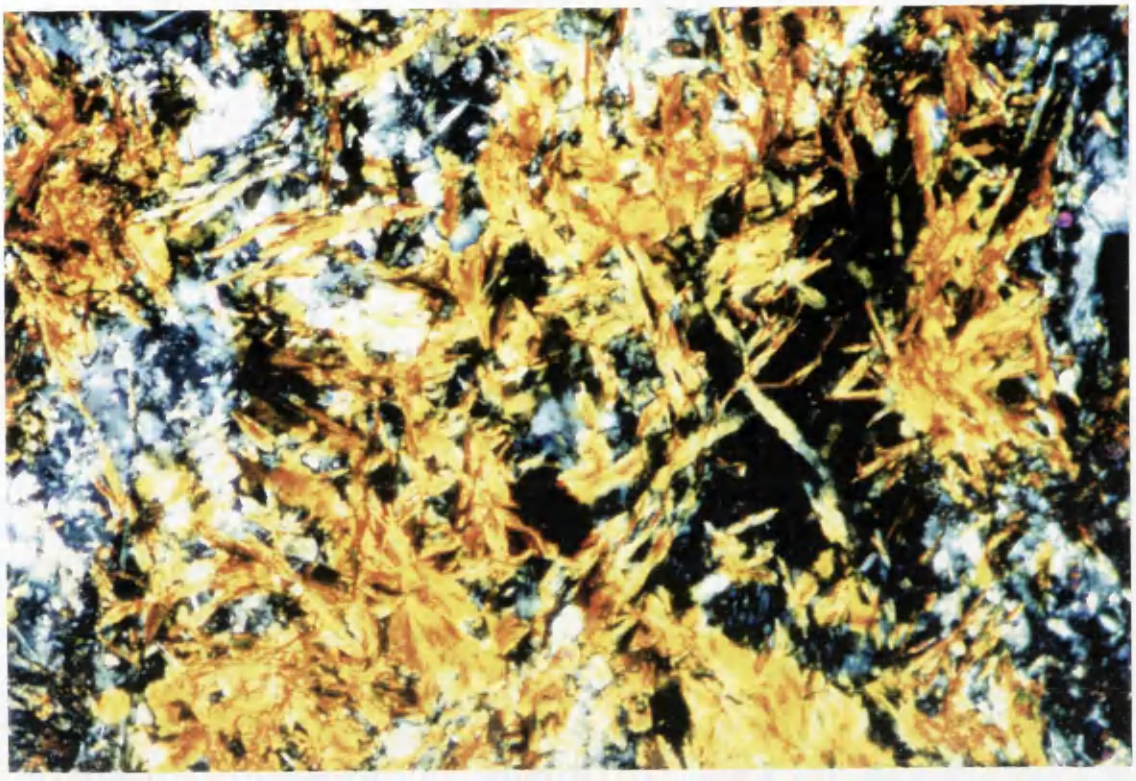

Plate.14. photomicrograph of metabasaltic andesite showing aggregates of stilpnomelane. [Crossed Nicol] X10. Sample 364, Locality (39900-17275).

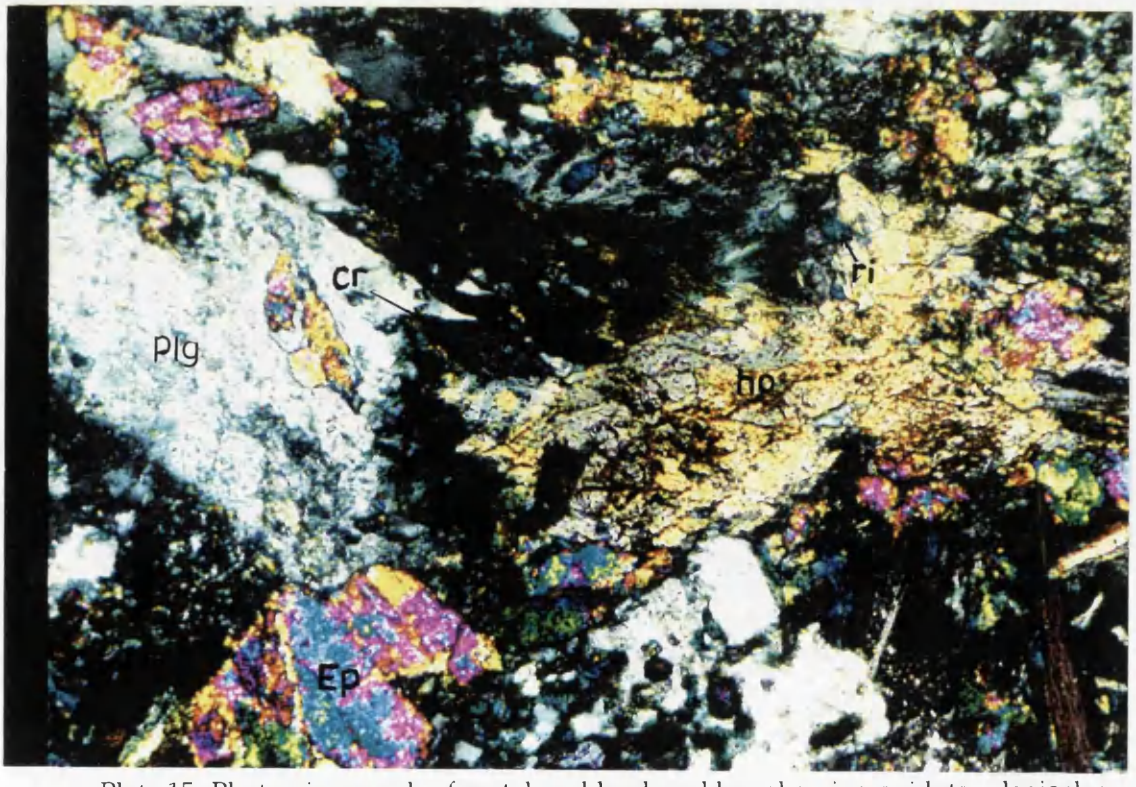

Plate.15. Photomicrograph of metahornblende gabbro showing epidote, plagioclase, quartz, chlorite and hornblende which was replaced by crossite and riebeckite [Crossed Nicols] X 2.5. Sample 379, Locality (37250-28550).
Plg: Plagioclase, cr: Crossite, ri: riebeckite, ho: hornblende, Ep: epidote.

Plate.16. Photomicrograph of dacite showing sieve texture [Crossed Nicol] X2.5. Sample 265, Locality (39200-12950).

VI - GEOCHEMISTRY

153 rock samples have been analyzed for major and trace elements, 12 metapelitic rocks, 10 metabasic schists, 18 Calc silicate rocks, 16 carbonate rocks, 18 psammite, 10 quartzites, 8 metacherts, 20 metahornblende gabbros, 4 metadolerites, 9 metabasaltic andesites, 14 metatrachyandesites, and 14 dacites. 18 rock samples have been analyzed for REE elements, 2 metahornblende gabbros, 2 metadolerites, 2 metatrachyandesites, 2 metabasaltic andesites, 2 dacites, 1 psammite, 1 quartzite and 6 metacherts.

The majority were analyzed by a Philips PW 1450 sequential X-ray fluorescence (XRF) spectometer with an on - line microcomputer for data processing at the Department of Geology & Applied Geology, Glasgow University. A few samples were analysed for REE by ICP methods and Instrumental Neutron Activation Analysis at the Scottish Universities Research and Reactor Centre (by Nuclear Activation Services) (see chapter 2).

6.1. PSAMMITE AND QUARTZITE

The chemical compositions of the psammites and quartzites are given in Tables 38, 39, 40.

The Pettjohn et al. (1972) diagram as modified by Herron (1988) classifies sandstones using the ratios Log (Fe_2O_3/K_2O) and Log (SiO_2/Al_2O_3).

The quartzites with 90-98 wt % SiO_2 and the psammites with 76-89 wt % SiO_2 are mostly litharenites (Fig. 22) by Herron's (1988) method.

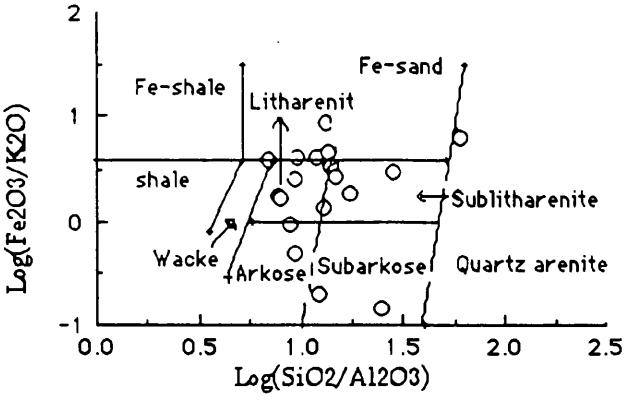

Fig. 22 Classification of psammites after Herron (1988).

Major and trace element variations are shown on Harker variation diagrams (Fig. 23). This suggests a strong input of detrital acidic igneous rock or re-worked sandstone or quartzite with concentration and depletion of resistant zircon into certain almost quartz - pure layers. Such a situation is typical of many beach sands with mechanical and chemical destruction of all but the most resistant minerals.

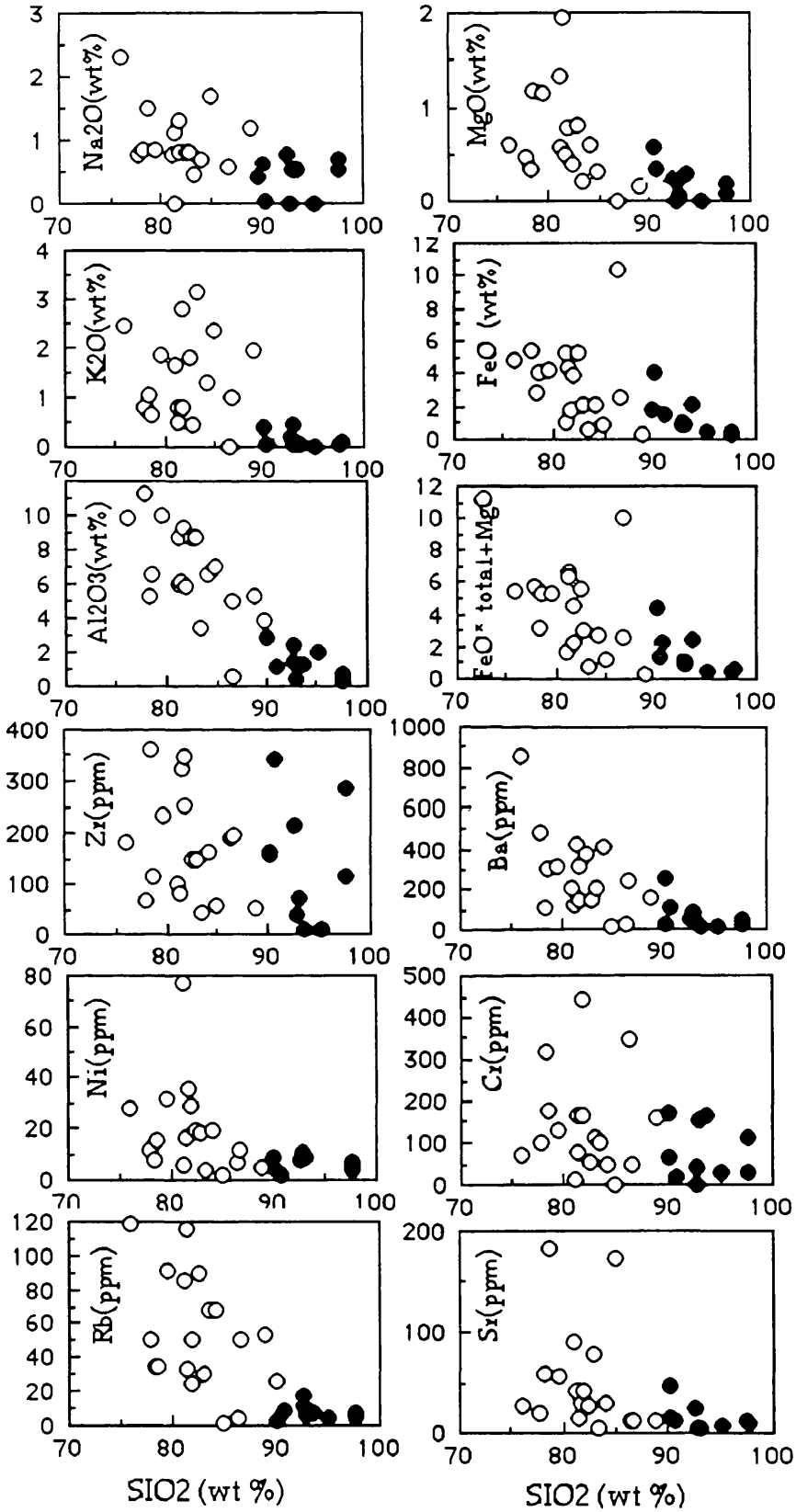

Fig. 23. Harker variation diagrams of the some major oxides and some trace elements for psammite (○) and quartzite (●).

Niggli numbers have been used by Van de Kamp et al. (1976) and Van de Kamp and Leake (1985) in geochemical provenance studies of

unconsolidated sand and sandstones. As pointed out by the authors Niggli numbers eliminate the effect 'of the closed array' where quartz (predominately SiO_2) is the dominant mineral in sandstones. Niggli values are based on the molecular proportions of Al_2O_3, CaO, FeO_{tot} +MgO+MnO and Na_2O+K_2O independent of the value of SiO_2 (Niggli, 1954).

Niggli mg vs Niggli si (Fig. 24) shows si enrichment exceeding that formed in igneous rocks, i, e. these clastic sediments extend outside the igneous field which was separated by Van de Kamp and Leake , (1985).

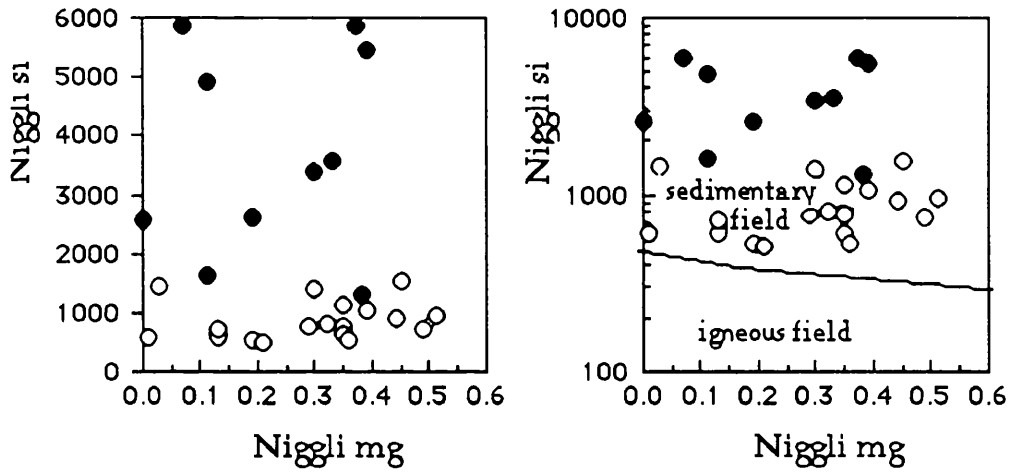

Fig. 24. Plot of Niggli mg vs Niggli si for psammite (○) and quartzite (●).

Niggli al-alk has been shown by Van de Kamp and Leake (1985) to be a good measure of the abundance of original clay mineral in a sediment and also that many trace and some major elements are largly fixed in clay minerals in typical sediments. Fig. 25 shows that Cr, Zr, Th, Sr and Niggli ti and other elements show no correlation with al-alk. The lack of positive correlation of Zr and Ti with al-alk is particularly significant as these correlation are very strong in all shales (eg Senior and Leake, 1978). The chemistry indicates that detrital clay minerals (illite, montmorillonite) were probably not significant in these rocks, with Ti and Zr not being absorbed on clay minerals but probably added in resistant detrital grain like zircon and rutile.

Van de Kamp and Leake (1985) give typical values of >30 al-alk for shales and clay-rich rocks. The high al-alk values in the Kadinhani psammite reflect the high percentage of muscovite and the relativly low feldspar content (Ab and K- feldspar both have al-alk =0). The detrital

muscovite may be responsible for the rather high Cr values as Cr readily enter muscovite.

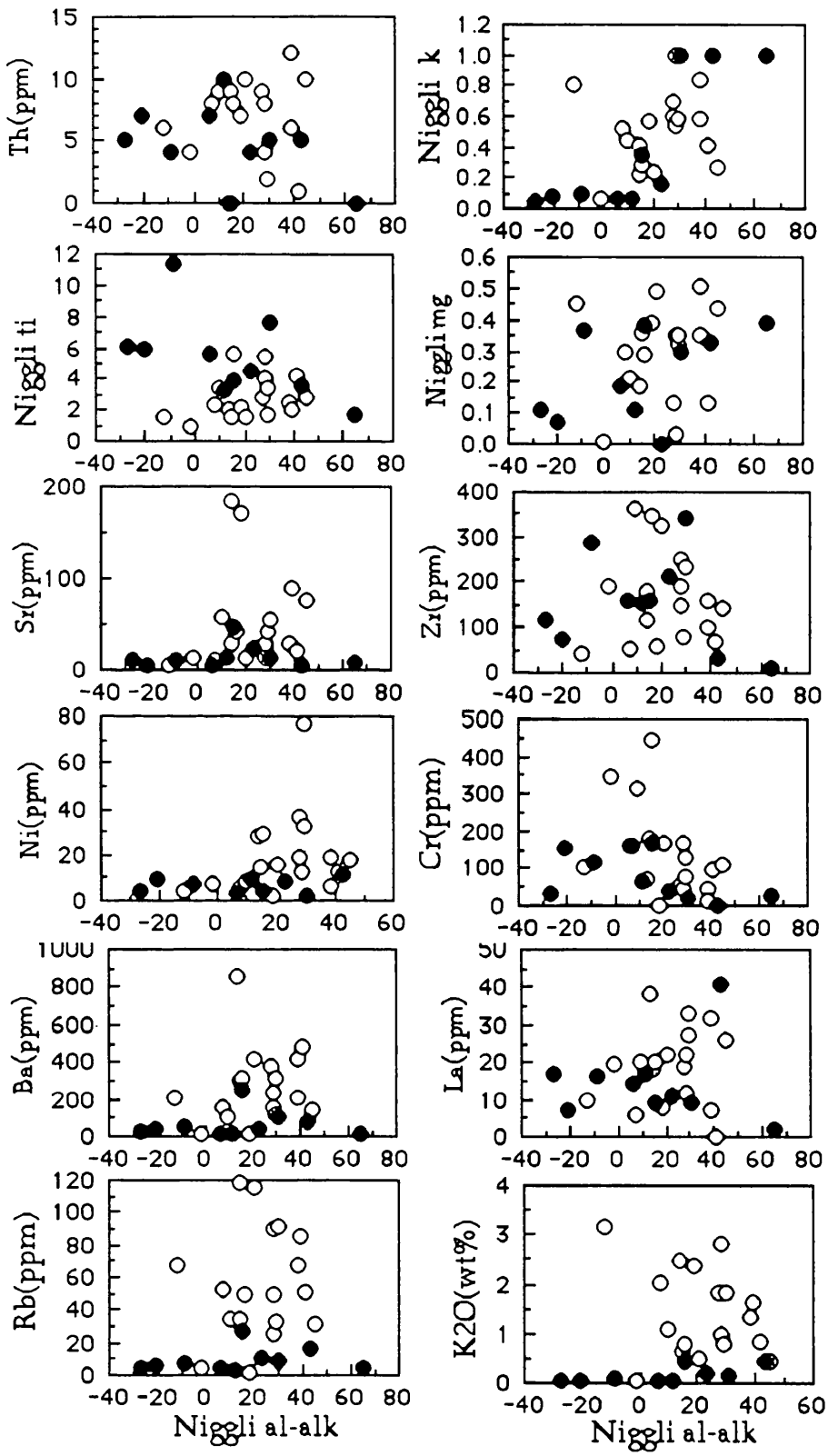

Fig. 25 . Major oxides and trace element values vs Niggli al-alk for psammite (○) and quartzite (●).

Al_2O_3 has positive correlation with Ga as is favoured by their similiar ionic radii and charges. Rb exhibit very good positive correlations with K_2O which indicates that both elements were in mica and K-feldspars (Fig. 26). FeO*(total) exhibits a good positive correlation with MgO (Fig. 26) which indicates that these elements are held in the mafic components although some Fe certainly came in magnetite minerals that are present in the rocks.

The association between Al and Ga is reflected in the high correlation between Al_2O_3 and Ga in both psammites and quartzite, Ga being widely distributed in all the Al-bearing minerals (Fig. 26).

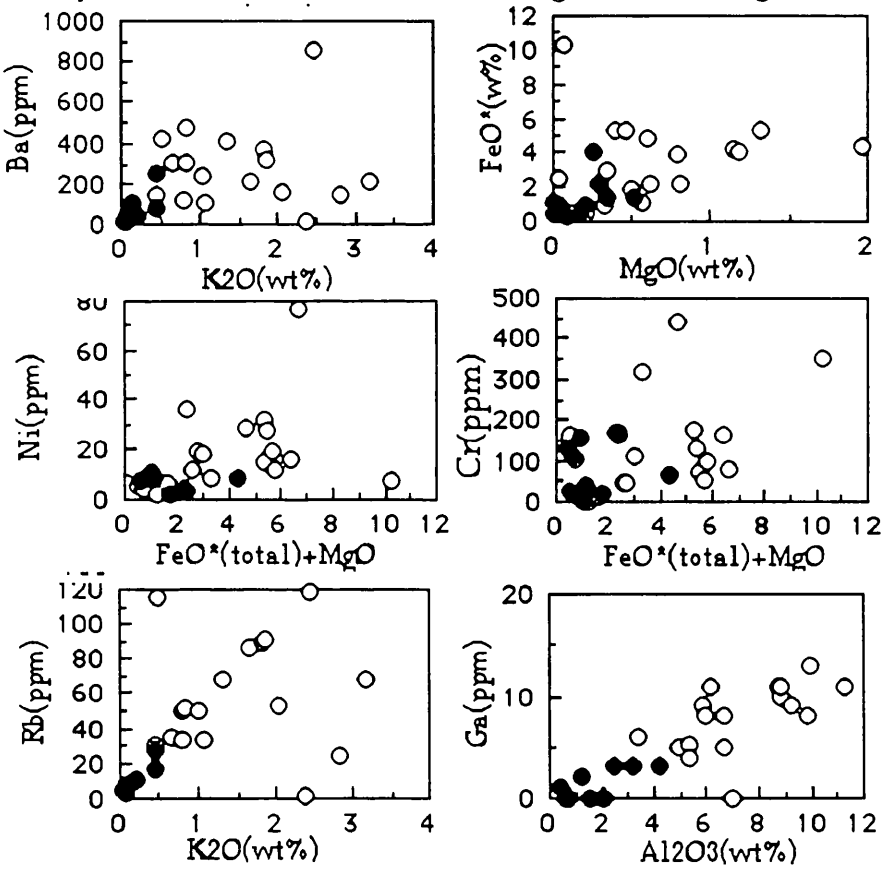

Fig.26. Major oxides and trace element plots for psammite (○) and quartzite (●).

Sr and La are low in the quartzite compared with the psammites. Sr is normally expected to be in plagioclase and carbonate in the sandstones. Ba, Ce and La are higher in the psammites, probably due to their concentrations in muscovite.

Tectonic Setting;

The chemical composition of sandstones in relationship to the tectonic setting of deposition has been studied by a number of authors

(Crook, 1974; Schwab, 1975; Maynard et al. 1982; Bhatia, 1983, Bhatia and Crook,1986). Clear chemical distinction is usually apparent between quartz-poor (58%-62%, SiO_2) intra-oceanic fore-arc sediments and quartz-rich (avg. 77%, SiO_2) passive margin, trailing-edge, sediments. However, subdivisions of active tectonic setting; strike slip orogens, active continental margins, and both continental and intra-oceanic back-arc basins, usually associated with intermediate-quartz (68% - 74%, SiO_2) sandstones show considerable overlap in both major and trace element geochemistry.

Bhatia (1983) has shown by the use of bivariate plots of selected geochemical parameters Log (K_2O/Na_2O vs SiO_2; Al_2O_3 /SiO_2 vs Fe_2O_3 + MgO and TiO_2 vs $Fe_2O_{3(total)}$ + MgO and of discriminant functions based on major element analyses, that sandstones of different sedimentary provenance and tectonic setting can be characterized geochemically. Bhatia (1983) noted that oceanic island arc sandstones dominantly derived from calc-alkaline andesites have higher abundance of TiO_2, Al_2O_3, Na_2O, and K_2O compared to sandstones. The continental island arc sandstones, dominantly derived from felsic volcanic rocks, have higher SiO_2, K_2O, and K_2O/Na_2O (=0.60) and lower $Fe_2O_{3(total)}$ +MgO than the oceanic island arc sandstones. The active continental margin sandstones are dominantly derived from the uplifted basement and reflect the composition of the upper continental crust in their higher SiO_2 and K_2O contents and K_2O/Na_2O =1. The passive margin type sandstones are significantly enriched in SiO_2 and depleted in Al_2O_3, TiO_2, Na_2O, and CaO and have a K_2O/Na_2O ratio >1. Although Roser and Korsch (1985) have criticized these criteria, Van De Kamp and Leake 1985 found that their results from the NE Pacific margin to be generally but not invariably compatible with those of Bhatia (1983).

When compared to the psammite and quartzite used in Bhatia's (1983) study, all the rocks consistently plot on the various diagrams (Fig. 27) in domains most closely related to the passive continental margin field or marginally fall into the active continental margin field (Fig, 27). On the discriminant function diagram (Fig. 28), the data give a clear indication of a passive margin type setting.

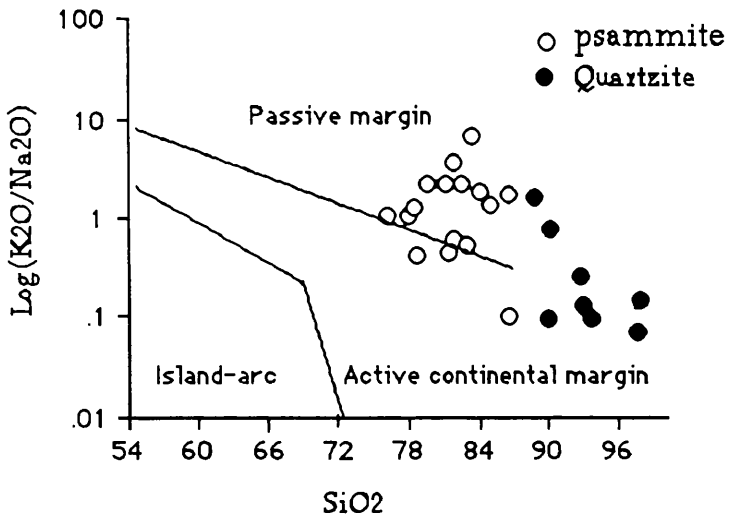

Fig. 27. Plot of log (K_2O/Na_2O)vs SiO_2 for quartzites and psammites , (after Bhatia, 1983).

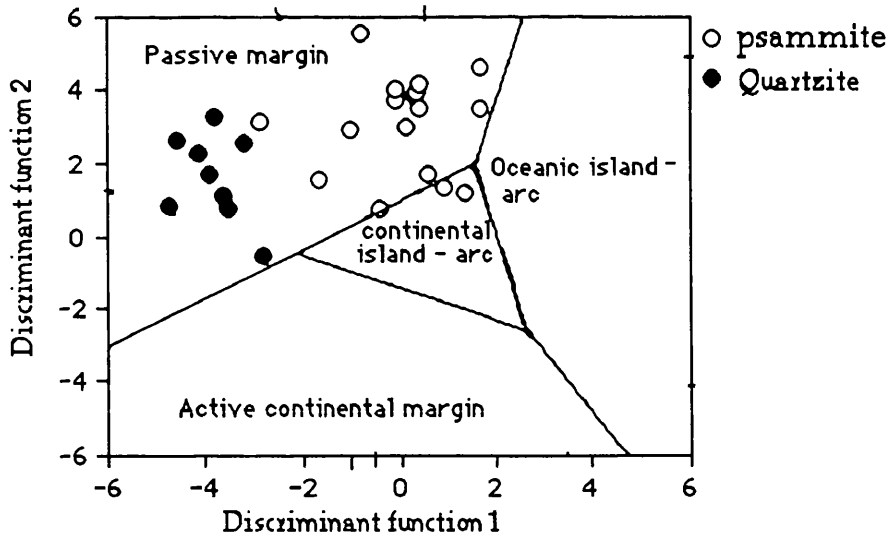

Fig. 28. Plot of discriminant functions F1 and F2 (as calculated by Bhatia, 1983) showing the position of psammites and quartzite.

When compared to the fields delimited by Roser and Korsch (1988), all rocks are of a quartzose sedimentary provenance source (Fig.29).

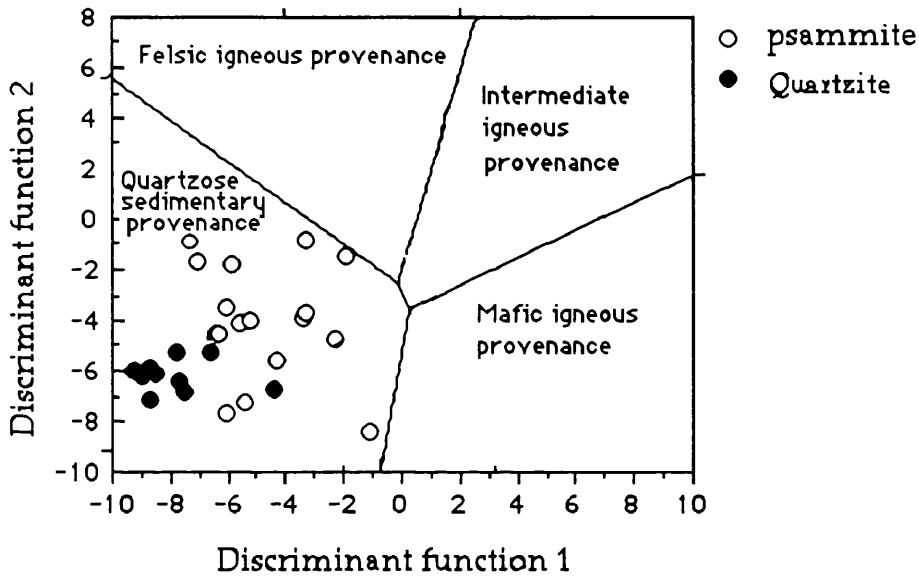

Fig.29. Plot of discriminant function F1 and F2 (as calculated by Roser and Korsch, 1988) showing the provenance of psammites and quartzite.

Relationship to general igneous trends;

The AFM diagram, with weight percent (Na_2O+K_2O), total Fe as FeO, and MgO, is widely used in studies of igneous rocks to display the distinctive enrichment trends (iron or alkali) of tholeiitic, alkaline and or, calc-alkaline suites. It has been shown by Robinson and Leake (1975) that sedimentary rocks have trends which mimic the alkali igneous enrichment trends, making the AFM diagram a relatively unsatisfactory tool to discriminate between metavolcanic and metasedimentary rocks in high grade metamorphic terranes. The psammites and quartzites define a trend similar to the alkali -rich trend of typical tholeiitic and calc-alkaline rocks on the AFM diagram (Fig. 30).

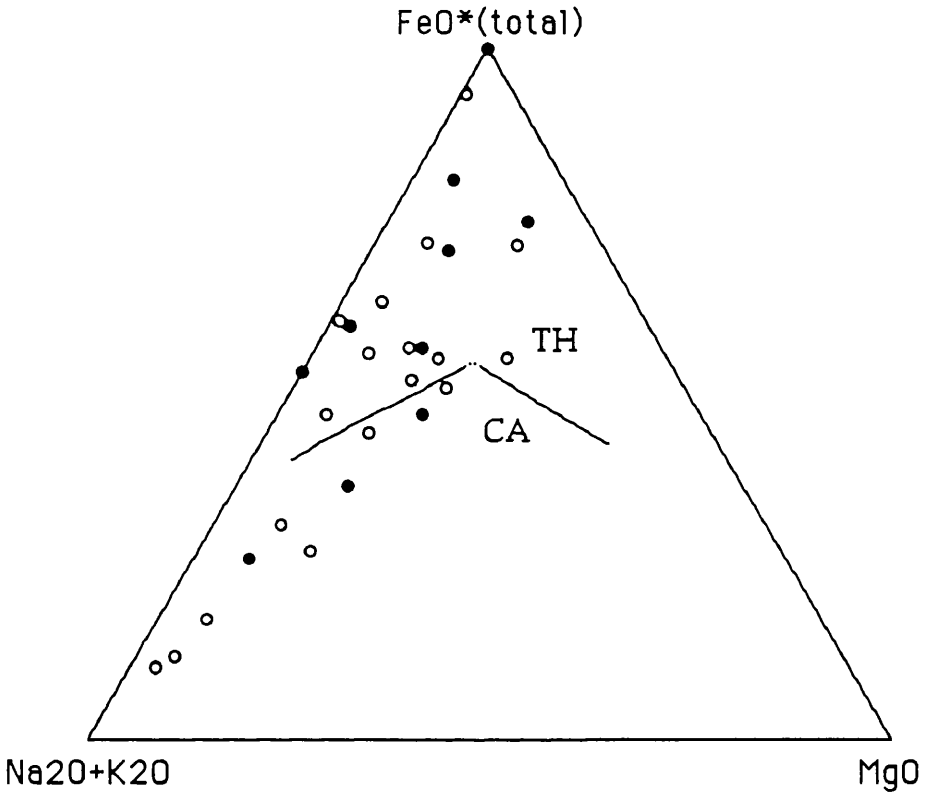

Fig.30. AFM diagram showing the distribution of psammite (○) and quartzite (●) from the study area compared to the general fields of tholeiitic (Th) and calk-alkaline CA) volcanic rocks.(after Robinson and Leake, 1975).

On the K_2O: Na_2O:MgO triangular diagram (Fig. 31), the majority of psammite show relative enrichment in K over Na compared to common acid igneous rocks, resulting in their plotting on the K_2O side of the igneous trend. The psammites and quartzite from the Kadinhani area can be interpreted from these diagrams as having either an acidic igneous source or be derived from re-worked sandstones or arkoses.

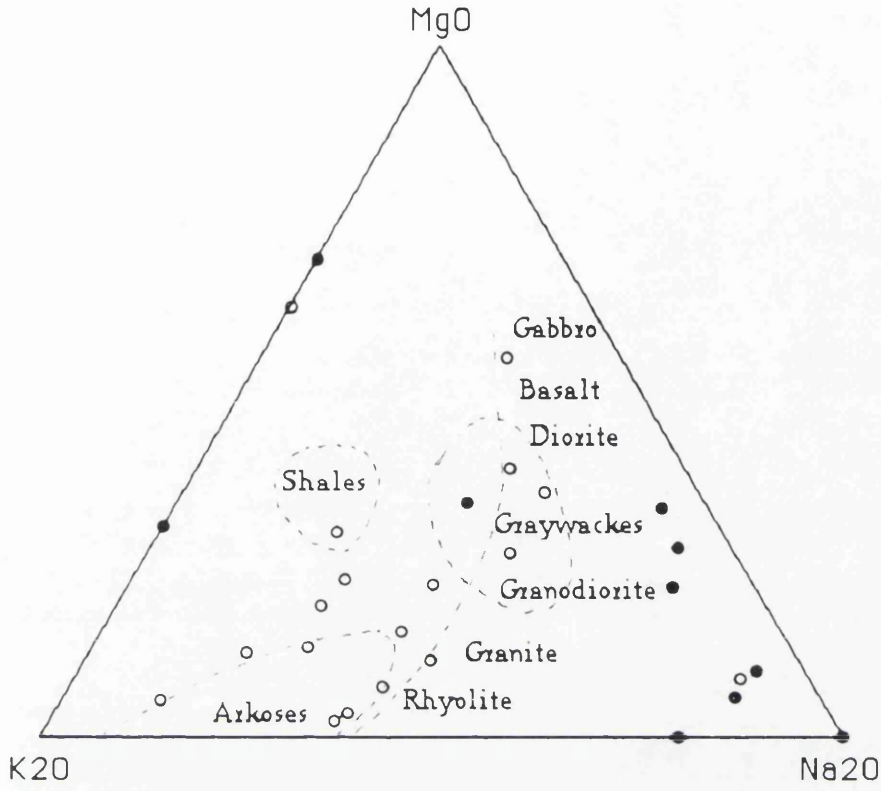

Fig.31. K2O:Na2O:MgO triangular diagram showing the trend of igneous rocks (after de la Roche, 1966), psammite (○) and quartzite (●)

Source material for the rocks;

Thorium has been shown to be immobile and enriched in deeply weathered soils (Kronberg et al. 1979). Probably the source terrain for the psammite and quartzite was low in Th (av. 7 for psammite, 5.9 for quartzite) compared to the average upper crustal value (10.7 ppm) recorded by Taylor and McLennan (1985). Low Th values may suggest that granitic detritus is low in these rocks. The La/Th ratios of the psammites and quartzite are 2.4 -2.6, in agreement with a value of 2.7 reported for the upper crust (McLennan et al., 1980), indicating the predominance of a felsic component in their source material (Fig. 32).

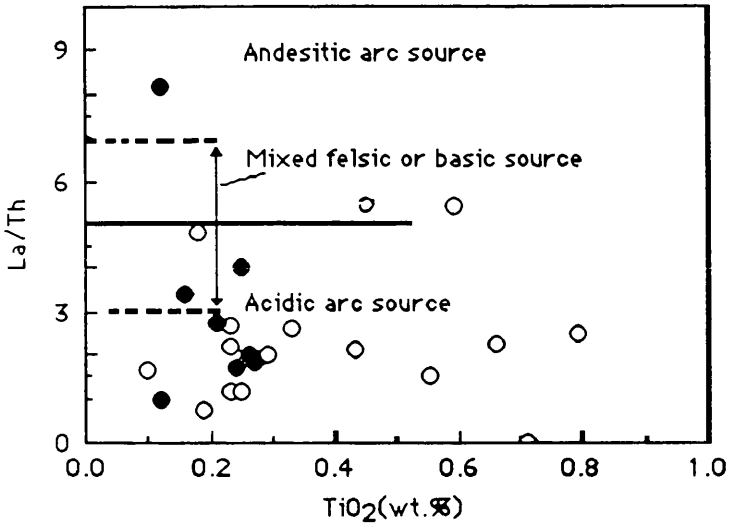

Fig. 32. La/Th vs. TiO_2 diagram showing the source of the Kadinhani psammite (○) and quartzite (●), (after Bhatia &Taylor, 1981; McLennan et al., 1984; Taylor & McLennan, 1985).

Rare earth elements;

The chondrite-normalized value of the psammites and quartzites from Kadinhani are plotted in Fig. 33 and are compared to the composite of N. American shales and upper continental crust (from Taylor et al., 1985). The REE patterns from the rocks are quite similar to NASC and upper continental crust REE patterns (Fig.33), but at lower concentrations due to the diluting effects of large volumes of quartz. The negative Eu/Eu* value is 0.63 for quartzite and 0.56 for psammites which are not significantly different from that obtained by Taylor et al., (1985) for a composite of N. American shales (0.70). The negative Eu anomalies may be interpreted as reflecting shallow, intracrustal differentiation resulting in Eu depletion in the upper crust, associated with the production of granitic rocks (McLennan, 1989).

The patterns remain very nearly parallel to each other and there is little difference between the quartzites and psammites, but the quartzites have lower Eu/Eu* and lower HREE than the psammites.

These REE characteristics are similar to cratonic sedimentary rocks. The general similarity of the REE patterns in the psammites and quartzites, variable LREE enrichment, Eu depletion and flat HREE reflect the sedimentary provenence. These indicate ultimate sediment sources dominated by granites with negative Eu anomalies (Taylor et al., 1986).

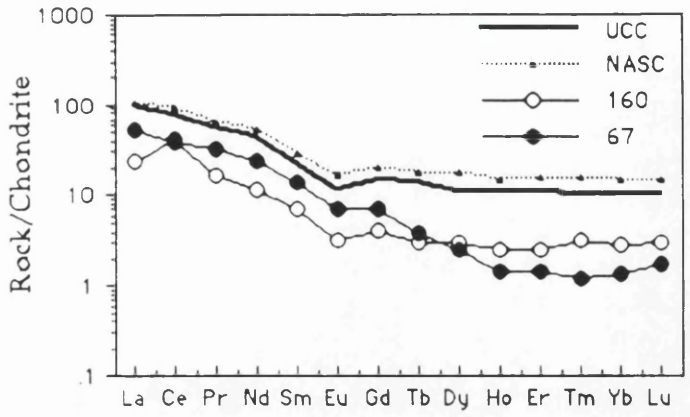

Fig. 33. Chondrite normalised REE patters for psammite (160) and quartzite (67) (UUC ;upper continental crust, NASC; North American shale composition) (after Boynton, 1984).

Table 38. Major and trace elements of psammites

Sa.NO	114	179	159	193	175	298	162	477	476	53
SiO_2	81.1	78.60	81.74	84.92	81.87	81.31	88.79	84.15	76.02	86.40
TiO_2	0.23	0.29	0.55	0.23	0.79	0.23	0.19	0.25	0.40	0.18
Al_2O_3	8.78	6.63	9.27	7.01	5.83	5.94	5.29	6.62	9.80	0.59
FeO	0.35	1.68	0.36	0.47	1.20	1.79	0.19	0.40	0.60	0.00
Fe_2O_3	0.80	2.59	1.52	0.48	2.75	3.69	0.21	1.77	4.32	10.22
MnO	0.01	0.05	0.03	0.02	0.03	0.01	0.0	0.03	0.02	0.30
MgO	0.57	1.18	0.50	0.32	0.78	1.32	0.12	0.61	0.60	0.06
CaO	0.02	3.36	0.08	0.03	1.21	0.00	0.03	0.08	0.00	0.0
Na_2O	0.76	1.49	0.80	1.71	1.31	0.00	1.25	0.70	2.31	0.59
K_2O	1.65	0.64	2.82	2.37	0.81	0.80	2.04	1.32	2.46	0.06
P_2O_5	0.15	0.06	0.05	0.05	0.03	0.02	0.01	0.06	0.08	0.05
CO_2	1.10	0.13	0.00	0.00	0.80	0.00	0.00	0.10	0.00	0.00
H_2O	3.13	2.00	2.10	1.90	3.15	1.33	2.50	1.63	1.96	0.35
TOTAL	98.5	98.7	99.8	99.5	100.6	96.4	100.6	97.2	98.6	100.8
Cr	12.	178	165	bdl	440	76	160	46	349	168
Co	2.	13	14	bdl	9	35	bdl	5	5	5
Ni	6	15	36	2	29	77	5	9	7	4
Cu	1	4	85	4	15	bdl	0	bdl	bdl	2
Zn	15	27	73	bdl	34	16	0	18	18	18
Ga	10	5	9	0	9	8	5	8	bdl	3
Rb	86	35	25	1	50	33	53	68	4	27
Sr	90	184	30	172	41	42	11	30	12	47
Y	8	17	17	6	16	18	12	10	12	0
Zr	99	116	251	59	349	81	54	162	190	161
Ba	205	304	150	10	308	117	1158	412	19	249
La	32	18	12	8	20	33	6	7	19	9
Ce	59	19	26	bdl	33	66	1	20.	30	16
Pb	9	3	8	1	8	9	9	7	3	9
U	bdl	bdl	bdl	bdl	bdl	3	bdl	1	0	5
Th	12	10	8	7	8	2	8	6	4	bdl

Coordinates of the analysed samples

114: 28020-23125
179: 30000-32500
159: 31700-33500
193: 28750-29750
175: 32825-33250
298: 33275-18500
162 31500-32900
53: 34750-21475
477: 30500-32650
476 30500-32650

Table 38. Continued

Sa.No	32	160	97 a	299	182	188	46	327	Ar.Mean
SiO_2	78.30	82.88	79.51	83.38	81.4	86.6	77.82	82.47	82.00
TiO_2	0.66	0.33	0.59	0.10	0.23	0.45	0.71	0.43	0.38
Al_2O_3	5.29	8.67	9.95	3.39	6.12	4.97	11.28	8.78	6.60
FeO	0.00	0.30	1.31	0.08	0	0.71	2.49	0.73	0.84
Fe_2O_3	2.91	1.85	3.06	0.45	4.42	1.88	3.28	4.63	2.82
MnO	0.02	0.05	0.05	0.03	0.05	0.45	0.05	0.06	0.07
MgO	0.35	0.81	1.15	0.21	1.96	0.04	0.46	0.40	0.63
CaO	7.01	0.07	0.12	0.00	0.07	0.00	0.00	0.00	1.10
Na_2O	0.84	0.81	0.84	0.47	1.10	0.58	0.78	0.81	1.00
K_2O	1.07	0.45	1.85	3.17	0.50	1.01	0.82	1.82	1.42
P_2O_5	0.03	0.01	0.09	0.00	0.06	0.00	0.02	0.01	0.05
CO_2	0.60	0.00	0.00	1.10	0.00	0.00	0.00	0.00	0.60
H_2O	1.90	1.30	1.66	3.50	2.75	2.00	1.92	0.00	2.06
TOTAL	99.00	97.90	100.20	95.90	98.70	98.70	99.60	100.10	98.90
Cr	317	110	127	102	164	47	98	55	145
Co	3	4	11	bdl	4	4	12	8	9
Ni	8	18	32	4	16	12	12	19	18
Cu	6	0	16	bdl	4	4	16	bdl	14
Zn	5	51	68	bdl	8	14	189	32	39
Ga	4	11	13	6	11	5	11	11	8
Rb	34	31	91	68	115	50	51	90	76
Sr	58	77	56	6	14	13	20	27	52
Y	27	17	22	8	18	19	14	15	15
Zr	363	146	235	43	324	193	67	148	169
Ba	105	139	312	210	419	240	477	373	289
La	20	26	27	10	22	22	0	19	18
Ce	46	85	38	13	45	22	11	34	31
Pb	5	54	12	4	4	3	51	11	12
U	bdl	1	bdl	bdl	bdl	bdl	2	bdl	2
Th	9	10	5	6	10	4	1	9	7

Ar.Mean: arithmetic mean

Coordinates of the analysed samples

32: 38250-21375
160: 31825-33750
97a: 31875-25325
299: 33375-18275
182: 30400-32675
188: 34800-33250
46: 34875-20425
327; 35050-33375

Table 39. Major and trace elements of Quartzites

Sa.No	116	468	97	60	67	198	51
SiO_2	92.66	90.18	97.53	90.68	97.67	93.58	92.93
TiO_2	0.21	0.36	0.16	0.27	0.25	0.26	0.12
Al_2O_3	3.00	3.18	0.31	1.53	0.71	1,28	0.38
FeO	0.80	0.43	0.79	0.50	0.39	1.79	0.51
Fe_2O_3	0.40	1.37	0.41	0.95	0.13	0.50	0.48
MnO	0.03	0.02	0.03	0.03	0.02	0.03	0.06
MgO	0.00	0.52	0.08	0.34	0.17	0.29	0.04
CaO	0.04	2.02	0.00	0.04	0.00	0.00	0.00
Na2O	0.78	0.55	0.71	0.00	0.53	0.53	0.52
K_2O	0.20	0.45	0.05	0.15	0.08	0.05	0.07
P_2O_5	0.04	0.02	0.01	0.02	0.00	0.00	0.00
CO_2	0.00	0.20	0.00	0.10	0.00	0.00	0.00
H_2O	0.00	2.30	0.00	0.61	0.00	2.10	1.20
TOTAL	98.16	101.6	100.00	95.22	99.95	100.41	97.30
Cr	41	117	31	19	113	163	155
Co	7	5	bdl	11	1	3	bdl
Ni	8	4	4	2	7	3	9
Cu	bdl	2	bdl	bdl	bdl	1	bdl
Zn	12	18	bdl	6	6	16	10
Ga	0	3	1	0	bdl	2	1
Rb	11	27	4	9	7	4	6
Sr	24	47	11	12.	10	6	5
Y	21	0	11	12.	15	8	9
Zr	214	161	115	341	288	162	73
Ba	43	249	24	103	46	19	38
La	11	9	17	9	16	14	7
Ce	25	16	26	36	29	17	11
Pb	5	9	5	13	5	7	5
U	bdl	0	bdl	0	bdl	bdl	bdl
Th	4	bdl	5	5	4	7	7

Coordinates of the analysed samples;

116: 25975-23000
468 31770-33250
97: 31875-25325
60 : 33900-21875
67: 33375-22625
198: 23800-21600
51: 33675-20750

Table 39. Contunued.

Sample No	219	143	57	Ar.Mean
SiO_2	90.06	92.78	95.10	93.31
TiO_2	0.24	0.12	0.04	0.2
Al_2O_3	4.25	2.49	2.00	1.91
FeO	0.60	0.00	0.00	0.72
Fe_2O_3	4.00	0.86	0.51	0.96
MnO	0.11	0.02	0.12	0.05
MgO	0.26	0.20	0.15	0.20
CaO	0.00	0.00	0.00	0.7
Na_2O	0.62	0.00	0.00	0.6
K_2O	0.06	0.45	0.00	0.17
P_2O_5	0.00	0.01	0.00	0.02
CO_2	0.00	0.00	0.00	0.0
H_2O	0.00	2.50	0.20	1.49
Total	100.25	99.43	98.13	98.95
Cr	67	bdl	27	81
Co	4	bdl	0	5
Ni	9	11	bdl	6
Cu	bdl	5	bdl	3
Zn	38	0	25	16
Ga	3	3	bdl	2
Rb	3	17	4	9
Sr	14	4	8	14
Y	13	15	5	12
Zr	157	33	8	155
Ba	19	81	16	64
La	17	41	2	14
Ce	16	13	bdl	21
Pb	29	6	3	9
U	bdl	bdl	bdl	0
Th	10	5	bdl	6

Ar. Mean: arithmetic mean

Coordinates of the analysed samples;

219: 25000-21300
143: 23525-24600
57 : 34200-21400

Table 40. Rare earth element data for psammite 160 and Quartzite 67.

Sample No	67	160
La	16.8	7.4
Ce	31.8	33.0
Pr	4.1	2.0
Nd	14.3	6.9
Sm	2.8	1.4
Eu	0.5	0.2
Gd	2.1	1.2
Tb	0.2	0.2
Dy	0.8	1.0
Ho	0.1	0.2
Er	0.3	0.6
Tm	0.5	0.1
Yb	0.3	0.6
Lu	0.1	0.1

Coordinates of the analysed samples;

67: 33375-22625
160: 31825-33750

6.2. METACHERT

From the mineralogical and petrographical data on the Kadinhani cherts it is clear that they consist entirely of microcrystalline quartz and chalcedony.

The chemical data are presented in Table 41 and 42. All types of chert average about 93% SiO_2 and 1.38 % Al_2O_3 with very little TiO_2 in most rocks. MnO and FeO are low in all siliceous rocks. The MnO content of the cherts ranges from 0.01 to 0.04 % with a mean value of 0.02%. One sample, 482, has high Fe_2O_3 content and contains the highest Cr, Zr, Ce, La contents in Table 41. Iron is present in most of the samples in the form of iron oxides (hematite). Most other elements occur in small amounts with the exception of Ba wihch ranges up to 889 ppm (sample 463) .

The SiO_2 concentration of the cherts decreases with increasing Al_2O_3, CaO, Na_2O_3, K_2O and Fe_2O_3 contents (Table, 41). There is a positive correlation between the Al_2O_3 and Na_2O+K_2O contents (Fig. 34) which is interpreted to indicate the presence of clay or feldspar. Al_2O_3 also has a positive correlation with FeO*(total), an association interpreted to be indicative of chlorite.

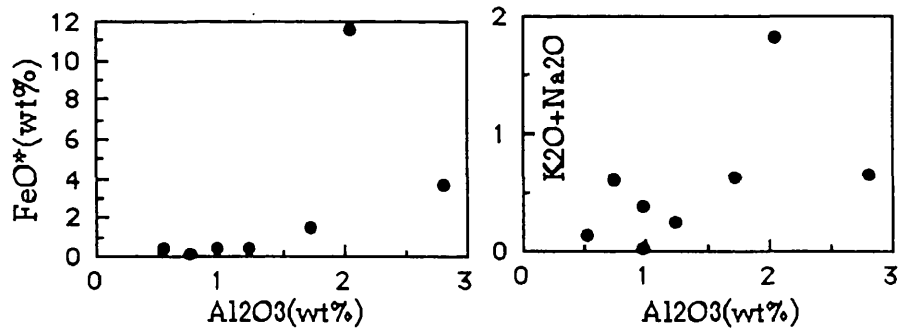

Fig.34. Plot of Al_2O_3 vs K_2O+Na_2O and Al_2O vs FeO*(total) in metachert.

Sugisaki et al. (1982) noted that the Al_2O_3/TiO_2 ratio of argillaceous sediments remains essentially constant from the continental shelf to the deep ocean floor environment, whereas the MnO/TiO_2 ratio shows a marked increase from shallow-water to pelagic environments in sediments.

The Kadinhani metachert averages 19 in Al_2O_3/TiO_2 and 0.3 in MnO/TiO_2 compared to average shallow-water chert values of 18-25, and 0.1-0.4 as recorded by Sugisaki et al.(1982). This suggests that the

Kadinhani metacherts have been deposited in a relatively shallow-water environment.

Ce anomaly values (Ce/Ce*) range from 0.7 to 1.16. Ce/Ce* does not change during diagenetic formation of chert lenses (Murray et al., 1992). Ce/Ce* correlates best with Al_2O_3, Na_2O, K_2O, and TiO_2 (Table 41), indicating that as the terrigenous input increases in abundance so does Ce/Ce*. The Ce anomaly generally approaches values of Ce/Ce* 0.86. This relationship is also shown by the broad positive association between Ce/Ce* and the aluminosilicate indices of Al_2O_3 and K_2O; note also that there is no relationship between Ce/Ce* and MnO or CaO (Fig. 35).

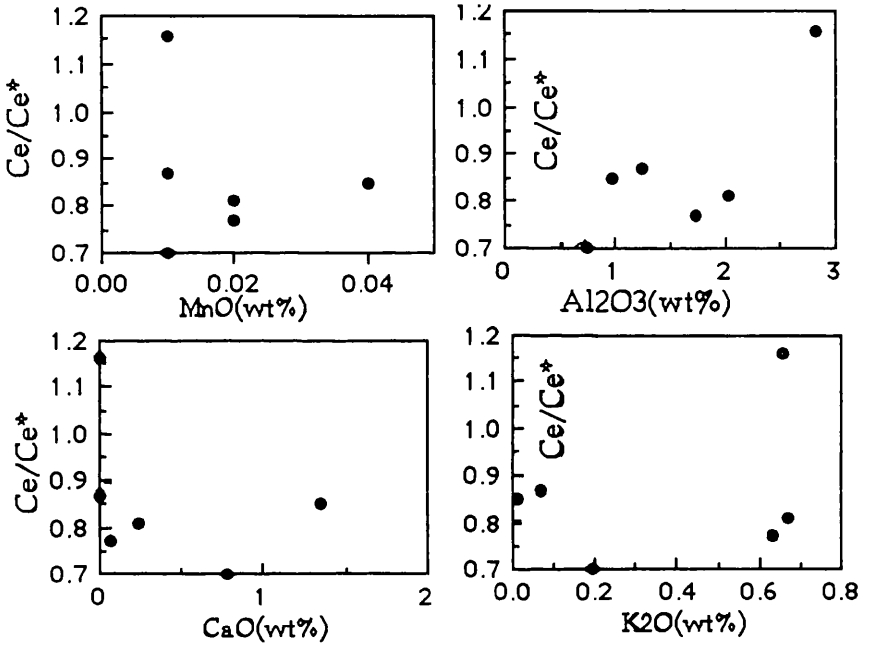

Fig. 35. Plot of Ce/Ce* vs. some major oxides for metacherts.

The positive correlation of REEs with Al_2O_3 (Fig. 36) implies that the terrigenous fraction is the dominant REE carrying phase (Murray et al., 1991). The positive correlation of REEs (total) with Fe_2O_3(total) indicates that the abundance of the metalliferous component is responsible for the variations in REE content.

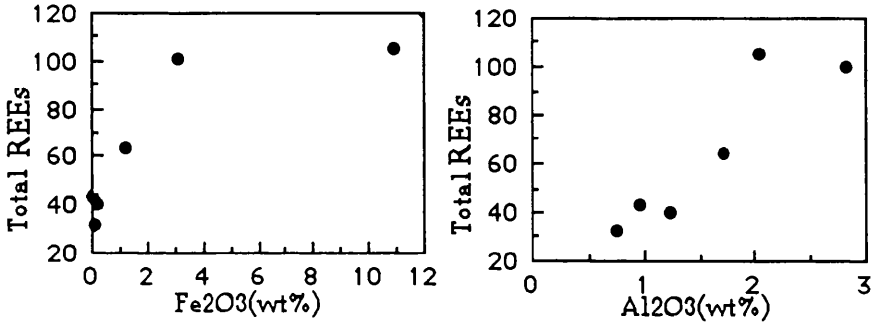

Fig. 36. The total REEs vs some major oxides for metacherts.

In figure 37, The plot of al-alk vs some REE and La, Ce, Eu and LREEs show positive correlation with al-alk. It sugges that clay mineral control the LREE in chert.

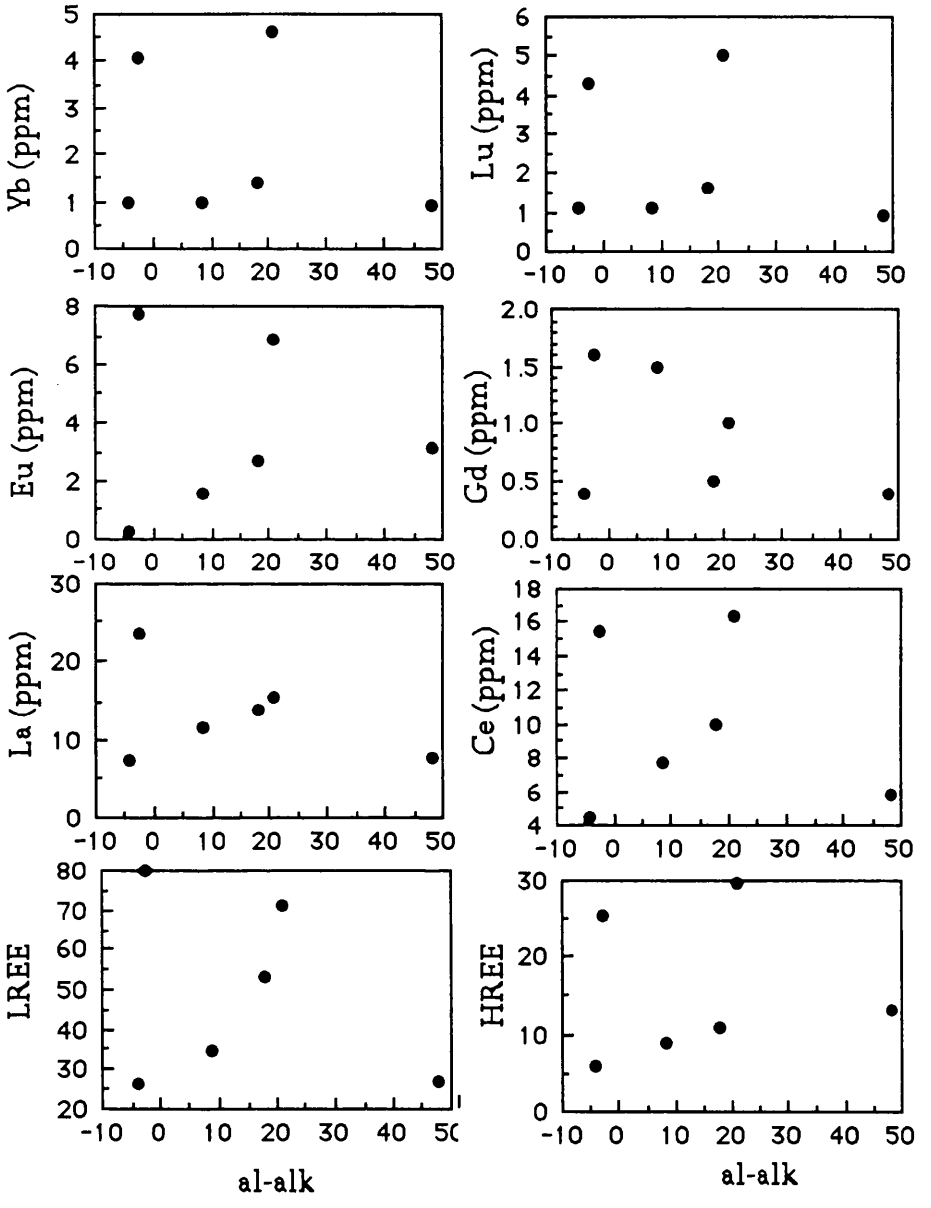

Fig. 37. Some REE vs al-alk.

The REE patterns (Fig, 38) show a small negative Ce anomaly. Large negative Ce anomalies are suggestive of deep-sea environments (Schimizu and Masuda, 1977).

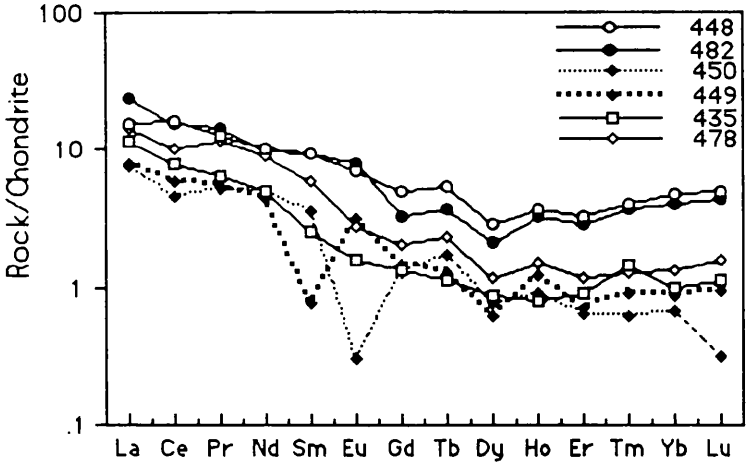

Figure 38. Chondrite -normalised rare earth element distribution patterns for metacherts from the Kadinhani area. Chondrite normalising values from Boynton (1984).

Chert and shale samples from Franciscan sequences deposited near a spreading ridge average Ce/Ce*=0.29; those deposited on the ocean-basin floor and not affected by metalliferous activity or continental input average Ce/Ce*=1.03. Chert and shale from the continental proximal Claremont Formation average Ce/Ce*= 0.93 (Murray et al., 1991).

Two depositional regimes can be identified; ocean-basin floor with Ce/Ce*~0.55 and continental margin (within ~100 km of a landmass) with Ce/Ce* ~0.90 to 1.30 and very low total REE (Murray et al., 1991).

Open-ocean sea-water displays extremely low Ce/Ce* values, mostly ranging from 0.2-0.3, due to preferential removal of oxidized Ce (cf. Elderfield, 1988). Courtois and Hoffert (1977), on two surface sediment transects from the central South Pacific toward South America, document a systematic change from deep sea surface sediments (Ce/Ce* 0.25) to continental margin sediment (Ce/Ce* 0.8 - 1).

Sample 450 shows a negative Eu anomaly, while sample 449 shows a positive Eu anomaly. The cause of the decreases in Eu/Eu* in chert may reflect a small loss of feldspar (Taylor and McLennan, 1985).

Most continental margin sediments display intermediate REE abundances, variable LREE enrichment and variable negative Eu anomalies, with Eu/Eu* in the range 0.6-1.0 (e.g., Mc Lennan et all., 1989,1990 a,b).

The chert samples from Kadinhani generally have Ce/Ce* 0.7 - 1.16. and Eu/Eu* ~ 0.8-1.4 (one sample (450) has Eu/Eu*-0.14 and one sample (449) has Eu/Eu* -5.3). The La/Yb ratio of the cherts normalized to chondrites range from 3.3 to 12. This ratio gives a measure of the light REE enrichment over the heavy REE relative to a chondrite average. The REE patterns (Fig. 38) from cherts suggest that they are thought to have formed in shallow-water environments.

Table. 41. Major and trace elements of Metacherts

Sa.No	448	463	482	449	450	435	478	473	Ar.Mean
SiO_2	89.85	97.14	84.52	92.41	93.02	98.34	94.40	94.98	93.08
TiO_2	0.11	0.04	0.17	0.04	0.07	0.06	0.07	0.06	0.07
Al_2O_3	2.81	0.53	2.04	1.24	0.75	0.97	1.72	0.98	1.38
FeO	0.62	0.05	0.80	0.26	0.02	0.00	0.28	0.06	0.26
Fe_2O_3	3.15	0.30	10.93	0.16	0.05	0.00	1.19	0.34	2.00
MnO	0.02	0.02	0.02	0.01	0.01	0.04	0.02	0.03	0.02
MgO	0.69	0.42	0.49	0.01	0.25	0.00	0.53	0.57	0.37
CaO	0.00	0.00	0.23	0.00	0.78	1.35	0.06	0.00	0.30
Na_2O	0.00	0.01	1.14	0.18	0.42	0.38	0.00	0.03	0.28
K_2O	0.66	0.12	0.67	0.07	0.19	0.01	0.63	0.00	0.29.
P_2O_5	0.13	0.01	0.12	0.00	0.05	0.02	0.02	0.00	0.04
LOI	0.40	0.76	0.84	0.33	1.10	0.25	0.35	0.00	0.37
Total	97.77	99.4	101.97	94.71	96.71	101.6	99.27	97.05	98.48
Cr	12	145	174	75	177	24	124	70	100
Co	25	4	7	bdl	bdl	bdl	0	bdl	4
Ni	51	3	4	1	2	2	6	0	8
Cu	0	bdl	bdl	bdl	bdl	6	31	bdl	5
Zn	31	bdl	4	0	5	0	11	0	6
Ga	2	bdl	5	1	0	0	2	1	1
Rb	23	6	14	13	7	12	22	15	16
Sr	165	12	9	19	10	14	4	3	29
Y	14	10	11	5	8	4	8	7	8
Zr	42	27	81	24	15	17	23	20	31
Ba	160	889	53	183	146	64	164	150	285
La	2	2	8	2	bdl	2	5	4	3
Ce	20	bdl	45	5	bdl	4	15	16	13
Pb	bdl	bdl	22	26	9	13	25	20	13
U	1	bdl	3	6	bdl	5	2	0	2
Th	3	bdl	8	bdl	bdl	bdl	bdl	bdl	1

Ar.Mean: Aritmetic mean

Coordinates of the analysed samples

448: 24500-22125
463: 24025-22750
482: 26625-27125
449: 25275-26875
450: 27375-28500
435: 39100-30750
478: 32000-29500
473: 40500-27500

Table 42. Rare earth element data for the cherts

sam. No	448	482	449	450	435	478
La	15.4	23.7	7.8	7.5	11.6	14.3
Ce	16.3	15.4	5.8	4.5	7.7	10.0
Pr	12.8	14.0	5.4	5.2	6.4	11.5
Nd	9.9	9.8	4.3	5.0	4.8	8.8
Sm	9.5	9.2	0.8	3.6	2.5	5.9
Eu	6.9	7.7	3.1	0.3	1.6	2.7
Gd	1.0	1.6	0.4	0.4	1.5	0.5
Tb	5.4	3.6	1.3	1.9	1.1	2.3
Dy	2.8	2.1	0.6	0.8	0.9	1.2
Ho	3.7	3.2	3.6	0.9	0.8	1.5
Er	3.2	2.9	0.7	0.7	0.9	1.2
Tm	4.0	3.7	0.9	0.6	1.4	1.3
Yb	4.6	4.1	0.9	0.7	1.0	1.4
Lu	5.0	4.3	0.9	0.3	1.1	1.6
Ce/Ce*	1.2	0.8	0.9	0.7	0.9	0.8
Eu/Eu*	1.3	1.4	5.2	0.2	0.8	0.8
total REEs	100.5	105.3	40.5	32.1	43.4	64.2

6.3. PELITE, BASIC SCHIST AND CALC SILICATE ROCKS

Metapelitic rocks have low CaO (< 1 wt %) and comprise phyllite, chlorite -chloritoid schist and chlorite- muscovite schist. Metabasic schists have (1-10 wt %) CaO and consist of albite-chlorite- actinolite -epidote schist. Calc silicate rocks have (>10 wt %) CaO and include chlorite-calc schist, calcite-epidote schist and calcite-muscovite - epidote schists. The major and trace - element compositions of these rocks are given in tables 43, 44 and 45.

The chemical characteristics of these three groups will be examined in order to determine the original sources of each group.

Discrimination between ortho- and para-amphibolites by geochemical means was undertaken by Leake (1964) and Van de Kamp (1969) using various Niggli values (al, alk, c, mg). Leake (1964) used the plot of Niggli c vs mg to demonstrate differences between pelitic rocks (with low c and mg values), mafic volcanic rocks (with intermediate c and mg values) and pure and impure carbonate rocks (with high c and mg values).

On the Niggli c vs mg diagram (Fig. 39) and Niggli al-alk vs c diagram (Fig. 40) the metapelitic rocks plot within the field of shales, the plagioclase and actinolite rich metabasic schists closely follow an igneous trend and the calc-silicate rocks plot in the field of pelite-limestone mixtures. These deductions are confirmed by a Niggli al-alk against c plot (Fig. 40) in which the same features re -occur but with the metabasic schists (except one sample) plotting in the field of igneous rocks, consistent with the igneous trend in Figure 40. These schists may have been basic tuffs in the pelites.

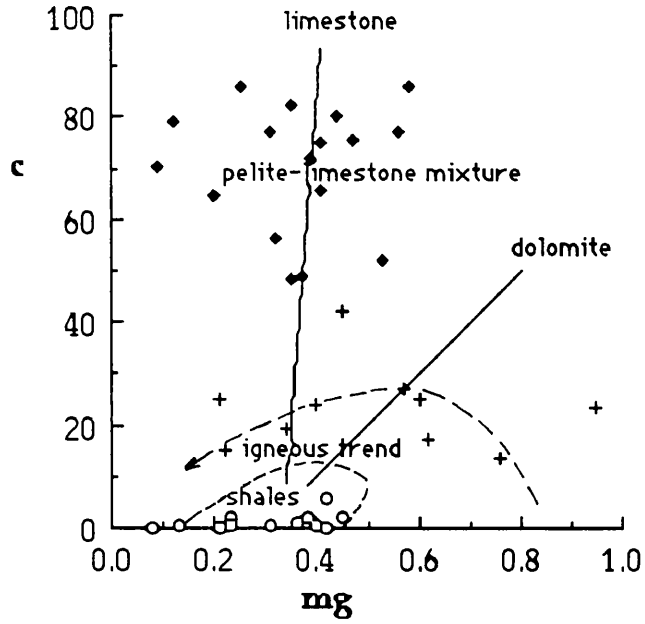

Fig. 39. Niggli c vs mg plot showing the fields of shales, dolomites, limestone and pelite-limestone mixtures as well as the igneous trend defined by the Karroo basalts (after Leake, 1964). metapelites (o), metabasic schist (+), calc silicate rocks (♦) from the studied area.

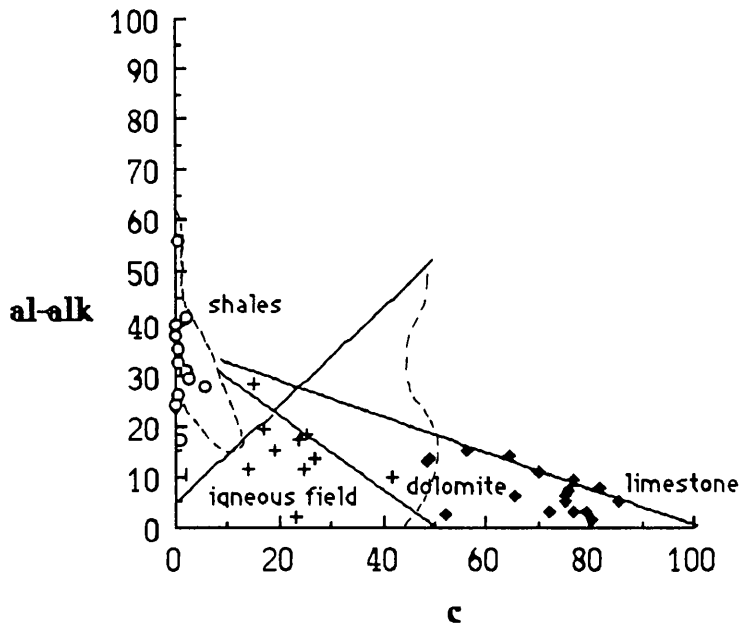

Fig. 40. Niggli al-alk : c plot showing the fields of shales, dolomites, limestones and the igneous field (after Van de Kamp, 1969). Data are metapelites (o), metabasic schist (+), calc silicate rocks (♦)

In figure 41, plots of Zr, Rb, Ba, Ni, Ga, La, Al_2O_3, K_2O and TiO_2 against al-alk for the metapelites show positive correlation. Senior and Leake (1978) suggest that all these elements are substantially added in sheet (mica and clay) minerals in pelites. Zr correlates poorly with al-alk (Fig. 41), probably because it is partly added in clay minerals and partly in detrital zircon in the original sediment. The calc silicate rocks show a similar positive correlation for al-alk and TiO_2, Al_2O_3, Rb and Ga but the remaining elements are more scattered as carbonate deposition influenced many trace elements. The metabasic schists plot off the sedimentary trend for TiO_2 which supports an igneous origin.

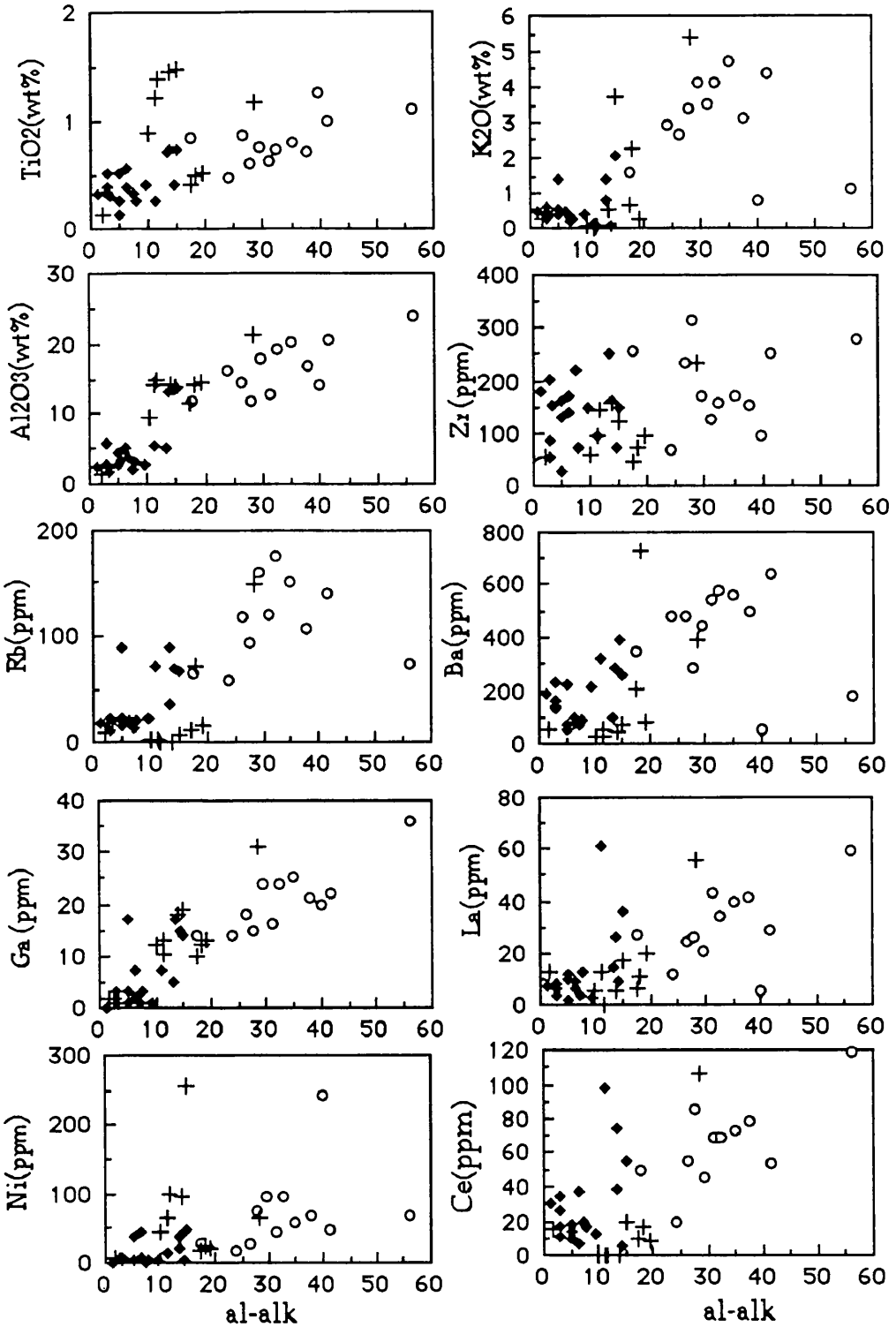

Figure 41. Plots of Niggli al-alk against La, Ni, Ga, Zr, Ba, Rb , Ce, TiO_2, Al_2O_3 and K_2O. metapelites (○), metabasic schist (+), calc silicate rocks (◆).

In figure 42, the K content is almost certainly due to the original presence of clay minerals and, or mica. As there are clear positive correlations between K and Ba, Th, Rb and Al_2O_3 in the metapelites these elements are clay-mineral related (probably illite).

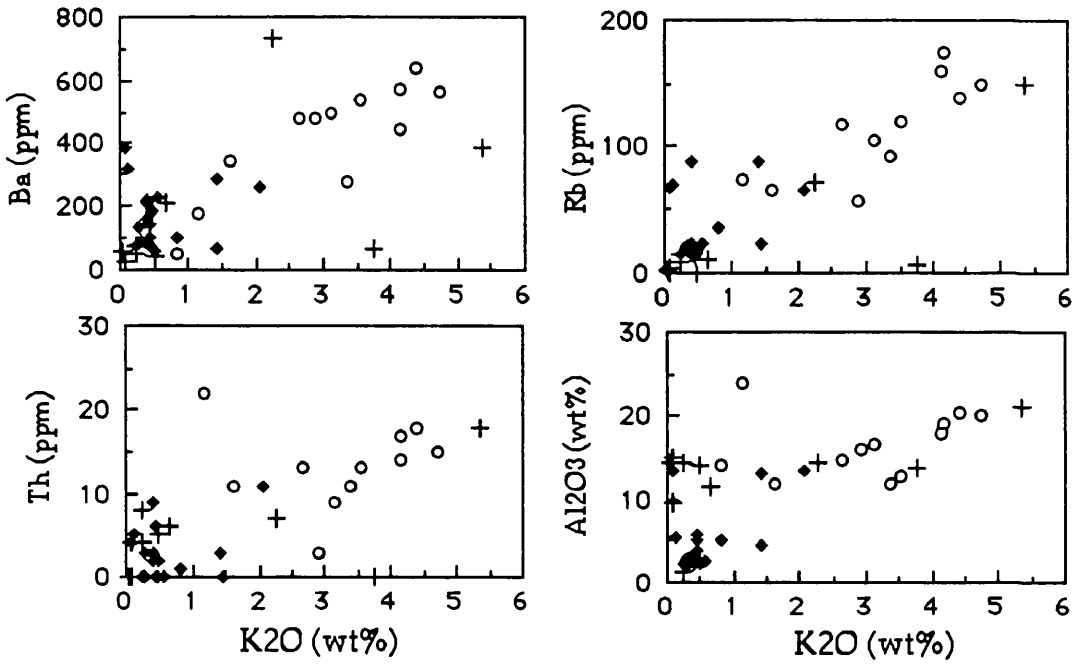

Figure. 42.Plots of K_2O against Rb, Ba, Th and Al_2O_3. metapelites (o), metabasic schist (+), calc silicate rocks (♦). CaO vs Sr is plotted (Fig. 43) and shows a positive trend for calc silicate rocks, and thus Sr was added in calcite.

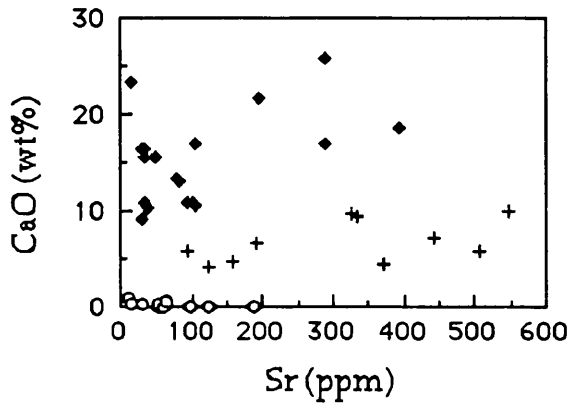

Fig. 43. CaO vs Sr diagram. metapelites (o), metabasic schist (+), calc silicate rocks (♦).

Zr/TiO_2 vs Ni plot has been used to test for sedimentary and igneous origins of rocks (Fig. 44). Igneous rocks generally have lower Zr/TiO_2 ratios than sedimentary rocks with the same Ni content. Although some overlap occurs, an optimum line dividing the field of sedimentary rocks from igneous rocks can be drawn. As Sr, Ti and Ni all tend to be relatively immobile during greenschist and amphibolite facies metamorphism (Cann 1970; Elliott 1973; Field and Elliott. 1974; Winchester and Floyd 1976, Winchester et al. 1980) , the concentration of these elements in the pelitic rocks will be approximately the same as in the original rocks. On this diagram, pelitic rocks, metabasic schist and calc silicate rocks from the Kadinhani area plot within the igneous field (Fig. 44). which since the rocks concerned are clearly sedimentary shows that this plot is not a reliable discriminator of sedimentary and igneous provenances.

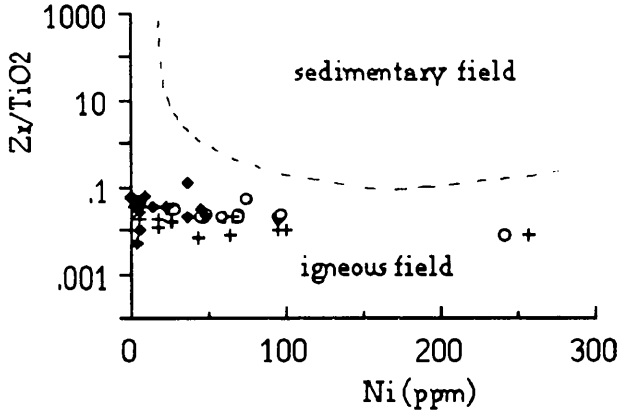

Fig. 44. Zr/TiO2 vs Ni diagram contrasting igneous and sedimentary (after Winchester et al, 1980). metapelites (o), metabasic schist (+), calc silicate rocks (♦)..

The pelitic rocks and calc silicate rocks fall in the tholeiitic and calc-alkaline fields on an AFM plot but the metabasic schists fall within the tholeiitic field only (Fig. 45).

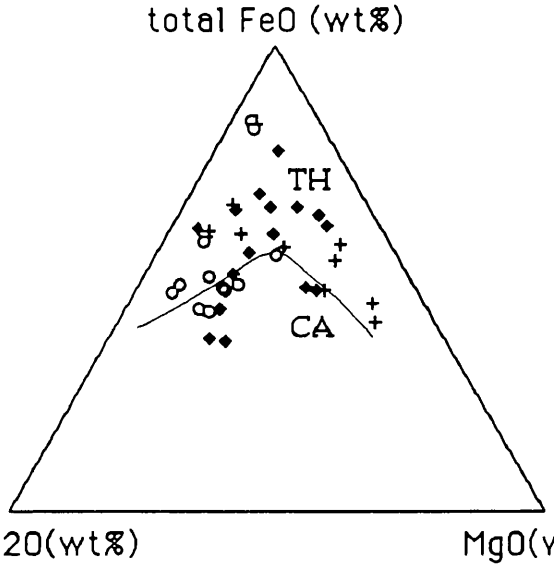

Fig.45.AFM diagram showing the distribution of metapelitic rocks from the study area compared to the general fields of tholeiitic (TH) and calk-alkaline (CA) igneous rocks (after Moore, 1977 and Zelt 1980). metapelites (○), metabasic schist (+), calc silicate rocks (◆)

A measure of the degree of weathering, termed the chemical index of alteration (CIA) has been used by Nesbitt and Young (1982) as an estimate of climatic conditions existing during the sedimentation of pelitic rocks. The chemical index of alteration is calculated from the formula :

$$CIA = (Al_2O_3 / (Al_2O_3 + CaO^* + Na_2O + K_2O)) X100$$

using molecular proportions, where CaO* represents the amount of CaO in silicate form. The influence of weathering increases with increasing values of CIA . Granites and granodiorites have CIA values of the order of 45 to 55 whereas shales and residual clays have much higher values (70 to 90) Clays formed primarily by mechanical processes at low temperatures are essentially ground down rock and thus have lower CIA values than residual clays and shales (Nesbitt and Young, 1982).

The metapelitic rocks have an average of 79.6 CIA value, metabasic schists averages 57.8 CIA and calc silicate rocks average of 15.4 CIA. An interpretation following Nesbitt and Young (1982) would be that the different types formed under somewhat different climatic conditions; the calc silicate rocks under colder climatic conditions than the other groups and the metapelites under considerably warmer conditions, slightly warmer than other group pelitic rocks and calc silicate rocks.

Table 43. Major Oxides and Trace elementsc of metapelitic rocks

Sa.No	151	231	208	104	107	48	35
SiO_2	65.90	66.70	55.40	67.40	69.46	61.70	58.80
TiO_2	1.26	0.99	1.10	0.61	0.64	0.47	0.81
Al_2O_3	14.10	20.50	23.95	12.70	13.82	16.10	20.10
FeO	9.59	0.64	0.00	1.19	0.79	7.12	4.39
Fe_2O_3	2.61	4.66	10.92	3.73	4.68	3.74	2.40
MnO	0.05	0.05	0.07	0.05	0.04	0.10	0.08
MgO	0.46	0.77	0.65	1.58	2.00	4.10	2.31
CaO	0.00	0.41	0.09	0.82	0.36	0.00	0.13
Na_2O	0.78	0.60	0.49	0.19	0.00	1.19	1.29
K_2O	0.82	4.40	1.15	3.37	3.54	2.90	4.73
P_2O_5	0.02	0.17	0.13	0.09	0.21	0.15	0.14
LOI	4.50	0.01	4.70	5.30	3.60	1.76	3.20
Total	98.60	99.80	98.56	97.00	99.14	99.18	98.40
Cr	633	130	144	355	68	76	146
Co	29	30	21	20	24	17	27
Ni	242	48	69	74	45	18	59
Cu	26	9	17	57	75	68	26
Zn	75	116	122	29	24	206	70
Ga	20	22.	36	15	16	14	25
Rb	bdl	140	74	93	120	57	150
Sr	205	31	122	11	15	20	61
Y	18	30	44	26	38	17	39
Zr	93	249	276	314	126	66	172
Ba	50	639	174	282	538	483	563
La	5	29	59	26	43	12	40
Ce	bdl	54	119	86	69	19	73
Pb	1	14	19	5	15	5	5
U	bdl	bdl	7	bdl	0	1	0
Th	bdl	18	22	11	13	3	15

Coordinates of the analysed samples

151: 32825-26750
231: 37200-16500
208: 25250-21300
104: 27500-25825
107: 28125-25900
48 33675-20475
35: 36375-18750

Table 43. Continued

Sa.NO	42	306	40	305	289	Ar. Mean.
SiO_2	65.60	65.60	73.30	70.50	62.30	65.22
TiO_2	0.70	0.77	0.84	0.88	0.73	0.81
Al_2O_3	16.70	18.00	11.80	14.55	19.20	16.8
FeO	4.59	4.19	3.00	1.44	3.90	3.4
Fe_2O_3	2.65	3.04	2.02	4.23	3.75	4.02
MnO	0.14	0.06	0.07	0.06	0.11	0.79
MgO	0.87	2.36	1.50	0.81	1.73	1.59
CaO	0.02	0.52	0.16	0.13	0.10	0.22
Na_2O	0.81	0.99	3.01	2.24	1.08	1.0.5
K_2O	3.13	4.13	1.62	2.65	4.16	3.04
P_2O_5	0.05	0.10	0.12	0.12	0.09	0.11
LOI	4.50	0.02	2.00	3.00	1.00	2.55
Total	99.30	99.80	99.40	99.66	98.10	98.14
Cr	196	190	80	90	139	146
Co	19	25	11	9	25	21
Ni	69	96	27	26	94	72
Cu	22	33	3	2	60	31
Zn	108	74	69	78	105	85
Ga	21	24	14	18	24	20
Rb	106	166	65	117	175	105
Sr	189	62	53	52	96	76
Y	35	25	32	29	31	30
Zr	154	173	256	234	158	189
Ba	499	445	348	484	575	423
La	41	21	27	24	34	30
Ce	78	45	50	55	69	55
Pb	14	6	12	9	11	8
U	bdl	bdl	bdl	bdl	bdl	0
Th	9	17	11	13	14	12

Ar. mean: Arithmetic mean

Coordinates of the analysed samples

42: 36150-18525
306: 36100-18150
40: 36375-18125
305: 36175-18300
289: 37675-18250

Table 44. Major oxides and trace elements of the metabasic schists.

Sa.No	154	286	47	281	283	79
SiO_2	60.40	54.56	46.78	52.80	66.86	64.40
TiO_2	0.50	1.47	1.18	0.53	0.41	0.12
Al_2O_3	14.30	14.86	21.10	14.40	11.5	7.21
FeO	4.49	4.75	1.39	3.85	3.83	0.43
Fe_2O_3	6.72	6.24	9.82	6.89	4.75	0.58
MnO	0.07	0.24	0.04	0.20	0.15	0.14
MgO	1.45	2.34	1.35	8.13	4.74	8.78
CaO	6.80	4.68	4.23	5.76	7.16	5.72
Na_2O	1.77	0.98	0.51	1.50	0.65	2.85
K_2O	2.26	3.76	5.37	0.24	0.66	0.24
P_2O_5	0.22	0.1	0.14	0.26	0.14	0.22
LOI	0.06	6.54	6.38	3.53	0.14	5.56
Total	99.0	98.1	98.34	98.20	100.5	96.25
Cr	129	395	160	124	120	180
Co	21	45	26	39	16	1
Ni	25	257	65	20	17	6
Cu	bdl	51	4	3	890	9
Zn	26	102	33	113	70	2
Ga	12	19	31	13	10	2
Rb	71	6	149	15	11	9
Sr	192	156	122	505	444	93
Y	18	20	29	17	18	17
Zr	73	120	233	94	46	55
Ba	730	69	388	77	208	50
La	11	17	56	20	6	13
Ce	17	20	106	8	10	15
Pb	12	2	8	12	11	9
U	bdl	bdl	bdl	1	bdl	bdl
Th	7	2	18	8	6	4

Coordinates of the analysed samples

154: 32250-28500
286: 38900-19100
47: 34400-20100
281: 40225-16450
283: 39425-17125
79: 31875-25375

Table 44. Continued

Sa.NO	5(7)	289b	41	62	Ar.Mean
SiO_2	60.80	49.90	46.40	50.00	55.30
TiO_2	0.90	1.21	1.45	1.40	0.51
Al_2O_3	7.36	15.30	14.10	14.90	13.5
FeO	3.35	3.90	6.87	3.09	3.6
Fe_2O_3	4.34	5.71	6.21	8.10	5.4
MnO	0.19	0.11	0.19	0.22	0.16
MgO	2.95	10.90	7.77	8.03	4.1
CaO	9.90	4.43	9.70	9.50	6.6
Na_2O	2.55	2.45	2.16	3.85	1.9
K_2O	0.08	0.03	0.50	0.07	1.3
P_2O_5	0.11	0.16	0.12	0.10	0.2
LOI	5.80	4.50	2.00	0.00	3.5
Total	98.3	97.1	97.5	99.3.0	98.3
Cr	197	245	359	390	230
Co	29	22	49	49	29
Ni	43	64	95	98	69
Cu	66	18	71	63	117
Zn	170	30	89	90	67
Ga	12	10	18	13	14
Rb	3	2	0	1	26
Sr	549	372	324	333	308
Y	25	45	36	39	26
Zr	60	92	157	142	107
Ba	29	55	44	25	162
La	5	13	5	bdl	14
Ce	bdl	bdl	bdl	bdl	32
Pb	3	4	4	3	6
U	bdl	bdl	bdl	bdl	0
Th	0	bdl	5	4	5

Ar. Mean: arithmetic mean

Coordinates of the analysed samples

5(7): 35400-22125
289b: 37675-18250
41: 36075-18400
62: 33250-22600

Table 45- Major oxides and trace elements of calc silicate rocks

Sa.No	411	464	467	425	81	65	271	278	163
SiO_2	42.10	45.45	43.81	37.46	61.42	62.22	75.16	71.28	73.22
TiO_2	0.52	0.57	0.12	0.74	0.34	0.32	0.40	0.25	0.26
Al_2O_3	4.53	5.03	3.42	13.12	2.60	2.28	3.81	3.00	2.63
FeO	1.00	4.32	0.00	1.36	0.79	0.00	1.02	0.19	0.39
Fe_2O_3	0.66	1.87	1.28	5.65	1.34	1.42	0.52	1.07	0.95
MnO	0.04	0.10	0.19	0.32	0.31	0.14	0.15	0.13	0.14
MgO	0.79	2.33	0.89	2.09	0.16	0.57	0.50	0.31	0.20
CaO	18.65	21.55	25.94	17.08	15.57	16.51	12.99	13.36	15.56
Na_2O	0.40	0.45	0.08	1.86	0.58	0.76	0.57	0.04	0.00
K_2O	1.43	0.45	0.41	1.41	0.57	0.49	0.44	0.30	0.50
P_2O_5	0.04	0.05	0.13	0.10	0.02	0.01	0.01	0.02	0.03
LOI	29.80	18.53	21.12	16.26	12.94	13.15	1.55	6.80	6.5
Total	100.00	100.70	97.4	97.45	96.64	97.87	97.15	96.95	98.38
Cr	18	60	13	89	166	34	161	18	191
Co	bdl	26	2	14	14	1	3	bdl	1
Ni	3	45	30	37	8	bdl	6	5	4
Cu	703	bdl	bdl	bdl	8	bdl	bdl	bdl	bdl
Zn	4	47	57	50	2	bdl	1	2	3
Ga	3	7	17	15	3	0	2	3	1
Rb	23	21	89	80	23	17	19	20	15
Sr	393	194	288	278	48	31	84	80	32
Y	10	22	29	29	10	18	16	17	20
Zr	28	170	160	167	202	181	140	72	131
Ba	68	76	219	288	230	186	102	92	56
La	2	9	10	26	8	7	6	13	12
Ce	14	37	18	74	26	30	7	16	10
Pb	6	13	23	23	7	11	8	4	7
U	6	6	8	8	1	0	bdl	bdl	bdl
Th	bdl	bdl	3	3	bdl	bdl	6	3	2

Coordinates of the analysed samples

411: 38375-15675
464: 31925-33235
467: 32450-33250
425: 32325-24825
81: 31750-25625
65: 23600-23325
271-s-: 40500-15500
278: 40375-16025
163: 30625-32100

Table. 45. continued

Sa.N0	410	426	469	485	61	293a	303	233	191	Ar. Mean
SiO_2	69.27	66.21	74.54	64.22	69.63	66.15	48.30	71.5	51.9	60.7
TiO_2	0.33	0.52	0.40	0.71	0.42	0.31	0.74	0.27	0.41	0.41
Al_2O_3	2.10	5.68	1.82	5.16	2.55	2.25	13.50	5.51	13.4	5.71
FeO	0.40	0.6	0.62	2.39	0.00	0.00	2.08	0.59	0.35	0.89
Fe_2O_3	1.17	2.11	0.44	2.45	1.09	2.64	5.86	3.98	7.23	2.3
MnO	0.06	0.12	0.03	0.05	0.07	0.15	0.12	0.11	0.23	0.14
MgO	0.71	1.58	0.25	1.39	0.70	0.85	1.45	0.26	1.14	0.89
CaO	10.58	10.71	9.25	10.41	10.83	10.84	16.90	16.40	23.2	15.3
Na_2O	0.00	2.58	0.50	0.05	0.05	0.48	0.00	0.50	0.91	0.55
K_2O	0.23	0.44	0.29	0.82	0.40	0.41	2.06	0.11	0.10	0.6
P_2O_5	0.01	0.04	0.02	0.05	0.02	0.01	0.09	0.01	0.07	0.04
LOI	9.0	10.0	7.98	10.32	8.95	11.16	8.13	2.10	2.52	1 0.8
Total	93.85	100.5	96.1	98.02	94.71	95.25	99.30	101.4	100.00	97.9
Cr	138	395	54	84	40	69	84	237	20	98
Co	0	45	0	9	1	28	17	5	5	10
Ni	0	257	5	22	2	4	49	14	5	23
Cu	bdl	51	1	bdl	3	bdl	0	2	bdl	42
Zn	1	102	2	43	1	1	40	23	16	22
Ga	1	19	2	5	1	1	14	7	15	6
Rb	14	6	17	35	23	21	66	70	68	35
Sr	105	156	30	39	35	95	104	34	16	103
Y	10	20	12	18	10	16	33	17	23	18
Zr	222	120	85	250	150	153	148	96	71	141
Ba	75	69	136	102	209	158	259	319	389	168
La	4	17	6	14	3	4	36	61	9	13
Ce	20	20	10	38	12	34	55	98	6	29
Pb	11	2	11	6	10	18	66	10	0	13
U	9	bdl	21	9	bdl	7	bdl	1	bdl	4
Th	bdl	2	bdl	1	8	2	11	5	4	4

Ar. Mean: Arithmetic mean

Coordinates of the analysed samples

410: 39800-15000
426: 32300-24875
469: 32500-33450
485: 37875-14825
61: 33925-22800
293a: 18650-33400
303; 33500-18200
233: 33225-33275
191: 29750-27875

6.4. GEOCHEMISTRY OF CARBONATE ROCKS

Geochemical analysis has aimed to determine the provenance and reconstruct the history of the sedimentary rocks.

Geochemical analyses of carbonate rocks are listed in Table 47. In table 46 the main chemical features of the different carbonate formations are compared. Al_2O_3 is believed to be a valid indicator of the original content of clay minerals in general and this has obviously influenced the concentrations of several other elements. Al_2O_3 shows a positive correlation with K_2O, total FeO and TiO_2 (Fig. 46) all of which are likely to be contained in clay minerals in different proportions. Where Al_2O_3 is zero or extremely low (eg sp. 287) clearly the SiO_2 cannot have been introduced into the original sediment in clay mineral or feldspar and was probably therefore either in traces of detrital quartz or in siliceous organisms.

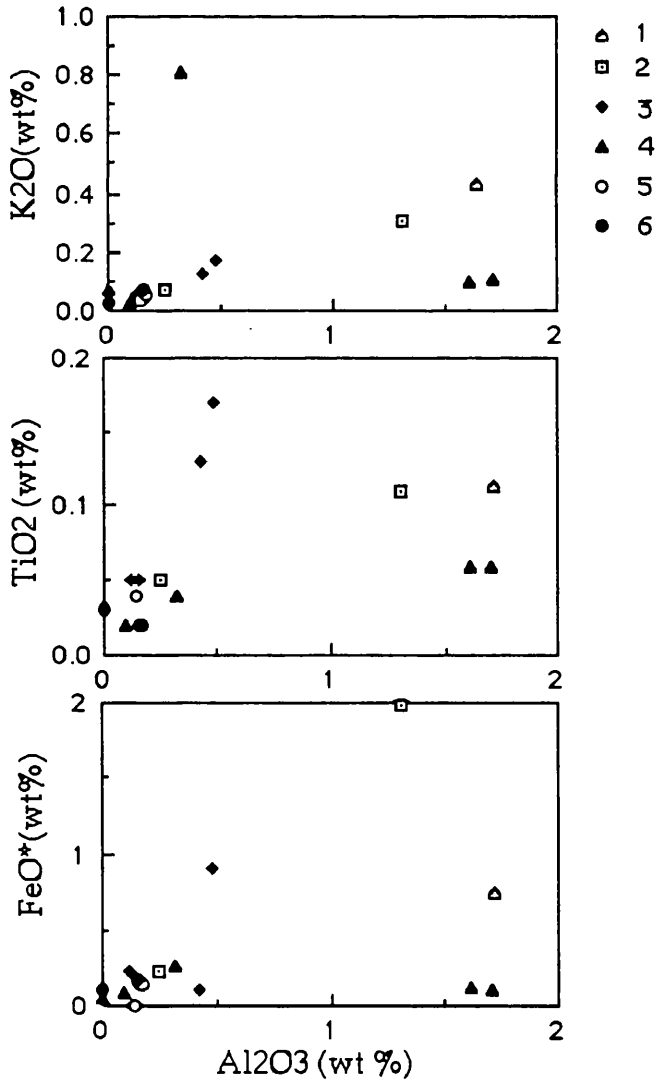

Fig.46. Plots against Al2O3 in carbonate rocks.

Strontium (Sr) is one of the most important minor elements in carbonate rocks especially in dolomites as discussed by Veizer and others (1978) who regarded Sr as an indicator of the derivation of the dolomite. Early dolomite with high Sr was interpreted as replacing aragonite while, in contrast, diagenetic dolomite with low Sr was interpreted as replacing other carbonates that lacked Sr (Veizer et al., 1978). When salinity increases the Sr content is also expected to increase, bearing in mind, however, that the most important factor which determines the amount of Sr in dolomite is the time of dolomitization. Early diagenetic fine crystalline dolomites have higher Sr contents than later diagenetic dolomites. The range of Sr in late diagenetic dolomites is typically 90- 300 ppm (Veizer and Demovic, 1974). The Sr content of the Kursunlu dolomites in the studied area is between 52 and 90 ppm, suggesting that the dolomites are late diagenetic (Table 55).

Weber (1964) and Wedepohl et al. (1972) concluded that Rb is concentrated in the clay fractions of the insoluble residue of the carbonate rocks. Degens et al. (1957) pointed out that there is no structural position for Rb in kaolinite but Rb can substitute for K in illite, montmorillonite and micas. Rb values are, 54 ppm for the Esiragili Formation carbonate and 15-69 ppm for calc-schist and 4-10 ppm for other rocks (Table 46). The Rb is most likely to be concentrated in the muscovite.

Ba was observed by Friedman (1969) to be low in marine limestones (less than 60 ppm) and high in the fresh water limestones (more than 60 ppm). The Ba contents which exceed 60 ppm in the Esiragili and Bagrikurt formations are rather high which might be due to the mixing of continental sediment.

Pb is 0-29 ppm in all the carbonate rocks except the calc-schist which has 29-69 ppm of Pb (Table 47). Wedepohl et al (1974) stated that calcite and dolomite cannot incorporate appreciable concentrations of Pb, because sea and interstitial waters usually contain very little Pb. He added that plants can concentrate large amounts of Pb and he quoted Koster (1969) that kaolinite can have higher than 40 ppm Pb. The high Pb content in the calc-schists is probably related to organic material or clay minerals.

Table 46. Some important major oxides and trace elements contents in different carbonate rocks .

	1	2	3	4	5	6
SiO_2	4.34	2.3-12.6	1.4 -3.2	0.1 - 4.2	0.1 - 0.7	0.9
TiO_2	0.13	0.02 - 0.14	0.06 -	0.03- 0.13	0.02-0.04	0.03
Al_2O_3	1.78	0.12-1.31	0.12-0.48	0.0-1.61	0.14-0.17	0.0
MgO	0.73	0.3	0.4 -0.8	0.5 -0.8	20.5-24.4	0.08
FeO total	0.79	0.2-2	0.1-0.9	0.05-0.3	0.2-0.2	0.1
Sr	91	15-649	11-1697	188-487	52- 90	163
Rb	54	15-69	4-10	5-9	4-6	0
Ba	131	79-310	0-96	0 -310	2-28	0
Pb	11	29-69	0-11	2-6	0-24	0

1-Esiragili Formation carbonate 2- Bagrikurt Formation calc-schist 3- Bagrikurt Formation block limestone 4-Kursunlu Formation Marble 5- Kursunlu Formation dolomite 6- Lorasdag Formation marble.

Table.47 . Major oxides and trace element concentrations of carbonate rocks

Sa.No	222 (4)	345 (4)	78 (4)	483 (4)	287 (4)	434 (5)	480 (5)	310 (6)
SiO_2	4.20	4.29	2.52	0.10	1.96	1.07	0.10	0.00
TiO_2	0.05	0.06	0.07	0.04	0.04	0.04	0.02	0.02
Al_2O_3	1.61	1.71	0.32	0.09	0.00	0.14	0.17	0.15
FeO	0.00	0.00	0.00	0.15	0.00	0.06	0.00	0.00
Fe_2O_3	0.13	0.11	0.26	0.02	0.05	0.01	0.00	0.00
MnO	0.03	0.03	0.01	0.01	0.02	0.02	0.02	0.00
MgO	0.71	0.62	0.54	0.52	0.84	22.08	24.38	20.54
CaO	54.60	53.64	54.92	54.84	53.74	28.91	33.09	29.33
Na_2O	0.30	0.30	0.41	0.23	0.75	0.06	0.03	0.00
K_2O	0.10	0.11	0.18	0.03	0.07	0.04	0.05	0.07
P_2O_5	0.00	0.00	0.00	0.01	0.00	0.01	0.02	0.01
LOI	39.19	39.70	40.63	42.25	42.83	46.64	42.34	47.67
Total	100.92	100.57	99.86	99.50	100.30	99.07	100.22	97.74
Cr	bdl	bdl	bdl	bdl	bdl	bdl	bdl	bdl
Co	bdl	bdl	bdl	bdl	bdl	bdl	bdl	bdl
Ni	2	2	bdl	0	2	1	bdl	3
Cu	5	bdl	bdl	5	bdl	bdl	bdl	bdl
Zn	bdl	bdl	5	bdl	59	bdl	6	bdl
Ga	1	0	bdl	bdl	bdl	bdl	bdl	0
Rb	5	6	5	9	0	5	4	6
Sr	188	246	221	487	339	52.0	90	73
Y	6	6	7	0	6	2	2	5
Zr	26	23	19	bdl	12	16	18	11
Ba	6	bdl	bdl	15	11	28	22	2
La	bdl	6	bdl	2	bdl	0	bdl	5
Ce	bdl	bdl	bdl	bdl	bdl	bdl	bdl	bdl
Pb	4	3	2	6	4	9	14	0
U	bdl	1	bdl	2	bdl	bdl	3	0
Th	9	6	bdl	bdl	1	bdl	bdl	3

Coordinates of the analysed samples

222: 37750-24825
345: 37300-25300
78: 37525-25500
483: 31825-30000
287: 39750-20675
434: 39500-32250
480: 31850-29700
310: 31800-29500

Table 47. Continued

Sa.No	423 (1)	90 (6)	163 (2)	201 (2)	487 (3)	461 (3)	458 (3)	38 (3)
SiO_2	4.31	0.92	2.30	12.58	1.38	2.04	2.43	3.21
TiO_2	0.13	0.03	0.05	0.11	0.06	0.06	0.04	0.02
Al_2O_3	1.78	0.00	0.25	1.31	0.48	0.42	0.15	0.12
FeO	0.50	0.00	0.00	0.59	0.50	0.05	0.0	0.00
Fe_2O_3	0.34	0.10	0.23	1.45	0.43	0.95	0.0	0.23
MnO	0.08	0.00	0.00	0.12	0.04	0.02	0.01	0.03
MgO	0.73	0.08	0.30	0.30	0.50	0.38	0.75	0.53
CaO	42.91	55.99	55.51	46.70	53.62	54.65	53.74	54.11
Na_2O	0.41	0.37	0.43	0.25	0.12	0.40	0.15	0.45
K_2O	0.43	0.03	0.07	0.31	0.17	0.13	0.05	0.05
P_2O_5	0.07	0.00	0.00	0.01	0.08	0.02	0.01	0.00
LOI	48.31	42.98	38.96	36.81	43.83	42.62	42.1	41.30
Total	100.00	100.50	98.0	99.00	100.79	101.74	99.43	99.46
Cr	66	bdl	41	65	bdl	243	bdl	bdl
Co	6	bdl	0	2	bdl	bdl	0	bdl
Ni	8	0	1	5	bdl	3	1	bdl
Cu	1	bdl	bdl	1	9	bdl	bdl	bdl
Zn	2	bdl	6	22	0	3	bdl	4
Ga	7	0	8	4	0	0	0	bdl
Rb	54	bdl	69	15	10	9	4	3
Sr	91	163	15	649	1697	11	147	210
Y	19	5	16	24	4	6	8	5
Zr	403	52	156	61	bdl	25	16	6
Ba	131	bdl	310	79	67	96	15	bdl
La	17	6	15	11	8	0	5	bdl
Ce	40	bdl	21	11	5	bdl	bdl	bdl
Pb	11	bdl	8	29	11	7	2	0
U	9	bdl	bdl	1	1	1	bdl	bdl
Th	0	2	8	7	bdl	bdl	bdl	bdl

Coordinates of the analysed samples

423: 35875-19350
90: 31600-21300
163: 30625-32100
201: 24050-21125
487: 36975-18025
461: 38000-16075
458: 38300-18525
38: 37375-19000

6.5. META - IGNEOUS AND IGNEOUS ROCKS

6.5.1. META - IGNEOUS ROCKS

Previous chapters showed that the rocks have been altered during metamorphism. Epidotization, sericitization, albitiziation, silicification and chloritization occur in the rocks.

During albitization of feldspar, Na was retained in albite microlites and phenocrysts, but the Ca, K and Rb ions were excluded. Sericite alteration is characterized by very strong K, Rb, and Ba enrichment and epidote provides a stable phase for the Ca displaced from the plagioclase. Chlorite alteration is characterized by moderate Mg enrichment.

The large ion lithophile elements (LILE) may have been affected by metamorphism so the relatively immobile elements are mostly used in the petrogenetic interpretation of the meta - igneous rocks. Ti, Y, Zr, Nb, Ga, Cr, Ni, P and REE often do not change substantially during low-temperature metamorphism (Volkova et al, 1992). They are generally considered to be relatively immobile during alteration or metamorphic processes and have therefore been used to elucidate the petrogenesis of meta-igneous rocks. (Field &Elliott 1974; Cann 1970; Pearce & Cann 1973 ; Floyd & Winchester 1978).

6.5.1.1. METATRACHYANDESITE AND METABASALTIC ANDESITE

The major oxides, trace element contents and CIPW norm values for the metatrachyandesites are given in Table 48, and data for the metabasaltic andesites are given in Table 49. Rare earth element data for both of the rocks are given in table 50.

On the Zr/TiO_2 vs. Nb/Y diagram (Fig. 47) the meta volcanic rocks generally plot in the trachyandesite and basaltic andesite fields (Fig. 47). Similar features are seen on the Zr/TiO_2 vs. Ga diagram (Fig. 48). The TiO_2 vs. Zr/P_2O_5 plot (Fig. 49) confirms the sub-alkaline character of these metavolcanics.

On diagram (Fig. 50) the metatrachyandesites plot in the calc-alkaline field, and the metabasaltic andesites partly in the calc-alkaline and partly in the tholeiite field.

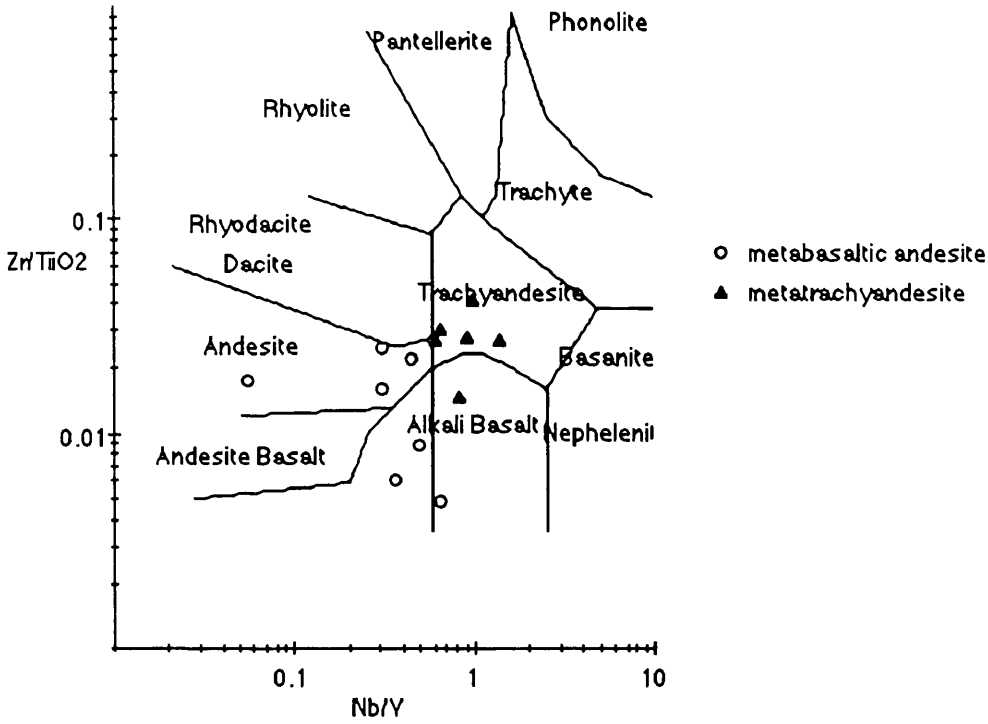

Fig. 47. Zr/TiO2 vs Nb/Y diagram showing the composition of metavolcanic rocks types from the Kadinhani area. Field boundaries are from Winchester & Floyd (1977).

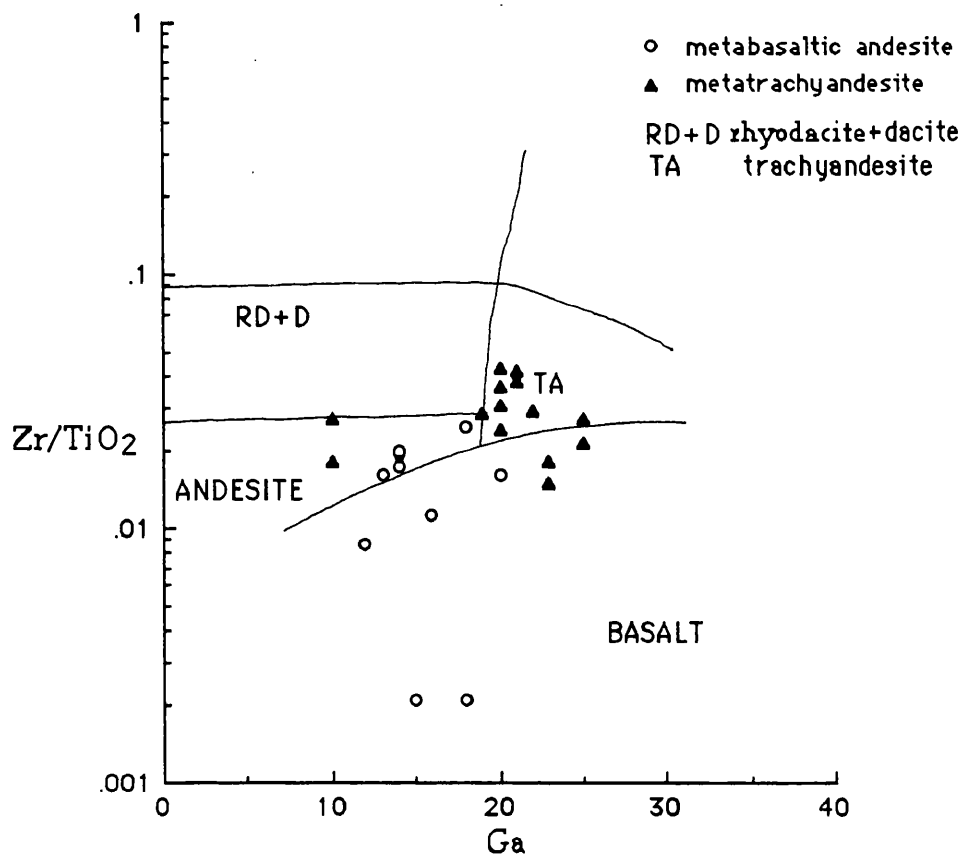

Fig.48. Zr/TiO2 vs Ga variation diagram showing distribution of metavolcanics. Field boundaries are from Winchester & Floyd(1977).

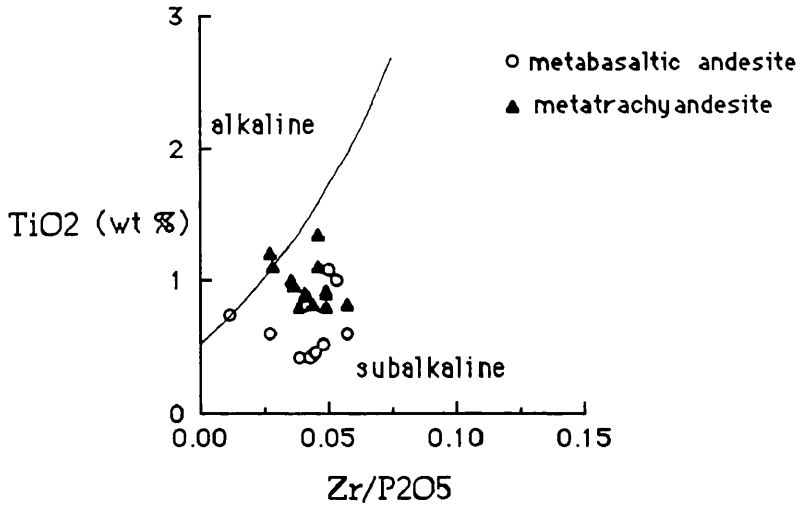

Fig. 49. TiO_2 vs Zr/P_2O_5 discrimination diagram revealing the original magma types. Field boundaries are from Floyd& Winchester (1975), and Winchester & Floyd (1976).

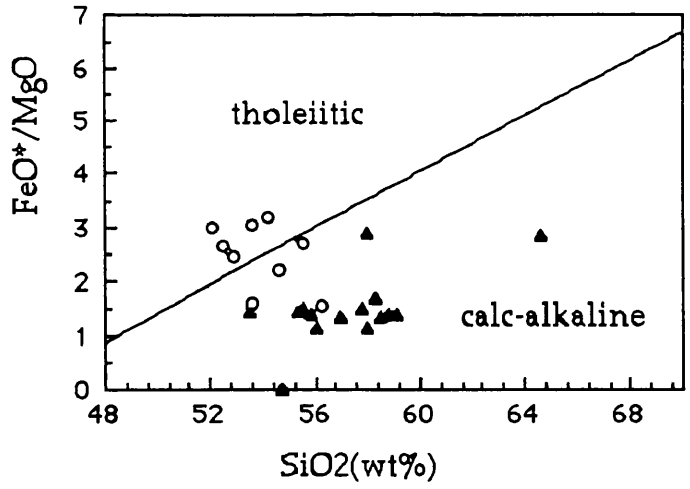

Fig. 50. SiO_2 vs FeO*/MgO diagram for metavolcanics rock (after Gill, 1981; and Ewart, 1982). Metatrachy andesite (▲) and metabasaltic andesite (o)

The major and trace element variations against SiO_2 are shown in Fig. 51. The weak negative correlation between Al_2O_3 and SiO_2 suggests that plagioclase was present in the liquidus phase in the metavolcanic rocks (Mc Millan & Dungan, 1986). Most of the element variation in the metabasaltic andesite plots show considerable scatter. However with increasing SiO_2, Zr, P_2O_5 and K_2O show positive correlation, some

elements and oxides such as Rb, MgO, FeO and TiO_2 show negative correlations in the metatrachyandesite.

Depletion of FeO, MgO and enrichment of K_2O, with increasing SiO_2 reflect the crystallization of hornblende, plagioclase and pyroxene in the metatrachyandesite (Romick et al, 1992).

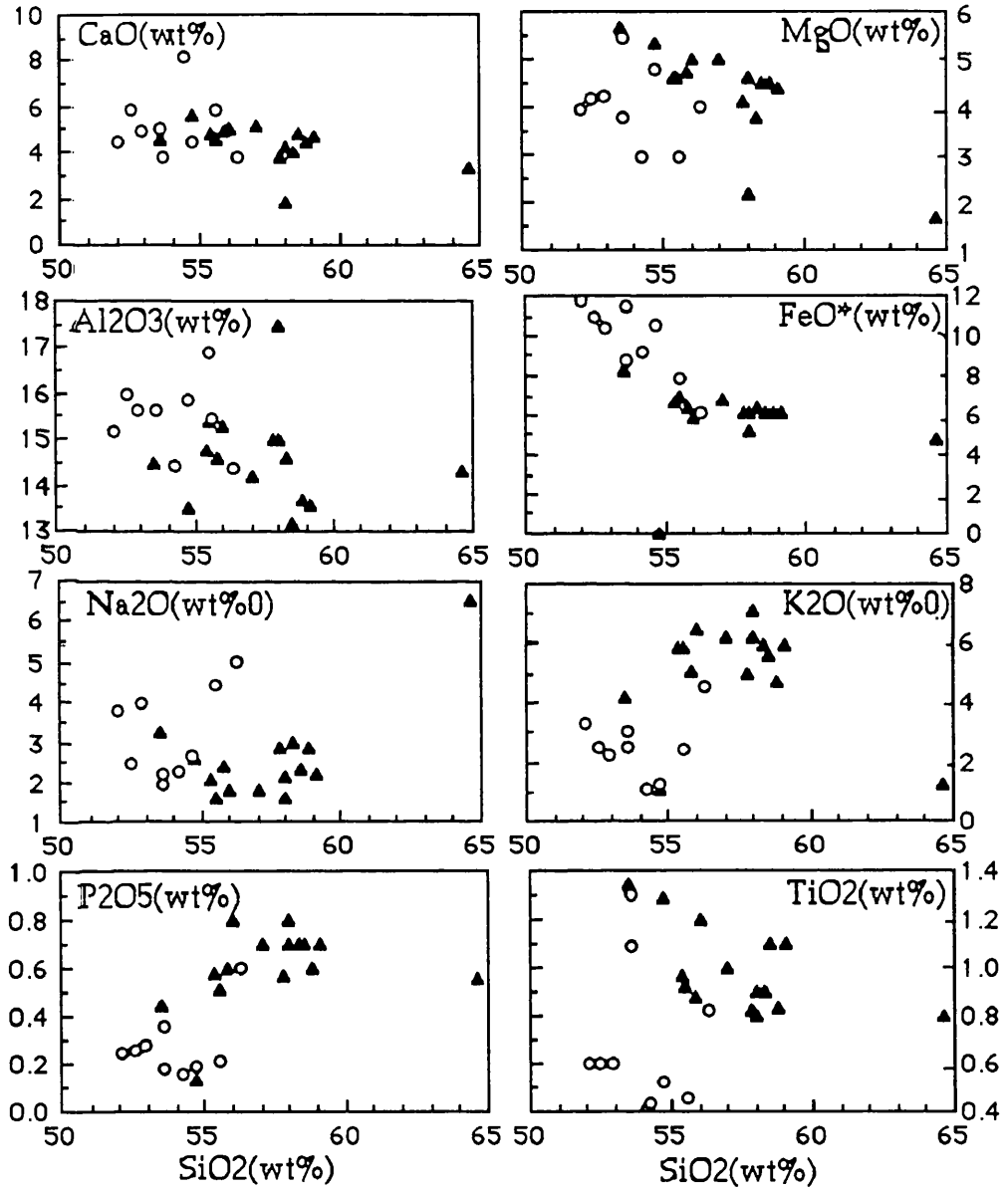

Figure 51. Harker diagram showing variation of major oxides and trace elements in the metavolcanic rocks, metatrachyandesite (▲) and metabasaltic andesite (o).

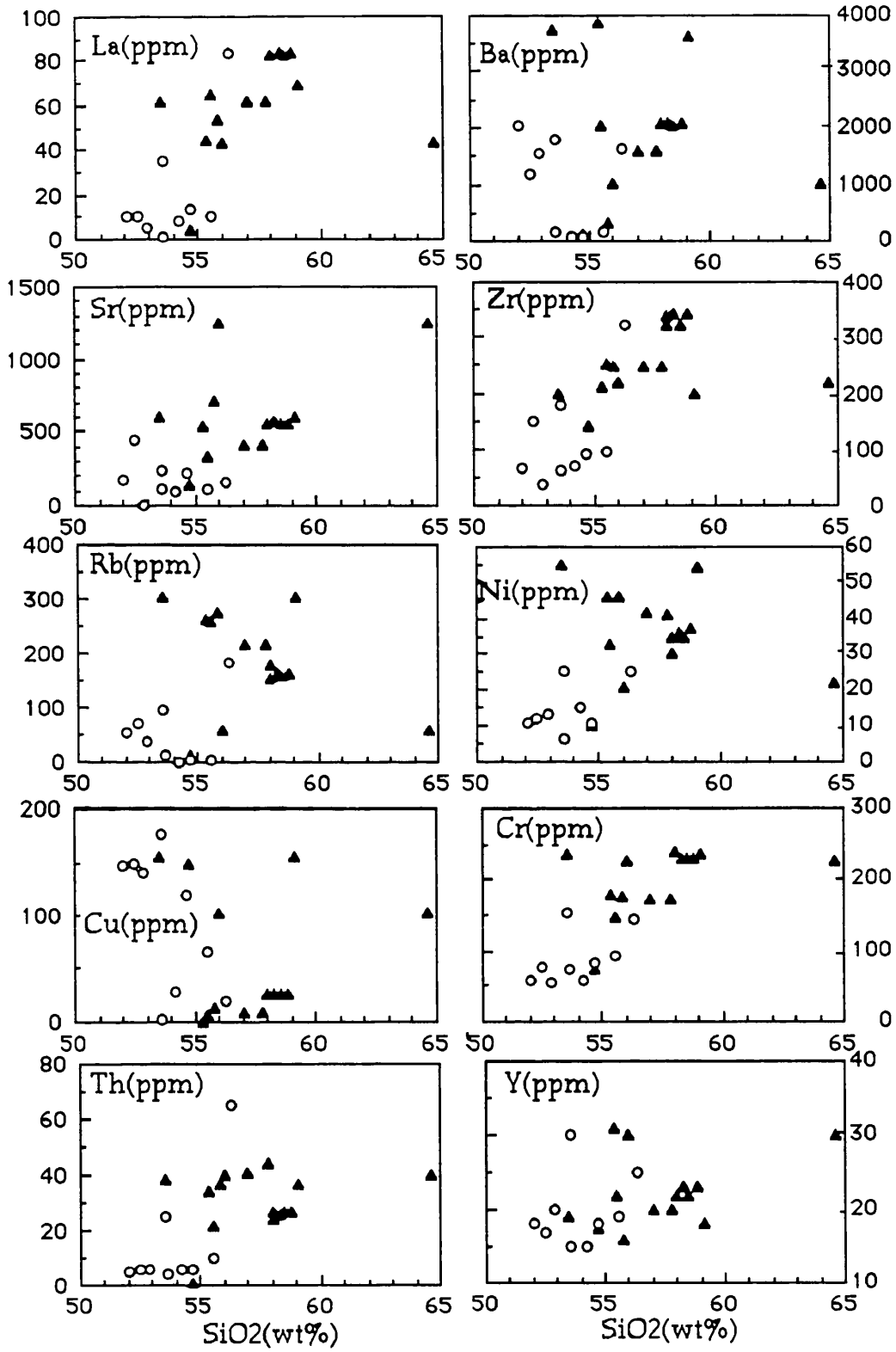

Fig. 51. Continued, metatrachyandesite (▲) and metabasaltic andesite (○).

The major and trace element data of the metavolcanic rocks are plotted against Niggli mg in Fig. 52. Niggli ti, Zr, Cr, and Ni show positive correlations with Niggli mg. These variation trends are consistent with known igneous fractionation trends; in particular, the samples with the greatest iron-enrichment show the highest levels for the incompatible elements (cf. Wager and Brown, 1967).

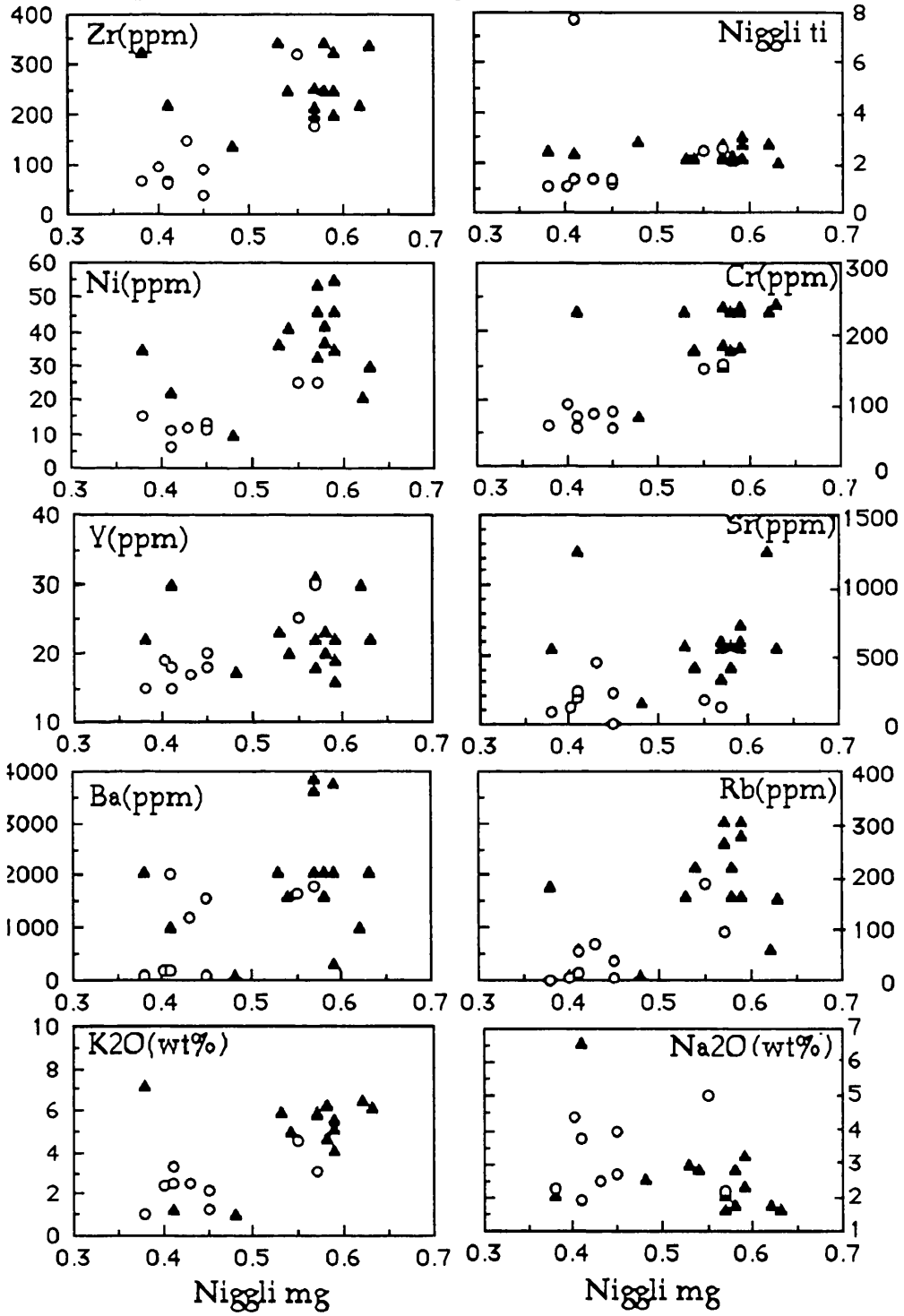

Fig. 52. Plots of major oxides and trace elements and Niggli ti versus Niggli mg, metatrachyandesite (▲) and metabasaltic andesite (o).

The TiO_2 versus Zr plot (Fig. 53) shows that the meta basaltic andesites lie within in the Arc Lava field whereas metatrachyandesites fall in the Within- Plate lava field.

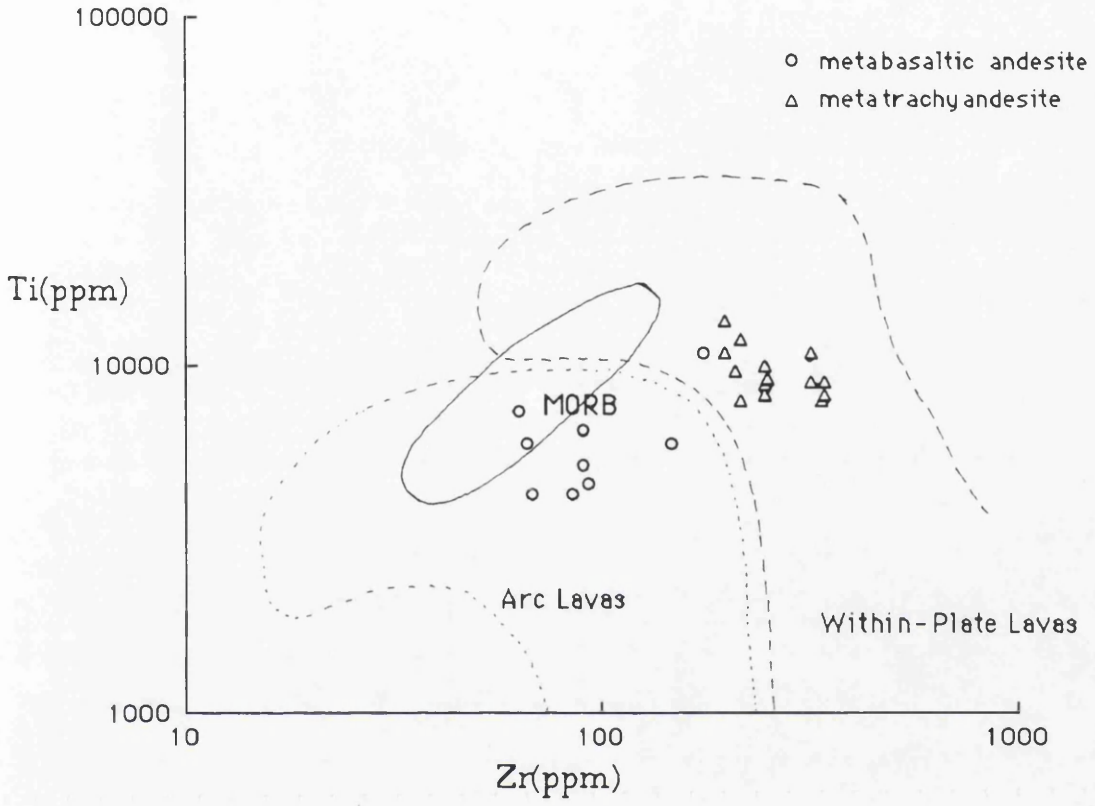

Fig. 53. Ti vs. Zr Plot for the metavolcanic rocks of the Kadinhani area. Field boundaries from Pearce (1982) and Pharaoh & Pearce (1984).

The effects of fractionation can be accommodated by plotting incompatible element Y against a compatible element such as Cr. Data for the Kadinhani metavolcanics rocks are plotted on the Cr-Y discrimination diagram (Fig. 54). The rocks are again consistent with a volcanic arc for the metabasaltic andesites and within-plate affinity for the metatrachyandesite

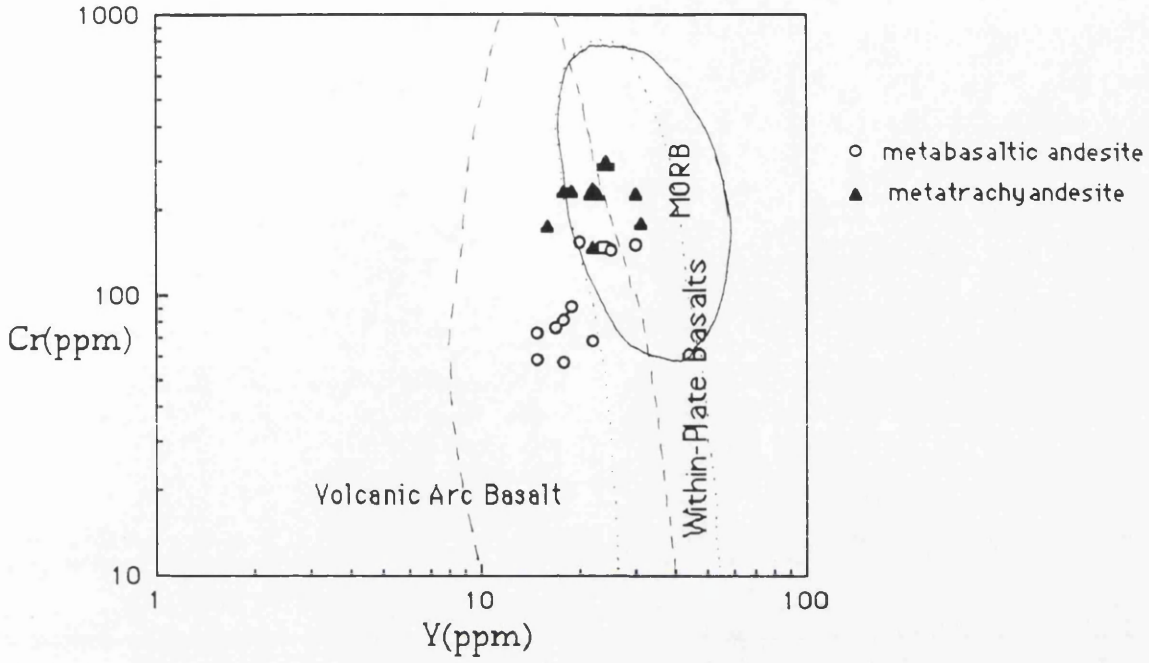

Fig.54. Cr versus Y Plot showing the distribution of metavolcanic rocks . Field boundaries from Pearce (1982).

These deductions are further supported by Zr/Y ratios for the rocks studied. Pearce (1983) showed that when a basalt suite has been identified as having a volcanic arc character, plotting the Zr/Y ratio against Zr provides an effective means of discriminating between oceanic and continental arc settings. Furthermore, basalts from the continental arc environment have high Zr/Y ratios relative to those of oceanic arc settings because the Zr derived from an enriched sub-continental mantle source is added to the subduction component. Accordingly, the meta basaltic andesites studied can thus be characterized as those of continental arc affinities (Fig. 55).

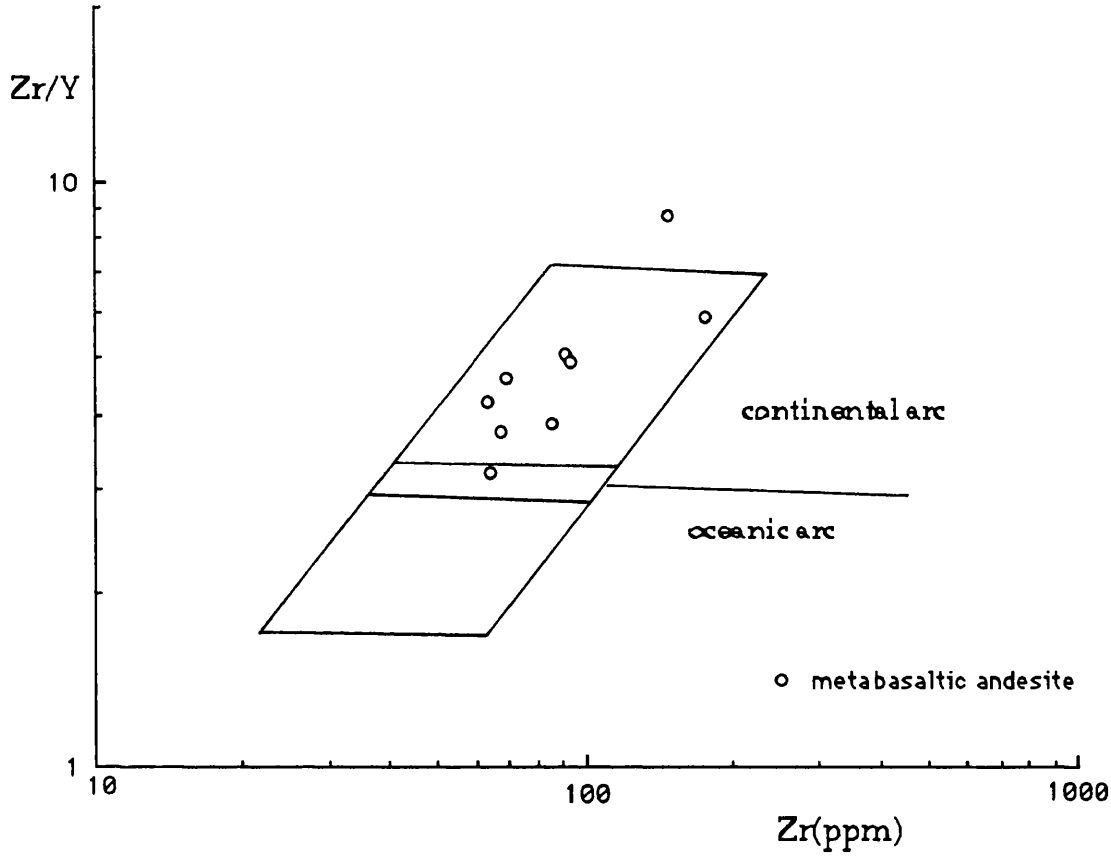

Fig. 55. Zr/Y versus Zr oceanic - continental volcanic arc discrimination diagram (Pearce,1983) showing the distribution of metabasaltic andesites from the Kadinhani area.

It has been shown that in volcanic arc environments, subduction zone enrichment of lithospheric mantle, locally coupled with crustal assimilation in zones of thickened crust, generally yield magmas with enchanced concentrations of large-ion Lithophile (LIL) elements such as K,Rb, Th, U, LREE etc. (Jakes et al., 1972; Gill, 1981; Pearce, 1982 and Tokel, 1987).

The Kadinhani metavolcanic rocks have low contents of Nb, and Nb/Y ratios ranging from 0.29 to 0.75 for the metabasaltic andesite, and 0.46-1 for the metatrachyandesites, These ratios are typical of a subalkaline magmatic series with Nb/Y <1 (Pearce & Gale 1977).

The MORB - and Primitive mantle - normalized incompatible element patterns of the rocks are shown in Figures 56, 57. Average samples of metavolcanic rocks from the area are plotted on N-MORB and Mantle - normalized incompatible element diagrams (Figures, 56 and 57).

The negative Nb anomaly (Fig. 56 and 57) is interpreted as representative of the composition of the subduction - related source material. The high LILE enrichment may be the result of crustal contamination since all likely contaminants contain large negative Nb anomalies (Dupuy et al. 1979; Taylor & Maclennan 1981; Weaver et al., 1983: Pearce 1983).

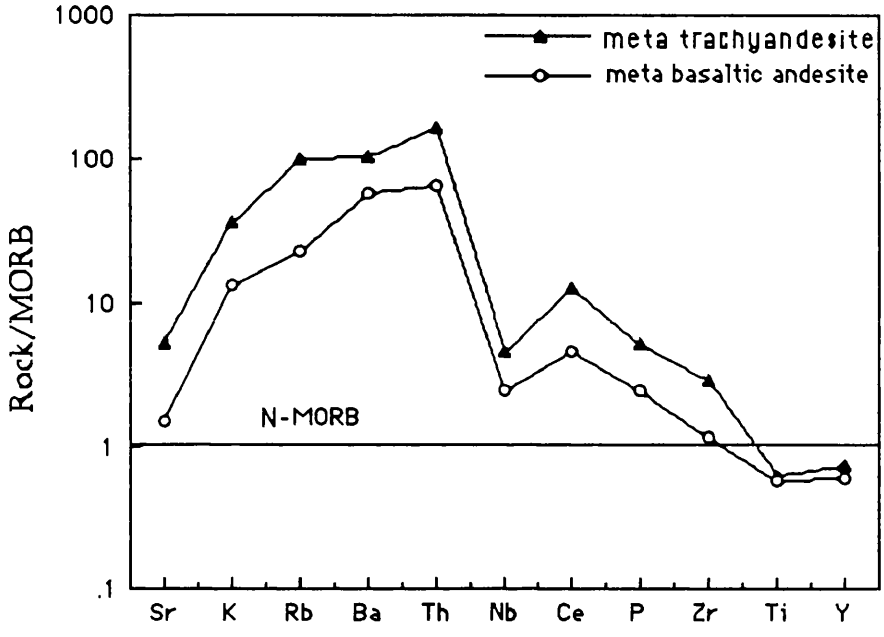

Fig. 56. MORB-normalizing incompatible element patterns for averages of the metabasaltic andesites and metatrachyandesites from the Kadinhani area. Normalizing values are as cited in Pearce (1982).

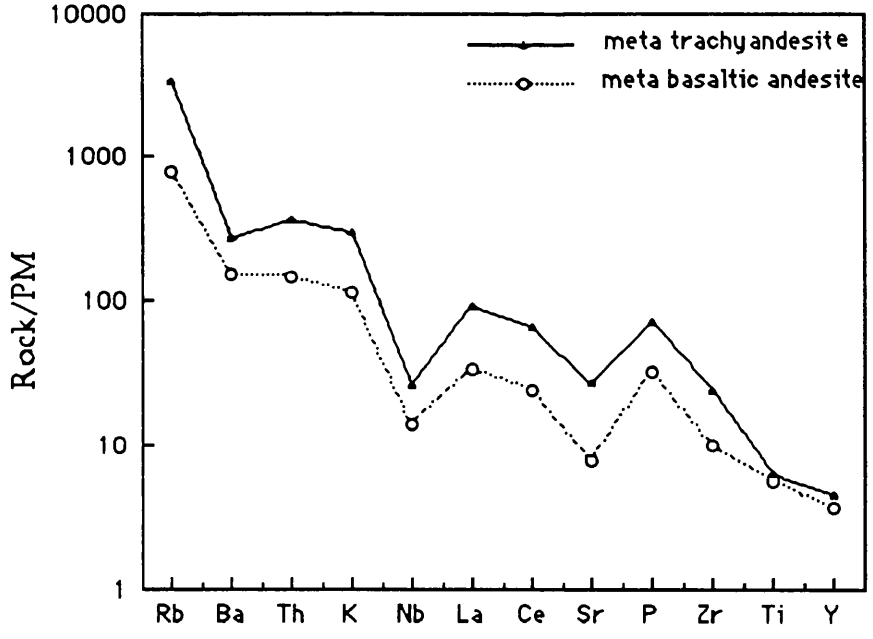

Fig. 57. Primordial mantle (PM) normalized multi-element patterns for averages of metatrachyandesite and metabasaltic andesite from the Kadinhani area. Normalizing values as cited in Wood et al. (1979).

Samples exhibit moderate enrichment in light REE and LIL (as shown by Th), and show depletion in Nb as reflected in the negative anomaly. These features indicate the presence of a subduction component in the genesis of these rocks (Pearce, 1982). The rocks are characterized by a general enrichment in Sr, K, Rb, Ba and Th, and selective enrichment in Ce and P compared to MORB (Fig. 56). This enrichment has been attributed to the introduction of aqueous fluids, and possibly sediment - derived melt, from a subducted oceanic lithosphere into the overlying mantle wedge (Best 1975; Kay 1977; Saunders & Tarney 1979; Pearce 1982, 1983).

Chondrite - normalized REE patterns for the metavolcanic rocks from the Kadinhani area (Fig. 58) generally show a strongly fractionated REE pattern with LREE/HREE ratios (La/Lu) =24-25 for metatrachyandesite and 15-27 for meta basaltic andesite. Both rocks display strongly fractionated patterns. Plagioclase fractionation is evident from the slight development of a negative Eu anomaly in metatrachyandesite. The flat HREE pattern may indicate amphibole fractionation.

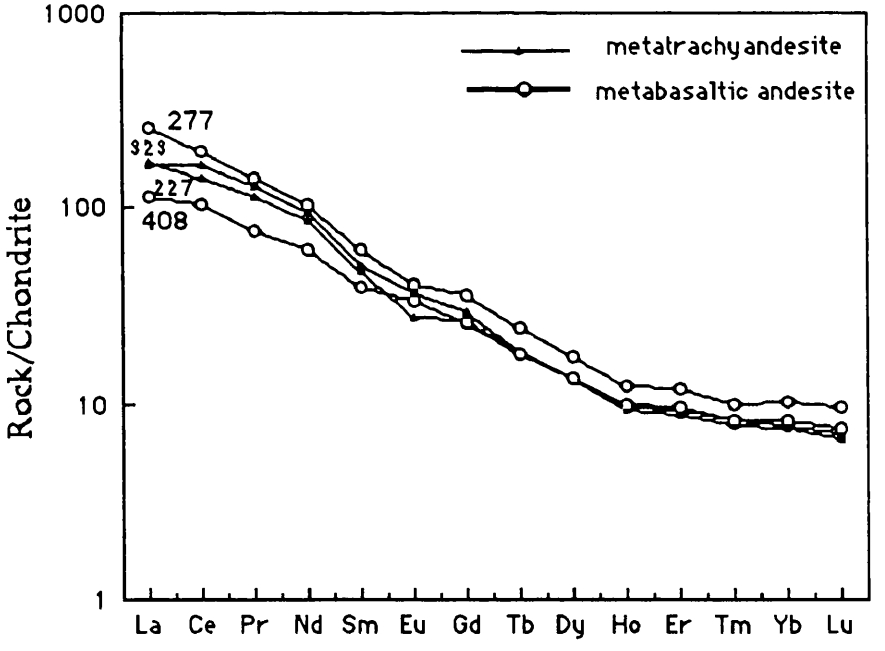

Fig 58. Chondrite - normalized rare earth element patterns for metatrachyandesite and meta basaltic andesite from the Kadinhani area. Chondrite normalizing values from Boynton (1984).

The strongly fractionationated and enriched REE patterns of the metavolcanics from the study area indicate that the conditions of formation of these rocks may have involved continental crust.

Petrogenesis;

Metabasaltic andesites are identified as continental arc types showing transitional between calcalkaline and tholeiite characters but the metatrachyandesites are calcalkaline in composition. Thus, metavolcanics studied show similarities in terms of chemical composition and tectonic setting and came from a subduction related zone.

The metavolcanic rocks were apparently derived from very similar enriched continental source regions, although systematic variations in bulk composition and in compatible element abundances do not imply significant differences in melting. They thus form a genetically related comagmatic suite.

Both rocks show marked enrichment in most incompatible elements (LILE, LREE) compared to N-MORB (Fig. 56).

The geochemistry as a whole indicates that the metavolcanics may have been derived from a subcontinental lithospheric source enriched in LIL and HFS elements. Such enrichments may have occurred in the source region prior to magma generation and / or during the ascent of magma through the thick continental crust.

Table. 48-Major Oxides, Trace Elements and CIPW Norms of the Metatrachyandesites

SA.No	227a	170	167	169	172	173	166
SiO_2	56.00	57.00	58.30	58.50	59.10	58.00	58.00
TiO_2	1.20	1.00	0.90	1.10	1.10	0.90	0.80
Al_2O_3	15.30	14.20	14.60	13.20	13.60	17.50	15.00
FeO	2.45	3.35	3.50	2.50	3.25	4.60	2.44
Fe_2O_3	3.59	3.78	3.25	3.85	3.27	2.06	3.00
MnO	0.15	0.15	0.10	0.10	0.10	0.11	0.21
MgO	5.00	5.00	3.80	4.50	4.40	2.15	4.61
CaO	5.10	5.15	4.00	4.80	4.70	1.87	4.25
Na_2O	1.80	1.80	3.00	2.35	2.20	2.09	1.62
K_2O	6.50	6.25	5.95	5.60	5.95	7.15	6.18
P_2O_5	0.80	0.70	0.70	0.70	0.70	0.80	0.70
CO_2	0.00	0.00	0.20	0.10	0.00	0.30	0.15
H_2O	2.17	1.60	1.88	2.25	1.60	1.97	2.92
TOTAL	100.06	99.98	100.18	99.55	99.97	99.50	99.88
Cr	227	171	230	229	235	232	239
Co	9	21	20	19	28	22	20
Ni"	21	42	35	35	54	35	30
Cu	103	9	25	26	155	26	25
Zn	48	77	70	69	96	64	64
Ga	10	20	21	22	23	20	19
Rb	59	215	161	160	303	180	155
Sr	1243	411	561	551	604	550	549
Y	30	20	23	22	18	22	22
Zr	218	248	342	322	200	322	340
Nb							
Ba	1030	1596	2065	2058	3650	2071	2070
La	43	61	82	81	69	81	82
Ce	104	122	139	141	137	145	130
Pb	38	4	4	3	114	5	5
U	3	1	bdl	bdl	0	bdl	bdl
Th	40	41	26	27	37	27	24
Ap	1.91	1.65	1.67	1.67	1.67	1.91	1.69
Il	2.34	1.94	1.75	2.16	2.15	1.76	1.57
Or	39.35	37.70	35.93	34.22	35.81	43.55	37.82
Ab	15.65	15.48	25.97	20.55	18.94	18.27	14.21
An	14.83	12.48	9.00	9.21	9.86	4.21	15.96
C	0.00	0.00	0.00	0.00	0.00	4.92	0.00
Mt	4.03	5.29	4.57	4.42	4.59	2.93	4.23
He	0.69	0.00	0.00	0.66	0.00	0.00	0.00
Di	4.47	7.01	5.23	8.32	7.24	0.00	0.89
Hy	10.67	10.64	9.30	7.72	9.03	10.59	11.99
Q	5.88	7.63	6.42	10.89	10.52	11.62	11.33
Cm	0.04	0.04	0.04	0.04	0.04	0.04	0.07

Coordinates of the analysed samples

170: 32985-32200
167: 32990-32300
169: 32875-32250
172: 29950-32100
173: 30065-32125
166: 32875-32275
227a: 33025-32200

Table. 48- Continued

Sa.NO	371	374	372	164	227	323	370	373	Ar.Mean
SiO_2	57.80	55.35	55.80	58.80	64.62	55.50	54.70	53.50	57.39
TiO_2	0.82	0.97	0.88	0.83	0.80	0.92	1.29	1.34	0.99
Al_2O3	15.00	14.70	14.60	13.70	14.30	15.40	13.80	14.50	15.00
FeO	2.81	3.49	2.57	3.27	1.48	4.60	6.56	2.85	3.31
Fe_2O3	3.54	3.52	4.12	3.23	3.45	2.76	5.09	5.70	3.60
MnO	0.07	0.10	0.11	0.11	0.06	0.11	0.19	0.10	0.10
MgO	4.12	4.62	4.71	4.49	1.69	4.83	5.33	5.66	4.32
CaO	3.80	4.81	4.99	4.51	3.37	4.62	5.62	4.59	4.41
Na2O	2.82	2.07	2.37	2.83	6.57	1.61	2.58	3.26	2.59
K_2O	4.98	5.84	5.11	4.67	1.22	5.84	1.06	4.14	5.09
P_2O_5	0.57	0.58	0.59	0.60	0.56	0.51	0.13	0.44	0.60
CO_2	0.35	0.20	0.15	0.36	0.00	0.40	0.10	0.21	0.16
H_2O	3.00	3.18	3.50	2.61	1.90	2.52	3.50	3.65	2.55
TOTAL	99.68	99.43	99.50	100.01	100.02	99.62	99.95	99.94	99.70
Cr	171	178	174	230	227	147	74	236	200
Co	21	19	23	20	10	19	25	27	20
Ni"	41	46	46	37	22	33	10	55	36
Cu	9	bdl	13	25	103	6	1	1	40
Zn	78	72	80	72	48	81	96	95	74
Ga	20	25	19	20	10	24	16	22	19
Rb	216	263	276	161	59	260	11	305	185
Sr	411	541	711	560	1242	325	148	603	600
Y	20	24	19	21	10	25	17	23	19
Zr	248	212	247	343	218	251	139	200	256
Nb	13	16	17	21	14	15		19	16
Ba	1596	3861	3333	2065	1030	2054	114	3750	2156
La	62	44	54	83	43	65	4	62	61
Ce	122	105	119	140	104	122	9	137	118
Pb	4	4	18	4	39	9	4	115	27
U	1	5	0	bdl	3	bdl	bdl	0	1
Th	44	34	37	27	40	22	1	38	31
Ap	1.39	1.42	1.46	1.44	1.35	1.25	0.32	1.11	1.45
Il	1.65	1.94	1.78	1.63	1.56	1.84	2.60	2.77	1.96
Or	31.20	36.50	32.00	28.60	7.44	36.60	6.61	16.59	30.66
Ab	25.30	18.50	21.20	24.70	57.30	14.50	23.10	29.95	22.72
An	11.40	14.50	12.00	11.20	3.25	15.60	24.40	13.79	12.11
C	0.00	0.00	0.00	0.00	0.00	0.00	0.00	0.00	0.00
Mt	4.98	4.95	5.22	4.57	2.19	3.93	7.13	4.49	4.50
He	0.00	0.00	0.38	0.00	1.83	0.00	0.00	2.33	0.39
Di	3.65	5.32	7.87	6.28	7.96	4.17	3.35	6.05	5.18
Hy	8.56	11.35	8.77	10.40	0.65	15.20	17.70	12.50	10.33
Q	11.70	5.28	9.04	11.00	16.30	6.70	14.50	10.30	9.93
Cm	0.04	0.04	0.04	0.04	0.04	0.03	0.02	0.04	0.40

Ar.Mean:arithmetic mean

371: 32875-32325
374: 32925-32125
372:: 29975-32175
164: 32625-31725
323: 33050-32300
373: 33050-32275
370: 32500-31650
227: 33025-32250

Table 49. Major oxides , Trace Elements and CIPW norms of the MetaBasaltic Andesite

Sampel No	272	409	405	364	274
SiO_2	52.89	52.49	53.59	52.04	55.55
TiO_2	0.60	0.60	1.30	0.60	0.46
Al_2O_3	15.65	15.96	15.63	15.16	15.46
FeO	4.65	5.76	5.23	4.72	5.55
Fe_2O_3	6.19	5.78	6.71	7.50	2.92
MnO	0.15	0.17	0.21	0.20	0.16
MgO	4.24	4.15	3.75	3.96	2.93
CaO	4.89	5.86	3.78	4.49	5.85
Na_2O	3.97	2.46	1.93	3.78	4.42
K_2O	2.19	2.50	2.51	3.28	2.41
P_2O_5	0.28	0.26	0.18	0.25	0.21
CO_2	0.55	0.40	0.15	0.47	0.50
H_2O	3.50	3.10	3.21	2.26	2.11
TOTAL	99.75	99.49	98.18	98.71	98.53
Cr	55	77	74	58	91
Co	29	27	31	26	13
Ni"	13	12	6	11	bdl
Cu	140	11	175	145	66
Zn	114	81	157	119	79
Ga	14	15	18	14	15
Rb	37	70	13	53	6
Sr	191	443	231	178	111
Y	20	17	15	18	19
Zr	37	149	63	53	6
Nb	7	5	10	9	bdl
Ba	1559	1204	176	2045	166
La	5	10	1	9	10
Ce	16	21	5	22	18
Pb	6	6	9	9	9
U	bdl	0	4	bdl	bdl
Th	6	6	4	5	10
Ap	0.69	0.65	0.46	0.60	0.51
Il	1.23	1.21	6.41	1.19	0.89
Or	13.83	15.77	15.05	20.45	2.42
Ab	54.43	22.24	23.44	33.83	37.89
An	20.58	26.8	18.66	15.54	26.97
C	0.00	0.00	2.44	0.00	0.00
Mt	8.54	7.88	6.24	10.22	4.15
He	0.00	0.00	2.09	0.00	0.00
Di	2.74	1.95	0.00	4.95	0.83
Hy	12.19	14.48	10.53	9.38	13.83
Q	5.57	8.77	14.43	3.58	12.28
Cm	0.02	0.01	0.02	0.01	0.01

Coordinates of the analysed sample

272: 39825-17175
409: 40500-17500
405: 39875-17250
407: 40100-17325
364: 39900-17275
274: 40100-17375

Table 49. Continued

Samp.No	277	406	404	408	Ar.Mean
SiO_2	56.30	54.22	54.67	53.58	53.92
TiO_2	0.82	0.43	0.52	1.09	0.71
Al_2O_3	14.40	14.44	15.90	15.67	15.36
FeO	2.47	5.88	6.64	2.16	4.78
Fe_2O_3	3.87	3.95	4.54	6.79	5.35
MnO	0.10	0.18	0.20	0.14	0.16
MgO	4.00	2.93	4.79	5.43	4.02
CaO	3.85	8.79	4.45	5.07	5.21
Na_2O	5.00	2.26	2.66	2.21	3.17
K_2O	4.55	1.06	1.20	3.02	2.52
P_2O_5	0.60	0.16	0.19	0.35	0.26
CO_2	0.38	0.90	0.20	0.35	0.42
H_2O	1.89	3.95	1.90	3.54	2.82
TOTAL	98.23	99.15	98.00	99.40	99.04
Cr	143	59	82	152	88
Co	15	21	24	10	22
Ni"	25	15	11	25	13
Cu	19	27	119	3	94
Zn	172	81	215	61	120
Ga	20	14	13	18	16
Rb	184	2	5	94	51
Sr	165	87	222	115	193
Y	25	15	18	30	20
Zr	320	69	91	175	121
Nb	8	7	1	9	8
Ba	1653	74	92	1791	973
La	84	8	13	35	19
Ce	162	8	15	77	38
Pb	46	8	9	3	12
U	7	0	0	0	1
Th	65	6	6	24	14
Ap	1.39	0.42	0.44	0.86	0.30
Il	1.92	0.89	0.98	2.22	1.87
Or	17.18	14.14	11.18	15.08	13.9
Ab	42.72	20.73	30.87	23.96	32.22
An	17.19	31.47	20.78	22.70	22.29
C	0.00	0.00	2.02	0.00	0.49
Mt	4.80	5.58	6.35	3.12	6.37
He	0.45	0.00	0.00	4.23	0.75
Di	11.45	11.99	0.00	1.37	7.83
Hy	4.75	8.55	19.18	13.83	11.85
Q	4.46	9.74	7.94	12.41	8.78
Cm	0.03	0.02	0.01	0.03	0.01

Ar.Mean: Arithmetic mean

Coordinates of the analysed samples

277: 33025-32250
406: 40400-17550
404: 40400-17500
408: 40550-17450

Table. 50. Rare earth element data for the meta trachyandesite 227, 323 and metabasaltic andesite 408, 277.

Sample No	227	323	408	277
La	171.1	167.8	116.3	259.9
Ce	143.9	166.5	105.2	197.5
Pr	114.1	128.8	76.9	141.5
Nd	87.4	95.0	61.9	105.1
Sm	48.0	50.3	40.0	61.1
Eu	27.5	37.3	33.1	40.0
Gd	27.3	29.2	26.1	36.4
Tb	18.0	18.3	18.2	24.2
Dy	13.6	13.7	13.6	17.6
Ho	9.5	9.3	9.9	12.3
Er	9.2	8.8	9.4	11.7
Tm	8.1	7.5	8.1	9.9
Yb	7.6	7.4	8.1	10.2
Lu	7.1	6.6	7.4	9.7

Coordinates of the analysed samples

227; 33025-32250

323: 33050-32300

408: 40550-17450

277: 33025-32250

6.5.1.2. METAHORNBLENDE GABBRO AND METADOLERITE

Petrography, mineral chemistry, and relict mineral assemblages indicate that dykes of metahornblende gabbro (with primary hornblende) and metadolerite occur with different mineralogical compositions. Geochemical data will be used to find out if these rock types could be petrogenetically related. Using the CIPW norms classification scheme of Streckeisen and Le Maitre (1979) these rocks plot in the diorite gabbro - monzo diorite,monzo gabbro fields (Fig. 59).

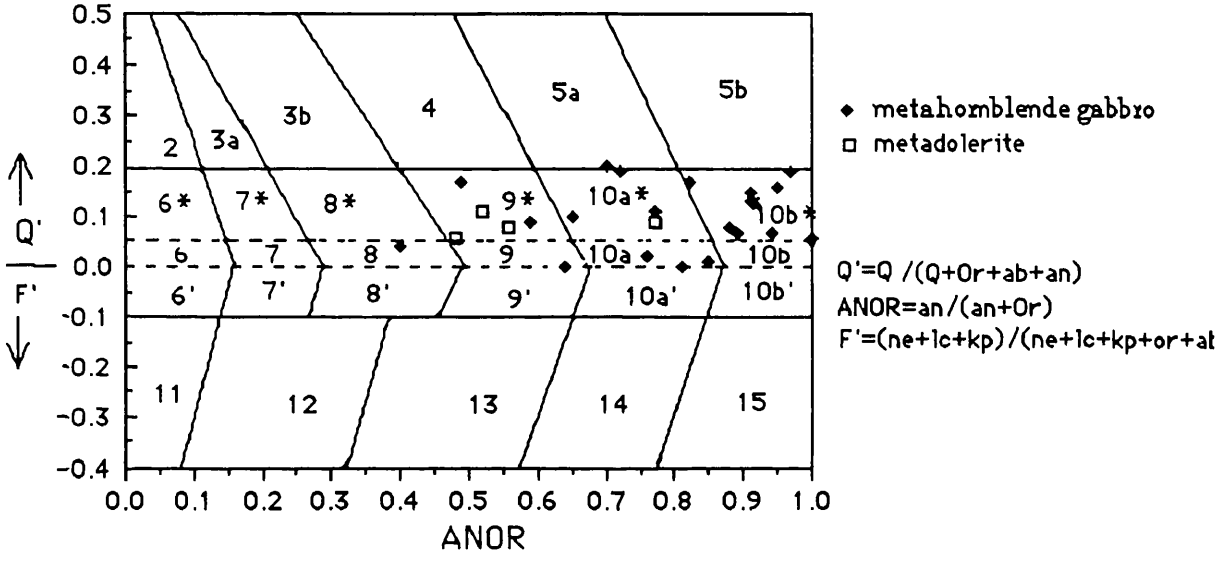

Fig. 59. CIPW nomenclature and classification of the metahornblende gabbro and metadolerite from the Kadinhani area, ANOR vs.Q' plot after Streckeisen and LeMaitre (1979). Field names: 2. alkali-feldspar granite; 3a,3b.granite; 4.granodiorite: 5a,5b.tonalite; 6.alkali-feldspar syenite; 7. syenite; 8. monzonite; 9.monzodiorite monzogabbro; 10a,10b. diorite gabbro; 11.foid syenite;12. foid monzosyenite; 13. foid monzodiorite monzogabbro; 14.foid diorite gabbro; 15. foidolite. * indicates prefix "quartz", ' indicates prefix "foid bearing".

The metahornblende gabbro and metadolerite rocks belong to the subalkaline rock series (Figure, 60) according to the classifications of Floyd and Winchester (1975) and Winchester and Floyd (1976). On the alkali vs. SiO_2 plot (Fig. 61) the metahornblende gabbros mostly plot in the tholeiite field and the metadolerites in the calcalkaline field but some of the gabbros do straddle the boundary.

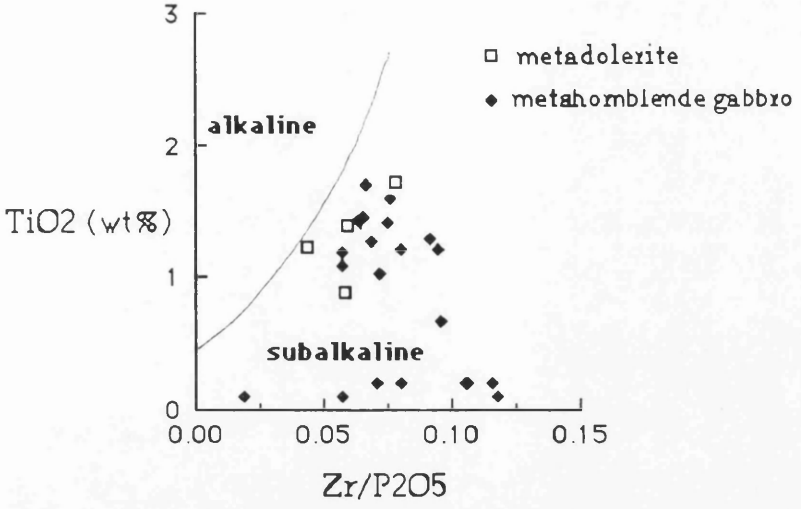

Fig. 60. Zr/P_2O_5 versus TiO_2 discrimination diagram used to reveal the original rock or magma type. Field boundaries from Floyd& Winchester (1975) and Winchester and Floyd (1976).

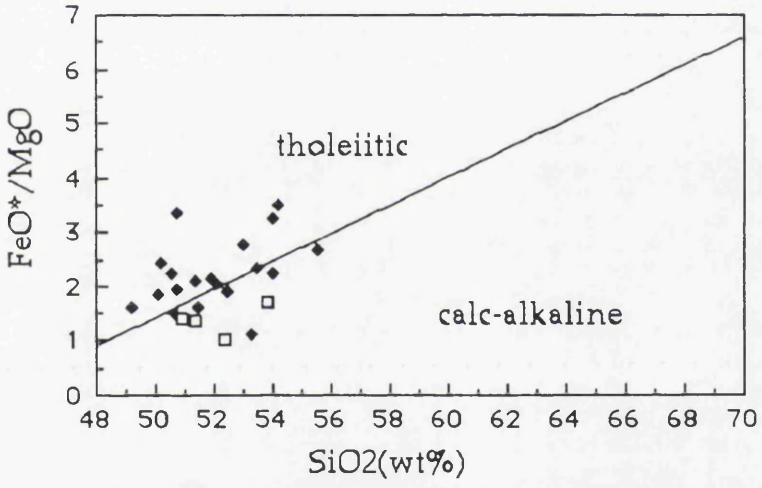

Figure 61. SiO_2 vs FeO*/MgO for metahornblende gabbro (♦) and metadolerite (□) (after Gill, 1981 and Ewart, 1982).

The major oxides and trace elements compositions of the metahornblende gabbro are presented in Table 51 and for the metadolerite in Table 52. Rare earth element data for both of the rocks are given in table 53.

The incompatible element ratios of the metadolerites and the metahornblende gabbros (K/Nb, K/Ba, P/Ce, Rb/Sr, Zr/Nb, Zr/Y, K/Rb, Ce/Y, and Ba/Zr) differ from each other. The differences in incompatible element ratios may have arisen by extensive plagioclase, clinopyroxene, apatite, and Ti-magnetite fractionaton (Mikhalsky et al., 1993).

The metahornblende gabbro shows a large range of mg-numbers

(mg=(mol 100 X Mg/(Mg+Fe)) between 33.30-61.30, but, the metadolerites have mg-numbers between 25.60 - 31.40.

Figure 62. illustrates Harker variation diagrams for metahornblende gabbro and metadolerite.

Since Ba and K have large ionic radii, these elements tend to concantrate in amphibole, which has a large vacant site (Yamamoto, 1984). The increase in Ba and K with increasing SiO_2 suggests the onset of amphibole fractionation in the evolution of the metahornblende gabbro. Depletions in CaO and MgO and enrichment in K_2O reflect the crystallization of hornblende in the metahornblende gabbro. The decrease in TiO_2,CaO and MgO reflects crystallization of ilmenite and augite in metadolerite. La, Zr, and P_2O_5 contents decline slightly with increasing SiO_2 in the metadolerite.These depletions correlate with the presence of apatite phenocrysts and zircon inclusions in pyroxene phenocrysts in metadolerite. The slight increase in Na_2O indicates that plagioclase was dominant crystalline phase in metahornblende gabbro. Sr is generally, strongly concentrated into plagioclase (Jensen, 1973). Thus, the steep, positive trend of Sr suggests that the start of plagioclase fractionation was considerably delayed in metahornblende gabbro. Zr and Y increase with increasing SiO_2 showing that separation of zircon did not occur in metahornblende gabbro. Generally, depletions in compatible elements (Ni and Co) and enrichment in incompatible elements (Ba, Y and Ce) indicate the existence of crystal fractionation processes in the metahornblende gabbro.

Furthermore, Harker variation diagrams suggest hornblende and minor plagioclase fractionation in the metahornblende gabbros, and augite and ilmenite fractionation in the metadolerites.

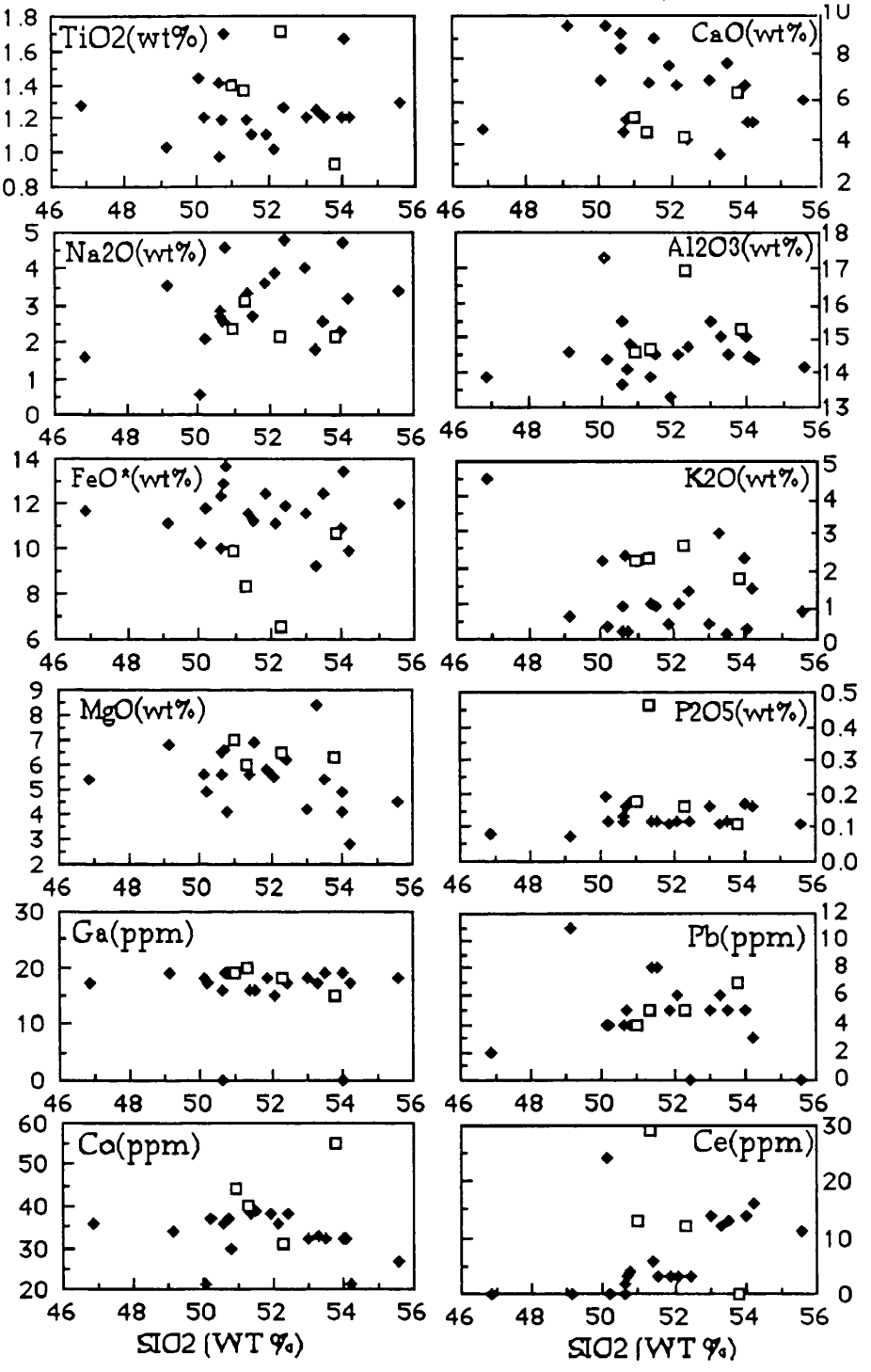

Fig. 62. Harker diagrams showing variation of major oxides and trace elements in Metahornblende gabbro (♦) and metadolerite (□).

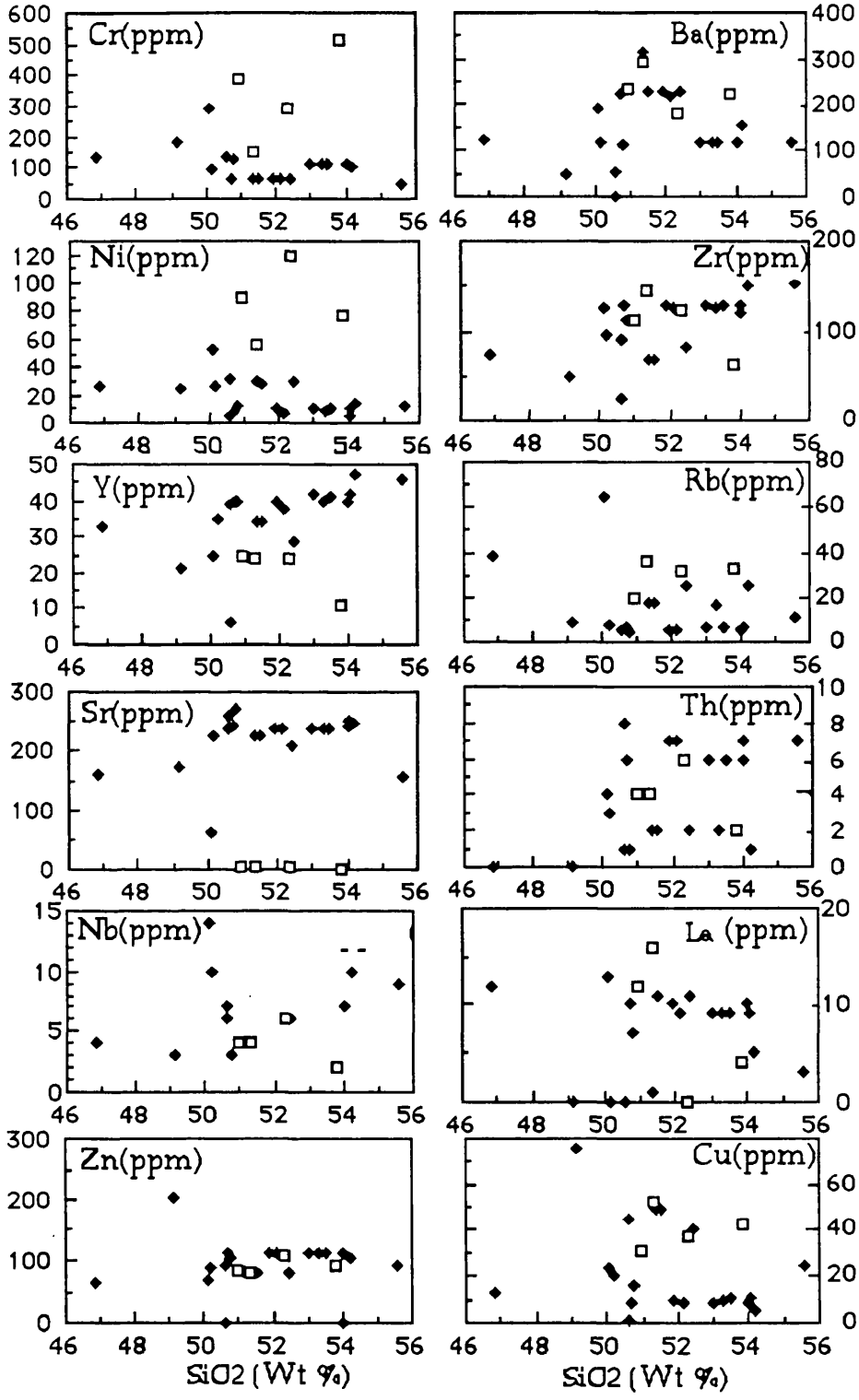

Figure 62. continued, metahornblende gabbro (♦) and metadolerite (□)

Plots of Cr and Ni against Zr show different trends for the two rock types confirming their distinctness (Figure, 63). In the metadolerite, Cr content decreases with increasing Zr, suggesting significant clinopyroxene fractionation (Ernst et al., 1991). However, in metahornblende gabbro Y

shows positive trend with increasing Zr, suggesting hornblende fractionation and significant plagioclase accumulation in the evolution of the rocks.

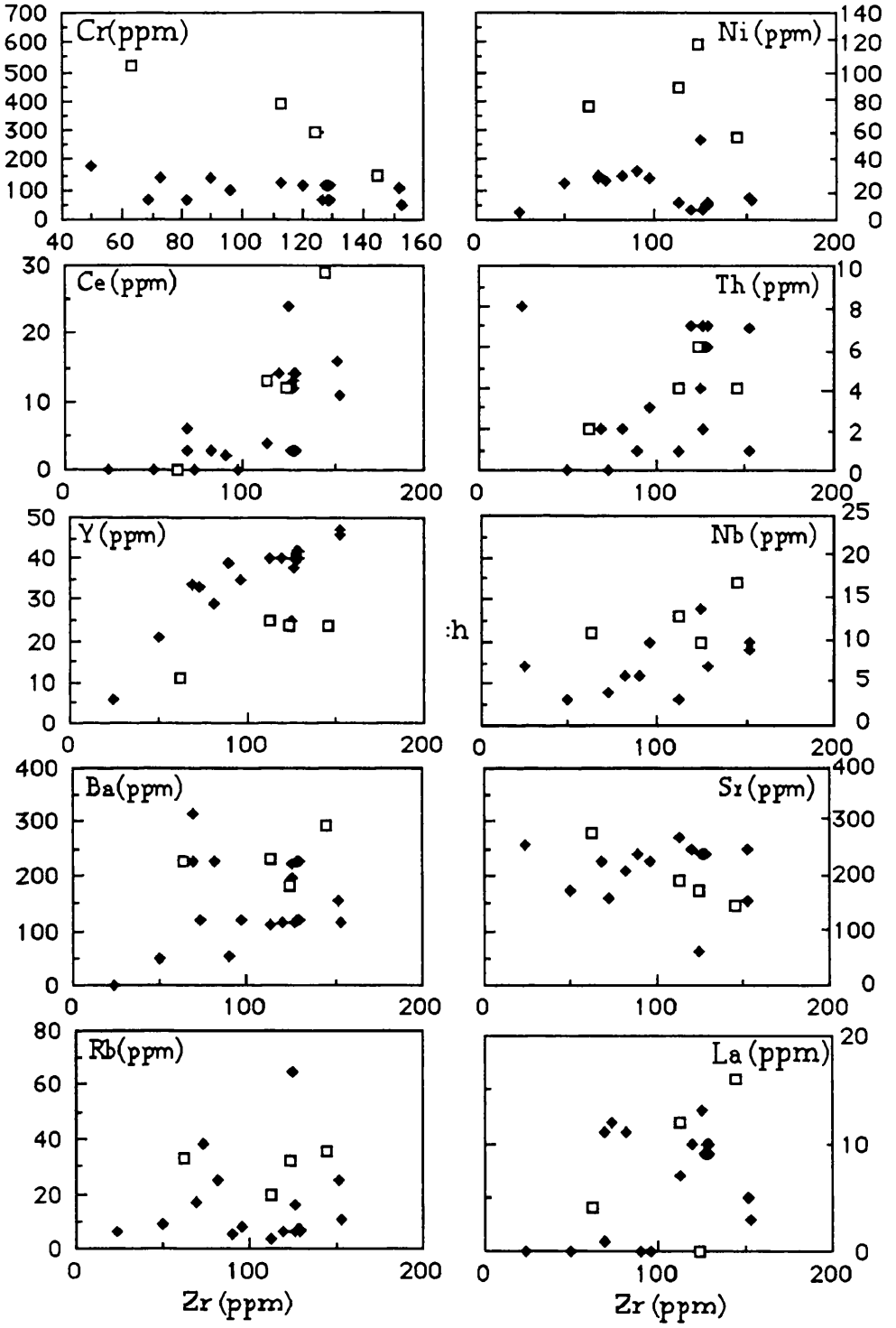

Figure 63. Trace elements concentrations vs. Zr, metahornblende gabbro (♦) and metadolerite (□).

All major and trace element data are also plotted against Niggli mg in Figure 64 and 64a. Negative correlations between Niggli mg and Nb, Zr, Y, P_2O_5, TiO_2 and Na_2O and poor positive correlations with Cr, and Ni are present in metahornblende gabbro. These trends suggest that the parent magma of the metahornblende gabbros are likely to represent low degrees of partial melting (Mikhalsky et al., 1993). In the metadolerite Y is negatively correlated whereas Ba, Fe_2O_3, total FeO*, and CaO are positively correlated with Niggli mg, representing major plagioclase and ilmenite control in the evolution of the rocks (DePaolo, 1981).

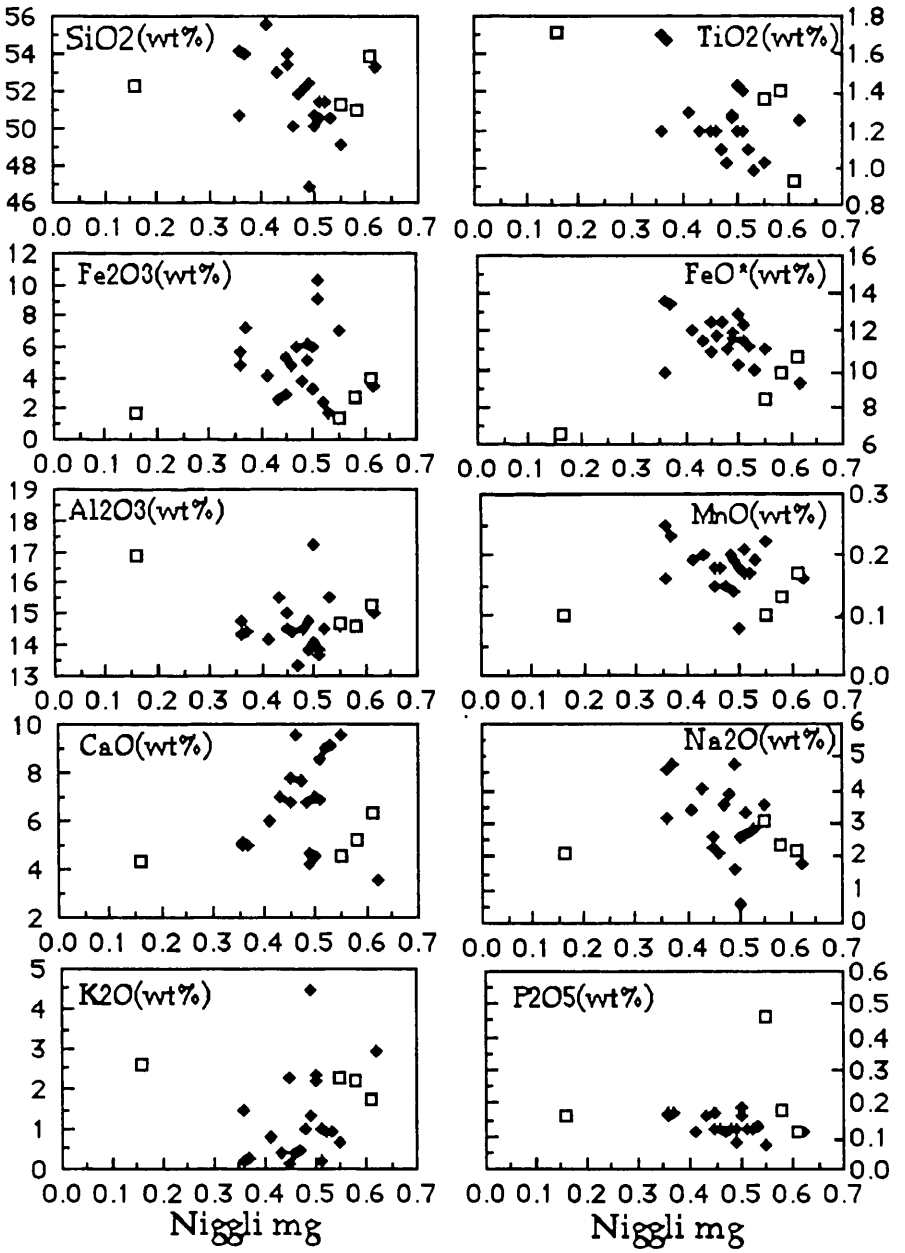

Figure.64.Plots of major oxides versus Niggli mg, metahornblende gabbro (♦) and metadolerite (□). FeO*: total.

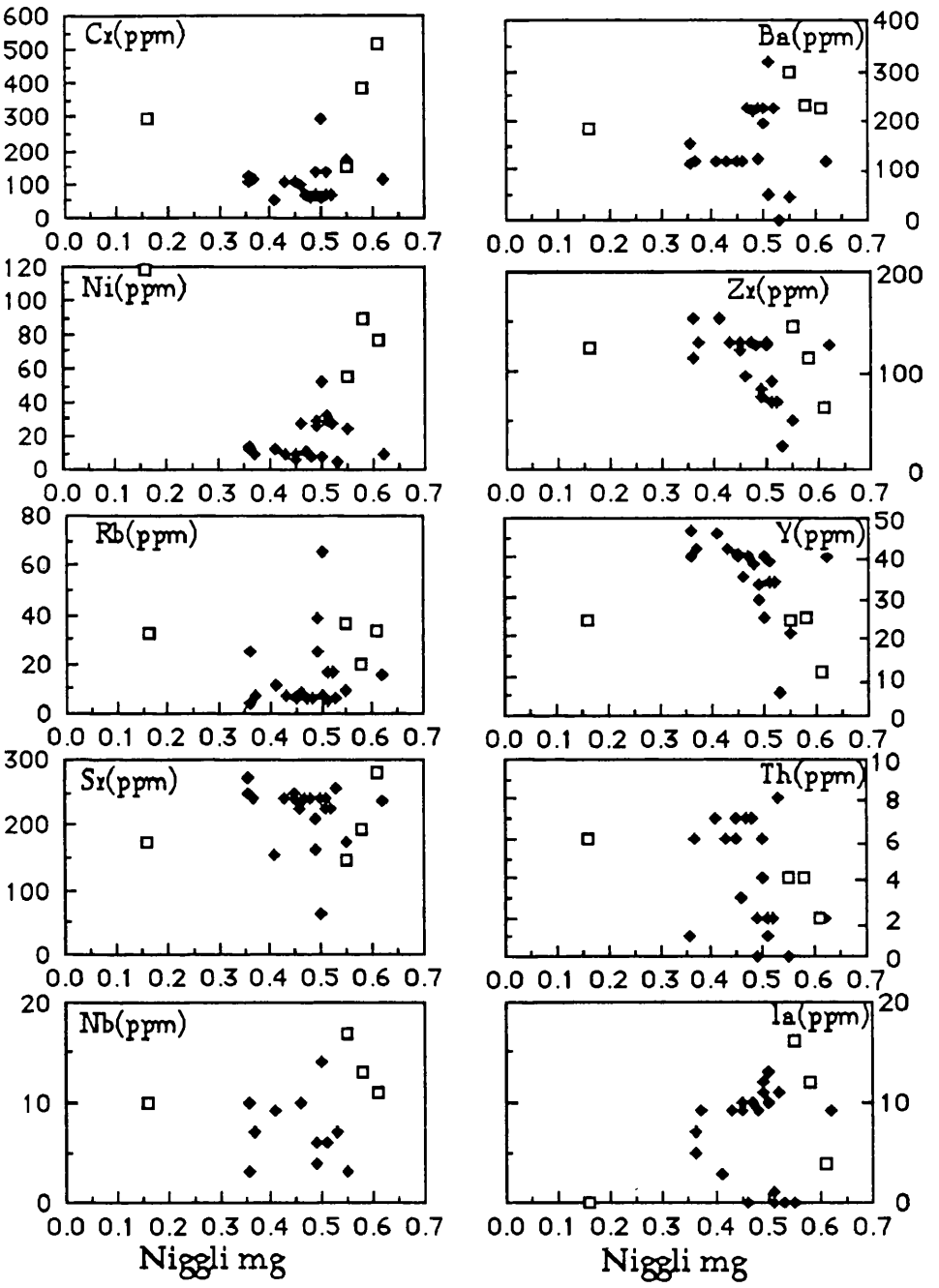

Figure.64a.Plots of trace elements versus Niggli mg, metahornblende gabbro (♦) and metadolerite (□).

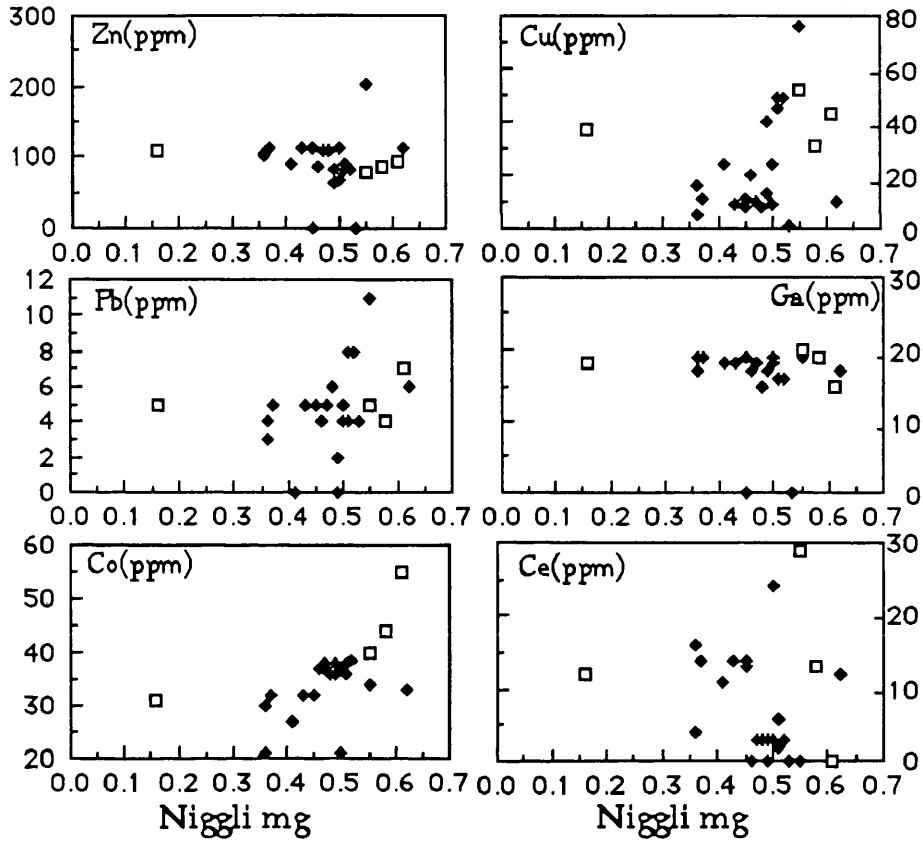

Fig. 64a. Continued, metahornblende gabbro (◆) and metadolerite (□).

In a Ti versus Zr plot (Fig. 65), both the metahornblende gabbro and the metadolerite plot in the Mid- Ocean - Ridge Basalt (MORB) field. However, in the metadolerites most of the geochemical data (e.g. REE) indicates that the rocks are related to within-plate lavas.

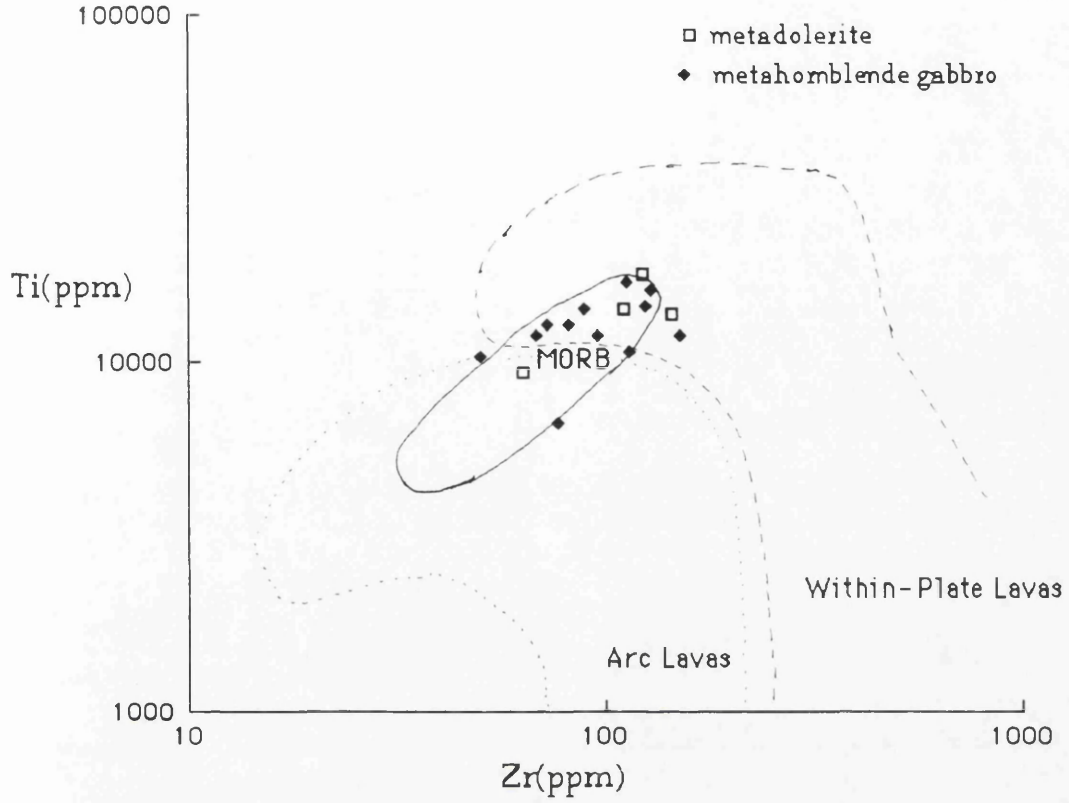

Fig. 65. Ti versus Zr for the metahornblende gabbros and metadolerites of the Kadinhani area. Field boundaries from Pearce (1982) and Pharaoh&Pearce (1984).

On the TiO_2 (wt%) versus Zr/P_2O_5 diagram of Floyd et al. (1975) the metahornblende gabbros fall in the field of abyssal tholeiites (Fig. 66).

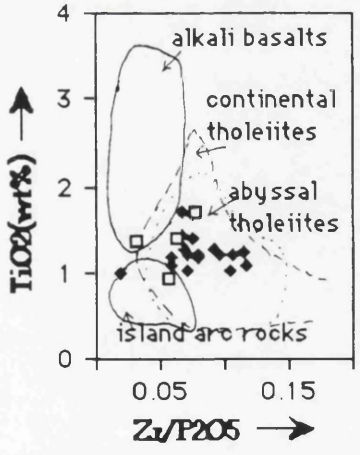

Figure. 66. Zr/P_2O_5- TiO_2 diagram of the metahornblende gabbro (♦) and metadolerite (□), after Floyd et al (1975).

The geochemical characteristics of the metahornblende gabbros are illustrated on N-MORB and Primitive Mantle - normalized patterns (Figures 67-68) which demonstrate that the gabbros are similar to

tholeiitic N-MORB but relatively enriched in K,Th, Rb, Ba, Nb and depleted in Ce and Ti.

The metadolerites are enriched in Rb, K, Ba, Th, Ce, P and Nb and depleted in Ti and Y relative to MORB, being calc-alkaline metadolerites, indicated by enrichment in K, Rb, Ba, Nb, Ce, P, Zr, and Ti compared with the tholeiitic meta hornblende gabbros as seen on MORB - normalized patterns (Figure, 67). These characteristics may be due to the involvment of subcontinental lithosphere in magma genesis as shown by Pearce (1983). The patterns (enrichment in LILE relative to HFSE) suggest that both upper mantle (sub-continental lithosphere) and subduction components may have been involved in the genesis of the metadolerites in a continental margin environment (Watters et al., 1987).

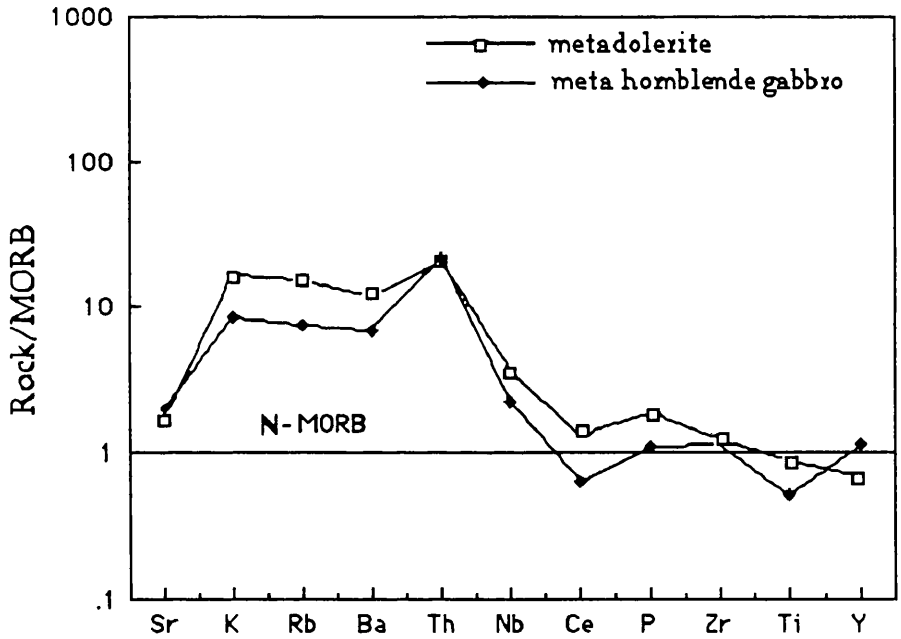

Fig.67. MORB-normalized patterns for averages of metahornblende gabbros and metadolerite samples from the Kadinhani area. Normalizing values as cited in Pearce (1982).

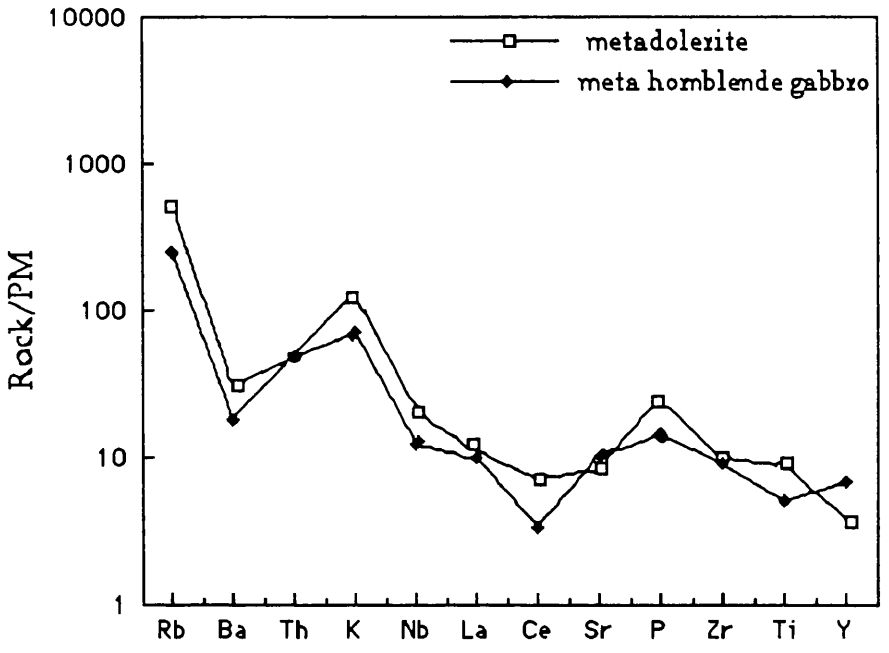

Fig. 68. Primordial mantle - normalized multi-element patterns for averages of the metahornblende gabbros and the metadolerites from the Kadinhani area. Normalizing values as cited in Wood et al. (1979).

The slight downwards depleted, patterns of the HREE (Fig. 69) profiles in the metadolerite could be explained by the fractionation of clinopyroxene which has larger crystal / liquid distribution coefficients for middle REE than for light or heavy REE in basic liquids (Luhr & Carmichael, 1980).

During the evolution of mafic melts the La/Yb ratio is frequently a good indicator of fractional crystallization. In the metadolerites, $(La/Yb)_N$ is 6-12 showing moderate fractionation, during fractional crystallization of plagioclase, the La/Yb ratio will decrease in the residual liquid because this mineral preferentially incorporates the light rare earth elements (LREE) over the heavy REE. During pyroxene fractionation, however, the La/Yb ratio will increase in the residual liquid. A small increase of La/Yb with decreasing mg-number can be explained by pyroxene fractionation (Bosbach et al, 1991).

The metadolerites are LREE enriched with $(Ce/Sm)_N$ =2.5, (Fig. 69), which are similar to those of subduction- related magmas (Wood, Joran & Trevil, 1979; Wood, 1980; Pearce, 1982, 1983). The more fractionated and LREE- enriched character of the metadolerites indicates that the evolution of the rocks involved continental crust (Watters et al, 1987).

The REE (Fig. 69) patterns of the metahornblende gabbros are quite different being almost flat with no LREE enrichment or depletion and slightly negative Sm-Lu slopes, being a pattern characteristic of MORB.

The $(La/Yb)_N$ ratio for the metahornblende gabbro is 1-1.4 implying only slight differentiation of the initial magmas and closeness in their composition to the parent magma (Volkova et al., 1992).

One sample of the metahornblende gabbro has a significant positive Eu anomaly, probably reflecting the accumulation of plagioclase (Stosch and Lugmair, 1987).

These patterns are similar to the bulk of REE profiles of ocean floor basalts (Schilling, 1971, 1975). Rare-earth element patterns from the least fractionated meta hornblende gabbro show a similarity that corresponds with tholeiitic suite types implying a probable worldwide similarity of source and process in the production of ocean - ridge type magma (Arth, 1981).

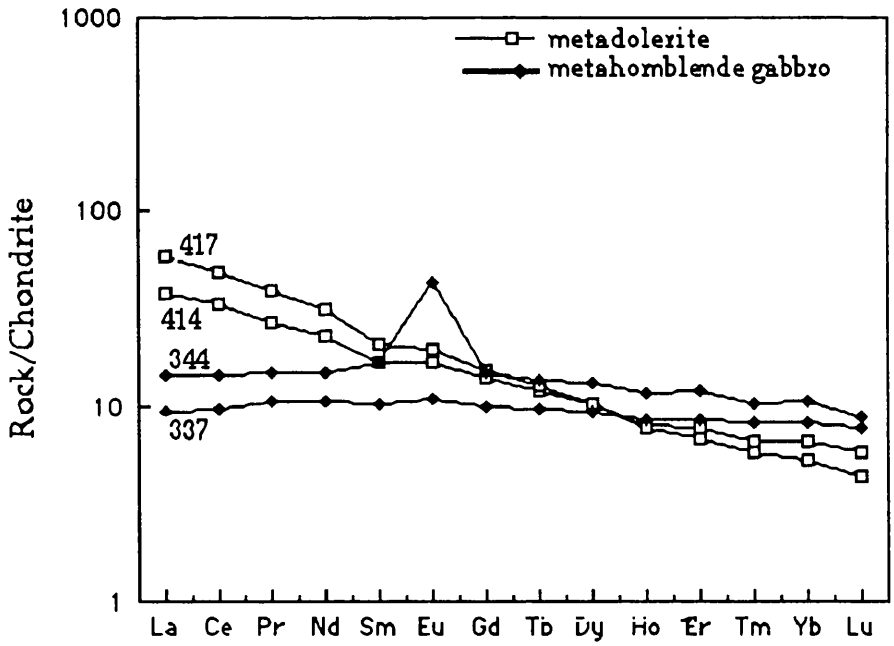

Fig. 69. Chondrite - normalised rare earth element distribution patterns for the metahornblende gabbro and metadolerites from the Kadinhani area. Chondrite normalising values from Boynton(1984).

Petrogenesis;

Geochemical consideration of the metadolerites and metahornblende gabbros shows that these two rocks types are distinct. Therefore, they should have been derived from different magmatic sources.

The metahornblende gabbros show a large range of mg-numbers (=100 (Mg/Mg+Fe^{+2})) between 33.30 and 61.30, but the metadolerites have a small range of mg=25.60 - 31.40. Since fractionation of hornblende requires a hydrous magma and does not pass into augite fractionation the two magmas are not related. This is also suggested by the metadolerite having relatively high Ni (56-119 ppm) and Cr (150-516 ppm) compared to the metahornblende gabbros which have low Ni (5- 53 ppm) and Cr (0-294 ppm) despite being less fractionated as regards mg. These relationships are only compatible with two different and unrelated magmas.

Many element ratios of the metadolerites and the metahornblende gabbros (K/Nb, K/Ba, P/Ce, Rb/Sr, Zr/Nb, Zr/Y, K/Rb, Ce/Y, and Ba/Zr) are quite different.

The metahornblende gabbros are tholeiitic showing significant iron enrichment whereas the metadolerites are calc alkaline with lack of iron enrichment. Major and trace element variations suggest that crystal fractionation played an important role in the evolution of both rocks; hornblende in metahornblende gabbro, and augite and Fe-Ti oxide fractionation in metadolerite.

The metahornblende gabbros have low Ni (average ~18 ppm, see table 51) contents. The low Ni contents of the rocks imply that even the most mafic rocks are not primary mantle derived melts (Atherton, 1985). Moreover, both rock types do not represent primary melt features, and thus they have originated from different parental magma sources.

The relative role of continental crust and upper mantle in the petrogenesis of continental igneous rocks is often difficult to evaluate. These difficulties are exaggerated in dealing with metamorphosed igneous rocks. A major problem concerns whether there is the petrogenetic relationship between the metahornblende gabbros and the metadolerites.

In the metahornblende gabbros, REE patterns and compositional data suggest derivation from a parental source similar to tholeiitic MORB- type melts. Formation of such a parental MORB- type melt is

commonly ascribed to small percent of partial melting of relatively undepleted mantle source and, possibly followed by small degrees of fractional crystallization (e.g. Cullers and Graf, 1984b).

The metahornblende gabbro was derived from source a similar to mid-ocean- ridge type parent. The low abundance of Nb and other elements with high ionic potential (e.g. Ti) in the metahornblende gabbro may be a result of their retention in residual phases stable in a hydrated mantle source region (Kay, 1977, Pearce, 1982). The metadolerite reveals parental magma was similar to subduction related lavas in a continental margin environment, involving a mix of subcontinental lithosphere and subduction components.

The normalized incompatible element patterns (Fig. 67) of the calc-alkaline continental metadolerites, are enriched in K,Rb, Ba, Nb, Ce, P, Zr and Ti, compared with the tholeiitic oceanic metahornblende gabbros. These characteristics may be due to the involvement of subcontinental lithosphere in magma genesis as shown by Pearce (1983). Furthermore both upper mantle (sub-continental lithosphere) and subduction components can be identified in incompatible element patterns of metadolerite from continental margin environments (Watters et al, 1987).

In conclusion, metahornblende gabbro and metadolerite are not cogenetic, and were derived from different magmatic sources.

Table 51. Major Oxides, Trace Elements and CIPW norms of the Metahornblende Gabbro.

Samp. No	186 a	225	224	73	77	77 a
SiO_2	53.50	51.50	53.30	54.00	50.60	53.00
TiO_2	1.20	1.10	1.25	1.20	0.98	1.20
Al_2O_3	14.50	14.50	15.00	15.00	15.50	15.50
FeO	7.90	9.77	6.47	8.91	9.21	8.06
Fe_2O_3	5.39	2.40	3.44	2.88	1.71	2.54
MnO	0.15	0.17	0.16	0.18	0.19	0.20
MgO	5.41	6.94	8.39	4.9	6.54	4.17
CaO	7.80	8.95	3.50	6.75	9.16	7.00
Na_2O	2.57	2.72	1.82	2.27	2.82	4.02
K_2O	0.14	0.94	2.95	2.24	0.95	0.39
P_2O_5	0.12	0.12	0.11	0.17	0.13	0.16
CO_2	0.35	0.45	0.13	0.48	0.55	0.43
H_2O	1.75	1.35	2.00	1.75	2.21	3.20
TOTAL	100.78	100.91	98.52	100.75	100.55	99.87
Cr	110	65	111	110	bdl	110
Co	32.	38	33	32	bdl	32
Ni"	9	28	9	6	5	10
Cu	11	49	10	8	1	9
Zn	112	82	113	0	0	112
Ga	18	16	17	0	0	18
Rb	7	17	16	6	6	7
Sr	240	226	238	250	258	240
Y	41	34	39	40	6	42
Zr	128	68	126	119	24	128
Nb					7	
Ba	118	228	117	116	bdl	118
La	9	11	9	10	bdl	9
Ce	13	3	12	13	bdl	14
Pb	5	8	6	5	4	5
U	0	bdl	bdl	bdl	bdl	0
Th	6	2	2	7	8	6
Ap	0.28	0.30	0.28	0.42	0.33	0.39
Il	0.39	0.19	0.38	0.39	0.21	0.39
Or	0.83	5.67	18.02	13.65	5.85	2.48
Ab	22.50	23.60	15.90	19.79	24.70	35.95
An	28.6	25.16	17.13	24.91	27.84	24.40
C	0.00	0.00	2.82	0.00	0.00	0.00
Mt	7.46	3.40	4.84	4.07	2.45	3.63
He	0.00	0.00	0.00	0.00	0.00	0.00
Di	8.69	16.04	0.00	6.99	15.14	9.32
Hy	18.93	25.27	31.96	22.41	19.69	18.55
Q	12.15	0.11	10.37	7.08	3.56	4.58
Cm	0.03	0.02	0.03	0.03	0.00	0.03

Coordinates of the analysed samples

186a: 35250-32875
225: 37250-28550
224: 39000-29100
73: 40050-27400
77: 37750-25125
77a: 37825-25135

Table.51. Continued

Sam.No	353	312	309	326	337	431	383
SiO_2	51.90	50.70	52.12	50.77	49.15	50.19	50.08
TiO_2	1.10	1.19	1.02	1.70	1.03	1.20	1.44
Al_2O_3	13.30	14.10	14.50	14.80	14.63	14.4	17.24
FeO	7.19	7.64	8.16	8.79	4.56	6.98	7.64
Fe_2O_3	6.03	6.02	3.74	5.70	7.06	4.84	3.30
MnO	0.15	0.18	0.20	0.25	0.22	0.18	0.08
MgO	5.80	6.60	5.50	4.07	6.84	4.89	5.56
CaO	7.70	4.55	6.75	5.13	9.58	9.56	6.95
Na_2O	3.60	2.60	3.90	4.60	3.53	2.11	0.55
K_2O	0.45	2.35	1.00	0.21	0.64	0.38	2.17
P_2O_5	0.11	0.16	0.12	0.17	0.07	0.12	0.19
CO_2	0.51	0.30	0.46	0.33	0.60	0.61	0.45
H_2O	2.25	3.20	2.31	2.30	2.00	3.45	3.10
TOTAL	100.09	99.59	98.78	98.82	99.91	98.91	98.75
Cr	64	64	63	123	178	96	294
Co	38	37	36	29	134	37	21
Ni"	11	8	9	12	25	27	53
Cu	10	9	8	16	76	19	23
Zn	110	112	110	106	204	88	69
Ga	18	19	15	19	19	17	18
Rb	6	7	6	4	9	8	65
Sr	240	241	239	272	172	226	62
Y	40	439	38	40	21	35	25
Zr	129	128	126	113	50	96	125
Nb				3	3	10	14
Ba	226	226	220	110	47	119	193
La	10	10	9	6	0	bdl	13
Ce	3	3	3	4	bdl	bdl	24
Pb	5	5	6	4	11	4	4
U	bdl	bdl	bdl	bdl	6	bdl	bdl
Th	7	6	7	1	0	3	4
Ap	0.25	0.39	0.30	0.42	0.18	0.30	0.46
Il	0.21	0.39	0.40	3.40	1.97	2.47	2.88
Or	2.77	15.01	6.20	1.30	3.96	2.42	13.59
Ab	31.97	23.77	34.59	41.00	31.00	19.28	4.90
An	19.76	21.44	20.00	20.00	23.00	30.95	35.20
C	0.00	0.00	0.00	0.00	0.00	0.00	1.90
Mt	8.36	8.38	5.30	7.96	9.65	6.80	4.69
He	0.00	0.00	0.00	0.00	0.00	0.00	0.00
Di	15.90	1.45	11.71	4.56	20.10	15.68	0.00
Hy	15.13	25.39	19.92	16.48	8.86	11.94	23.22
Q	5.08	3.51	1.26	4.44	0.78	9.92	12.94
Cm	0.01	0.02	0.01	0.03	0.04	0.01	0.05

Coordinates of the analysed samples

353: 38875-31050
312: 40225-27250
309: 40375-25375
326: 35250-32800
337: 37125-28575
431: 23375-22990
383: 38750-27000

Table.51. Continued

Sam.No	368	344	377	339	357	186	313	Ar.Mean
SiO_2	50.59	51.38	54.20	55.59	52.42	54.04	50.86	51.98
TiO_2	1.41	1.19	1.20	1.29	1.27	1.67	1.28	1.24
Al_2O_3	13.68	13.84	14.35	14.16	14.75	14.43	13.87	14.6
FeO	2.22	2.77	5.56	8.15	7.55	7.00	6.10	7.03
Fe_2O_3	10.32	9.04	4.85	4.19	5.10	7.13	6.19	5.09
MnO	0.21	0.17	0.16	0.19	0.19	0.23	0.14	0.18
MgO	5.55	5.55	3.83	4.47	6.23	4.12	5.37	5.53
CaO	8.52	6.85	4.97	6.05	4.23	5.02	4.64	6.66
Na_2O	2.70	3.31	3.20	3.40	4.77	4.75	3.59	3.14
K_2O	0.21	1.00	1.44	0.77	1.36	0.29	2.48	1.11
P_2O_5	0.12	0.12	0.16	0.11	0.12	0.17	0.80	0.16
CO_2	0.58	0.4	0.26	0.18	0.14	0.38	0.30	0.39
H_2O	3.00	2.93	3.33	1.65	1.20	0.90	3.25	2.35
TOTAL	99.11	98.55	97.51	100.20	99.34	100.13	98.87	98.65
Cr	135	67	106	50	65	111	137	103
Co	36	38	21	27	38	32	35	31
Ni	32	29	14	13	29	10	26	18
Cu	45	49	5	24	39	11	13	22
Zn	90	82	103	90	82	112	64	92
Ga	15	16	17	18	17	19	17	15
Rb	5	17	25	11	24	7	38	14
Sr	238	226	248	155	207	240	160	219
Y	39	34	47	46	29	42	33	36
Zr	90	69	151	152	82	129	73	105
Nb	6		10		6	7	4	7
Ba	52	316.78	155	117	228	119	121	147
La	bdl	1.00	4	3	11	9	12	7
Ce	2	5.95	16	11	3	14	bdl	7
Pb	4	8.00	3	4	bdl	5	2	5
U	bdl	bdl	bdl	bdl	bdl	0	bdl	bdl
Th	1	1.96	1	7	2	6	bdl	4
Ap	0.30	0.30	0.39	0.27	0.30	0.39	0.21	0.38
Il	2.92	2.43	2.48	2.50	2.46	3.22	2.75	1.62
Or	1.36	6.38	9.27	4.66	8.27	1.71	13.00	6.72
Ab	24.95	30.28	29.52	29.35	41.53	41.03	15.14	26.98
An	26.90	21.56	22.37	21.60	15.21	17.62	19.72	23.15
C	0.00	0.00	0.00	0.00	0.00	0.00	0.00	0.23
Mt	2.05	4.52	6.77	5.91	7.13	9.78	8.54	6.08
He	8.07	5.22	0.00	0.00	0.00	0.00	0.00	0.66
Di	14.34	11.13	2.75	6.82	4.48	5.42	4.47	8.74
Hy	8.46	9.78	10.19	17.02	18.89	11.62	16.33	17.50
Q	10.42	7.07	16.00	11.60	0.00	8.87	2.78	6.62
Cm	0.03	0.01	0.03	0.02	0.01	0.03	0.03	0.02

Am.Mean: Arithmetic mean

Coordinates of the analysed samples

368: 39750-31705
344: 40250-27750
377: 37200-28550
339: 38950-29075
357: 40125-27750
186: 35250-32800
313: 40200-27625

Table 52. Major Oxides values, Trace element and CIPW norms of the Metadolerite

Sampel No	413	417	414	415	Ar.Mean
SiO_2	50.95	51.32	52.32	53.82	52.10
TiO_2	1.40	1.36	1.71	0.93	1.35
Al_2O_3	14.61	15.66	16.89	15.28	15.61
FeO	7.80	7.73	5.35	7.53	7.10
Fe_2O_3	2.82	1.39	1.79	3.88	2.47
MnO	0.13	0.10	0.10	0.17	0.12
MgO	7.00	6.05	6.51	6.31	6.46
CaO	5.20	4.59	4.35	6.37	5.12
Na_2O	2.34	3.11	2.12	2.17	2.93
K_2O	2.18	2.26	2.61	1.71	2.43
P_2O_5	0.18	0.36	0.16	0.11	0.22
CO_2	0.49	0.37	0.39	0.53	0.44
H_2O	3.20	3.61	3.70	1.10	2.65
TOTAL	98.30	98.01	98.00	99.91	98.76
Cr	388	150	295	516	337
Co	43	39	31	54	42
Ni	90	56	119	76	85
Cu	31	52	37	43	40
Zn	85	78	107	92	90
Ga	19	20	18	15	18
Rb	20	36	32	33	30
Sr	193	144	173	280	198
Y	24	23	24	11	21
Zr	113	145	124	63	111
Nb	13	17	10	11	12
Ba	232	295	184	225	234
La	12	16	bdl	4	8
Ce	13	29	12	bdl	13
Pb	4	5	5	7	5
U	bdl	bdl	bdl	3	1
Th	4	4	5	2	4
Ap	0.42	0.61	0.53	0.30	0.60
Il	2.67	2.59	1.34	1.97	2.23
Or	12..88	13.34	27.81	21.40	20.75
Ab	19.80	26.3	21.52	20.64	22.48
An	21.52	18.72	30.37	27.39	27.48
C	0.00	0.00	0.00	0.00	0.00
Mt	4.10	2.02	3.32	5.52	3.78
He	0.00	0.00	1.80	0.00	0.45
Di	0.00	0.00	0.00	3.57	4.11
Hy	27.32	26.00	1.89	15.30	11.47
Q	4.71	2.42	10.00	4.90	6.36
Cm	0.08	0.03	0.07	0.00	0.04

Ar. Mean: arithmetic mean

Coordinates of the analysed samples

413: 39350-22000
417: 39750-22125
414: 38650-22500
415: 38600-22325

Table 53. Rare earth element data for the metahornblende gabbro 344, 337 and metadolerite 414, 417.

Sample No	344	337	414	417
La	14.4	9.3	38.3	58.5
Ce	14.5	9.6	33.5	49.0
Pr	15.0	10.3	27.1	39.3
Nd	15.0	10.4	22.8	31.7
Sm	16.7	10.1	16.8	20.8
Eu	42.6	10.8	17.1	19.9
Gd	14.8	9.9	49.1	15.5
Tb	13.6	9.6	11.8	12.6
Dy	13.3	9.3	10.1	10.1
Ho	11.6	8.5	8.0	7.7
Er	12.0	8.5	7.7	6.8
Tm	10.3	8.2	6.4	5.7
Yb	10.5	8.2	6.5	5.2
Lu	8.7	7.7	5.8	4.3

Coordinates of the analysed samples

344: 40250-27750
337: 37125-28575
414: 38650-22500
417: 39750-22125

6.5.2. IGNEOUS ROCKS

DACITE

Dacites have been classified according to a total alkali versus silica (TAS) diagrams (Fig. 70). The rocks fall within the high-K dacites field on SiO_2 vs K_2O diagram (Fig, 71). They are also plotted on a normative colour index vs. normative plagioclase composition diagram (Fig, 72).

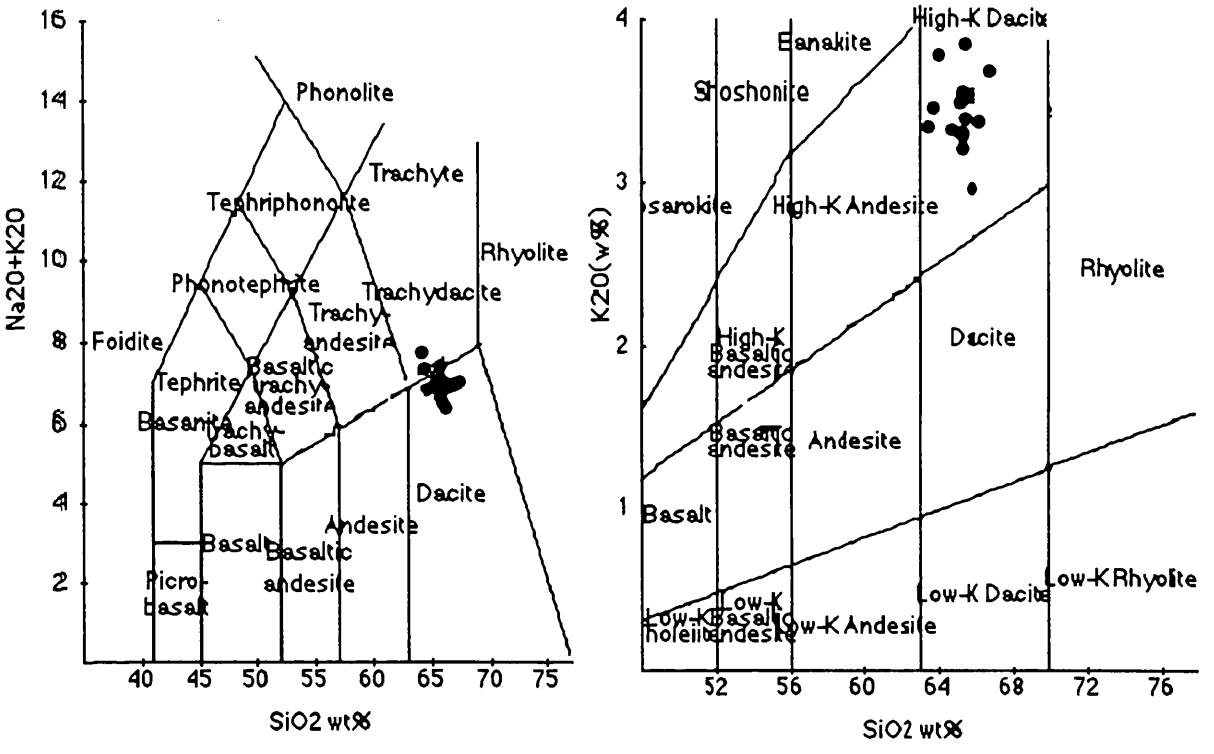

Fig ure 70, 71. Chemical classification diagrams of dacite. (70) SiO_2 vs. totall alkali plot (LeBas et al.,1986) and (71) SiO_2 vs. K_2O plot (Peccerillo and Taylor, 1976).

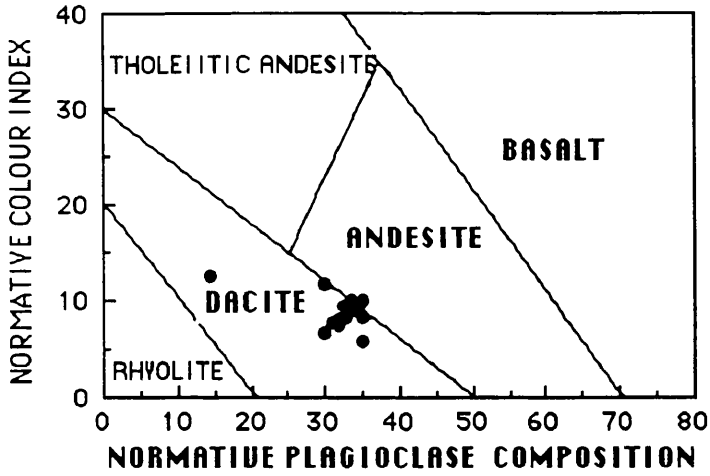

Figure. 72. Plot of normative plagioclase composition versus normative colour index for dacite (after Irvine and Baragar, 1971).

The dacites are typicaly calcalkaline in composition according to the classification schemes of Irvine and Baragar (1971), and Gill (1981) and Ewart, (1982) (Fig. 73, 74). On an AFM diagram, the rocks show little iron enrichment and plot in the calc-alkaline field (Fig. 75).

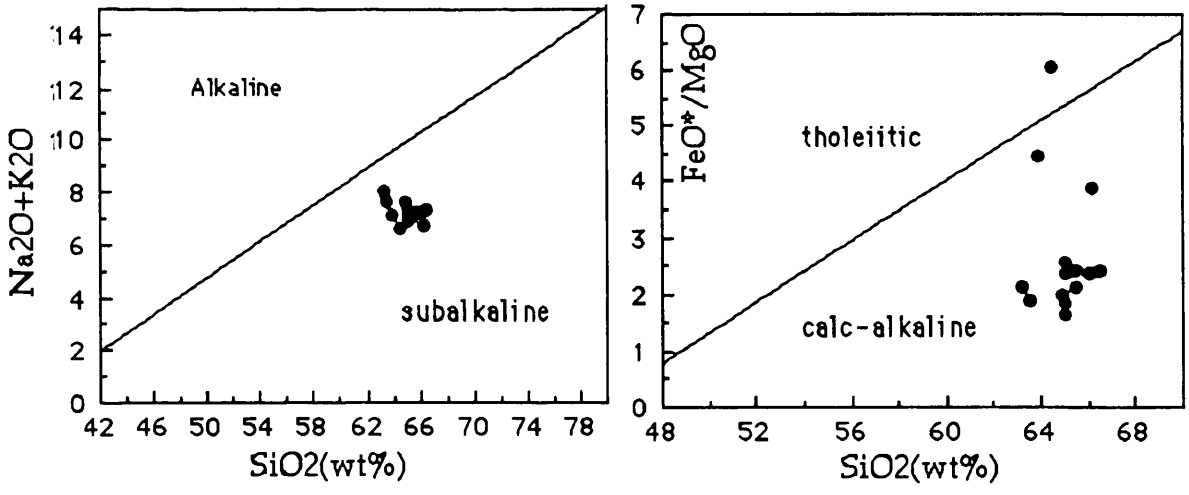

Fig.73. Chemical discrimination of dacites based on SiO_2 vs. Na_2O+K_2O plot (after Irvine and Baragar, 1971) and (74); SiO_2 vs. FeO*/MgO plot (after Gill, 1981; Ewart, 1982).

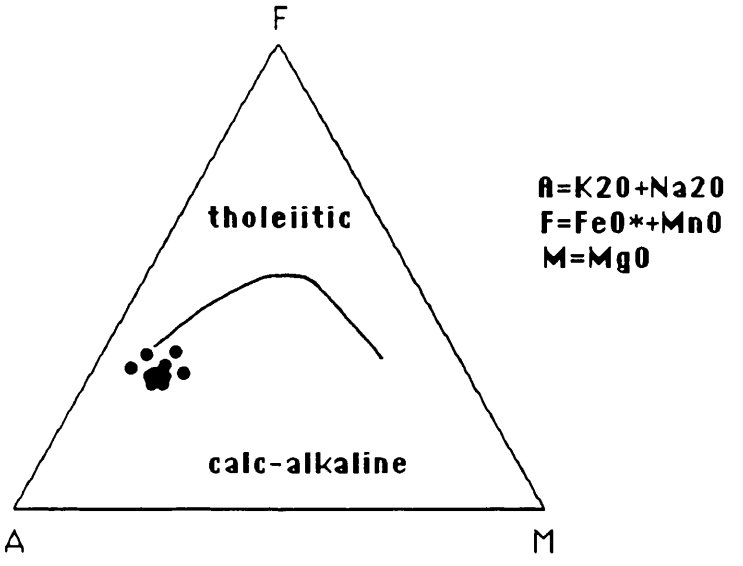

Fig. 75. AFM diagram showing the composition of dacites. The thick line seperates tholeiitic and calc-alkaline compositions (Irvine & Baragar, 1971).

Major, trace elements and CIPW norms are listed in Table 54 and Rare element analyses are given in table 55.

Figure 76 is a Harker variation diagram for the dacites. TiO_2, CaO , MgO and Th decrease with increasing SiO_2. Sr, Nb and Y increase with increasing SiO_2 contents. These variations suggest that crystal fractionation of mafic minerals played a significant role in the genesis of the dacite (Peccerillo et al., 1976). Depletions of CaO and MgO with increasing SiO_2 content, reflect the crystallization of hornblende, plagioclase and pyroxene (Romick et al, 1992). The decrease in TiO_2 reflects crystallization of titaniferous magnetite (Barton et al, 1986). Generally, trace elements show considerable scatter on the variation diagrams. However, systematic trends are shown by most of the major elements and are broadly consistent with crystallization of the observed phemocryst phases in the rocks.

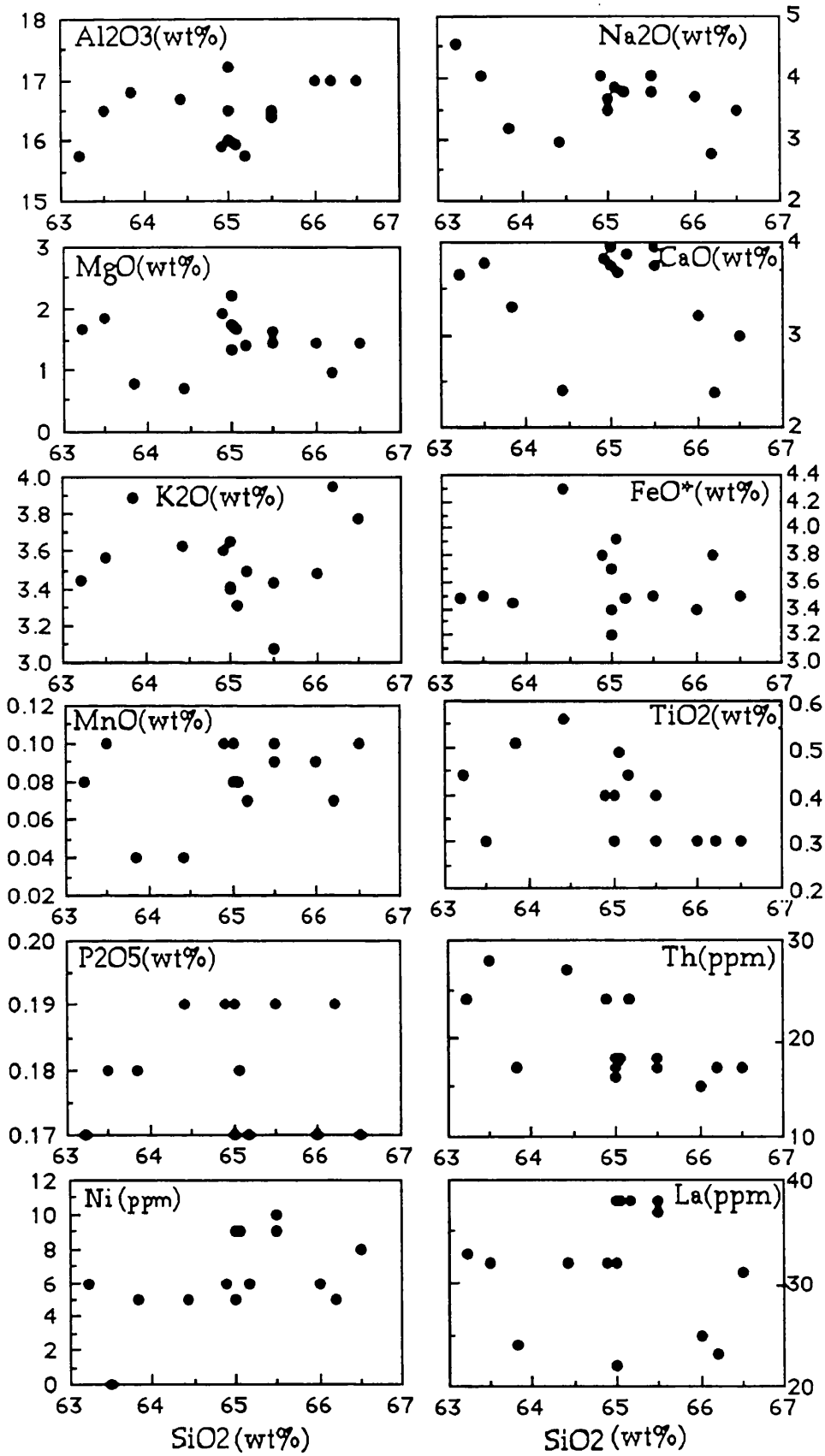

Fig. 76. Harker diagram showing variations of major oxides and trace elements for dacites .

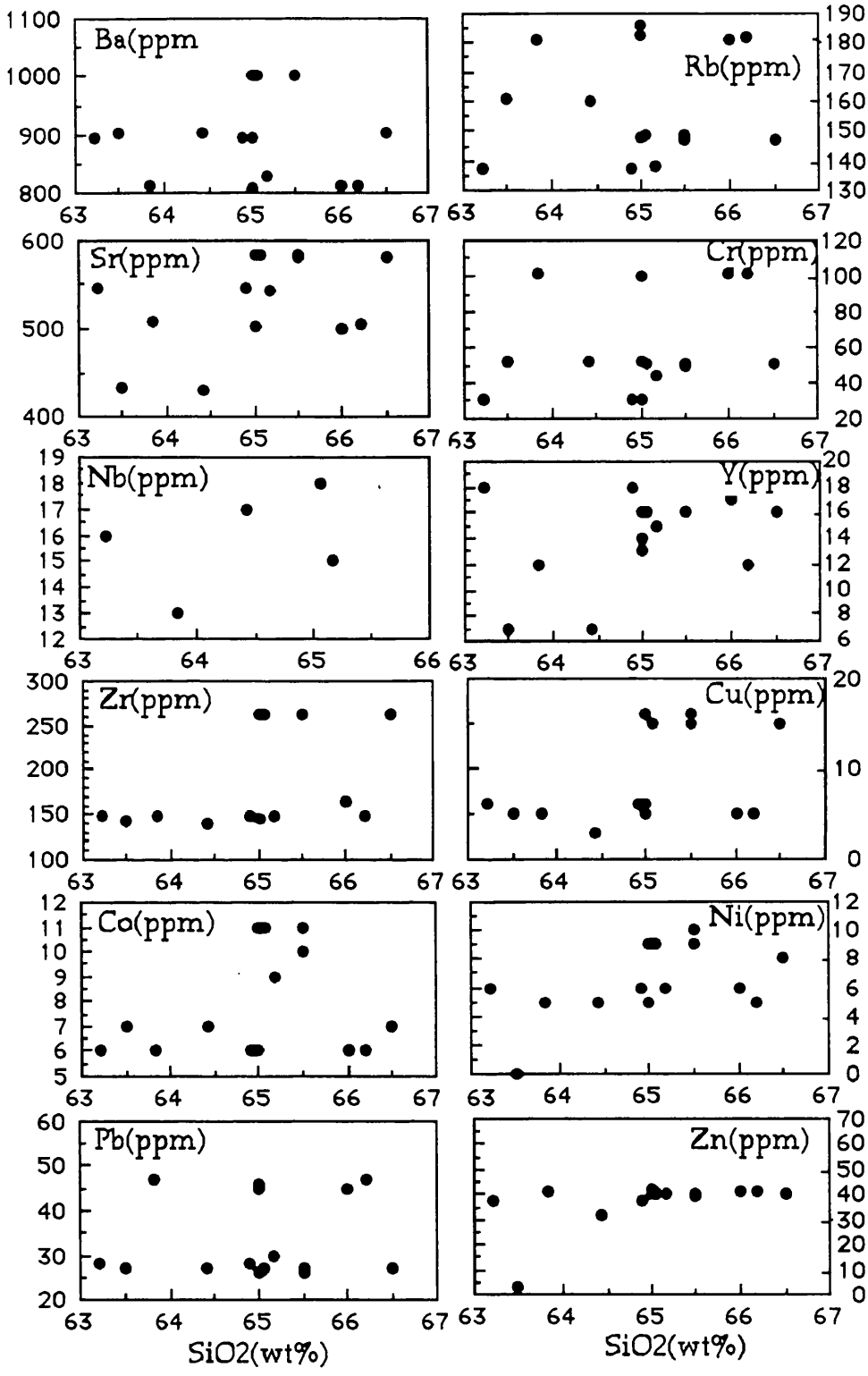

Fig. 76 continued.

Dacites have relatively high La/Y and Nb/Y ratios, compared with typical calcalkaline orogenic suites (Gill, 1981). Lambert and Holland (1974) described J and L- type trends, which lead respectively to depletion and enrichment in Y content in a calcalkaline series. The J and L-trends have been used for hornblende, and pyroxene controlled differentiation

trends respectively, as these minerals can be critical in determining trend direction.

In the Y versus CaO plot (Figure, 77), the dacites plot on the Y depleted side of the standard calcalkaline trend as obtained by pyroxene and plagioclase - dominated fractionation (Lambert and Holland, 1974). Thus, they define a J -type trend suggesting hornblende controlled fractionation (Figure, 77).

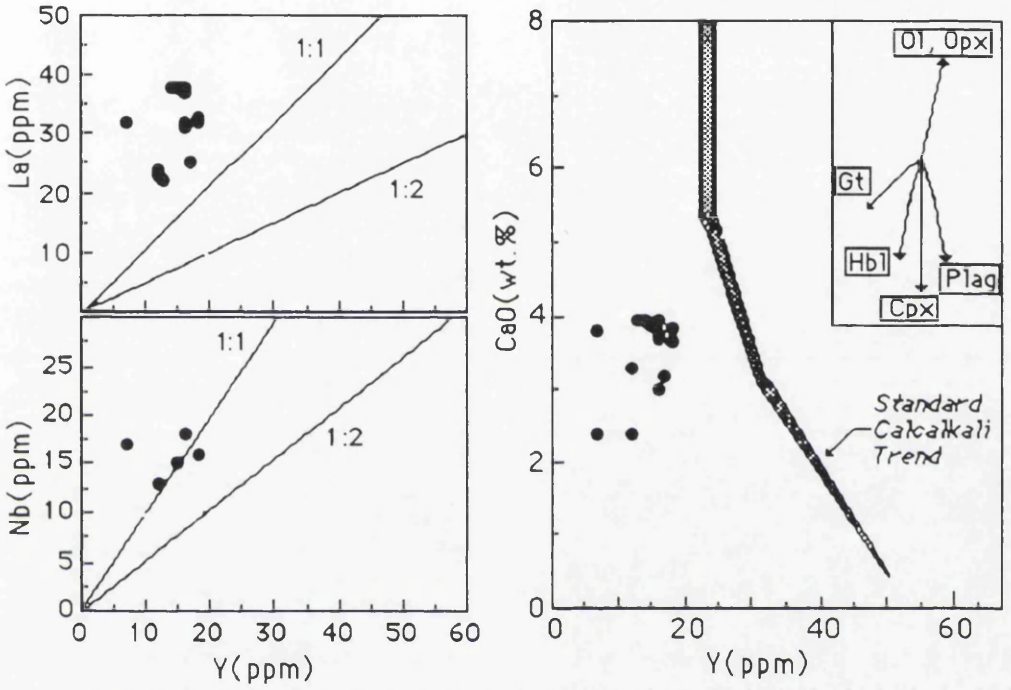

Fig. 77: Y versus Nb, La and CaO plots for dacites. The standard calcalkaline trend is from Lambert and Holland (1974).

Chondrite -normalized REE distribution patterns of two dacite samples are shown in Fig. 78. The REE patterns are highly fractionated, exhibiting steep slopes with $(La/Lu)_N$ ratios ranging between 21-22. The patterns are slightly concave upward. No important Eu anomaly (Eu/Eu*= 0.95) was found in the rocks. Generally, REE patterns are similar to those of orogenic calc-alkaline suites (Gill,1981). Trace element characteristics (e.g., low Y(7-18)) and depleted HREE patterns could be accounted for by extreme amphibole- fractionation (Defant et al, 1991).

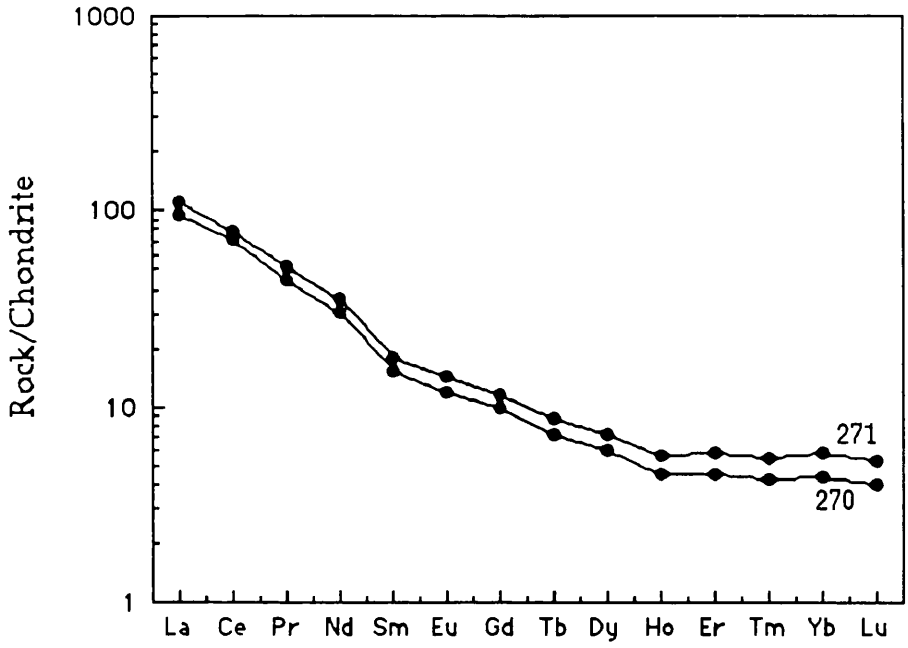

Fig. 78. Chondrite-normalized rare earth element distribution patterns for dacites from the Kadinhani area. Chondrite normalizing values from Boynton (1984).

Petrogenesis

Dacites have low to moderate concentrations of in Nb (15-18 ppm), Zr (141-263 ppm) and Y (7-18 ppm) which are characteristics of orogenic calcalkaline associations (Gill, 1981). They also show REE patterns similar to that of the orogenic high - K calc-alkaline rocks (e.g, Gill, 1981).

The data suggests that the dacites evolved mainly by fractional crystallization, possibly from an intermediate composition. The geochemical data are also consistent with a hydrous crystallization assemblage in which hornblende was one of the primary phenocrysts and exerted a major control on the crystallization history particularly in the K-rich dacite. The Harker diagrams show that amphibole fractionation played an important role in the modification of the calc-alkaline magma.

Dacites exhibit disequlibrium textures such as oscillatory zoning and sieve texture in plagioclase. Oscillatory zoning in plagioclase can be related to magma mixing (Hollister and Gancarz, 1971; Nakamura 1973). Sieve textures in plagioclase result from the dissolution of plagioclase (Tsuchiyama, 1985) probably due to influxes of new magma.

According to petrographic observations and geochemical data, both magma mixing and crystal-fractionation have been involved in the evolution of these dacites.

Table. 54. Major Oxides , Trace Elements and CIPW Norms of dacite

Sa.No	265a	269a	269ab	270a	271a	241	243
SiO_2	66.20	65.50	65.50	64.90	64.50	65.00	65.00
TiO_2	0.30	0.30	0.40	0.40	0.30	0.30	0.40
Al_2O_3	17.60	16.40	16.50	15.90	16.50	17.20	16.00
FeO	1.20	1.66	1.60	2.61	2.25	1.37	1.65
Fe_2O_3	2.72	2.07	2.06	1.45	1.47	1.96	2.21
MnO	0.08	0.10	0.09	0.10	0.10	0.08	0.10
MgO	0.98	1.45	1.64	1.92	1.87	1.73	2.21
CaO	2.38	3.95	3.75	3.82	3.79	3.95	3.95
Na_2O	2.78	4.04	3.79	4.05	4.02	3.67	3.47
K_2O	3.95	3.07	3.43	3.60	3.57	3.41	3.40
P_2O_5	0.19	0.19	0.19	0.19	0.18	0.19	0.19
CO_2	0.41	0.08	0.15	0.25	0.33	0.41	0.50
H_2O	0.88	1.16	0.36	0.46	0.72	0.72	1.18
Total	99.67	99.97	99.40	99.60	99.60	99.99	100.26
Cr	101	50	51	30	52.07	100.04	52.12
Co	5	10	11	6	7.36	6.22	11.31
Ni	5	9	10	6	5.02	4.97	5..1
Cu	5	15.	16	6	3.01	5.00	6.02
Zn	41	40	39	36	33.24	42.11	41.99
Ga	18	19	20	18	19.67	18.01	17.89
Rb	182	148	147	137	161.21	186.36	183.13
Sr	505	584	582	544	431.80	503.93	503.08
Y	12	16	16	18	7.01	13.20	14.01
Zr	149	262	262	147	141.90	145.75	145.04
Ba	812	1002	1002	893	901.21	810.11	1002.01
La	23	37	38	32	31.97	22.31	38.06
Ce	48	55	55	51	54.09	47.12	53.20
Pb	47	27	26	28	26.89	46.02	45.01
U	1.	bdl	bdl	bdl	4.02	1.00	bdl
Th	17	18	17	24	28.02	15.90	17.02
Ap	0.46	0.44	0.46	0.44	0.44	0.44	0.44
ill	0.58	0.57	0.77	0.76	0.59	0.57	0.76
Or	24.20	18.20	20.70	21.50	21.68	20.20	19.90
Ab	24.40	34.26	32.70	34.50	34.85	31.10	29.10
An	10.90	18.07	17.60	14.70	16.89	18.40	17.80
C	4.03	0.00	0.21	0.00	0.00	0.72	0.00
Mt	2.82	2.94	2.92	2.07	2.10	2.16	4.36
He	0.67	0.00	0.00	0.00	0.00	0.00	1.45
Di	0.00	4.20	0.00	2.57	0.94	0.00	0.25
Hy	2.54	2.42	4.71	6.45	6.68	7.49	5.33
Q	29.00	18.75	19.60	16.60	15.68	18.60	20.40
DI	77.70	71.21	73.00	72.70	72.22	70.00	69.40
NCI	5.95	10.14	8.42	11.80	9.31	9.20	10.10
NPC	31.00	33.53	35.00	29.90	32.64	34.20	34.90

Coordinates of the analysed samples

265a: 39200-12950
269a: 38025-15800
269ab: 37400-15400
270a: 37225-15600
271a: 37675-15675
241: 37400-15300
243: 37575-15450

Table 54. Continued

Sam.No	242	242a	243a	268	269	270	271	265	Ar.Mean
SiO_2	65.00	66.50	66.00	65.17	65.06	63.22	64.42	63.83	64.98
TiO_2	0.30	0.30	0.30	0.44	0.49	0.44	0.56	0.51	0.40
Al_2O_3	16.50	17.00	17.00	15.76	15.93	15.75	16.87	16.81	15.41
FeO	1.87	1.87	1.44	0.83	0.92	1.79	0.92	0.59	1.37
Fe_2O_3	1.71	1.81	2.10	2.71	3.10	1.86	3.47	2.91	2.24
MnO	0.09	0.10	0.09	0.07	0.08	0.08	0.08	0.04	0.08
MgO	1.34	1.45	1.44	1.41	1.66	1.65	0.72	0.78	1.55
CaO	3.75	3.00	3.20	3.87	3.68	3.65	2.40	3.30	4.85
Na_2O	3.67	3.50	3.72	3.78	3.87	4.55	2.97	3.17	3.73
K_2O	3.65	3.78	3.48	3.50	3.31	3.45	3.63	4.89	3.60
P_2O_5	0.17	0.17	0.17	0.17	0.18	0.17	0.19	0.18	0.18
CO_2	0.58	0.33	0.41	0.32	0.30	0.27	0.20	0.12	0.31
H_2O	1.12	0.60	0.88	0.70	0.90	1.00	0.90	0.65	0.81
TOTAL	99.76	100.41	100.24	99.40	99.80	99.89	99.40	99.79	99.82
Cr	30	51	101	44	51	30	52	101	59
Co	6	7	6	9	11	6	7	6	7
Nii	9	8	6	6.	9	6	5	5	6
Cu	16	14	5	bdl	15	6	3	5	7
Zn	40	39	41	40	39	37	32	41	39
Ga	20	20	17	20	19	18	20	18	19
Rb	148	147	181	138	149	137	160	181	159
Sr	583	582	501	542	584	545	431	507	528
Y	16	16	17	15	16	18	7	12	14
Zr	262	263	165	147	262	146	141	148	185
Nb				15	18	16	17	13	16
Ba	892	901	812	829	1003	892	901	813	898
La	32	31	25	38	38	33	33	24	34
Ce	51	54	47	57	54	51	54	48	52
Pb	26	27	45	30	27	28	27	47	33
U	bdl	bdl	bdl	0	bdl	bdl	4	1	1
Th	18	17	15	24	18	24	27	17	20
Ap	0.42	0.39	0.42	0.41	0.42	0.42	0.44	0.41	0.44
ill	0.57	0.57	0.57	0.85	0.97	0.85	1.10	1.01	0.73
Or	22.43	22.46	20.80	21.04	19.92	20.92	22.16	29.84	21.72
Ab	31.72	29.77	31.80	32.56	33.33	48.13	25.97	27.74	32.13
An	17.82	13.87	14.84	15.99	16.67	8.09	11.06	15.69	15.22
C	0.11	2.11	1.76	0.00	0.00	0.00	4.07	0.75	0.91
Mt	2.44	2.58	2.98	1.32	1.37	2.65	1.17	0.28	2.33
He	0.00	0.00	0.00	1.73	2.06	0.00	2.54	2.63	0.73
Di	0.00	0.00	0.00	1.85	0.58	7.38	0.00	0.00	1.18
Hy	4.91	5.02	4.02	2.71	3.94	1.68	1.82	2.04	4.10
Q	19.85	23.09	22.66	20.78	20.63	9.76	29.59	19.52	20.3
DI	72.62	68.00	72.27	74.39	73.87	78.82	77.72	77.11	73.36
NCI	7.91	8.16	7.58	8.45	8.93	12.56	6.63	5.96	9.00
NPC	3100	31.78	31.82	32.94	33.34	14.40	29.87	35.12	31.96

Ar. Mean: Arithmetic mean

DI: Differentiation index

NCI: normative colour index

NPC: normative plagioclase composition

Table. 55. Rare earth element data for the Dacite

Sample No	271	270
La	96.1	111.5
Ce	72.3	78.3
Pr	45.2	52.4
Nd	30.3	35.5
Sm	15.4	18.2
Eu	11.8	14.5
Gd	9.8	11.7
Tb	7.2	8.7
Dy	5.9	7.3
Ho	4.5	5.6
Er	4.5	5.8
Tm	4.2	5.2
Yb	4.3	5.8
Lu	4.0	5.2

Coordinates of the analysed samples

242: 37500-15200

242a: 37500-15250

243a: 37500-15450

268: 38025-15375

269: 37825-15675

270: 37120-15475

271: 37700-15650

265: 3925-13000

VII - METAMORPHISM

In this chapter an attempt will be made to determine the variation in the grade of metamorphism across the mapped area. According to petrographic evidence, two prograde regional metamorphic events occurred, but mineral assemblages and critical minerals for the precise determination of the pressure and temperature conditions of metamorphism are generally absent.

The presently accepted criteria (for example, Winkler, 1967, p.161) for classifying rocks in the blueschist facies as opposed to the greenschist facies surprisingly does not include the presence of sodic amphibole. Terranes containing both greenschist and blueschist have been generally classified as transitional between the greenschists and the blueschists facies (Turner, 1968; Ernst and other, 1970, p.201). Although it is only a point of terminology, the question is worth considering; should the boundary between the greenschist and blueschist facies be set where with increased pressure crossites first become stable, and the assemblage albite + actinolite + iron oxide became unstable or should it be set where the assemblage albite+ actinolite (without iron oxide) becomes unstable, and the composition range of sodic amphibole expands into the glaucophane field ? Because the sodic amphiboles are so easily recognized, the most logical place to arbitrarily set this facies boundary would seem to be at the point where crossites are first stable, thus, according to this scheme; 1) The presence of glaucophane or crossite plus epidote indicates the blueschist facies. This same conclusion was made by Ernst in 1963. (2) The assemblage albite plus actinolite plus iron oxide indicates the greenschist facies as does the stable co-existence of albite with chlorite.

The Stability Fields of Minerals of the Study Area:

The experimental and hypothetical phase relationships of Ca-Na amphiboles, Ca-silicate, sheet silicates, carbonate, and magnetite minerals are discussed below.

PRESSURE AND TEMPERATURE

Compositions of the Ca-amphiboles and crossite can be used to estimate the pressure of metamorphism (Raase 1974; Brown 1977). The plotting of the amphibole from actinolite to crossite on the $NaM4\text{-}Al^{IV}$ diagram of Brown (1977) for the metahornblende gabbro and the plotting of

the crossite on the same diagram for the metatrachyandesite (Figure 79. a, b) suggest a metamorphic pressure of 3-6 Kbar for the metahornblende gabbro, and 6-7 Kbar for the metatrachyandesite,

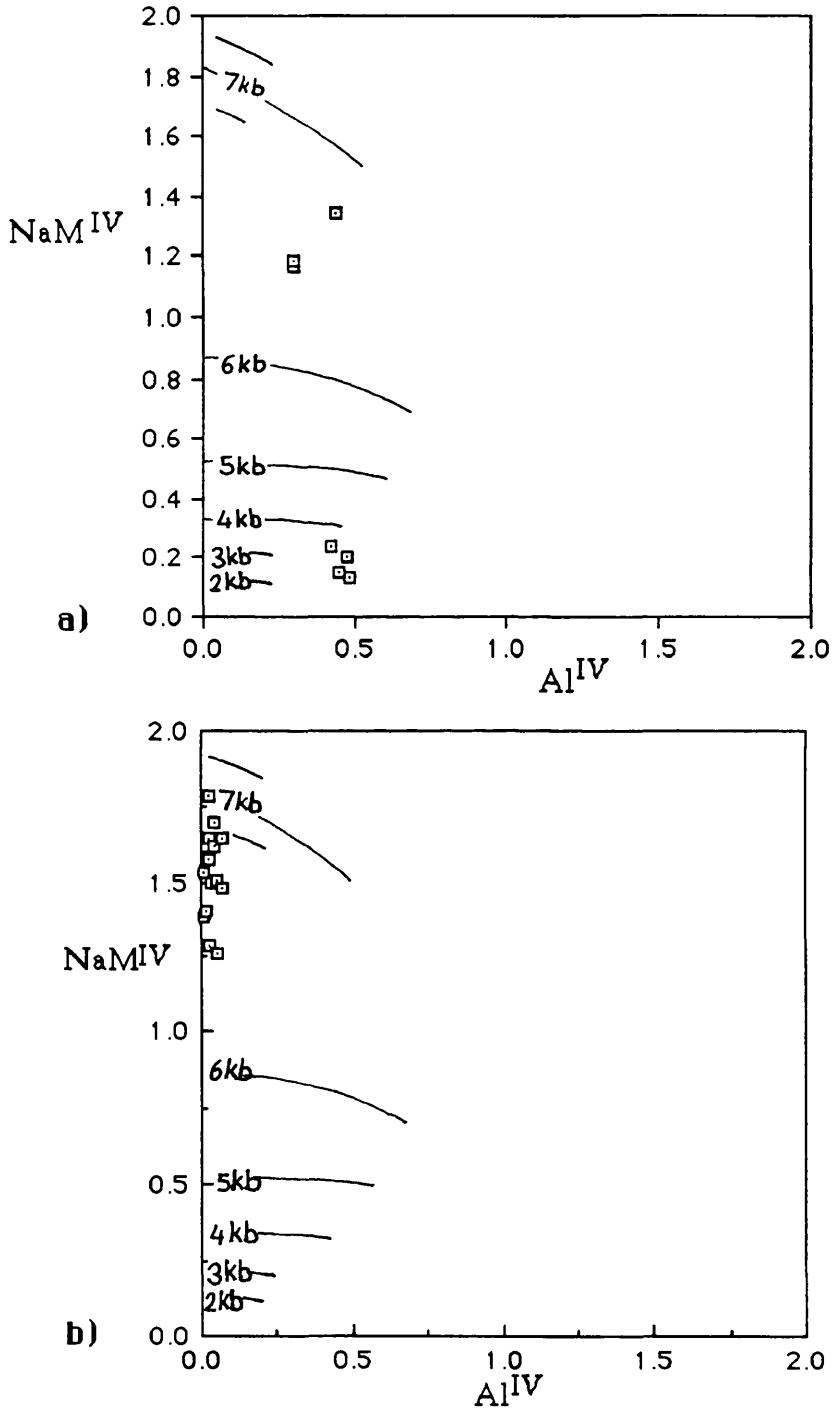

Fig. 79. Tentative estimate of the relationship between pressure of metamorphism and NaM^{IV} vs AL^{IV} in the metahornblende gabbro (a) and metatrachyandesite (b). Diagram based on Brown (1977).

The plotting of hornblende and actinolite on the AlVI-Si diagram of Raase (1974) suggests a metamorphic pressure of about 5 kbar or more than 5 kbar for metabasic schist and metabasaltic andesite (Fig. 80. a,b).

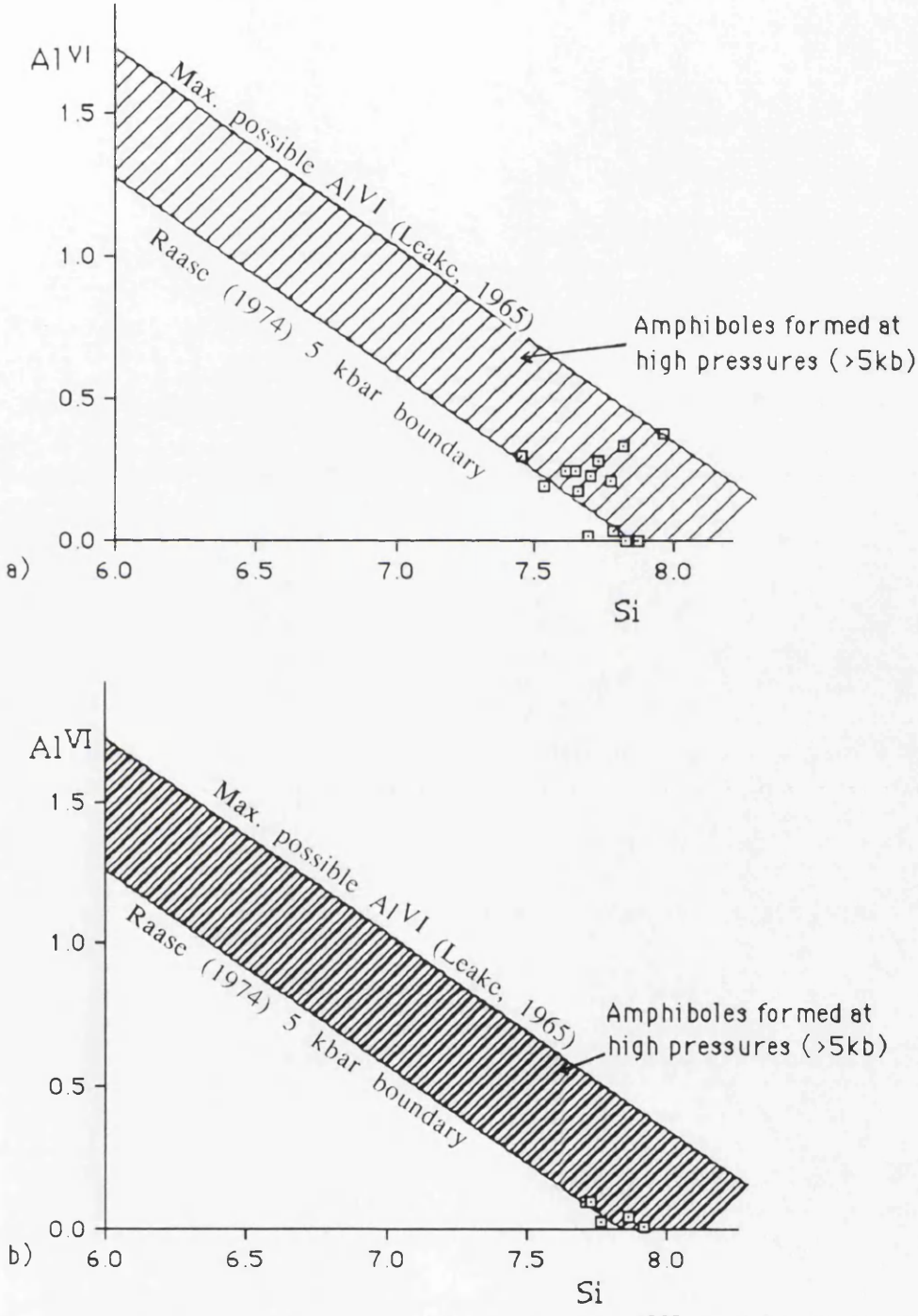

Fig.80. Hornblende analyses plotted on an Al^{VI} against Si diagram (after Raase, 1974), for metabasic schist (a) and metabasaltic andesite (b) .

The temperature obtained from hornblende-plagioclase geothermometers suggest that the temperature during metamorphism was about 521(±75)-482 (±75) °C , and the pressure about 3-6 Kbar for metahornblende gabbro, 431(±75) - 400(±75) °C and the pressure about 5-7 Kbar for the metabasaltic andesite , and 426 (±75)-395 (±75) °C and the pressure about 5-7 Kbar for metabasic schist. These estimates are based on Blundy and Holland's (1990) plagioclase-hornblende geothermometer. The temperatures seem to be rather high for blueschist rocks which rarely exceed 400 ^{o}C.

NaM^{IV} poor calcic amphibole is sequentially replaced first by a deeper green to green blue winchitic amphibole, and then by a blue riebeckite. The extremely low NaM^{IV} content of the actinolite suggests that the metamorphism was initiated with low pressure, greenschist facies conditions and only later became of blueschist facies.

The following reaction might come closest to the true magnesio-riebeckite - forming reaction;

24 edenite + 16 albite + 15 magnetite + 48 Co3 + 56H2O = 20 magnesio-riebeckite + 15 clinochlorite + 48 calcite + 11 quartz.

The presence of glaucophane indicates relatively high pressures (>6 Kbar at 400 °C; Maresch, 1977). Glaucophane is almost invariably found only in low - temperature metamorphic rocks which belong to the high-pressure type (Miyashiro, 1972). In particular, glaucophane requires a minimum of 4 Kbar PH2O and is probably not stable above 550°C, but it is stable above 350 ^{o}C(Maresch, 1977). These maximum possible stability limits are essentially compatible with the high-pressure, low temperature conditions deduced for glaucophane from metamorphic terranes (Maresch, 1977).

The common coexistence of both sodic and calcic amphiboles and their compositional trends are characteristic and at the lowest grade, only riebeckite or crossite appear. With increasing grade, alkali amphibole first becomes enriched in the glaucophane component, which later coexists with actinolite to define a compositional gap, and finally occurs as winchite and presumably hornblende (Liou & Maruyama, 1987).

The metatrachyandesite includes pumpellyite. The coexistence of pumpellyite, chlorite, epidote, actinolite and quartz indicates metamorphic conditions near those for the reaction;

Pumpellyite+chlorite+ quartz=epidote=actinolite+H2O at H2O =7 Kbar, T=370 °C (Nitsch, 1971). In an Al:Fe:Mg diagram (Figure 81) most of the pumpellyites plot in the high pressure field and are rich in Al.

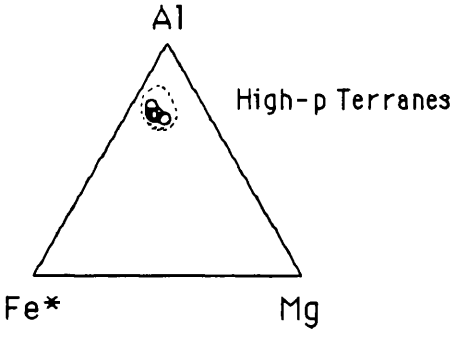

Fig.. 81. Compositional variations of pumpellyite under high-pressures after Evarts & Schiffman, (1983).

The pistacite component of epidote from the area varies from 23.3 to 32.0%. Coombs et al (1976) suggest that the tendency for pistacitic epidote from 26 to 39 %Ps crystallize at low temperatures (Miyashiro and Seki, 1958) is related to a general tendency for decreasing fO_2 with advancing metamorphism.

The pressure- temperature metamorphic environment is estimated for epidote by Black and Brothers (1977) to have been ~350°C, 7 kbar; by Feiminger (1982) to have been 350-40°C; P_{total}~P_{fluid} 5-7 Kbar.

In Figure 82. the atomic proportions of Mg^+ vs Na+ K in mica minerals are plotted. A clear relationship is shown between a low Na content and a high Mg content. The fields are superimposed on the diagram, which indicates, low pressures (L) and medium to high pressure (H) with the samples from the present area plotting mostly in the high pressure field.

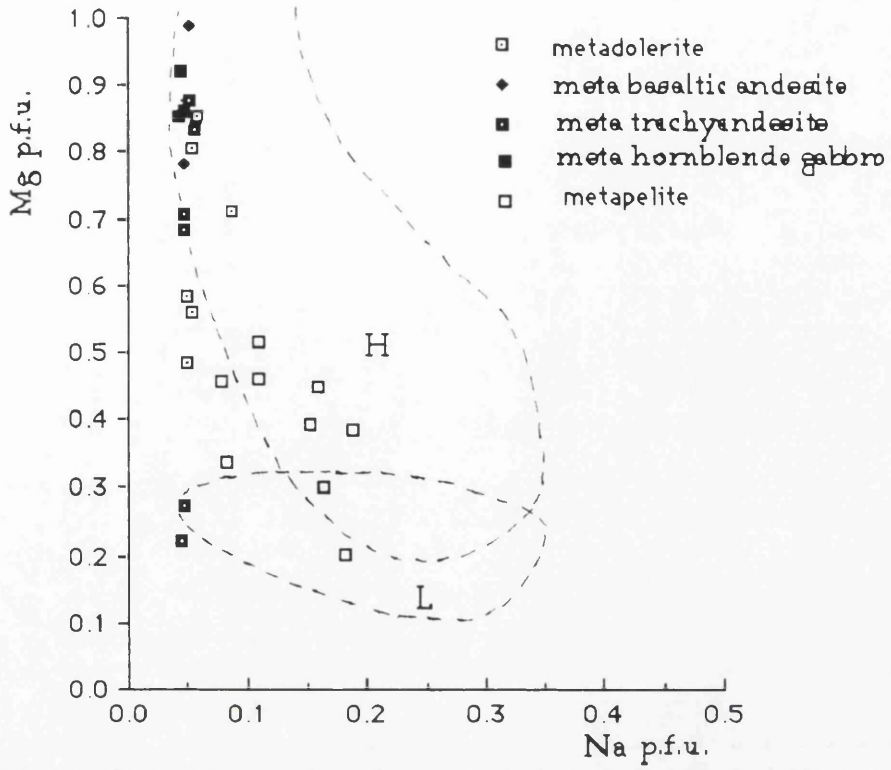

Fig. 82. Plot of Mg against Na for muscovite and white mica analyses from high (H) and low (L) pressure area (After Cipriani et al., 1971).

The experimental work of Velde (1965) and Massone & Schreyer (1987) shows that phengite with Si content > 3.3 crystallizes under rather high P/T conditions. In the study area the Si content in phengite in the metatrachyandesite is more than 3.3.

From the common association with quartz + muscovite + chlorite, chloritoid in the study area is thought to have been produced by reactions similar to those proposed by Seidel and Okrusch (1975). These mineral assemblages are indicative of metamorphic conditions in excess of 4-5 Kbar at 380-400 °C.

In an Al:Fe:Mg diagram most of the chlorite from the area plots within the compositional field of chlorites from greenschist facies rocks (Figure 83).

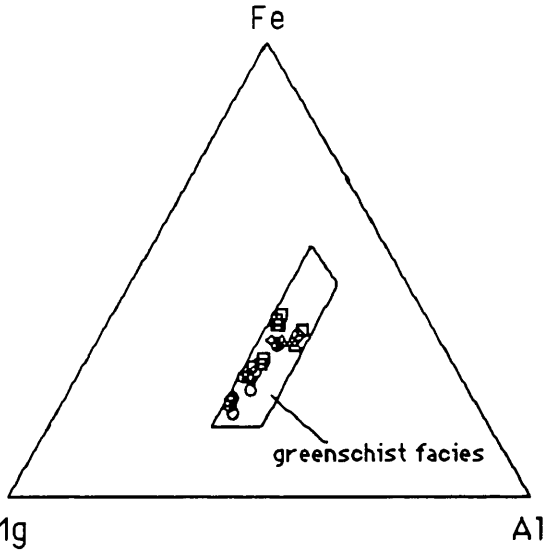

Fig. 83. Chlorite Al-Fe-Mg compositions from the greenschist facies after Velde (1977, Figure 31b).

Stilpnomelane is frequently associated with high pressure metamorphic minerals and is less common in low pressure assemblages (Miyashiro & Shido, , 1973). The stability of stilpnomelane varies widely and is strongly dependent on the bulk rock chemistry . For example, stilpnomelane is often present in low-grade metabasites (Winkler, 1979) and very low-grade metamorphosed iron formations (Deer et al, 1966).

The albite ($Ab_{99 \text{ to } 95}$) component of the plagioclase is very high, which agrees with low temperatures.

Ankerite is fine to medium grained. The coarseness of ankerite is related to the diffusion of cations during very low-grade metamorphism. Perrault (1955) suggested that ferroan dolomites represent replacement of earlier materials.

The TiO_2 content of the magnetite minerals from the area is between 0-0.6 wt%. Metamorphic magnetite in the greenschist facies contains only 0.03 to 0.69 wt % TiO_2 (Abdullah and Atherton, 1964).

Metacherts and schists include graphite. Based on X-ray difraction work and by comparison with metamorphic mineral facies, Landis (1971) determined graphitization to begin at a temperature of at least 300 °C with fully-ordered graphite appearing not before 450°C; pressures were thought to range between 2 and 6 Kbar. In a similar study, Gray (1974) obtained data of 300-500 °C and over 3 Kbar respectively.

Most of the metamorphic minerals from the different type rocks studied are given in Table 56. It must be appreciated that most rocks contain disequilibrium assemblages as the blueschist metamorphism did not recrystallize all the earlier greenschist assemblages.

Table. 56. Metamorphic minerals in the greenschist and blueschist metamorphisms for different rocks in the studied area.

Minerals	meta bast. andesite		meta trac.ands.		metabasc. schist		meta hbl. gabb.		meta dolerite		meta sediments	
	G	B	G	B	G	B	G	B	G	B	G	B
Magn.-hornblende					------		-------					
Winchite				------		------		------				
Ferro winchite				------				------				
Riebeckite				------								
Mag. riebeckite			------	------	------	------						
Richterite					------							
Actinolite	------		------		------		-------				-------	
Actinol.-hornblende					------		-------					
Ferro-glaucophane		-----		------								
Crossite				------				------				
Pumpellyite				------								
Chloritoid											------	
Albite	------	-----	------	------	------	------	------	------	-------	------	------	------
Stilpnomelane	------											
Muscovite	------	-----	------	------	------	------	-------	------	-------	------	-------	------
Phengite				------								
Epidote	------	-----	------	------	------	------	------	------	-------	------	-------	------
Ankerite											-------	------
Hematite	------	-----	------	------	------	------	-------	------	------	------	-------	------
Sphene	------	-----	------	------	------	------	-------	------	-------	------	-------	------
Brusvigite			------	------								
Ripidolite			------	------			-------	------			-------	------
Pycnochlorite	------	-----	------	------							-------	------
Diabanites							-------	------				
Graphite											-------	------

G: Greenschist

B: blueschist

The age of the metamorphism has not been determined. However, geological investigations to the north of the Menderes Massif and the Afyon-Bolkardag Belt suggest that the greenschist metamorphism seems to have been completed before the late Cretaceous and the blueschist metamorphism is " early Alpine" in age and is believed to have taken place during the late Cretaceous - early Eocene interval (see chapter, 8).

VIII. THE TECTONIC EVOLUTION OF TURKEY AND EVOLUTION OF THE PRESENT AREA.

Geologically, Turkey was created during the Alpine orogeny caused by the collision of Laurasia and Gondwanaland since the late Mesozoic. In the classical, four- fold tectonic subdivision of Turkey (Ketin 1966), the Pontides in the north can be assigned to Laurasia, whereas the Anatolides, Taurides, and the Border Folds belong to the Gondwanaland realm with the major Tethyan Izmir-Erzincan suture, separating the Pontides from the Anatolides (Figure 1 a).

During the Mesozoic and earlier, the Anatolides and Taurides formed a wide and extensive platform, the Anatolide Tauride platform (Sengor 1979), which was largely contiguous to Gondwanland but separated from it during the late Mesozoic by a narrow ocean -the Mesogea of Biju-Duval and others (1977) whose remnants are the Tekirova and Troodos ophiolites and the present Eastern Mediterranean. The closure of the Tethys ocean by subduction and the subsequent collision of the two continents led to the Alpine orogeny in Turkey.

The Pontides, Anatolides, and Taurides are subdivided in Figure 1a into several zones commonly separated by minor and often disputed sutures.

There are four major units in the Anatolides which are the Menderes Massif, the Afyon-Bolkardag Zone, the Tavsanli Zone, and the Kirsehir Massif. Also five major high-pressure metamorphic complexes are recognized in Turkey (Okay 1986). These are (1) the Tavsanli zone in western Turkey; (2) the metamorphic Alanya nappes; situated on the Mediterranean coast in southern Turkey; (3) the Bitlis Massif in eastern Turkey; (4) the Karakaya complex of the Pontides which has an extensive distribution in northern Turkey and (5) the Afyon -Bolkardag Zone which surrounds and lies to the east of the Menderes Massif and includes present area. The Menderes massif (sensu strico) in the west consists of gneisses and mica schists formed from remobilised Precambrian basement (Durr and others 1978; Sengor and others 1984b).The Afyon zone (Okay 1984a) forms the Paleozoic to Lower Tertiary sedimentary cover to the gneisses of the Menderes Massif, and has undergone medium to low grade Barrovian metamorphism along with the

Menderes Massif during the Eocene (Durr and others 1978; Caglayan and others 1980; Sengor and others 1984b). South of the Menderes massif the Afyon zone consists of a thick basal metaclastic sequence of Paleozoic age overlain by over one Km of Mesozoic marbles with a emery horizon. The marbles are succeeded by a slightly metamorphosed thin sequence of red micritic limestone and flysch with serpentinite and limestone olistoliths of Paleocene and early Eocene age.The switch from neritic to pelagic sedimentation in the Afyon Zone was caused by the emplacement of the Lycian Nappes, which lie tectonically over the lower Eocene flysch of the Afyon Zone (Durr and others1978). The emplacement of the Lycian Nappes was followed by a Barrovian type of regional metamorphism, which has affected the Menderes Massif, the Afyon Zone, and the basal parts of the Lycian Nappes (de Graciansky 1966; Basarir 1970;Dora 1981). In contrast, a well-documented Eocene HP - LT metamorphism exists in the Cyclades immediately to the west of the Menderes Massif(e.g.Altherr and others 1979; Blake and others 1981). The Afyon zone shows a similar stratigraphy and metamorphism to the northeast part of the Menderes Massif (cf.Okay 1984a).

North of the Menderes Massif, the northwest Turkish blueschist belt or the Tavsanli zone (Okay 1984b), comprised of volcanic and sedimentary rocks metamorphosed in the blueschist facies during the mid-Cretaceous, is partly thrust over the Afyon zone.

During the Mesozoic , the area of the Menderes Massif , Afyon Zone and the major part of the Taurides was a Bahaamian - type carbonate platform on continental crust.(Okay 1986).

Turkish blue schists share two common features with many other Alpine HP-LT metamorphic complexes; the short time span of the HP-LT metamorphism, and blueschist protoliths consisting mainly of sedimentary rocks deposited on continental crust. These features , which differentiate these blueschist from the Circum -Pacific HP-LT metamorphic complexes, are probably a reflection of the peculiar characteristics of the Tethys ocean(Okay 1986).

EVOLUTION OF THE PRESENT AREA

On the basis of previous knowledge and the new evidence presented in this thesis following history can be deduced.

The oldest rocks in the present area are of Silurian - Devonian age. The base of the Esiragili Formation, which is conglomerate outside the present area, was followed by sandstone, shale and carbonate as seen in the present area. The formation was deposited on a continental margin in Silurian -Devonian time. Transgressive processes were dominant during the deposition of these particular sediments. The following, Devonian Bagrikurt Formation contained shale, sandstones, quartzite, cherts, siliceous carbonates, conglomerates. Volcanism is also recorded in the formation with amigdaloidal trachyandesite, which is calc alkaline and of a within plate setting, basaltic andesite, which is transitional tholeiitic to calc alkaline and of continental arc character. All these rock types in the Bagrikurt Formation suggest that the present area was subjected to geotectonic activity in the Devonian-Carboniferous period. The volcanic rocks may be related to a continental margin and a continental arc of Hercynian oregeny.

Later, there was a return to shallow water conditions with the carbonate deposition of the Kursunlu Formation in Carboniferous time and the transformation of limestone into dolomite during early diagenesis. These carbonates, which reflect shelf environments, are cut by intrusive dykes which are hornblende gabbros which are tholeiitic and MORB in character, and dolerites which are calc-alkaline in character.

Considering all the above data and its position it is proposed that a back arc basin was developed in the this belt during the Devonian - Carboniferous. The opening of this basin was characterized by the dolerite which intruded the Kursunlu Formation.

All rocks in the present area have undergone intense deformation and greenschist metamorphism during the Alpine orogeny. The first phase of deformation (D_1) and a penetrative (S_1) was accompanied by the most important minerals, muscovite, chlorite, chloritoid, actinolite and stilpnomelane and grew during greenschist facies metamorphism.

The metasediments may have weathered and eroded until the Lorasdagi Formation carbonate was deposited in the an open shelf environment in Jurassic to Cretaceous time.

The second and the third phases of deformation (D_2, D_3) took place during blueschist metamorphic episodes and developed upright fold and crenulation cleavages (S_2, S_3) and lineation (L_2) and kink bands. The most important minerals, magnesio riebeckite, crossite, glaucophane, phengite, pumpellyite and albite were formed during the blueschist metamorphism. It is believed that this last metamorphism acted during late Cretaceous and Eocene time.

No further sediments were deposited in the present area till Late Miocene times. Sediments may be uplifted and eroded until the late Miocene. During late Miocene - Pliocene, a shallow lagoon formed by block-faulting accompanied by volcanism. The Osman Kayasitepe Formation limestone was deposited with volcanic material in a continental environment during the volcanism , which was calc alkaline and with orogenic high K dacitic magma and was influenced by the continental crust post collision tectonism and subduction.

After the lake dried out, some paleosoils formed. Alluvium developed by alteration of the various lithologies in streams in the Quaternary.

IX. CONCLUSIONS

1-The geological maps of the Kadinhani area at 1:25.000 scale covering 300Km^2 and have been completed (appendix-1).

2- The lithostratigraphic units of the Kadinhani area show the Esiragili Formation is the oldest Formation and includes metacarbonate, phyllite and psammite. This formation is overlain by the Devonian Bagrikurt Formation, of schist, phyllites, marbles, cherts, quartzites, basic schist, calc silicate, pelites and psammites and also metavolcanic rocks such as metatrachyandesite and metabasaltic andesite. The Formation was overlain by Devonian and Carboniferous age Kursunlu Formation limestone.

The meta - igneous rocks such as metahornblende gabbro and metadolerite cut the Permian limestone, which is outside the studied area, and older rocks in the present area.

The Lorasdagi Formation, of Jurassic-Cretaceous age, overlies the Kursunlu and Bagrikurt Formations unconformably and continues up to the unconformably overlying upper Miocene- Pliocene Osmankayasi Tepe Formation.

The upper Miocene-Pliocene is overlain by dacite which itself overlies limestone which is overlain by the Plio -quaternary Toprakli formation.

3-The psammite and quartzite samples from Kadinhani have a generally similar chemistry which suggests a similar source for these rocks which a passive or active continental margin setting. The geochemistry and especially the REE values suggest that the rocks were derived from a granitic, sedimentary, or metasedimentary acidic source, or sources.

4-The major oxides, trace elements, REE, and REE patterns in the cherts are in favour of deposition of the Kadinhani cherts in a basin not far from the continent and they have been deposited in a relatively shallow-water environment similar to recent continental shelf slope environments. In the metachert the main control in composition was clay which influenced Al, Fe and LREE.

5-The pelitic rocks in the Kadinhani area contain less than 1 % CaO and were originally shales in which the main control in composition was the sheet silicates (clay, mica, and chlorite) which influenced elements such as Zn, Rb, Ba, Ga, La, Al, K, and Ti. The sediments with 1-10 % CaO were originally rich in basic magmatic material and possibly formed tuffs in the pelites. The basic magma was probably tholeiitic basalt. The calc silicate rocks were originally impure siliceous limestones (not dolomites) with variable amounts of clay material (pelite) and Zn was added in clay minerals to the calc silicate rocks. The CIA values suggest that basic schist, pelitic rocks and calc silicate rocks have formed under somewhat different climatic conditions.

6- Carbonate rocks contain variable amounts of terrigenous material such as clay, muscovite, quartz and chlorite. The Sr composition of the dolomite in the area studied is very low and possibly of late diagenetic origin. Geochemical evidence supports the presence of very little detrital input into the carbonates in the area studied.

7-The petrology and geochemistry of the meta-igneous and volcanic rocks have been described.

8- The Ti, Cr, Ca, Al and Na contents of the clinopyroxenes in the metadolerite allows identification of a non-orogenic and calc alkali character. From the metatrachyandesite these elements allow discrimination of orogenic, tholeiitic and calc-alkali characters and from the metabasaltic andesite rock allows identification of orogenic and tholeiitic variation.

9- Amphibole and biotite mineral compositions from the dacites show typical orogenic character.

10-The petrology and geochemistry of the meta-igneous and volcanic rocks have been described. The meta-igneous and volcanic rocks are of a sub-alkaline (tholeiitic + calc-alkaline) character.

11-Petrochemical characteristics of the Kadinhani volcanic and meta-igneous rocks suggest that they may have been derived from subcontinental lithosphere, except the metahornblende gabbro which has MORB - REE characteristics. It is difficult to explain the intrusion of such a magma as dykes as into continental crust.

12-The geochemical data show that the rock types were produced in differing tectonic settings. The geodynamic system evolved with tension replaced by compression and a transition from initial oceanic volcanism to continental arc to continental orogenic volcanism.

13- The differences in geodynamic conditions are seen in the chemical and REE compositions of the meta-igneous and volcanic rocks. The best information on this is provided by the elements that are inert during low-temperature metamorphism i.e the highly charged lithophile elements Th, Zr, Nb, the REE, the transition group elements (Ti, Cr, Co) and P.

14-Small amounts of crustal contamination in the evolution of the rocks are indicated by high Rb, Ba and LREE contents.

15-The metahornblende gabbros are tholeiitic and their element concentrations plot in the mid-ocean ridge basalt (MORB) field. The metadolerite and metatrachyandesite are calcalkaline and their element concentrations plot in the fields of within plate basalts (WPB). Metabasaltic andesites show transition from tholeiitic to calc-alkaline and their element concentrations plot in the field of continental arc lavas (CAL).

16-The meta trachyandesite and metabasaltic andesite have similar REE patterns, Primordial mantle and N-MORB-normalized profiles, strongly suggesting a similar origin. However, the possibility of derivation of the metatrachyandesite from basaltic magma via crystal fractionation of mafic minerals conflicts with the degree of REE fractionation of the metabasaltic andesite.

17-The metahornblende gabbro was derived from source similar to a mid-ocean- ridge type parent. The metadolerites parental magma was similar to subduction related lavas in a continental margin environment, involving a mix of subcontinental lithosphere and subduction components.

18- Dacites show the characteristics of typical orogenic High - K dacites which contain high Al, low Ti, Nb, and REE. The rocks were evolved mainly by amphibole fractionation under hydrous conditions at shallow levels in the continental crust and probably formed by fractional crystallization from andesitic parental magmas.

19-Three phases of deformation (D_1-D_3) have been recognized in the present area. D_1 minor folds and D_1 cleavage are the dominant structural elements in the area. Oblique extension joints are the result of later brittle deformation. D_3 minor structures are only developed locally and no major fold related to this deformation occurs in the area. The microstructural and petrographic investigations show distinct phases of deformation and different metamorphic events.

20- A well developed schistosity is evident in rocks rich in sheet silicates, but carbonate-rich metasediments show only a faint schistosity. Some rocks show an additional crenulation cleavage. The crenulation cleavage as observed in thin sections, either consists of dark trains of iron oxides and opaque granules interspersed with dimensionally oriented phyllosilicates, or as aggregates of parallel dimensionally oriented phyllosilicates. The dominant mineral assemblage in the crenulation cleavage is muscovite and sericite-opaque minerals particularly where the host rock mineralogy is white mica - quartz-chlorite-amphibole-epidote and opaque minerals.

21- Diagnostic mineral assemblages and mineral chemistry have been documented for all the rocks in the studied area. Common minerals in the studied area are albite + crossite+ riebeckite+ glaucophane+ winchite+ actinolite+ hornblende+ chlorite+ biotite+ epidote+ pumpellyite+ chloritoid+ stilpnomelane+ calcite+ magnetite+ quartz+ dolomite+ sphene+ sanidine+ siderite+ white mica+ hematite+ apatite+ antigorite and graphite. These are indicative of metamorphic conditions dealt with in the last chapter. Calcic plagioclase, augite,hornblende, biotite and salite are relicts from earlier igneous crystallization.

22- Seritization, chloritization, saussuritization and albitization are widely observed in the meta igneous rocks.

23- The compositional changes of minerals with increasing grade were determined. All Ca-Al silicates (pumpellyite and epidote), and phengite increase in Al_2O_3, amphibole changes from riebeckite through crossite- glaucophane and actinolite to winchite.

24-The studied area was metamorphosed first under the conditions of the greenschist facies and then later under the blueschist facies. The blueschist facies minerals are best developed in the metabasaltic andesite, and the metatrachyandesite. The presence of cogenetic calcic and sodic amphiboles in the metahornblende gabbro and metabasic schist are recognized as transitional between the greenschist - blueschist facies. The metabasaltic andesite, metatrachyandesite and metabasic schists are foliated and the foliation is parallel to S_1 in the surrounding metapelites, calc-schists and psammites. The most important minerals, muscovite, chlorite, chloritoid, actinolite, and stilpnomelane grew during the D_1 deformation under greenschist facies metamorphism. This metamorphism was accompanied by crystal - plastic deformation of albite and quartz. Chloritoid in the pelitic rocks shows evidence of syntectonic rotation and deformation, with wrapping of the foliation around the porphyroblasts, indicating a possible early syn-D_1 origin. These facts and the amphibole compositions in the rocks suggest that the greenschist facies metamorphism predated the blueschist facies metamorphism in the Kadinhani area.

25-The blueschist metamorphism gave rise to magnesio - riebeckite, crossite, glaucophane, phengite,pumpellyite and albite minerals.

26- The age of the metamorphisms has not been determined. The pressure-temperature metamorphic environment is calculated to have been 3-6 Kbar and 350-500 °C for greenschist facies in metapelitic rocks and metahornblende gabbro and metabasaltic andesite. They are composed of typical greenschist minerals which are chloritoid, actinolite, stilpnomelane, chlorite and epidote. The pressure-temperature metamorphic environment is calculated to have been 6-7 Kbar and 350-400 °C for blueschist facies in the metatrachyandesite which is composed of typical blueschist minerals namely albite, phengite, pumpellyite, magnesio riebeckite, crossite and glaucophane.

REFERENCES

Abdullah, M. I. & Atherton, M. P. 1964. The thermodynamic significance of magnetite in low grade metamorphic rocks. Am. Jour. Sci., 262, 904-917.

Altherr, R., Schliestedt, M., Okrusch, M., Siedel, E., Kreuzer, H., Harre, W., Lenz, H., Wendt, I. & Wagner, G. A. 1979. Geochronology of high-pressure rocks on Sifnos (Cyslades, Greece). Contrib. Mineral. Petrol., 70, 245-255.

Anderson, A. T. J. 1976. Magma mixing: petrologic process and volcanological tool. Journal of Volcanology and Geothermal Research., 1, 3-33.

Arth, J. G. 1981. Rare earth element geochemistry of the Island arc volcanic rocks of Rabaul and Talasea, New Britain. Geol. Soc. Am. Bull., 92, 858-863.

Atherton, M. P., Sanderson, L. M., & Warden, V. 1985. The volcanic cover; Chemical composition and the origin of the magmas of the Calipuy Group. In: W.S Pitcher et al., (eds) Magmatism at a plate edge; The Peruvian Andes, (Blackie/Halsted Press), 273-284.

Banger, N. 1987. Karadag (Sizma-Konya) cevresinin jeolojik-petrografik incelemesi. Yuksek lisans Thesis, Selcuk Universitesi Fen Bilimleri Enstitusu.

Barberi, F., Bizouard, H. & Varet, J. 1971. Nature of the clinopyroxene and iron enrichment in alkalic and transitional basaltic magmas. Contrib. Mineral. Petrol., 33, 93-107.

Barton, M., Huijsmans, P. P. 1986. Post-caldera dacites from the Santorini volcanic complex, Aegean Sea. Greece; an example of the eruption of lavas of near-constant composition over a 2,2 year period. Contrib. Mineral. Petrol., 94, 472-495.

Basarir, E. 1970. Bafa Golu dogusunda kalan Menderes Masifi guney kanadinin jeolojisi ve petrografisi. Ege universitesi Fen Fakultesi Ilmi Raporlar Serisi., 102, 42p.

Bayic, A. 1968. Sizma-Konya metaporfiritleri hakkinda. Maden Tetkik Arama Enstitusi Dergisi, Ankara., 70.

Best, M. G. 1975. Amphibole-bearing cumulate inclusions, Grand canyon, Arizona, and their bearing on silica undersaturated hydrous magmas in the upper mantle. Journal of Petrology., 16, 212-236.

Bhatia, M. R. & Taylor, S. R. 1981. Trace element geochemistry and sedimentary provinces:a study from the Tasman geosynclines Australia. Chem. Geol., 33, 115-125.

Bhatia, M. R. 1983,. Plate tectonics and geochemical composition of sandstones: Jour. Geol., 91, 611-627.

Bhatia, M. R., Crook, K. A. W. 1986. Trace element characteristics of graywackes and tectonic setting discrimination of sedimentary basins. Contrib. Mineral. Petrol., 92, 181-193.

Biju-Duval, B., Dercourt, J. & Le Pichon, X. 1977. From the Tethys ocean to the Mediterranean Seas: a plate tectonic model of the evolution of the Western alpine system., Editions Technip edn. Paris., 143-164. pp.

Black, P. M. & Brothers, R. N. 1977. Blue schist ophiolites in the melange zone, Northern New Calodonia. Contrib. Mineral. Petrol., 65, 69-78.

Blake, M. C, Jr., Bonneam, M., geyssant, J., Kienast, J. R., Lepurier, C., Malusk, H. & Papanikolaou, D. 1981. A geological reconnaissance of the cycladic blueschist belt,Greece. Geological society of America Bulletin., 92, 247-254.

Blundy, J. D. & Holland, J. B. 1990. Calcic amphibole equilibria and a new amphibole-plagioclase geothermometer. Contrib. Mineral. Petrol., 104, 208-224.

Bosbach, D., Stosch, G. & Seidel, E. 1991. Magmatic and metamorphic evolution of metagabbros in the Munchberg Massif, N. E.Bavaria. Contrib. Mineral.

Petrol., 107, 112-123.

Boynton, W. W. 1984. Cosmochemistry of the rare elements.Rare Earth Geochemistry. Elsevier, Amsterdam, 63-107. pp.

Brown, G. M. 1967. Mineralogy of basaltic rocks.1, Basalts. New York, İnter Science., 103-162. pp.

Brown, H. H. 1977. The crossite content of Ca-amphibole as a guate to pressure of metamorphism. Journal of Petrology., 18, 58-72.

Caglayan, A., Ozturk, E. M., Ozturk, Z., Saw, H. & Akat, U. 1980. Menderes masifi guneyine ait bulgular ve yapisal yorum. Jeoloji muhendisligi., 10, 9-17.

Cann, J. R. 1970. Rb, Sr, Y, Zr and Nb in some ocean floor basaltic rocks. Earth and Planetary Science Letters., 10, 7-10.

Cipriani, C., Sassi, F. P. & Scolari, A. 1971. Metamorphic white micas: definition of paragenetic fields. Schweiz. Min. Petr. Mitt., 51, 259-302.

Coombs, Ds., Hordyski, R. & Naylor, Rs. 1976. Occurrence of prehnite-pumpellyite facies in northern Maine. Am. J. Sci., 268, 142-156.

Courtois, C. & Hoffert, M. 1977. Distribution des terres rares dans les sediments superficiels du Pacifique sud-east. Bull.Soc.Geol.Fr., 19, 1245-1251.

Crook, K. A. W. 1974. Lithogenesis and geotectonics:. Special publication of the society for Economic paleontologist and Mineralogist., 304-310. pp.

Cullers, R.L. and Graff, J. L. 1984 b. Rare earth elements in igneous rocks of the continental crust: intermediate and silicic rocks ore petrogenesis. Elsevier, Amsterdam, 275-316 pp.

de Graciansky, F. C. 1966. Le Massif Cristallin du Menderes (Taurus Occidental, Asie minevre). Un exemple possible de vieux socle granitique remobilise. Revue de Geographie Physique et de geologie dynamique., 8, 289-306.

de la Roche, H. 1966 Sur l'existence de plusierurs facies geochimiques dans les schistes paleozoiques des Pyrenees Luchonnaises. Geol. Rundschau., 55, 274-301.

De Paolo, D. J. 1981. Trace element and isotopic effects of combined wallrock assimilation and fractional crystallization. Earth Planet Sci. Lett., 53, 189-202.

Deer, W. A., Howie, R. A. & Zussman, J. 1966. Rock-Forming Minerals.,. Longman, London.

Deer, W. A., Howie, R. A. & Zussman, J. 1982. Rock-Forming minerals. Longman, London.

Degens, B. T. & Williams, P. G. and Keith, M. L. 1957. Environmental studies of Carboniferous sediments, I, Geochemical Criteria for differentiating marine from fresh water shales. Bull. Am. Ass. Petrol. Geol., 41, 2455-2472.

Dogan, A. 1975. Sizma-Ladik (Konya) civa sahasinin jeolojisi ve maden yataklari sonuclarinin incelenmesi. Yuk.Muh.Diploma calismasi, Istanbul Universitesi Fen Fakultesi.

Dora, O. 1981. Menderes Masifinde Petroloji ve feldspat incelemeleri. Yerbilimleri., 7, 54-63.

Dupuy, C., Leyreloup, A. & Vernieres, J. 1979. The lower continental Crust of the Massif Central (Bournac, France)-with special reference to REE, U,and Th composition, evolution, heat-flow production. Physics and Chemistry of the Earth., 11, 401-415.

Durr, S., Altherr, R., Keller, J., Okrusch, M. & Seidel, E. 1978. The Median Aegean Crystalline Belt: stratigraphy, structure, Metamorphism;. Schweizerbart, Stuttgrat, 455-476 pp.

Elderfield, H. 1988. The oceanic chemistry of the rare -earth elements. Phil.trans. Roy. Soc. London, A 325, 105-126.

Elliott, R.B., The chemistry of gabbro/ amphibole transitions in south Norway. Cont. Min. Petr., 38, 71-79, 1973.

Eren, Y. 1993. Eldes-Derbent-Tepekoy- Sogutozu (Konya) arasinin jeolojisi,. Doktora, Selcuk Universitesi Fen Bilimleri Enstitusu.

Ernst, W.G. 1963b. Petrogenesis of glaucophane schists. J.Petrology, 4, 1-30.

Ernst, W.G., Seki, Y. & Onuki, H.Gilbert, M.C. 1970. Comparative study of the low-grade metamorphism in the California Coast Ranges and the outher metamorphic belt of Japan. Geol.Soc.America.Mem., 124, 276p.

Ernst, W.G., Harker, B.R., Barton, M.D. & Sen,G. 1991. Occurence, geochemistry and igneous petrogenesis of magnesian metavolcanic rocks from the WTrPz belt, Central Klamath Mountains, northern California. Geological Society of America Bulletin., 103, 56-72.

Evarts, R.C. & Schiffman, P. 1983. Submarine hydrothermal metamorphism of the del Puerto Ophiolite,California. Am.J.Sci., 283, 289-341.

Ewart, A. 1979. A reviev of the mineralogy and chemistry of Tertiary-Recent dacitic, rhyolitic, and related salic volcanic rocks. Trondhjemites, Dacites, and Related Rocks. Elsevier., Amsterdam.

Ewart, A. 1982. The mineralogy and petrology of Tertiary-Recent oeogenic volcanic rocks: with special reference to the andesitic-basaltic compositional range. Oreogenic Andesites and Related Rocks. John Wiley, New York, 25-95 pp.

Feininger, T. 1982. Glaucophane schist in the Andes at Jambalo, Columbia. Can.Mineral., 20, 41-8.

Field, D. & Elliott, R.B. 1974. The chemistry of Gabbro/ amphibolite transitions in south Norway. Contrib. mineral. Petrol., 47, 63-76.

Floyd, P.A. & Winchester, J.A. 1975. Magma type and tectonic setting discrimination using inmobile elements. Earth Planetary Science Letters, 27, 211-218.

Floyd, P.A. & Winchester, J. A. 1978. Identification and discrimination of altered and metamorphosed volcanic rocks using inmobile elements. Chemical Geology, 21, 291-306.

Friedman, G. M. 1969. Trace elements as possible environmental indicators in carbonate sediments. In: G.M.Friedman (eds.), Depositional environments in Carbonate Rocks. 14, Soc.Econ.Palaeontologist Mineralogist, Spec. Publ., 193-198.

Gill, J. B. 1981. Orogenic Andesites and Plate Tectonics. Springer, Berlin.

Goger, E. & Kiral, K. 1969. Kiziloren dolayinin jeolojisi. M.T.A. Rapor ; 5204 (yayinlanmamis).

Gray, D. R. & Durney, D. W. 1974. The development of cleavage and differentiation in crenulated rocks from southeastern Australia. Geol.Soc.Aust.Tectonies and Structural Newsletter., 3, p.22(Abst.).

Guzel, A. 1983. Sarayonu-Kadinhani (Konya) dolayinin hidrojeoloji incelemesi. Doktora tezi, S.U.Muh-Mim.Fak.

Harvey, P.K. & Atkin, B. P. 1981. The rapid determination of Rb, Sr and their ratios in geological materials by X-ray fluorescence spectrometry using a rhodium X-ray tube. Chemical Geology., 32, 291-301.

Harvey, P. K., Taylor, D. M., Hendry,R.D., Bancroft,F. 1973. An accurate fusion method for the analysis of rocks and chemically related minerals by X-ray fluorescence spectrometry,. X-ray spectrometry., 21, 33-44.

Hawthorne, F. C. 1981. Crystal chemistry of the amphiboles in amphiboles and other Hydrous Pyriboles-Mineralogy,. Mineralogical Society of America., 1-95 pp.

Herron, M. M. 1988. Geochemical classification of terrigenous sands and shales from core or log data. J.Sed.Petrol., 58, 820-829.

Hey, M. H. 1954. A new review of the chlorites. Mineralogical Magazine, 30, 272-92.

Holl, R. 1966. Genese und altersstellung von vorkommender Sb-W-Hg formation in der Turkei und auf Chios / Griechenland. PhD., Munchen.

Hollister, L. S. & Gancarz, A. J. 1971. Compositional sector-zoning in clinopyroxene from the Narce area, Italy. Am. Miner., 56, 959-79.

Huebner, J. S. 1980. Pyroxene phase equilibria at low pressure. Pyroxenes Review in Mineralogy. Miner.Socie. of America., 213-280.

Irvine, T. N. & Baragar, W.R.A. 1971. A guide to the chemical classification of the common volcanic rocks. Can.J.of Earth Sci., 8, 523-548.

Jakes, P. & White, A. C. R. 1972. Major and trace elements abundances in volcanic rocks of orogenic areas. Geol. Soc. Am. Bull., 83, 29-40.

Jensen, B. B. 1973. Patterns of trace element partitioning. Geochim. Cosmochim. Acta., 37, 2227-2242.

Johnson, M. C., Rutherford, M. J. 1989. Experimental calibration of the aluminum in hornblende geobarometer with application to Long valley caldera (California) volcanic rocks. Geology., 17, 837-841.

Kaaden, G. V. D. 1964. Konya vilayeti, Kursunlu-Ladik sahasindaki zincifre zuhurlari hakkinda not. M.T.A. 3539 (Yayinlanmamis) .

Kay, R.W. 1977. Geochemical constraints on the origin of Aleutian magmas. American Geophysical Union, Washington,D.C., 229-242 pp.

Ketin, I. 1966. Tectonic units of Anatolia (Asia minor). Maden Tetkik arama

Enstitusu Bulteni., 66, 23-35.

Koster, H. M. 1969. Beitrag zur Geochimie - der kaoline. Japan., 273-280 pp.

Kovenko, V. 1939. Konya mintikasindaki Sizma Koyu civa madeni Maden Tektik Arama Enstitusu. 3837 (Yayinlanmamis), .

Kronberg, BI, Fyfe WS, Leonardos OH, Santos AM. 1979. The geochemistry of some Brazilian oils: element mobility during intense weathering. Chem. Geol., 24, 211-229.

Kuno, H. 1950. Petrology of Hakone volcano and adjacent areas, Japan. Geological Society of America Bulletin., 25, 957-1020.

Kuo, L. & Kirkpatrick, R.J. 1982. Pre-eruption history of phyric basalts from DSDP legs 45 and 46: evidence from morphology and zoning patterns in plagioclase. Contrib. Mineral. Petrol., 79, 13-27.

Lambert, R. S. J., Holland, J. G. 1974. Yttrium geochemistry applied to petrogenesis utilizing calcium Yttrium relationships in minerals and rocks. Geochim. Cosmochim. Acta., 38., 1393-1414.

Landis, C. A. 1971. Graphitization of dispersed carbonaceous material in metamorphic rocks. Contrib.Mineral.Petrol., 30, 34-45.

Le Bas, M. J., Le Maitre, R. W., Streckeisen, A. & zanettin, B. 1986. A chemical classification of volcanic rocks based on the total alkali silica diagram. Journal of Petrology., 27, 745-750.

Leake, B. E. 1964. The chemical distinction between ortho- and para amphibolites,. J.Pet., 5-2, 238-254.

Leake, B. E. 1965. The relationship between composition of calciferous amphibole and grade of metamorphism,. London, 299-318 pp.

Leake, B. E., Hendry, G.L., Kemp, A., Plant, A.G., Harrey, P.K., Wilson, J.R., Coats, J.S., Aucott, J.W., Lunel, T. & Howarth, R.J. 1969. The chemical analysis of rock powders by automotic x-ray fluorescence. Chem.Jeology., 5, 7-86.

Leake, B. E. 1978. Nomenclature of amphiboles. American Mineralogist, 63, 1025-1052.

Leterrier, M., Maury, R.C., Thonon,P., Girard,D. Marchal,M. 1982. Clinopyroxene composition as a method of identification of the magmatic affinities of paleo-volcanic series. Earth Planet. Sci.Letters, 59, 139-154.

Liou, J. G., Maruyama, S. & Cho, M. 1987. Very-Low grade metamorphism of volcanic and volcaniclastic rocks-mineral assemblages and mineral facies. Blackie, Glasgow, 59-112 pp.

Loomis, T. P. 1982. Numerical simulations of crystallization processes of plagioclase in complex melts: The origin of major and oscillatory zoning in plagioclase. Contrib. Mineral. Petrol., 81, 219-229.

Luhr, J. F.Carmichael, I.S.E. 1980. The Colima volcanic complex Mexico. Contrib. Mineral. Petrol., 71, 343-372.

Maresch, W. V. 1977. Experimental studies on glaucophane: an analysis of present knowledge. Tectonophysics., 43, 109-125.

Massone & Schreyer. 1987. Phengite barometry based on the limiting assemblage with K-feldspar, phlogopite, and quartz. Contrib. Mineral. Petrol., 96, 212-224.

Maucher, A. 1964. Konya Vilayeti Ladik ve Sizma cevrelerinde bulunan civa zuhurlarinin gezilmesine ait rapor. Maden Tetkik Arama Enstitusu., 3695 (yayinlanmamis) .

Maynard, J. B., Valloni,R.and Yu,H-s. 1982. Composition of modern deep-sea sands from arc related basins. Journal of the geological Society of London special publication, 531-562 pp.

Mc Lennan, S. M. & Taylor, S. R. 1980. Th and U sedimentary rocks: crustal evolution and sedimentary recycling. Nature, 285, 621-624.

Mc Lennan, S. M., Taylor, S. R.& Mc Gregor, V. R. 1984. Petrogenesis of the Kirkpatrick Basalt, solo Nunatak, North Victoria Land, Antartica. Contrib. Mineral. Petrol., 87, 101-108.

Mc Lennan, S. M. McCulloch, M. T., Taylor, S. R & Maynard, J. B.,. 1989. Effects of sedimentary sorting on neodymium izotopes in deep -sea turbidites. Nature., 337 (6207), 547-549.

McLennan, S. M. 1989. Archean sedimentary rocks and the archean mantle. Lunar and planetary Institute., Houston,TX.

McLennan, S. M., Taylor, S. R., Mcculloch,M.T. and Maynard,J.B. 1990a. Geochemical and nd-sr isotopic composition of deep-sea turbidites. partI; Implications for crustal evolution. Geochim.Cosmochim.Acta (submitted).

McLennan, S. M., Taylor, S. R., McCulloch, M. T. and Maynard, J. B. 1990b. Geochemical and Nd-Sr isotopic composition of deep sea turbidites.Part II: Sedimentological and plate tectonic controls. Geochim.Cosmochim.Acta.

McMillan, N. J. & Dungan, M. A. 1986. Magma mixing as a petrogenetic process in the development of the Toas Plateau volcanic field, New Mexico. J.Geophys. Res., 91, 6029-45.

Mikhalsky, E. V & Sheraton, J. W. 1993. Association of dolerite and Lamprophyre dykes Jett Peninsula (Prince Charles Mountains, East Antartica). Antarctic Science, 5 (3), 297-307.

Miyashiro, A. & Seki, Y. 1958. Enlargement of the compositional field of epidote and piemontite with rising temperature. Am. J. Sci., 256, 423-430.

Miyashiro, A. 1972. Metamorphism and related magmatizm in plate tectonics. Am. J. Sci., 272, 629-656.

Miyashiro, A. & Shido, F. 1973. Progressive compositional change of garnet in metapelite. Lithos., 6, 13-20.

Moore, J. M. 1977. The geology of Namiesberg, northhern Cape. Bull.Precambr. Res. Unit. Univ.Cape Tawn., 20, 69.

Motorcu, A. 1987. Ladik-Sizma (Konya) bolgesi civa yataklari. Yuksek lisans., Selcuk Universitesi Fen Bilimleri Enstitusu.

Murray, R. W., Buchholtz Ten Brink, M. R., Gerlach, D. C.,Russ, G. P., III, and Jones, D. L. 1991a. Rare earth, major and trace elements in chert from the Franciscan complex and Monterey Group, California: Assessing REE sources to fine-grained marine sediments. Geochim. Cosmochim. Acta., 55, 1875-1895.

Murray, R. W., Buchholtz Ten Brink, M. R., Gerlach, D. C., Russ III, G. P., Jones, D. L. 1992. Rare earth, major, and trace element composition of Monterey and DSDP chert and associated host sediment: Assessing the influence of chemical fractionation during diagenesis. Geochemica et Cosmochimica Acta., 56, 2657-2671.

Nakamura, N. 1973. Origin of Sector-zoning in igneous clinopyroxenes. Am.Min., 58, 986-990.

Nesbitt, H. W. & Young, G. M. 1982. Early proterozoic climate and plate motions inferred from major element chemistry of lutites. Nature, 299, 715-717.

Niehoff, W. 1964. 1/100000 olcekli Aksehir ve (91/1,91/3,91/4) ilgin paftalari Yaz calismalari hakkinda rapor.Maden Tetkik Arama Enstitusu., 3387 .

Niggli, P. 1954. Rocks and Mineral deposits. Freeman, San Francisco, 559pp .

Nitsch, K. H. 1971. Stabilitatsbeziehungen von prehnit- und pumpellyit haltigen paragenesen. Contrib. Mineral. Petrol., 30, 240-260.

Nixon, G.T. & Pearce, T. H. 1987. Laser-interforometry study of oscillatory zoning in plagioclase: The record of magma mixing and phenocrysts recycling in calc-

alkaline magma chambers,Iztaccihuati volcano, Mexico. American Mineralogist., 72, 1144-1162.

Okay, A. I. 1984-a. Distribution and characteristics of the Northwest Turkish blueschists. Geological society of London special Publication, 455-466 pp.

Okay, A.I. 1984-b. Kuzeybati Anadolu'da yer alan metamorphic kusaklar. Ketin symposium., 83-92.

Okay, A. I. 1986. High-pressure/low-temperature metamorphic rocks of Turkey. Geological Society of America Memoir, 164, 333-347.

Pearce, J. A. & Cann, J. R. 1973. Tectonic setting of basic volcanic rocks determined using trace element analyses. Earth and Planetary Science Letters, 19, 290-30.

Pearce, J. A. & Gale, G. H. 1977. Identification of ore deposition environment from trace-element geochemistry of associated igneous host rocks. Institute of Mining and Metallurg, London, 14-24 pp.

Pearce, J. A. 1982. Trace element characteristics of Lavas from destructive plate boundaries. In: Thorpe, R.S. (eds) Andesites: Orogenic andesites and related rocks. John Willey, New York, Chichester, 525-548 pp.

Pearce, J. A. 1983. Role of the sub-continental lithosphere in magma genesis at active continental margins. In: Hawkesworth, C.J. & Norry, M.J. (eds) continental Basalts and mantle Xenoliths. Shiva, Cheshire, 230-249 pp.

Pearce, T. H. & Kolisnik, A. M. 1990. Observations of plagioclase zoning using interference imaging. Earth Science Reviews, 29, 9-26.

Peccerillo, A. & Taylor, S. R.,. 1976. Geochemistry of Eocene calc-alkaline volcanic rocks from the Kastamonu area, northern Turkey. Contrib. Mineral. Petrol., 58, 63-81.

Pehlivan, A. N. 1976. Etibank Konya civa isletmesi Sizma-Ladik sahalarina ait rapor. Maden Tetkik Arama Enstitusu., 5757 .

Perrault, G. 1955. Geology of the Western margin of the Labrador Trough. Ph,D. Thesis, Toronoto.

Petrascheck, W. E. 1964. Konya vilayeti Ladik civa madeninin 1/25000 olcekli harita etudu hakkinda ana rapor, Maden Tetkik Arama Enstitusu., 3788 (yayinlanmamis).

Pettijohn, F. J., Potter, P. E. and Siever, R. 1972. Sand and sandstones. Springer-Verlag., Berlin-Heidelberg,

Pharaoh, T. C. & Pearce, J. A. 1984. Geochemical evidence for the geotectonic setting of early proterozoic meta-volcanic sequences in Lapland. Precambrian Research, 10, 283-309.

Pilz, R. 1937. Konya-Sizma civa ve bakir madenleri hakkinda rapor. Maden Tetkik Arama Enstitusu, 544, .

Poldervaart, A. & Hess, H. H. 1951. Pyroxenes in the crystallization of basaltic magma. Journ.Geol., 59, 472.

Raase, P. 1974. Al and Ti contents of hornblende, indicators of pressure and temperature of regional metamorphism. Contrib. Mineral. Petrol., 45, 231-236.

Ramsay, J. G. & Huber, M. I. 1983. The techniques of modern structural geology:1 strain analysis. Akademic Press, London.

Riley, J. P. 1958. Simultaneous determination of water and carbondioxide in rocks and minerals,. Analyst, 83/982, 42-49.

Robinson, D., and Leake, B.E. 1975. Sedimentary and igneous trends in AFM diagrams. Geol.Mag., 112, 305-307.

Romick, Jay. D., Kay, S. M., & Kay, R.W. 1992. The influence of amphibole fractionation on the evolution of calc-alkaline andesite and dacite tephra from the Central aleutions, Alaska. Contrib. Mineral. Petrol., 112, 101-118.

Roser, B. P., and Korsch, R. J. 1988. Provenance signatures of sandstone - mudstone suites determined using discriminant function analysis of major element data,. Chem. Geol., 67, 119-139.

Roser, B. P., Korsch, R.j. 1985. Plate tectonics and geochemical composition of sandstones: a discussion. J.Geol., 93, 81-84.

Saunders, A. D. & Tarney, J. 1979. The geochemistry of basalts from a back-arc spreading centre in the East Scotia Sea. Geochimica et Cosmochima Acta, 43, 555-72.

Saunders, A. D., Norry, M. J. & Tarney, J. 1991. Fluid influence on the trace element compositions of subduction zone magmas:Phil.Trans. R.Soc.Lond., A 335, 377-392.

Schilling, J. G. 1971. Sea-floor evolution; rare-earth evidence, Philos.Trans. R.Soc.London,Ser.A, 268, 663.

Schilling, J. G. 1975. Rare-earth variations across ' normal segments' of the Reykjanes ridge, 60-53 N, mid-atlantic ridge, 29 s and east Pacific rise, 2-19 S, and evidence on the composition of the underlying low-velocity layer. J.Geophys. Res., 80, 1459-1473.

Schumacher, Prof. 1937. Sizma madenindeki civa zuhurlarina ait rapor Maden Tetkik Arama Enstitusu., 545 (yayinlanmamis).

Schumacher, J. C. 1991. Empirical ferric iron correction: necessity, assumptions, and effects on selected geothermobarometers. Mineralogical Magazine, 55, 3-18.

Schwab, F. L. 1975. Framework mineralogy and chemical composition of continental margin-type sandstone. Geology., 3, 487-490.

Sengor, A. M. C. & Kidd, W. S. F. 1979. Post-collisional tectonics of the Turkish - Iranian plateau and comparison with Tibet. Tectonophysics, 55, 361-376.

Sengor, A. M. C., Satir, M. & Akkok, R. 1984b. Timing of tectonic events in the Menderes Massif, Western Turkey: Implications for tectonic evolution and evidence for Pan American basement in Turkey. Tectonics, 3, 693-707.

Senior, A. & Leake, B.E. 1978. Regional metasomatism and the geochemistry of the Dalradian metasediments of Connemera, Western Ireland. j. Pet., 19, 585-625.

Seidel, E., Okrusch, M. & Schubert, W. 1975. Chloritoid-bearing metapelites associated with glaucophane rocks in W.Crete. Contrib.Mineral. Petrol., 49, 105-115.

Shimizu, H., Masuda, A. 1977. Cerium in chert as an indication of marine environment of its formation. Nature, 266, 346-348.

Sibley, D. F., Vogel, T. A., Walker, B. M. & Byerly, G. 1976. The origin of oscillatory zoning in plagioclase :A diffusion and growth controlled model. American Journal of Science., 276, 275-284.

Spear, F. S. & Kimball, K. 1984. RECAMP-A FORTRAN 4 program for estimating Fe+3 contents in amphiboles. Computers Geosci., 10, 317-325.

Stosch, H. G. & Lugmair, G. W. 1987. Geochronology and geochemistry of eclogites from the Munchberg Gneiss Massif, FRG. Terra Cognita, 7, 163.

Streckeisen, a. & LeMaitre, R. W. 1979. A chemical approximation to the modal QAPF classification of the igneous rocks. Neues Jahr. Mineral. Abh., 136, 169-206.

Sugisaki, R., Kinoshita, T. 1982. Major element chemistry of the sediments on the central Pacific transect, Wake to Tahiti, GH80-1 cruise. Geol. Surv. Jpn.,

Cruise Rep., 18, 293-312.

Taylor, S. R. & Mc Lennan, S. M. 1981. The composition and evolution of the continental crust: rare earth element evidence for sedimentary rocks. Phil.Trans. R.Soc.London., A 301, 381-399.

Taylor, S. R., and McLennan,S.M. 1985. The continental Crust; its composition and evolution. Blackwell scientific puplications, Oxford, U.K.

Taylor, S. R., Rudnick, R. L., Mc Lennan S. M., Eriksson K.A.,. 1986. Rare earth element patterns in archean high-grade metasediments and their tectonic significance. Geochim. Cosmochim.Acta., 50, 2267-2279.

Tokel, S., Ercan, T., Akbasli, A., Yildirim, T., Fisekci, A., Selvi, Y., Olmez, M. & Can, B. 1987. Orta Anadolu Neogene toletitic Provensi:Magma jenezi ve carpisma sonu litosfer dinamigi. METU Journal of Pure and Applied Sciences., 21, 1-3, 461-477.

Tsuchiyama, A. 1985. Dissolution kinetics of plagioclase in melt of the system diopsite-albite-anorthite and the origin of dusty plagioclase in andesites. Contrib. Mineral. Petrol., 84, 1-16.

Turner, F. J. 1968. Metamorphic petrology. Mc Graw-hill, New York, 403p.

Ustundag, A. 1987. Sizma-Kursunlu-Meydan-Bagrikurt (Konya) koyleri arasindak Karadag cevresinin jeolojisi. Yuksek lisans, Selcuk Universitesi Fen Bilimleri Enstitusu.

Van de Kamp, P.C. 1969. Origin of amphibolites in the Beartooth Mountains - new data and interpretation. Bull.Geol.Soc.Am., 80, 1127-1136.

Van de Kamp, PP.C., Leake, B. E., and Senior, A. 1976. The petrography and geochemistry of some Californian arkoses with applications to identifying gneisses of metasedimentary origin: Jour. Geology., 84, 195-212.

Van de Kamp, P. C. and Leake, B. E. 1985. Petrography and geochemistry of feldspathic and mafic sediments of the northeastern Pacific margin.

transactions of the Royal Society of Edinburgh: Earth Sciences., 76, 411-419.

Veizer, J., Demovic, R. 1974. Strontium as a tool in facies analysis. J. Sediment. Petrol., 44, 93-115.

Veizer, J., Lemieux, J. Jones, B., Gibling, M. R., Savello,J. 1978. Paleosalinity and dolomitization of lower paleozoic carbonate sequence, Somerest and Prince of Wales islands, arctic Canada. Can.Jour.Earth Science., 15, 1448-1461.

Velde, B. 1965. phengite micas: Synthesis, stability and natural occurence. Am.Journ. of Sci, 263, 886-913.

Velde, B. 1977. Clays and clay minerals in Natural and Synthetic systems. Elsevier.

Volkova, N. I., Med'nichenko, A.K., Gofen, G. I. & Varzieyeva, T. B. 1992. The geochemical features of the metabasites and the geodynamic setting of their formation in the Fankaratega Greenschist Belt. Geochemistry International, 29 (11).

Wager, L. R., Brown, G. M. 1967. Layered igneous rocks. Freeman, San Francisco.

Watters, B. R. & Pearce, j. A. (1987). Metavolcanic rocks of the La Ronge Domain in the Churchill Province, saskatchewan: geochemical evidence for a volcanic arc origin. Geological Society Special Publication, 33, 167-182.

Weaver, B. I., Marsh, N. G. & Tarney, J. 1983. Trace element geochemistry of basaltic rocks from the Rio Grande Rise, South Atlantic, DSDP leg 72, Hole 516. 457-466 pp.

Weber, J. N. 1964. Trace element composition of dolostones and dolomites and its bearing on the dolomite problem. Geochim.Cosmochim. Acta., 28, 1817-1868.

Wedepohl, K. H., Correns, C.W, Shaw, D. M., Turekian, K. K., Zemann, J. 1972.

Handbook of Geochemistry. Springer-Verlag Berlin, Heidelberg., New York.V.II/3.

Wedepohl, K. H., Correns, C. W., Shaw, D. M., Turekian, K. K., Zemann, J. 1974. Handbook of Geochemistry. Springer-Verlag Berlin, Heidelberg, New york, V.II/4.

Weisner, K & Lehnert-Thell, K. L. 1964. Sizma-Ladik civa yataklari. Maden Tektik Arama Enstitusu Maden Etud Rap. 551.

Weisner, K. 1968. Konya civa yataklari ve bunlar uzerindeki etudler. Maden Tektik Arama Enstitusu dergisi, Ankara, 70.

Winchester, J. A. & Floyd, P. A. 1976. Geochemical magma type discrimination application to altered and metamorphosed basic igneous rocks. Earth Planetary Science Letters, 28, 459-469.

Winchester, J. A. & Floyd, P. A. 1977. Geochemical discrimination of different magma series and their differentiation products using immobile elements. Chemical Geology, 20, 325-343.

Winchester, J. A., Park, R. G., Holland, J. G. 1980. The geochemistry of lewisian semipelitic schists from the Gairloch district, wester Ross. Scott.j.Geol., 16, 165-179.

Winkler, H. G. F. 1967. petrogenesis of metamorphic rocks. springer-Verlag, New York, 237pp.

Winkler, H. G. F. 1979. Petrogenesis of metamorphic Rocks,. 5th edn. springer-Verlag., New York,

Wood, D. A., Joron, J. L. & Treuil, M. 1979. A re-appraisal of use of trace elements to classify and discriminate between magma series erupted in different tectonic settings. Earth and Planetary Science Letters, 46, 326-336.

Wood, D. A. 1980. The application of a Th-Hf-Ta diagram to problems of tectonomagnetic classification and to establish the nature of crustal

contamination of basaltic lavas of the British Tertiary volcanic provence. Earth and Planetary Science letters, 50, 11-30.

Yamamato, M. 1984. Origin of calc-alkaline andesite from Oshima volcano, north Japan. J.Fac. Sci. Hokkaido Univ. Ser., IV-21, 77-131.

Zelt, G. A. D. 1980. Granulite-facies metamorphism in Namaqualand, South Africa. Precambr.Res., 13, 253-274.

A GEOLOGICAL MAP OF KADINHANI AREA, KONYA — TURKEY

APPENDIX- 1

HUSEYIN KURT – 1993

CROSS SECTIONS FOR THE GEOLOGICAL MAP OF KADINHANI, TURKEY

APPENDIX - 2

Huseyin Kurt - 1993